# LOW-GRADE REGIONAL METAMORPHISM OF PALEOZOIC ROCKS IN THE MIDLAND VALLEY OF SCOTLAND

Lesley Jayne Evans

A Thesis Submitted for the Degree of PhD
at the
University of St Andrews

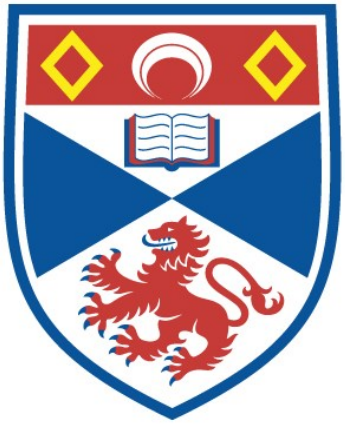

1988

# LOW-GRADE REGIONAL METAMORPHISM OF PALAEOZOIC ROCKS IN THE MIDLAND VALLEY OF SCOTLAND

*LESLEY JAYNE EVANS*

Thesis presented for the degree of

Doctor of Philosophy

JULY 1987



ProQuest LLC.
789 East Eisenhower Parkway
P.O. Box 1346
Ann Arbor, MI 48106 – 1346

CERTIFICATE

I certify that *LESLEY JAYNE EVANS* has been engaged in research at the University of St Andrews and that she has fulfilled the conditions of Ordinance General No 12, and that she is qualified to submit the accompanying thesis in application for the degree of Doctor of Philosophy. She was admitted under this Ordinance in October 1982.

I certify that the following thesis is based on the results of research carried out by me, and that it is my own composition, and that it has not previously been presented for a higher degree.

CONTENTS

*ABSTRACT*

*Low-grade burial metamorphism in the Midland Valley of Scotland, has been investigated with reference to the Silurian sediments and to the Carboniferous volcanics.*

*In the Silurian sediments, facies definitive phyllosilicates are absent. Thin-section examination indicates that cementation was early and despite strong deformation, the lack of cleavage is related to the isotropic dispersal of domains during burial. Scanning electron microscopy and X-ray diffraction define clay mineral assemblages which characterize the transformation of montmorillonite to illite during burial. Illite crystallinity, $b_0$ and conodont alteration, show values consistent with this transformation and are indicative of diagenetic/anchizone conditions. Metamorphism is related to Siluro-Devonian syn-sedimentary burial. Despite tentative links between the Midland Valley and the Southern Uplands during the Llandovery, the relative simplicity of the burial metamorphic sequence in the former region suggests that the Silurian trough became palaeo-geographically distinct.*

*The Carboniferous volcanics have undergone burial metamorphism in the zeolite facies, which occurred once the bulk of the lavas had been extruded, and following burial beneath the Central and Ayrshire Basins. Alteration was dominated by hydrothermal processes and has resulted in the production of early greenstones, later burial metamorphic zones and palaeo-geothermal plumes. Seven zones have been defined upon the distribution of amygdale minerals. Thin-section examination however divides the zeolite facies in the Midland Valley into an upper analcime and a lower laumontite zone.*

*Mineralogical assemblages are conducive with metamorphism at a) $P_{fluid}$ = 2-4(?)kb at 200 °C and b) $P_{fluid}$ = 2 kb at 350-420 °C, for the zeolite zones and the palaeo-geothermal plumes respectively. These values are compatible with burial depth estimates, with homogenization temperatures in fluid inclusions and with calcite-water fractionation temperatures. Water/rock ratios indicate that metamorphism was related to the flow of seawater and meteoric water through the volcanic sequences. Evidence for episodic boiling in fluid inclusions indicates fluid convection occurred, and was related to fracturing associated with a change from a lithostatic to a hydrostatic pressure regime. Seismic pumping was related to fracturing and to re-newed magmatic activity in shallow chambers beneath the Midland Valley.*

*ACKNOWLEDGEMENTS*

*I would like to thank Dr G J H Oliver for his supervision during the preparation of this thesis. Dr A Fallick and Dr J Kinnaird are thanked for their guidance, concerning the application of stable isotope and fluid inclusion analyses respectively. Fruitful discussion with fellow research students and members of staff is also gratefully acknowledged.*

*Analytical work was carried out at St Andrews University and at the Scottish Universities Research and Reactor Centre. The technical advice of the staff at these institutes was invaluable. I particularly wish to thank A Reid, D Herd, A Mackie, J Allan, R Batchelor, S Edwards and Ward for their assistance.*

*Miss K Finlay typed this thesis, and is highly praised for her patient deliverance of the final copy. No thanks could be enough.*

*I am indebted to the Natural Environment Research Council for supporting this research through grant GT4/82/GS/95, and to NERC, the Russell Trust and to the Geography and Geology Departments of St Andrews University for supporting a visit to Iceland. Jack Jarvis is thanked for his assistance in this matter.*

*My greatest thanks go to my parents, family and friends for their constant support and encouragement.*

LIST OF FIGURES

Page No

Page No

## LIST OF TABLES

LIST OF PLATES

Plate 4B: Scanning electron photomicrograph of illite whiskers (i) growing in pore space. Top left, smectite (sm) forms primary pore lining. Bottom right, pitted detrital quartz grain (qtz).

Plate 5A: Scanning electron photomicrograph of chlorite (chl) rosettes; individual stacks consist of lobate-edged chlorite plates.

Plate 5B: Scanning electron photomicrograph of chlorite (chl) rosette growing into pore space. Top right, detrital mica plates.

Plate 6: Typical flood basalt scenery in the Clyde Plateau Lavas. Photograph taken looking eastwards over Loch Humphrey. Individual flow units dip southwards. Overlay: - - fault bounded margin of area; - mineralogical isograds parallel contours (see text, chapter 2.2 for explanations of mineral zones).

Plate 7A: Photograph of calcite cemented greenstone agglomerate. Bottom left, consolidated ash. Top right, basaltic clasts traversed by late calcite veins.

Plate 7B: Photograph of lava tube in metabasalt infilled with early platy heulandite (heu) and late druzy quartz (qtz).

Plate 8A: Photograph of spherulitic quartz, retrieved from veinlets in metabasalt. Arrow points to haematite trails growing along partings within the quartz.

Plate 8B: Photograph of botryoidal prehnite growing on vitreous acicular thomsonite.

Plate 9A: Photograph of late isositetrahedral analcime crystals. Centre left, associated early acicular thomsonite.

Plate 9B: Photograph of opaque radial natrolite clusters.

Plate 10A: Photograph of vitreous silbite sheafs growing on quartz in a geode.

Plate 10B: Photograph of vitreous coffin-shaped heulandite crystals growing into a geode.

Plate 11A: Photograph of prehnitized metabasalt. Consisting of pseudo-hexagonal clusters of prehnite, which extend into amygdales (top left).

Plate 11B: Cross-section through botryoidal prehnite extending into a vein. Note the textural similarities between plate 11A and 11B.

Plate 12A: Photograph of hydrothermally altered basalt from Beith quarry, in the Clyde Plateau Lavas. The dark band is the

haematized flow top.

Plate 12B: Photograph of hydrothermally altered metabasalt from the Icelandic rift zone, Krafla.

Plate 13A: Photomicrograph of plagioclase showing rim replacement textures. Coronas are infilled with chlorite and sericite.

Plate 13B: Photomicrograph of plagioclase phenocryst showing patches of incipient albite crystallization. Dusty speckles are of sphene. Veins, amygdales and groundmass laths show similar replacement by albite.

Plate 14A: Photomicrograph of albitized plagioclase phenocryst sitting in opaque analcimitized metabasalt.

Plate 14B: Enlargement of plate 15A, to show fasicule bundles of albite.

Plate 15A: Photomicrograph to show the interstitital growth of radial chlorite, from glass (plane-light).

Plate 15B: Photomicrograph of prehnitized (bottom) and analcimitized (top) metabasalt. The alteration front cuts the amygdale margin transversally (see overlay).

Plate 16A: Photomicrograph of analcimitzed metabasalt in plane-light. Analcime is characteristically dusty, and

replaces the groundmass and feldspar phenocryst, as well as growing into amygdales. The centre of the amygdale is infilled with natrolite radials.

Plate 16B: Photomicrograph, as above, taken in cross-polars.

Plate 17A: Photomicrograph of icositetrahedral analcime projecting into amygdale from analcimitized metabasalt. Within the amygdale, late radial natrolite is seen to grow upon early analcime.

Plate 17B: Photomicrograph of pseudomorphed feldspar phenocryst in analcimitized metabasalt. The left-hand side of the crystal is replaced by natrolite, and right-hand side by analcime.

Plate 18A: Photomicrograph of laumontized metabasalt, in plane-light. The opaque mineralogy preserves the primary igneous textures.

Plate 18B: Photomicrograph, as above, under cross-polars. Relict igneous textures are difficult to observe, and are incompletely replaced by aggregates of radiating laumontite. Sphene and opaque ores form inclusions in laumontite.

Plate 19A: Photomicrograph of partially pseudomorphed pyroxene in analcimitized metabasalt. The pyroxene is in its

extinction position; replacement is by prehnite.

Plate 19B: Photomicrograph of prehnitized metabasalt. Sphene and opaque ores form inclusions in prehnite.

Plate 20A: Photomicrograph of early opaque icositetrahedral analcime overgrown by late prehnite.

Plate 20B: Photomicrograph of amygdular laumontite.

Plate 21A: Photomicrograph of analcimitized metabasalt. Amygdales infilled with chlorite, calcite and idiomorphic sphene.

Plate 21B: Photomicrograph of accicular prehnite bows growing into geode.

Plate 22A: Photomicrograph of amygdular stilbite, heulandite and quartz, growing tangentially from analcimitized metabasalt. Haematite coats the amygdale rim and heulandite crystals. The stilbite is seen to actively replace heulandite.

Plate 22B: Photomicrograph of prehnitized metabasalt. The dark areas characterise replacement by epidote. Top centre, equant partially isotropic hydro-grossular grows into geode. Bottom centre early icositetrahedral analcime has been pseudomorphed by calcite.

Plate 23A: Photomicrograph of spherulitic vein ferrierite in basalt.

Plate 23B: Photomicrograph of spherulitic stilbite and quartz growing into geode in analcimitized metabasalt.

Plate 24A: Photomicrograph of prehnite, showing optical continuity between occurrences in a vein and a pseudomorph. The prehnite is in analcimitized metabasalt.

Plate 24B: Photomicrograph of analcime (centre), calcite (tangential) and prehnite. The calcite replaces analcime.

Plate 25A: Photomicrograph of fluid inclusions (1-11) in thomsonite at Tf = -76.6 $^{o}$C.

Plate 25B: Photomicrograph of fluid inclusions (1-11) in thomsonite at Tf = -37.2 $^{o}$C.

Plate 26A: Photomicrograph of fluid inclusions (1-11) in thomsonite at Tf = -34.7 $^{o}$C.

Plate 26B: Photomicrograph of fluid inclusions (1-11) in thomsonite at Tf = -33.2 $^{o}$C. The temperature was held constant to allow one single large ice-crystal to grow.

Plate 26C: Photomicrograph of fluid inclusions (1-11) in thomsonite at room temperature.

Plate 27A: Photomicrograph of L+V and V+L-type secondary inclusion trails in laumontite at room temperature.

Plate 27B: Photomicrograph of above inclusions at 151.5 $^{o}$C.

Plate 27C: Photomicrograph of above inclusions at 153.6 $^{o}$C. Note the small amount of liquid remaining in the tip of the central inclusion.

LIST OF APPENDICES

# INTRODUCTION

The aim of this thesis is to study the effects of low-grade burial metamorphism in the Palaeozoic rocks of the Midland Valley of Scotland.

This thesis is divided into two parts. Part One, is concerned with the investigation of clay mineral alteration in the Silurian sediments. This has been investigated in the following chapters with reference to:-

1.1 The geological background

1.2 Petrography

1.3 Clay mineralogy

1.4 Illite crystallinity and $b_o$ spacing

1.5 Discussion

This research was undertaken as an adjunct to work in the British Caledonides (Oliver and Leggett, 1980; Oliver *et al*, 1984; Bevins and Rowbotham, 1983; Roberts and Merriman, 1985; Merriman and Roberts, 1985; Thomas, 1986). The main concern was to determine the low grade metamorphic history of the Midland Valley Silurian and to establish whether similarities in the metamorphic style existed between the Southern Uplands and the Midland Valley. The results are of importance to evolutionary models (McKerrow *et al*, 1977; Leggett *et al*, 1979 and 1982, Bluck, 1983 and 1984) for the Scottish Caldeonides, and to the terrane concept (Bluck, 1984).

Part Two of this thesis is concerned with the investigation of

hydrothermal alteration in the Carboniferous Volcanics of the Midland Valley, Scotland. This has been investigated in the following chapters, with reference to:-

2.1 The geological history

2.2 Hydrothermal alteration in Carboniferous Midland Valley lavas

2.3 Petrography

2.4 Mineral chemistry

2.5 Fluid inclusion studies

2.6 Stable isotope studies

2.7 Discussion

This research was undertaken to determine the low grade metamorphic history of the Carboniferous rocks in the Midland Valley and to establish the hydrothermal processes operating during burial in metabasic rocks.

**Geological Setting:** The Midland Valley is a rift basin, the margins of which are defined by the Highland Boundary and Southern Uplands Faults. The area between these faults consists mostly of Devonian and Carboniferous volcanics and sediments. Small inliers of Lower Palaeozoic rocks (Silurian) occupy a linear belt (contained within folded Devonian strata) in the southern Midland Valley. Ordovician sediments occur at Girvan. Silurian sedimentation reflects a change from marine to terrestrial strata. The latter, plus associated calc-alkaline volcanism, characterize the Devonian. The Carboniferous Period is characterized by the accummulation of

alkaline flood basalts in the western Midland Valley, with smaller outcrops of more explosive volcanicity in the east. Sedimentation is characterized by deltaic basins.

The Lower Palaeozoic of the Midland Valley (pre-Upper Devonian) does not show any continuity across the boundary faults. Suggesting that the graben was not in its present position until the Upper Palaeozoic. Consequently, the Lower Palaeozoic of the Midland Valley has been interpreted (Bluck, 1984) as a suspect terrane (see chapter 1.1 for further discussion). The Carboniferous history of the Midland Valley is related to differential movements on the basement structures, associated with the failed opening of the Palaeozoic European Rift System (Francis 1978a, b).

**Diagenesis vs Low Grade Metamorphism:** The PT range to be investigated, covers the gradual transition from diagenesis to low grade metamorphism. Where, diagenesis produces changes near the rock surface under low pressure and low temperature conditions equivalent to those exposed during sedimentation; and where metamorphism records mineralogical changes induced by increased temperatures and pressures in consolidated rocks. Diagenesis therefore transforms loose particles to sediments by compaction and cementation, whilst the original fabric of the rock is maintained. In low grade metamorphism the original fabric of the rock is maintained in hand specimen, whilst changes are recognized in thin section which may be associated with the development of mineral parageneses at precise PTs.

The distinctions likely to be quoted by sedimentologists and metamorphic petrologists regarding the end of diagenesis and the beginning of metamorphism, are quoted below:-

1 For a sedimentologist: Diagenesis stops at a depth in all sedimentary rocks once compaction (and hence fluid expulsion) and cementation stops (Winkler, 1979) ie at a depth at which all interconnecting pore spaces have been sealed. By this definition, in a shaley sequence undergoing alteration the transformation of mixed-layered illite-montmorillonite to illite (resulting in the continuous expulsion of water) must be a process characteristic of diagenesis. However, observation of 'no interconnecting pore spaces in all sedimentary rocks' is a poor criterion on which to base the definition of a metamorphic rock, since channelways may have developed in the sediments after the peak of the metamorphic/diagenetic episode.

2 For a metamorphic petrologist: Diagenesis ends once mineral parageneses are observed which cannot have originated in a sedimentary environment (Winkler, 1979). For example mixed-layered chlorite- montmorillonite, associated with illite-montmorillonite, has not yet been observed as a detrital phase (see chapter 1.5). Consequently chlorite-montmorillonite, and by association illite-montmorillonite, must be metamorphic mineral parageneses.

Since (as evident from above) the last disappearance of interconnecting pore spaces obviously need not coincide with the first appearance of metamorphic mineral parageneses, it would be more adviseable to accept mineralogical criterion rather than physical criterion to define the beginning of metamorphism. However, only certain mineralogical parageneses are suitable for defining the beginning of metamorphism. For example, the assemblage

quartz-calcite may exist from diagenesis through to high grades and is consequently non-definitive. In metabasites Coombs *et al*, (1959) recognized analcime. heulandite and laumontite as the lowest temperature metamorphic minerals. Whilst in metapelites the beginning of metamorphism may be associated with the development of illite-montmorillonite provided that it can be proved to alter to illite with increasing grade.

Throughout this thesis, the prefix 'burial' is only used in connection with those low grade metamorphic rocks where the fact of burial can be reasonable well established.

# PART ONE

# BURIAL METAMORPHISM OF THE SILURIAN INLIERS

**Corrigendum**

The author would like to draw attention to the fact that in Chapter 1.3, the scale bars in figures 1.3.2, 1.3.3 and 1.3.4 have been misplaced by a factor of $0.3^{o}2\theta$ with respect to the diffractogram peaks.

## 1.1 Geological Background

### 1.1.1 Aims

The aim of this chapter is to review the literature on the sedimentological, stratigraphical and structural history of the Silurian inliers as a background to the investigation of burial metamorphism in the Midland Valley.

### 1.1.2 Sedimentology and Stratigraphy

Lower Palaeozoic sediments occupy a linear belt (extending for 120 km) along the southern margin of the Midland Valley. Here, Silurian strata of variable age is exposed in inliers (fig 1.1.1) at:-

i) Girvan - Main Outcrop (nomenclature after Cox and Toghill, 1973).
- Coastal sections of Craigskelly and Woodland Point.

ii) Central Regions - Lesmahagow
Hagshaw
Eastfield
Carmichael

iii) Pentland Hills - North Esk
Loganlee
Bavelaw Castle

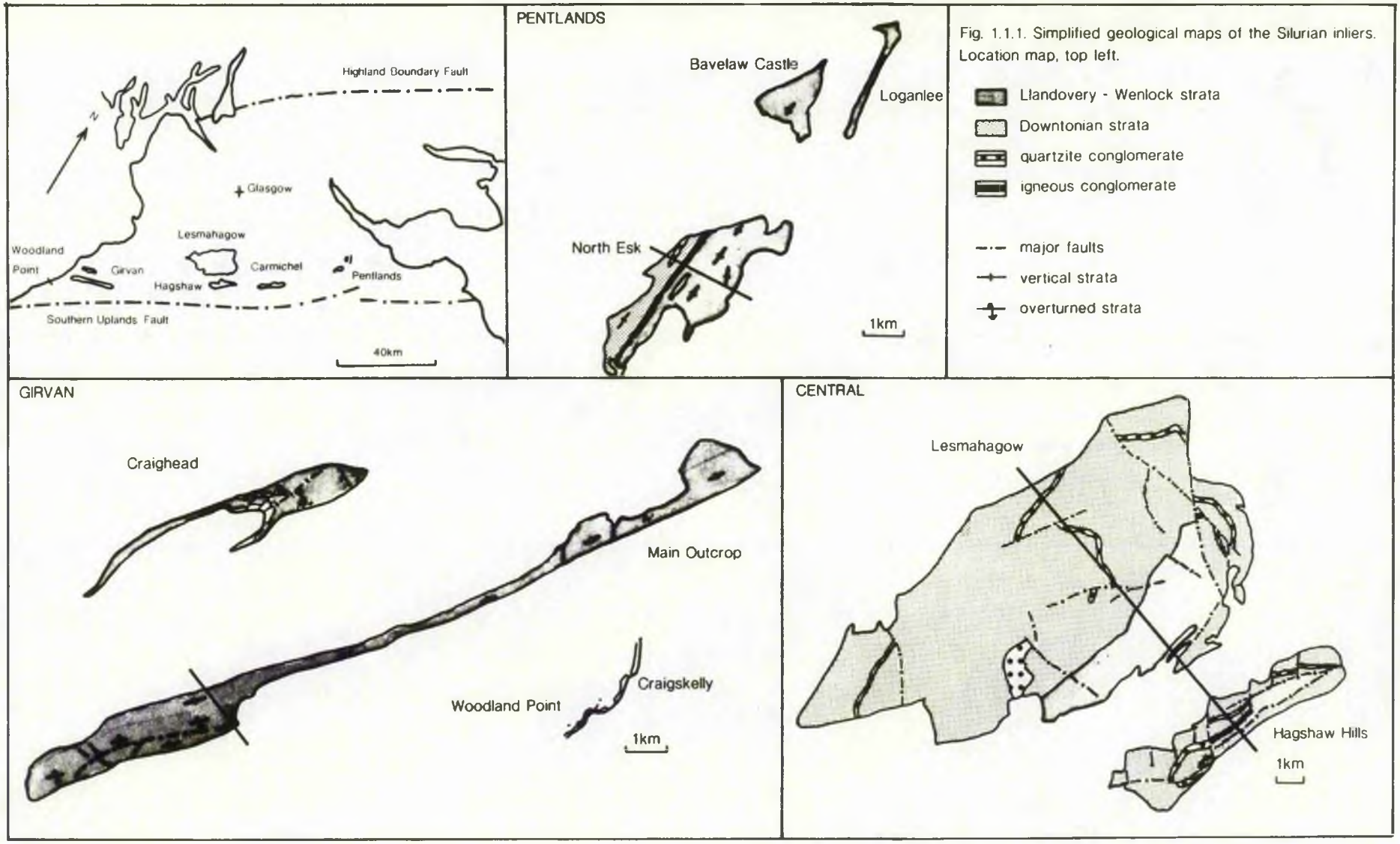


Fig. 1.1.1. Simplified geological maps of the Silurian inliers. Location map, top left.

Each inlier contains a slightly different part of the Silurian succession; a brief account of which is given below. More detailed accounts of the sedimentological, stratigraphical and faunal development of the inliers are given in Pringle (1948); Anderton *et al*, (1979); Walton (1983); and Cameron and Stephenson (1985).

Girvan

At Girvan, the base of the Silurian succession is seen at all three inliers in contact (one of overstep and overlap) with the Ordovician.

The sequence (fig 1.1.2) is characterized by a limited number of lithologies. Sedimentation commenced with the development of the Lady Burn Conglomerate (comprised of ophiolitic detritus) in the Craighead Inlier (in the M. acuminatus zone) and with the Craigskelly Conglomerate on the coast (in the M. cyphus zone). The latter may be compared with the Ordovician Corsewall Point Conglomerate (Longman *et al*, 1979).

The Conglomerates are overlain by fossiliferous sandstones which have a characteristic shelly fauna of corals, polyzoa, brachiopods and trilobites, which testify to shallow marine shelf conditions. These in turn are overlain by a succession of deeper water turbidites, consisting of grey-green mudstones and shales, with occasional graptolitic horizons. From the graptolite bands, initial sedimentation is placed just below the M. cyphus zone (Ruddion); and, the Mid Llandovery (Fronian) unconformity within the M. sedgwickii zone. The graptolites are the equivalent of those seen in the Birkhill Shales of the Southern Uplands.

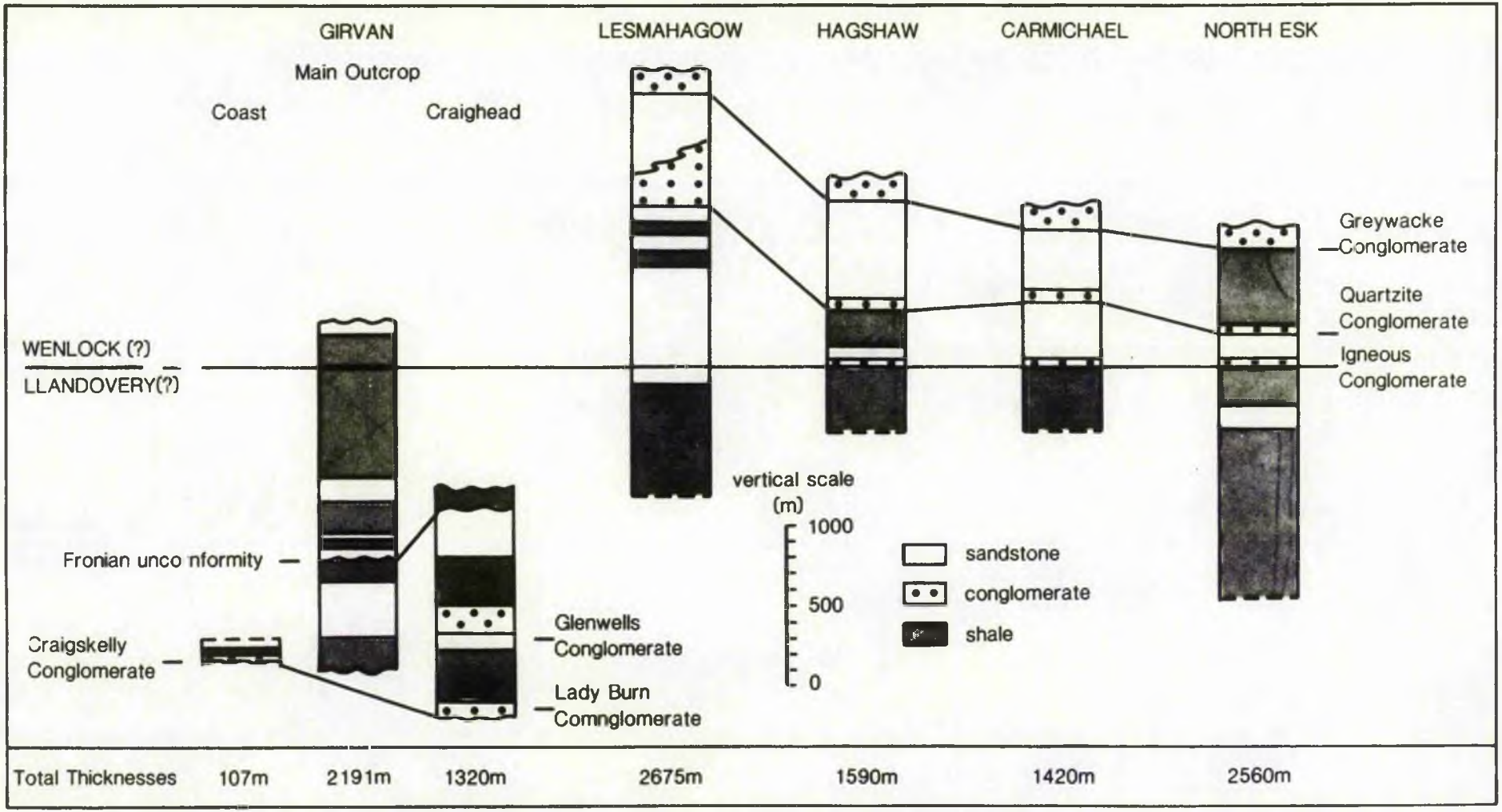


Fig. 1.1.2. Silurian successions in the inliers of the Midland Valley. (modified after, Cocks and Toghill(1973): Cameron and Stephenson(1985) ).

Turbidite sedimentation was punctuated in the M. gregarius zone by the development of the deltaic Quartzite Conglomerate horizon (know locally as the Glenwells Conglomerate - reflecting a change from turbidite deposition to the development of sub-sea fans in the south (Walton, 1983)), and in the M. maximus subzone by the development of red beds.

A marine transgression was responsible for the return to turbiditic and graptolitic deposition. This transgression was expressed in the stratigraphic column (fig 1.1.2) as the Fronian unconformity. A marine regression terminated turbidite deposition and was followed by a return to turbiditic and graptolitic deposition. This was terminated by brackish/fresh-water deposition of the Wenlock Straiton Grits.

Central Regions

The fullest sequence of Silurian sedimentation in the central regions is given by the Lesmahagow inlier. Sedimentation spans from the Llandovery into the Ludlow (Seldon and White, 1983).

The succession begins with a marine turbidite unit (the Kip Burn Formation), bearing bivalve and arthropod horizons. The faunas reflect a change from marine to quasi-marine conditions. A period of sandstone and shale sedimentation characteristic of deltaic/paralic conditions ensued; unfossiliferous except for two fish-bearing horizons.

This regressional theme continued into the Wenlock with the deposition of the deltaic Quartzite Conglomerate and associated fluviatile sediments.

The Hagshaw Hills succession is similar to that at Lesmahagow.

It is composed of a lower turbidite unit (within which brachiopods [Glassia and Howellella] and graptolites [M. vomerinus] indicate an Upper Llandovery age of sedimentation [Rolfe and Fritz, 1966]), and an upper shallow marine horizon.

Unlike Lesmahagow, the junction between marine and quasi-marine conditions is marked by the development of the Igneous Parishholm Conglomerate. Equivalents of which are also found in the Carmichael and Pentland Hills inliers (fig 1.1.2).

The Carmichael inlier records the transition from marine turbidites to red bed facies. The turbidites contain M. crenulata c.f. vars. M. vomerinus, thus placing an Upper Llandovery age upon the rocks and allowing comparison with the Hagshaw Hills inlier.

The Eastfield inlier is composed of unfossiliferous sandstones and is therefore undated.

Pentland Hills

In North Esk, the largest of the inliers, the succession begins with fossiliferous mudstones; containing the brachiopods Craniops and Glassia and the trilobites Acernaspis and Harpidella (Tipper, 1976). Rare graptolites, Koremagraptus and Monoclimacis c.f., M. vomerina, of Upper Llandovery age occur.

A sequence from flaggy greywacke to sandstone and conglomerate (igneous) to red mudstone and sandstone of Wenlock age follows.

Both Bavelaw and Loganlee successions resemble the lowermost mudstones and flaggy sandstones of North Esk. These however, have a more varied Llandoverian fauna.

Summary

Sedimentation, initiated in the lowermost Llandovery, occurred in a distinct Midland Valley basin (Rolfe, 1961).

An early period of southerly and northerly directed turbidite deposition is recognized (Leggett, 1980) in the Girvan inlier alone (post Turriculatus zone, sedimentation was northerly directed; sedimentation commencing without apparent unconformity). Palaeocurrent data is conspicuously absent for the Girvan area. Comparison of the basal conglomerates with the Ordovician conglomerates of the Southern Uplands (Pringle, 1948; Longman *et al*, 1979) and the graptolitic and shelly faunas with those of Moffat (Lapworth, 1882) and Galashiels (Cocks and Toghill, 1973) respectively, tentatively suggests that detritus in Girvan was derived from an Ordovician provenance in the Southern Uplands, comprising early erosion of volcanic rocks and later erosion of greywackes and conglomerate (McGiven, 1968).

Elsewhere a period of northerly directed sedimentation (Rolfe, 1961) characterized by shallow marine sandstones, paralic sediments and red beds, followed turbitite activity at the Llandovery-Wenlock boundary: this marked the beginning of the marine regression in the Midland Valley. In regions east of Girvan, this change was clearly marked by the Igneous (Pentlands), Fence (Carmichael) and Parishholm (Hagshaw) Conglomeratic horizons.

The Igneous Conglomerates thicken eastwards and south-eastwards (Leggett, 1980) towards a likely provenance of oceanic lithosphere exposed in the Southern Uplands (Rolfe, 1961). However, Bluck (1984) strenuously denies a Southern Uplands source, suggesting instead that the igneous conglomerate was derived from an

acid to basic volcanic terrane of basement rocks. By the end of the Llandovery, the Midland Valley trough was palaeogeographically distinct from the Southern Uplands.

Higher in the succession, the Quartzite Conglomerate (thickening pointing to a source at Tinto; Walton, 1983), provides another important marker horizon in a comparatively unfossiliferous sequence.

Similar clast compositions led Walton (1963, 1983) to surmise that both the Igneous and Quartzite Conglomerates had a likely provenance in the Southern Uplands. Longman *et al,* (1979) and Bluck (1984) however, concluded from a study of Ordovician conglomerates at Girvan that the accretionary prism could not have been in its present position during the Silurian and that a more probable source for the Silurian conglomerates would be the underlying crystalline continental basement (a metamorphic basement of predominantly granulite facies rocks, which Upton *et al,* (1984) believe to unconformably underlie the Silurian successions in the Midland Valley). Although, Oliver and McKerrow (1984) commenting on a study of seismic velocities by Hall *et al,* (1983), liken the basement to greenschist facies metagreywackes of accretionary origin. Both Oliver and McKerrow's (1984) and Upton *et al's* (1984) basement concepts could account for similarities in clast content for detritus derived from both northern and southerly sources.

A third Greywacke Conglomerate overlies the sequence in most inliers, derived from sources to the south-east and north-east (Bluck, 1984). Radiometric studies by Thirlwall (1983) indicate that the Conglomerate was of late Silurian age, although floral and faunal evidence (Richardson, 1967; Westoll, 1977) suggests a Devonian age.

### 1.1.3 Structure

Throughout the southern Midland Valley, Silurian strata is preserved in the cores of openly folded Lower Devonian anticlines. The observed variety in the degree and style of folding is attributed to involvement in two orogenic episodes:-

i) Upper Silurian

ii) Mid Devonian

Both episodes display uniform Caledonian trends. Structural cross-sections are presented in figure 1.1.3.

**Upper Silurian Deformation**

Upper Silurian orogeny is expressed in the Girvan and Pentland inliers. Deformation in the Pentlands is characterized by steeply dipping, structurally simple, asymmetric folds which are overturned to the southeast (Tipper, 1976; Rolfe, 1961). At Girvan (Main outcrop and coastal exposures), steeply dipping isoclinal folds are overturned to the north-west (south of Girvan) and to the south-east (north of Girvan) (Rolfe & Fritz, 1966). Williams (1959), recognized five pre-Devonian fold phases. In the Midland Valley $D_1$ is characterized by isoclinal folds and thrusts, whilst kink-bands are associated with $D_2$. These phases are prevalent in the Southern Uplands, and are developed in association with cleavage in $D_1$ and with monoclines in $D_2$ (McKerrow *et al*, 1977). Although the style of deformation in Girvan is similar to that of the Southern Uplands, progressive and diachronous deformation of the style postulated for the latter (Walton 1983) ie the development of high angle strike,

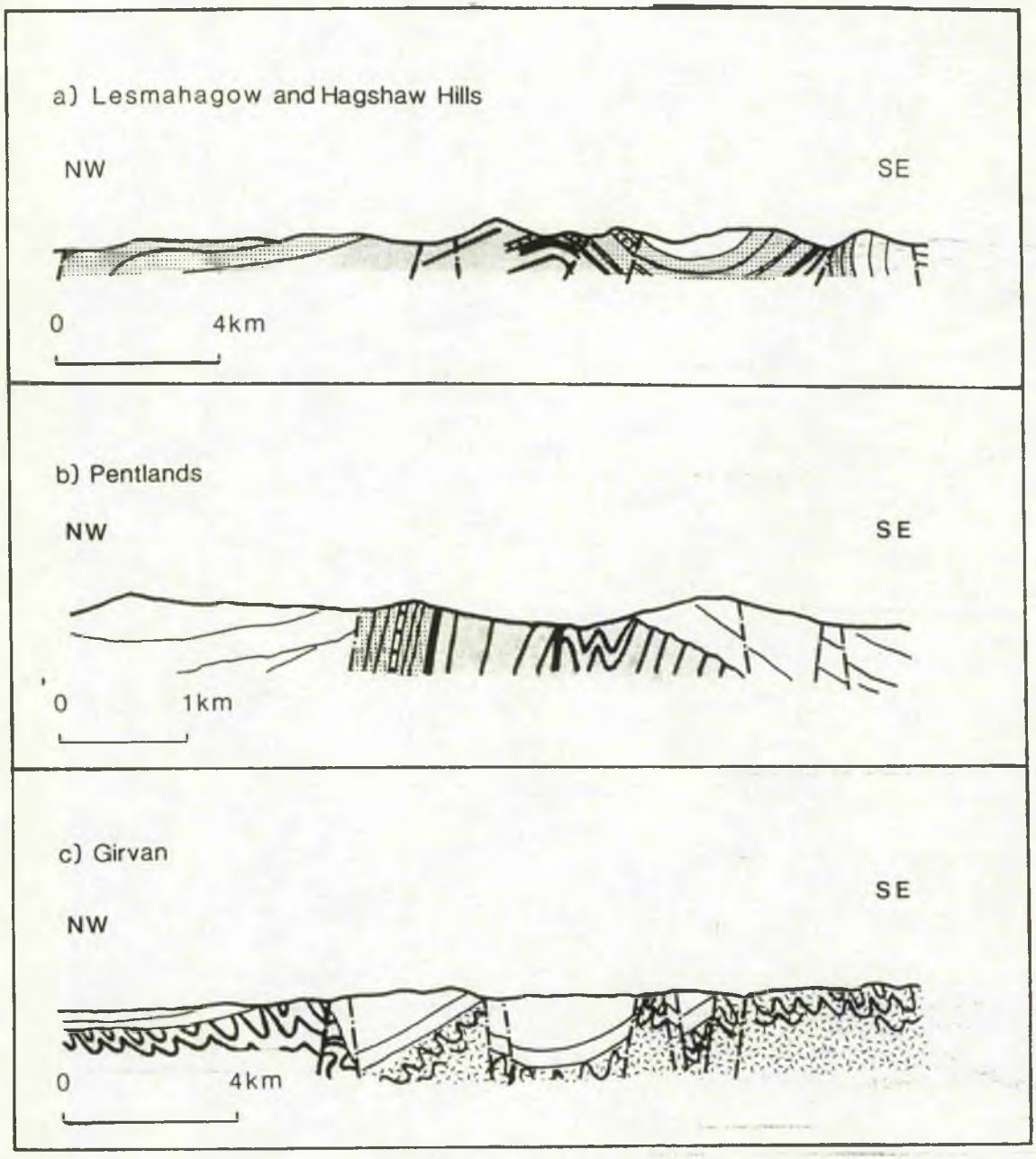


Fig. 1.3.1. Cross-sections through the Midland Valley Silurian. Key Llandovery & Wenlock strata Downtonian strata Ordovician strata Devonian strata quartzite conglomerate igneous conglomerate intrusions —·— major faults

wrench and normal faults associated with rotation, does not affect the Girvan area. These features, coupled with the decreased development of cleavage northwards from the Southern Uplands and with the lack of cleavage in the Midland Valley, are consistent with a decrease in tectonic activity from the south. Consequently the structural style developed in the Midland Valley differs from that seen in the Southern Uplands.

**Mid Devonian Deformation**

Deformation developed in the Mid Devonian, folding Lower Devonian and Silurian strata. Upper Devonian strata overlies the sequence with unconformity on the Lower Devonian (Walton, 1983).

Deformation is characterized by broad open folds in Lesmahagow (pericline, elongated to the north-east; steeper south-eastern limb) and in the Hagshaw Hills (asymmetric anticline; steeper south-eastern limb overturned by reverse fault). At Girvan, the Craighead inlier forms a simple open anticline, plunging to the north-east. Whilst in the Main Outcrop, Devonian deformation is characterized by three north-east to south-west trending fault phases (Williams, 1959).

### 1.1.4 Terrane Concepts for the Midland Valley Silurian

The Midland Valley is essentially a fault-bounded block, disposed between areas of contrasting lithology. Sedimentation across the Highland Boundary Fault is evident in the Cambro-Ordovician sequences of Dunnottar (near Stonehaven, where Dalradian clasts occur in the Segannan sediments) and from the Lower Devonian onwards. Suggesting that a major structural and sedimentological discontinuity existed between the Midland Valley and

the Scottish Highlands in Silurian times. Movement on the bounding faults was essentially associated with rifting in the Carboniferous (see chapter 2.1). Prior to this Lambert and McKerrow (1976) found evidence for lateral movement on the faults. Whilst Bluck (1984) indicates that the Midland Valley could not have lain adjacent to the present Scottish Highlands until the Lower Devonian. To the south of the Midland Valley lies the allochthonous Southern Uplands accretionary prism. According to Bluck (1984) the Southern Uplands did not provide detritus for the Midland Valley in the Silurian, rather a volcanic arc presently buried beneath the Southern Uplands provided the detritus. It appears that the southern margin may also have been divorced from the Midland Valley during the Silurian. In this respect, the Midland Valley may have been a suspect terrane (Bluck, 1984) during the Lower Palaeozoic.

Within this terrane, a variety of explanations have been presented to account for the differences in deformational and sedimentological histories between each inlier and between the inliers and the main trough in the Southern Uplands:-

1 McKerrow *et al*, (1977) and Leggett *et al*, (1979) proposed that the Midland Valley inliers represented individual upper slope basins.

2 Leggett *et al*, (1982) proposed that the Midland Valley sediments represent a fore-arc dividing the Highlands (arc-basement) from the Southern Uplands (trench-accretionary prism).

3 Bluck (1983) proposed that the Midland Valley Silurian collected in an inter-arc basin. Following the interpretation

of the Ordovician sequence stratigraphically above the Ballantrae Complex at Girvan as having formed in proximal fore-arc basin.

4 Bluck (1984) also proposed that the Midland Valley Silurian may have suffered latteral displacement, since the geological history of the Midland Valley cannot be reconciled with it lying adjacent to the Dalradian during all of the Lower Palaezoic.

Since:- i) During the time of maximum Dalradian uplift (c450 Ma), no detritus with a provenance in local Dalradian-type terrains has been found.

ii) During the mid-Devonian, regions north of the Highland Boundary Fault experienced widespread sedimentation whilst uplift occurred in the Midland Valley.

iii) Movement which juxtaposed the Midland Valley and the Scottish Highlands produced little sedimentation. The relationship is presently a thrust contact. Large scale thrusting would have produced substantial thicknesses of sediment.

All the above concepts appear to require a displacement of the elements of a destructive margin (ie of the trench, fore-arc and arc), without disrupting the sequence of tectonic units.

### 1.1.6 Conclusions

Sedimentary, stratigraphical and structural evidence indicates that the Silurian inliers formed geographically distinct areas, which have been interpreted (in Walton, 1983) as inter-arc (Bluck, 1984), fore-arc (Leggett *et al*, 1982) and/or upper slope basins (McKerrow *et al*, 1977 and Leggett *et al*, 1979). Despite tentative links between the Girvan region and Moffat, geological evidence indicates that the Silurian of the Midland Valley developed in a separate terrane distinct from the Southern Uplands.

## 1.2 Petrography

### 1.2.1 Aims

1 To determine thin-section characteristics associated with diagenesis

2 To determine authigenic sheet silicate structures with the aid of scanning electron microscopy (SEM)

### 1.2.2 Thin-section examination

A representative selection of wackes and marine sandstones from the Midland Valley have been examined. Localities are given on fig 1.3.1.

The marine sandstones are dominated by angular quartz clasts with subordinate acid igneous and feldspar clasts, set in a matrix of haematite, illite(?) (plate 1a), and chlorite.

Wackes typically consist of mineral (quartz, feldspar, muscovite, biotite, chlorite) and lithic clasts (quartzite; igneous-trachytes and pyroxene-bearing hypabyassal rocks) set in a matrix of clays and calcite.

In coarse wacke bands, clasts are often enclosed in calcite cement. Finer bands typically show a preferred orientation of detrital minerals parallel to bedding (plate 1b). This is believed to be a sedimentary lamination rather than a metamorphic foliation, since the more resistant quartz and feldspar clasts are seemingly devoid of authigenic overgrowths and display either concavo-convex, point or long contacts. None of these features are representative of appreciable compaction.

The wacke and sandstone mineralogy of detrital quartz,

Plate 1A: Photomicrograph of early calcite (cc) cemented wacke. Key qt - quartz; dmi - detrital mica. l - point contacts.

Plate 1B: Photomicrograph showing preferred orientation of detrital micas parallel to bedding.

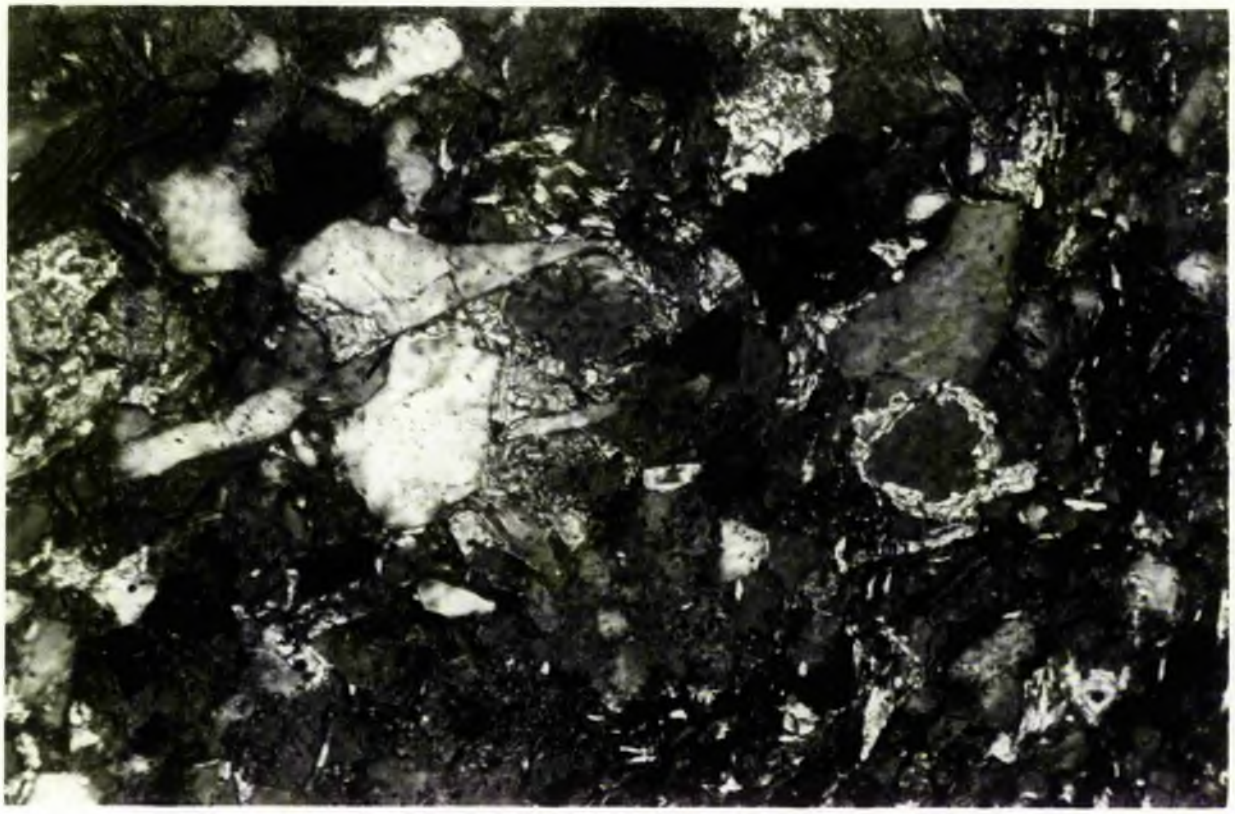

50μ

50μ

feldspar, calcite and white mica has been confirmed by X-ray diffraction and by scanning electron microscopy (SEM). In addition a matrix of clay minerals has been identified (see Chapter 1.3).

It is evident from the textural relationships of the clasts and from the non-development of pressure-solution seams, that the sediments cannot have been significantly compacted prior to lithification. Interestingly, the rocks (excluding those of Girvan Main Outcrop), clearly turbiditic wackes in the field, have a matrix component of 10% or less. This contrasts markedly with the Southern Uplands, where a matrix content in excess of 10% was interpreted by Oliver and Leggett (1980) to reflect metamorphic/diagenetic recrystallization. According to them, the unstable minerals in the Southern Uplands sediments have reacted to form the excess matrix component. At Girvan Main Outcrop, a similar increase in the matrix component is observed.

In the majority of greywacke thin-sections, clasts are cement (calcite) supported. This phenomenon (see below) could be attributed to overpressuring/montmorillonite dehydration (Powers, 1967), where water enriched in $Ca^{2+}$ and depleted in $Mg^{2+}$, is given off to pores during the burial reaction of montmorillonite to illite (at 2.5 to 5 km depth - Leeder, 1982). Velde (1977) establishes that $K^{+}$ fixation would have been an essential part of the reaction. The distinct absence of authigenic feldspar observed during SEM investigations (see section 1.2.3) suggests that the dissolution of feldspars may have been a probable source of $K^{+}$.

Plate 2A: Scanning electron photomicrograph of pitted detrital quartz grain (qt), coated with illite wiskers (i). Residual pore spaces infilled with montmorillonite plates (m).

Plate 2B: Scanning electron photomicrograph of neo-formed pyramidal quartz overgrowths.

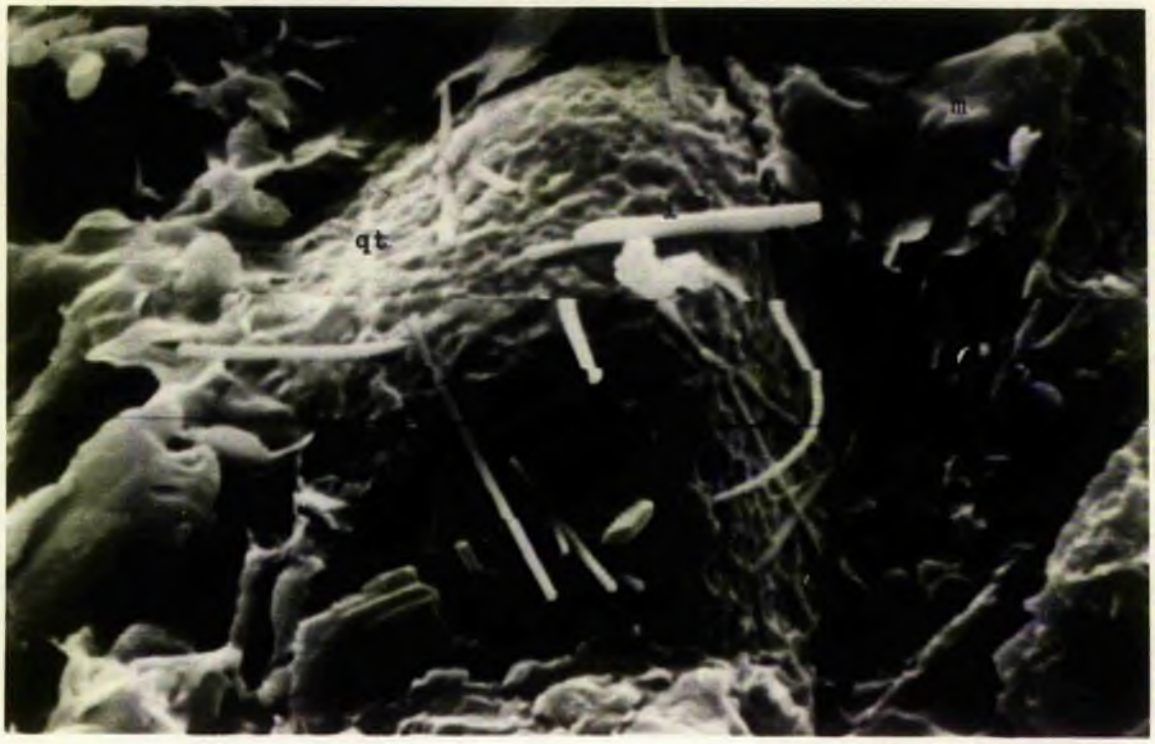


4μ

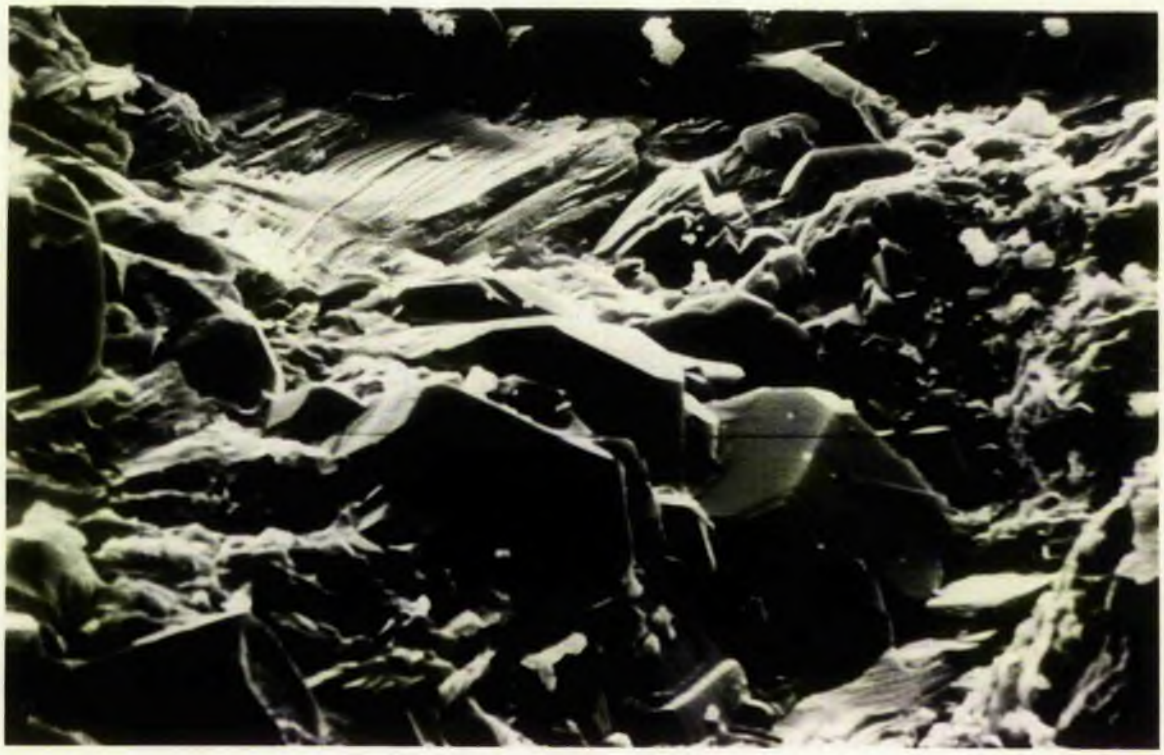

20μ

**Summary**

Thin-section analyses show that the coarse wacke bands and the shales have suffered variable amounts of compaction. In the shale bands, compaction would have reduced porosity and caused fluid expulsion whilst in the greywackes textural evidence indicates that compaction was hindered by early cementation/lithification. Cements may have been derived from those fluids expelled from the underlying shales.

Because of early lithification, zones of under-compacted sediments may have existed at depth. Such zones are often over-pressured as a result of either:-

i) the expansion of water in a closed space upon heating (Velde, 1977) or

ii) montmorillonite dehydration liberating excess water (Powers, 1967)

This concept is consistent with the conclusions of Magara (1975), who noticed that during the burial of mudrocks there was a tendency for water expulsion to lag behind burial transformations.

### 1.2.3 SEM examination

From thin-section examination, clay minerals appear to be an integral part of the matrix. To be of use in low grade metamorphic studies the authigenic nature of the clay minerals has to be established. This was determined with the use of the scanning electron microscope. The recognition of phases was made by comparison with photomicrographs from Welton (1984), Wilson and

Plate 3A: Scanning electron photomicrograph of residual pore space, infilled with boxwork montmorillonite (top left) and with illite plates (bottom centre).

Plate 3B: Scanning electron photomicrograph of authigenic illite plates (i) coating a detrital grain. Feldspar clast, top centre. Top left, honeycomb chlorite infills pore space.

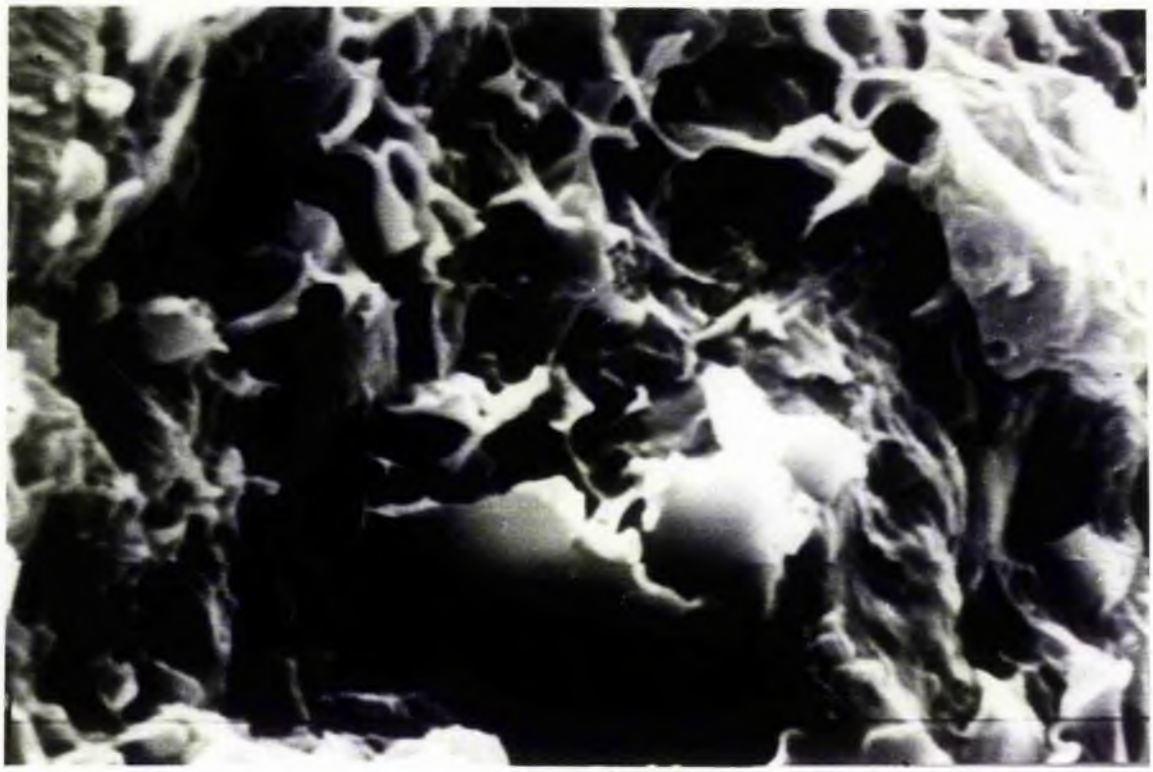

4μ

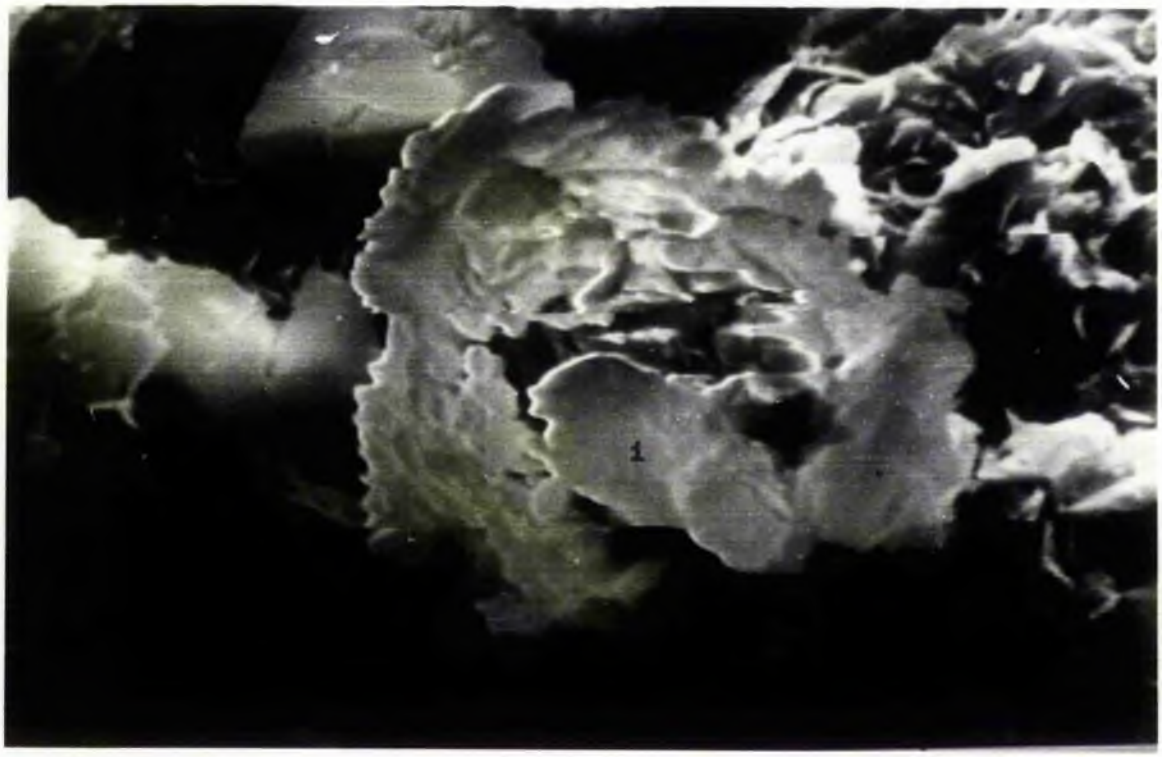


4μ

Pittman (1977) and Scholle (1979).

**Method**

Rock chips were mounted on aluminium specimen stubs. To aid conduction, grain and stub contacts were coated with silver paint. The stubs were placed in a SEM coating unit and sputter coated with 40-50 μm of gold.

The rock chips were examined on a Cambridge Scanning Electron Microscope, housed in the Gatty Marine Laboratory.

**Results**

**Quartz**

The majority of quartz grains examined were of detrital origin. Individual grains are characteristically well-rounded (plate 2a) and have pitted and etched surfaces.

Occasional neo-formed quartz (plate 2b) occurs as over-growths on detrital grains. These form euhedral pyrimidal crystals.

**Montmorillonite**

Authigenic montmorillonite is seen to form a meshwork structure (plate 3a) infilling pore spaces. The structure is similar to the honeycombe structure of chlorite (plate 3b). Montmorillonite may be distinguished from chlorite by its highly crenulated surfaces and by its inability to form crystalline laths.

**Mixed-layer Illite-Montmorillonite (I-M)**

Mixed-layer illite-montmorillonite (I-M) develops the characteristics of both illite and montmorillonite and may resemble

Plate 4A: Scanning electron photomicrograph of illite whiskers (i) forming a lattice work across a pitted detrital quartz grain.

Plate 4B: Scanning electron photomicrograph of illite whiskers (i) growing in pore space. Top left, montmorillonite (m) forms primary pore lining. Bottom right, pitted detrital quartz grain (qtz).


A

10μ

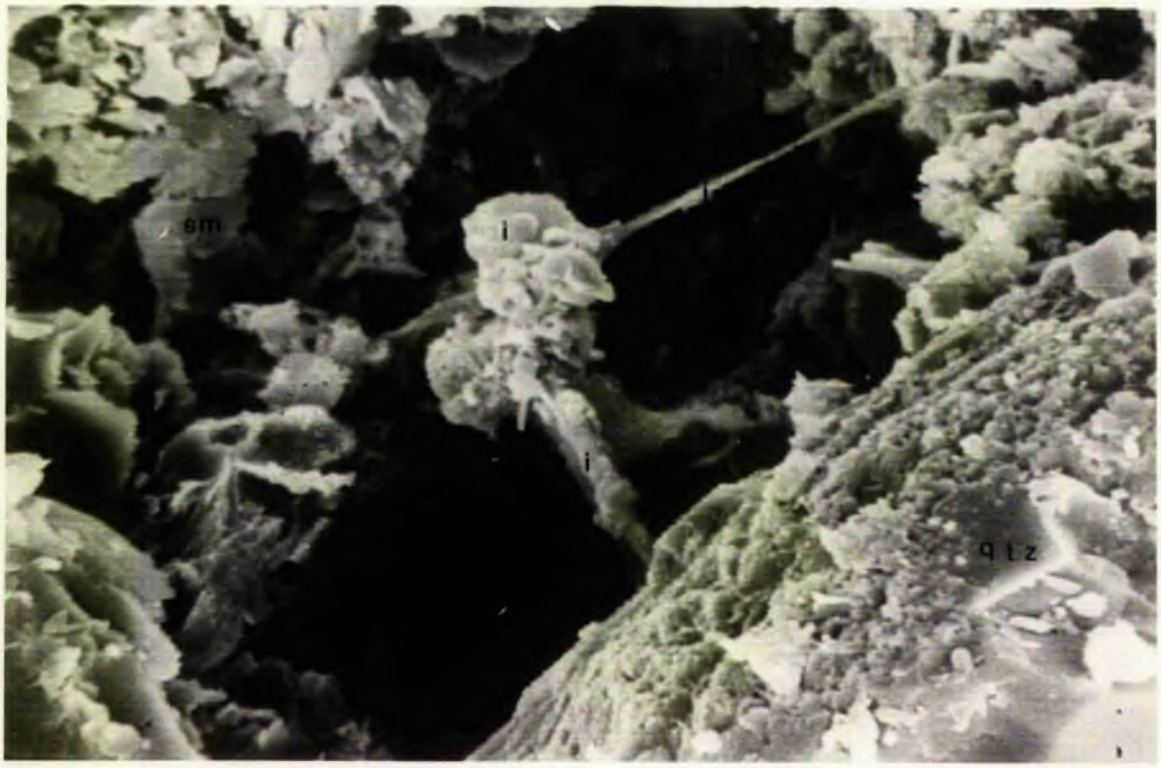


B

10μ

one more than the other depending upon the illite: montmorillonite ratio. I-M typically forms crenulated sheets (plate 3a) with convoluted edges.

Since it is often difficult to distinguish the convoluted edges of I-M from the wispy projections of illite plates, X-ray diffraction was always used to confirm the identification of phases (see chapter 1.3).

Illite

Illite occurs in two morphological forms. The commonest of these are authigenic plates that curl away from their point of attachment. These plates are characterized by short stubby projections at crystal edges (plate 3b). The second type are fine lath-like projections or whiskers that either coat grains (plate 4a) or infill pore spaces (plate 4b).

Chlorite

Two chlorite crystal habits have been recognized, ie honeycomb structure and chlorite rosettes. The honeycomb structure (plate 3b) consists of chlorite plates which display face to face and face to edge contacts. This is the main pore-filling structure.

Chlorite rosettes (plate 5a, b) consist of stacks of lobate edged plates.

Authigenic feldspar was not observed.

Plate 5A: Scanning electron photomicrograph of chlorite (chl) rosettes; individual stacks consist of lobate-edged chlorite plates.

Plate 5B: Scanning electron photomicrograph of chlorite (chl) rosette growing into pore space. Top right, detrital mica plates.

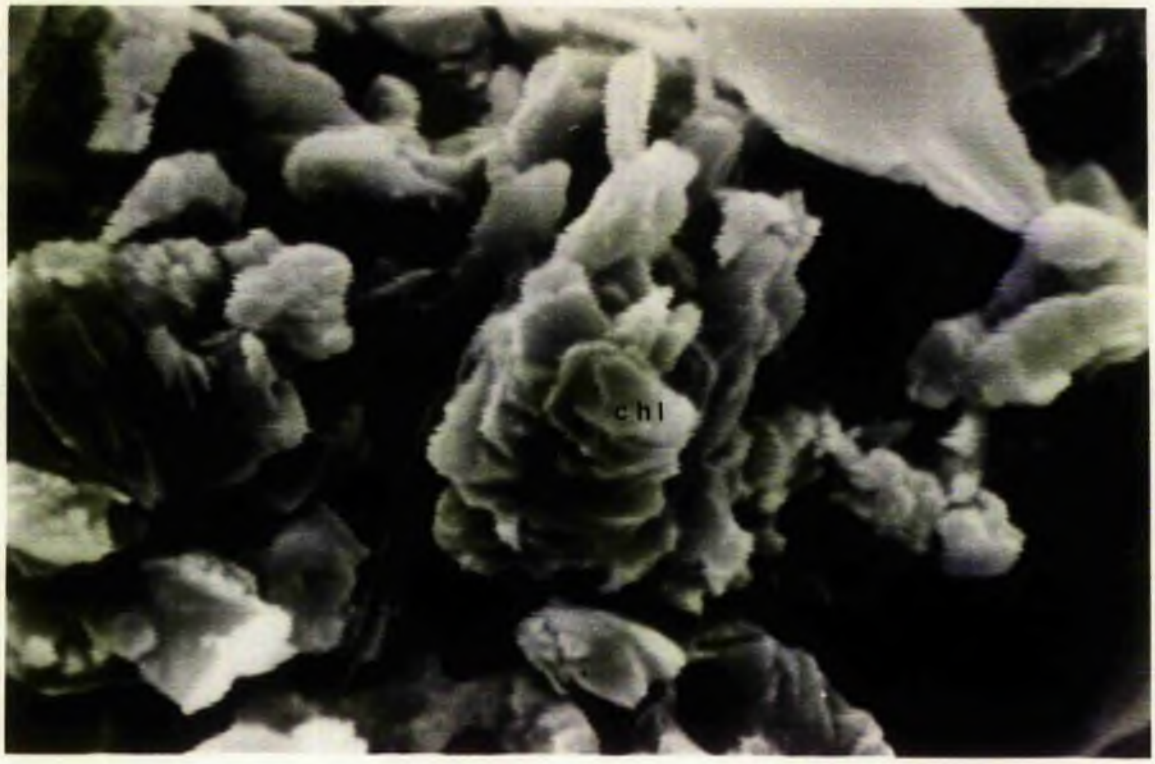


5A

4 μ

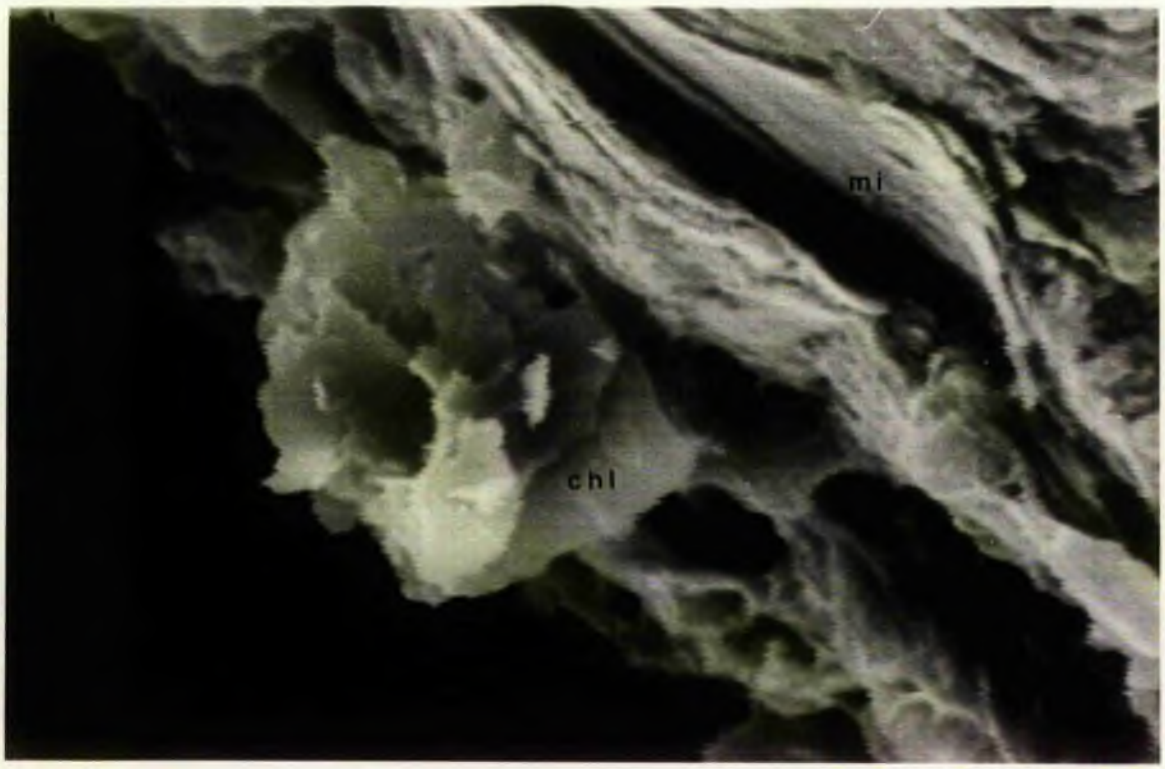


5 B

4 μ

**Summary**

Scanning electron micrographs show that the clays are clearly authigenic, since they are all seen to coat pitted and etched detrital grains and to infill pore spaces. Furthermore, the delicate habit of chlorite rosettes (plate 5a, b) and of illite whiskers (plate 4a, b) in particular,precludes transport of the grains as detrital minerals.

The authigenic clays (plus authigenic quartz) are seldom found together in association. Instead, two broad assemblages may be resolved, characterized by:-

GROUP 1: authigenic quartz, illite, honeycomb chlorite ± illite-montmorillonite

GROUP 2: montmorillonite, mixed-layer illite-montmorillonite, chlorite rosettes

Group 1 minerals are characteristically developed in the Girvan Main Outcrop and at the coastal exposures of Woodland Point and Craigskelly. Representative minerals of Group 2 are to be found in the Craighead, Central and Pentland inliers.

1.2.4 Conclusions

1. Thin-section examination has established that Silurian greywackes in the Midland Valley have suffered little or no compaction. Cementation was early and was associated with over-pressuring. This resulted in the transformation of montmorillonite to illite and in the generation of an excess matrix component in regions of enhanced burial metamorphism/diagenetic recrystallization.

2. Scanning electron microscopy has indicated the presence of low grade metamorphic phases. The distribution of two distinct groups and the association of illite plus quartz with rocks of a higher matrix content, apparently confirms that the burial metamorphic reaction, involving the conversion of montmorillonite to illite plus quartz, occurred.

The petrogenetic significance of these results will be discussed in Chapter 1.5.

## 1.3 Clay Mineralogy

### 1.3.1 Aims

To confirm SEM clay mineral identifications with the aid of X-ray diffraction techniques.

### 1.3.2 Introduction

Samples for analyses were collected at 500 m and 1 km intervals along northerly directed traverses from pelitic, greywacke, arenaceous and conglomeratic horizons, at the localities shown on figure 1.3.1.

Mineral determinations were made by X-ray identification of centrifugally separated 2 $\mu$ fractions of whole-rock powder (see 1.3.3). To aid the qualitative analyses of the clay minerals, diffractograms were obtained of:-

i) air-dried samples
ii) glycolated samples
iii) heated samples (at 600 $^{o}$C)
iv) acid treated samples (HCl heated to 80 $^{o}$C)
v) dimetholsulphoxide (DMSO) treated samples
vi) cation saturated samples

Details of preparations are given below. Sample lists and treatments are given in Appendix 1.3.1.

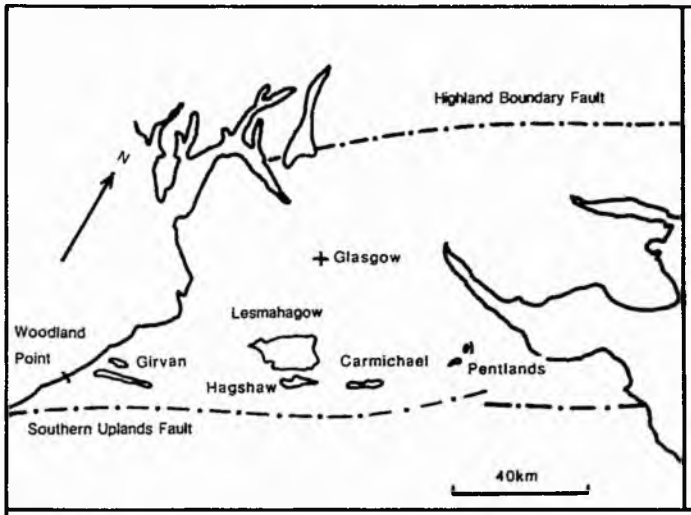


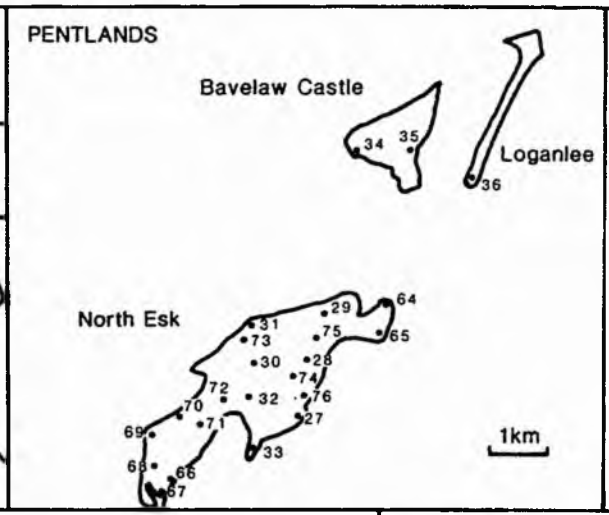


Fig. 1.3.1.

Sample localities in the Midland Valley Silurian.

- • localities
- —·— major faults

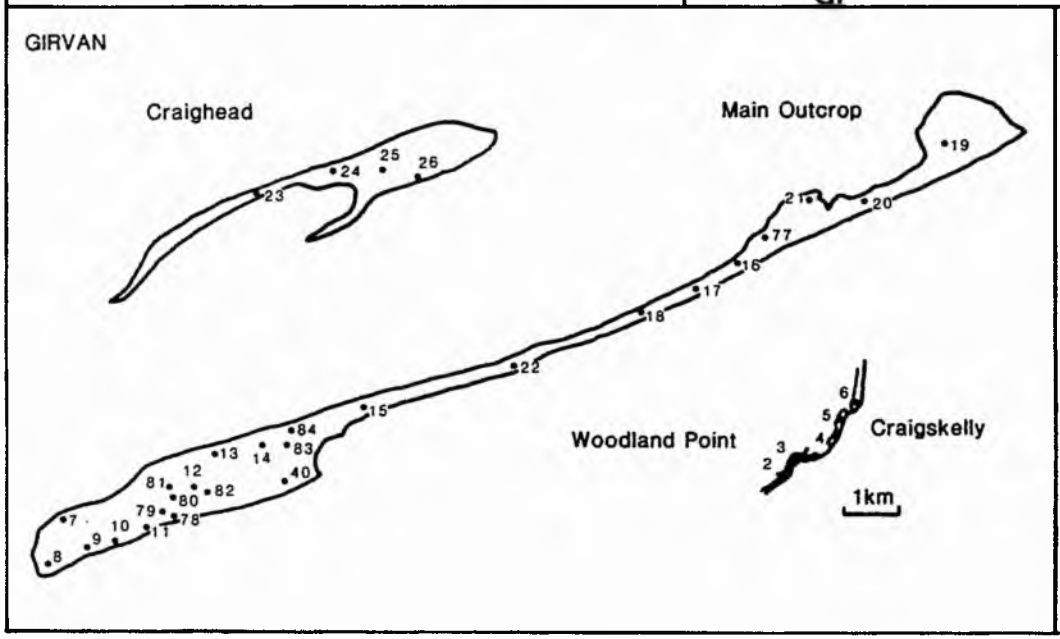


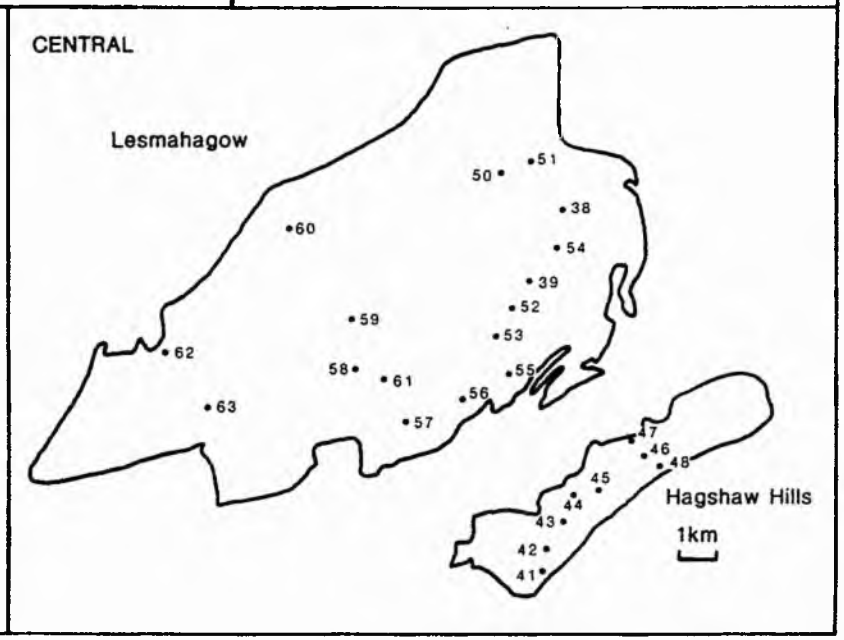

### 1.3.3 Qualitative Clay Mineral Analyses

#### Sample Preparation

All samples were stripped of weathered surfaces, and were dry-crushed for 10 seconds in a Tema mill. Water was mixed with a portion of the whole-rock powder of each sample. The slurries were placed in an ultrasonic bath for 20 min to facilitate particle disaggregation; D. Robinson (pers. comm.) recommends submersion for several hours rather than several minutes. The resulting mixture centrifuged, firstly for 40 seconds at setting 5, and then for 40 seconds at setting 7. The setting and timing of separations was determined by Thomas (1986). The objective was to obtain a good clay separate of $<2\mu$ grain size, relatively free of quartz, feldspar and detrital mica that may have been reduced to clay-size fractions during crushing. A. Kemp (pers. comm.) has confirmed the $<2\mu$ grain size of this separate using scanning electron microscopy. The resulting slurries were sedimented onto roughened glass-slides and allowed to dry. Sedimentation onto roughened slides enabled an orientated array of flakes to be produced, thereby, enhancing the intensity ratios of the basal reflections (Niskanen, 1964) (of value for the determination of illite crystallinity), whilst enabling identification of a particular species by its d-spacing.

#### X-ray Diffraction

Throughout this study, a Phillips PW 1394 vertical goniometer fitted with a monochromator was used under the following machine conditions:-

| | |
|---|---|
| Nickel filtered CuK $\alpha$ radiation | |
| Current | 36 kV at 18 mA |
| $2^{o}$ | Scatter slit |
| $1^{o}$, $1/6^{o}$ | divergence silts |
| $0.2^{o}$ | receiving slit |
| Ratemeter | 1 x $10^{2}$ c.p.s or 1 x $10^{3}$ c.p.s. |
| Time constant | 4 |
| Scanning speed | $1^{o}$ per $2\theta$ per min. |
| Chart speed | 1 cm per min. |

Diffractograms were run between 3-$65^{o}$ $2\theta$ and between 3-$30^{o}$ $2\theta$. D. Robinson (pers. comm.) recommends the use of a $4^{o}$ divergence slit for $b_o$ analysis.

Identification of discrete clay species was hindered by the presence of overlapping peaks due to similarities in the d-spacing of the minerals. The samples were therefore subjected to a series of analytical treatments.

**Glycolation**

Glycolation (MacEwan, 1944; Walker, 1949) is a simple method to test for the presence of mixed-layer expandable minerals. It is not to be regarded as the sole means of distinguishing between vermiculite and smectites (see Grim and Kulbichi, 1961).

Untreated slides were placed in a dessicator containing ethylene-glycol and heated to a temperature of 60 $^{o}$C for one hour. A diffractogram of the glycolated samples was run between 3-30 $^{o}$ $2\theta$ under the aforementioned conditions.

Heat treatment

Dehydration of different clay species occurs at specific temperature intervals (Thorez, 1976). Premounted, glycolated samples were subjected to heating for one hour in a furnace at:-

a) 100 $^{o}$C (Grim and Kulbichi, 1961) to test for mixed-layer minerals (Weiss and Rowlands, 1956; Hower and Mowatt, 1966).
b) 600 $^{o}$C (Grim and Bradley, 1951; Weaver, 1956), to test for kaolinite and chlorite.

Acid treatment

Dissolution methods were applied to clay-bearing samples to:-

a) remove contaminants eg carbonate and organic matter.
b) to test for the presence of chlorite (Kodama and Oinumai, 1963). Chlorite was soluble under the following circumstances:-

A quantity of dry whole-rock powder was placed in a 50 ml flask with some (2N) HCl and was left to boil on a stove, maintaining a temperature of 80 $^{o}$C, for eight hours. The samples were washed in distilled water and the clay fraction removed and prepared for analysis in the usual fashion.

DMSO treatment

Treatment of samples in dimetholsulphoxide (DMSO) is a positive test for kaolinite (Garcia and Camazano, 1968).

A portion of the 2 $\mu$ powder (pre-treated with heated hydrochloric acid) was refluxed in 50 ml of DMSO at 180 $^{o}$C for approximately 70 hours. Samples were washed clean in distilled water

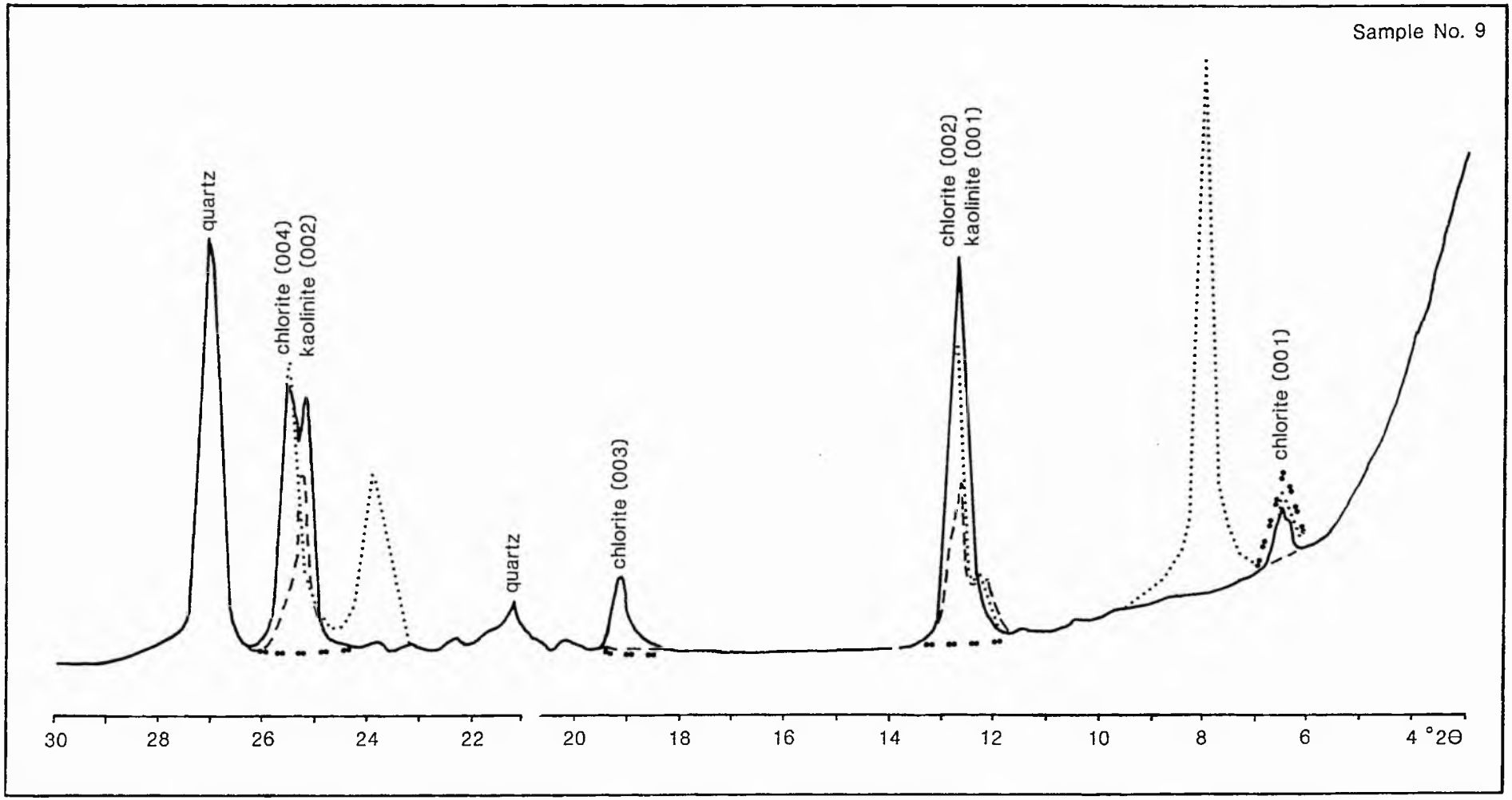


Fig. 1.3.2. Diffractograms of chlorite and kaolinite from the Midland Valley Silurian. Traces of, —— untreated and ethylene-glycolated sample, ····· DMSO treated sample, - - heated sample, – – HCl treated sample.

and prepared for analyses.

Cation-saturation

Clay samples may be saturated with either:-

a) potassium: enabling differentiation between varieties of smectite (results must be interpreted with great caution when distinguishing between smectites derived from different parental materials).

b) magnesium: separates the smectites in general from the vermiculites.

In this study Mg-saturation was used. Samples were saturated with (1N) Mg $Cl_2$ (Grim and Kulbichi, 1961) and then washed in distilled water until free of chloride. A portion of the 2 $\mu$ slurry was sedimented onto roughened glass slides and dried in a stove at 100 $^{o}$C for two hours. All samples were glycolated (Kisch, 1980a) and a diffractogram run under the usual machine conditions.

1.3.4 Results

1 Clay Minerals - Pure Species

Kaolinite

Kaolinite may be recognized by its (001) and (002) reflections at 7 Å and 3.5 Å respectively; which collapse upon heating at 600 $^{o}$C (Fig 1.3.2).

Due to the overlap of kaolinite (001) and (002) reflections with chlorite (002) and (004) in mechanical mixtures of sediment, a

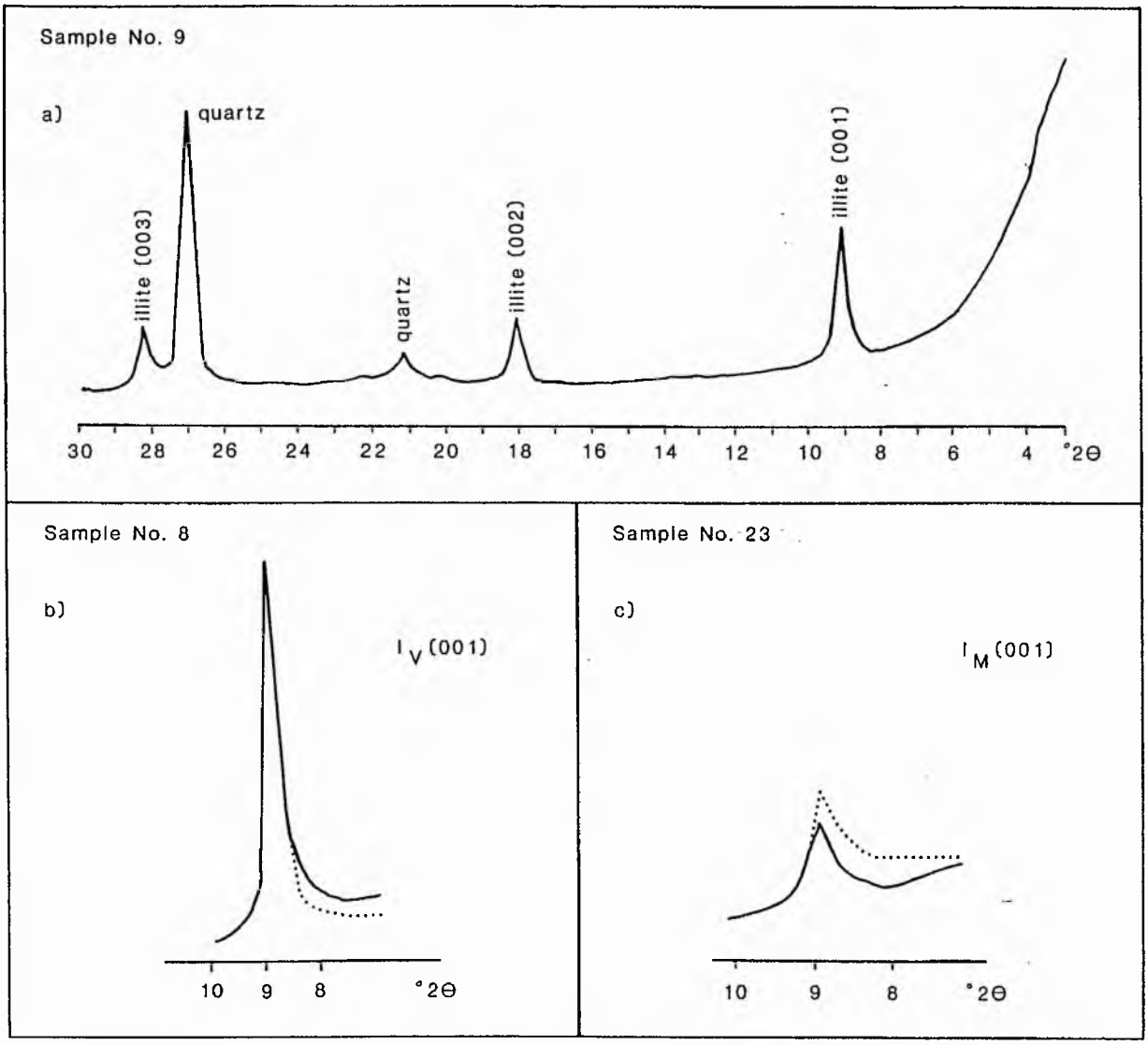


Fig. 1.3.3. Diffractograms of illite from the Midland Valley Silurian. a) illite proper b) illite with vermiculite behaviour c) illite with montmorillonite behaviour. Traces of, —— untreated samples, .....ethylene - glycolated samples. after Thorez 1976

slower scanning speed (Biscaye, 1964) or treatment with DMSO (Garcia and Camazano, 1968) may be used to resolve the reflections. As a result of DMSO treatment, the kaolinite (001) basal reflection at 7.15 Å moves to a new position at 11.18 Å, and 3.56 Å reflection to 7.15 Å; a new peak appears at 3.63 Å (Fig 1.3.2).

Chlorite

Chlorite was determined by its strong (002) and (004) reflections at 7.2 Å and at 3.6 Å, and by its weaker (001) and (003) reflections at 14.2 Å and at 4.7 Å respectively. Upon acid treatment the latter reflections were completely removed from the diffractogram (Kodama and Oinumai, 1963). Heat treatment at 600 °C (Grim and Bradley, 1951) succeeded in the removal of all, except the (001), peaks from the diffractogram (Fig 1.3.2).

Illite

Illite is characterized by its strong (001) basal reflection at 10 Å, which remains stable after heating (100 °C) and glycolation (Fig 1.3.3).

Some reflections show a slight asymmetry towards the low angle. Upon glycolation the apex of these minerals remains at 10 Å, whilst the shoulders are seen to expand or contract. These two varieties of illite are known as illite with montmorillonite behaviour ($I_M$) and as illite with vermiculite behaviour ($I_V$). They are not to be confused with illite-mixed-layer minerals, which develop their own characteristic pattern of d-spacings.

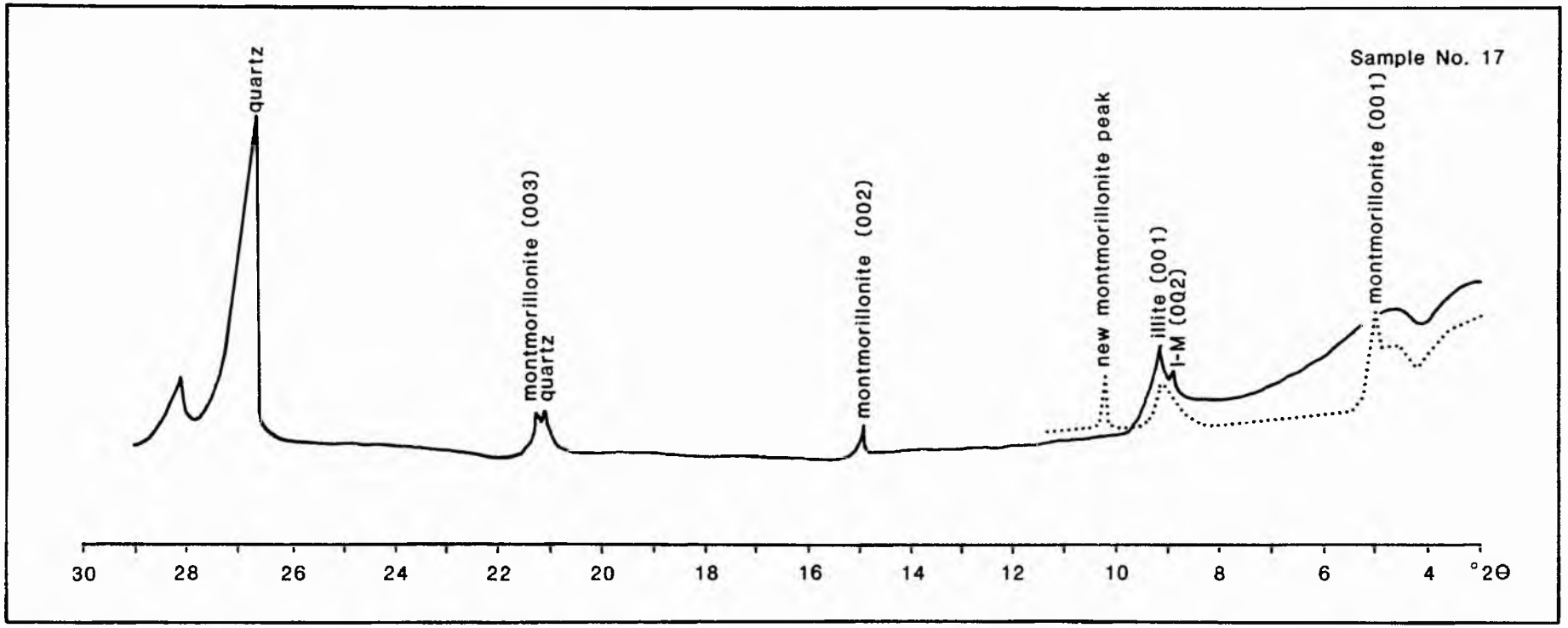


Fig. 1.3.4. Diffractograms of montmorillonite from the Midland Valley Silurian. Traces of,—— untreated sample,····· ethylene-glycolated cation-saturated sample.

### Montmorillonite

Montmorillonite is characterized by its 14 Å (001) reflection (Fig 1.3.4), which remains expandable even after heat (100 °C) and acid treatment (Martin-Vivaldi and Gallego, 1961).

Distinctive tests are glycolation (montmorillonite expanding towards the low angle) and cation-saturation (Grim and Kulbichi, 1961). Upon cation-saturation, montmorillonite remains expandable; the 10 Å illite peak is accompanied by a new montmorillonite peak at 8.99 Å, and the (001) montmorillonite peak shifts from 14 Å to 17.7 Å.

The behaviour of kaolinite, illite, chlorite, and montmorillonite in response to the treatments undertaken, have been summarized in Table 1.3.1. Where no indication of the effects has been given, the reflections are taken to be the same as for untreated air-dried samples.

A comprehensive list of the clay minerals discussed (including pure species and regularly and randomly interstratified) is given in appendix 1.3.2.

## 2 Interstratified/Mixed-layer Clay Minerals

### Introduction

In addition to the pure clay minerals described, interstratified species also occur. These consist of bi-mineralic mixtures of pure clays (regularly ordered).

The type of layers involved in the interstratifications can be determined from the treatments and subsequent reflection behaviour outlined in section 1.3.3 and in Tables 1.3.1 and 1.3.2.

Table 1.3.1

| Mineral | Layer Type | Characteristic refelections of natural samples (untreated) | Ethylene Glycolated | Heat Treated | Acid Treated | Mg-/EG Saturated | DMSO Treated |
|---|---|---|---|---|---|---|---|
| Kaolinite (ordered) | 1:1 | 7.15 Å (001) strong, sharp<br>3.58 Å (002) sharp, strong | | Collapses at 500 °C | | | 7.15 Å - 11.18 Å |
| Kaolinite (disordered) | 1:1 | 7.15 Å (001) less intense than kao s.s.. A-sym twds low angle<br>3.5 Å (002) a-sym twds high angle | | | | | New peak at 3.63 Å |
| Chlorite | 2:1 | 14 Å (001) weak<br>7 Å (002) strong, sharp<br>4.7 Å (003) weak<br>3.5 Å (004) strong, sharp | | 14 Å - 13.6 Å<br>001 peak enhanced<br>collapse of 002<br>003, 004 at 600 °C | Dissolves (N.B. variable resistance to treatment depending upon chlorite composition) | | |
| Swelling Chlorite (Cg) | 2:1 | 14 Å (001)<br>7 - 7.2 Å (002)<br>4.7 Å (003) | 14 Å - 17 Å<br>7-72 - 8.85 Å<br>4.7 Å - 5.85 Å | | | | |
| Illite | 2:1 | 10 Å (001) strong symmetry slight a-sym to low angle<br>5 Å (002) strong, sym-metric | 10 Å (001)<br>10 Å (001)-collapse of a-sym $I_V$<br>10 Å (001)-a-sym remains $I_M$ | 10 Å (001) | | | |
| Montmorillonite | 2:1 | 1 4 Å (001)<br>5.1 Å (003) | 1 4 Å - 17 Å<br>8.5 Å (002)<br>5.1 Å - 5.7 Å | 14 Å - 10 Å<br>5.1 Å - 5 Å | | 1 4 Å - 17 Å<br>10 Å - asym.<br>new peak at 8.99 Å | |

Table 1 Position in Å and behaviour of the characteristic clay mineral refelctions after treatments.

Table 1.3.2

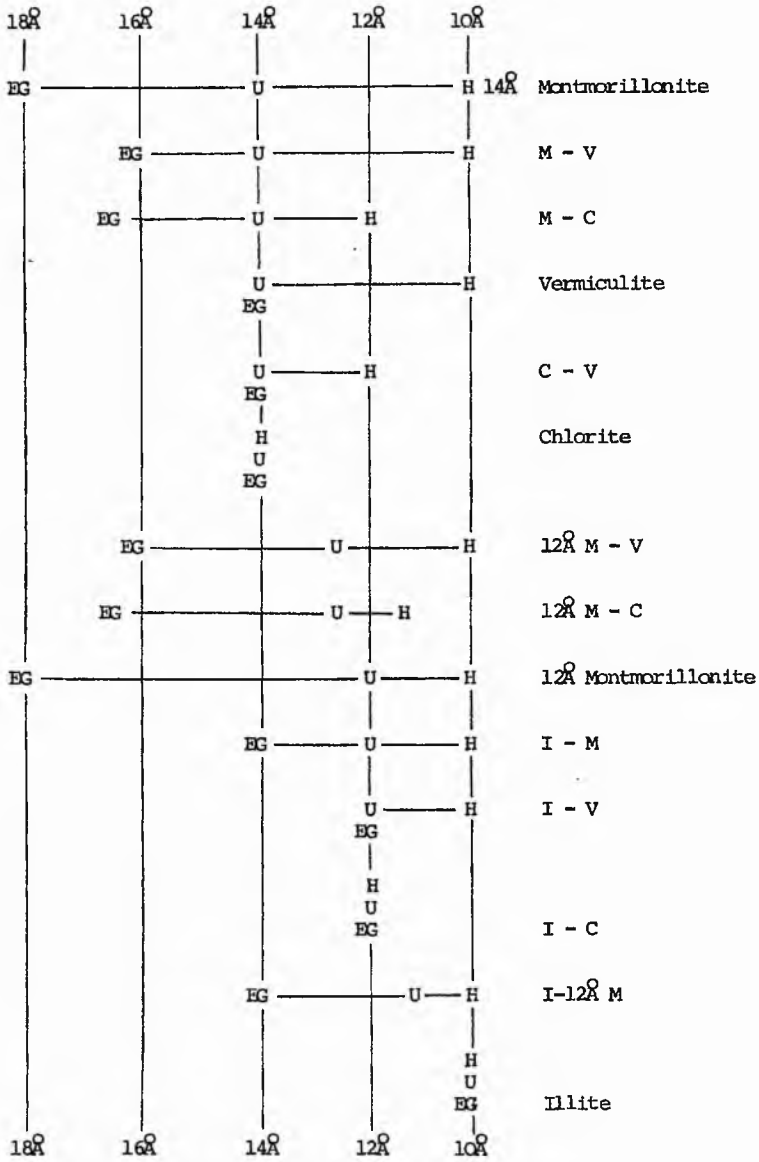


EG : Treatment with ethylene-glycol
U : Untreated sample
H : heated to 600 °C

Schematic representation of the behaviour of the reflections corresponding to basal spacing during X-ray diffraction after different treatments (after LUCAS, CAMEZ and MILLOT, 1959).

Within the Silurian sediments, the minerals that most commonly participate in these interstratifications are illite, montmorillonite, vermiculite and chlorite. These combine to produce:-

| | |
|---|---|
| illite-vermiculite (I-V) | (Fig 1.3.5a) |
| illite-montmorillonite (I-M) | (Fig 1.3.5b, c) |
| chlorite-vermiculite (C-V) | (Fig 1.3.6a) |
| chlorite-montmorillonite (C-M) | (Fig 1.3.6b) |

The combined (001) reflection of any particular mixed-layer structure lies beyond the range of sensitivity for the Phillips PW 1394 vertical goniometer. Discrimination between clay mixtures is therefore dependant upon the behaviour of the (002) reflection (at 12 Å - 14 Å, for air-dried samples) after glycolation and heat treatment. The position (in Å) of the (002) reflections of those mixed-layer (N, EG and heat treated) found in the Silurian sediments, are given in Table 1.3.2. The position of the (002) reflections of some other common interstratifications are given for comparison.

**Determination of regular or random structures in mixed-layer minerals**

To further interpretation, a distinction was made between randomly interstratified and regularly interstratified clay minerals. (See Reynolds and Hower (1970) and Thorez (1975) for discussion).

Regularly interstratified mixed-layers are characterized by a series of (001) reflections that do not correspond to those of a

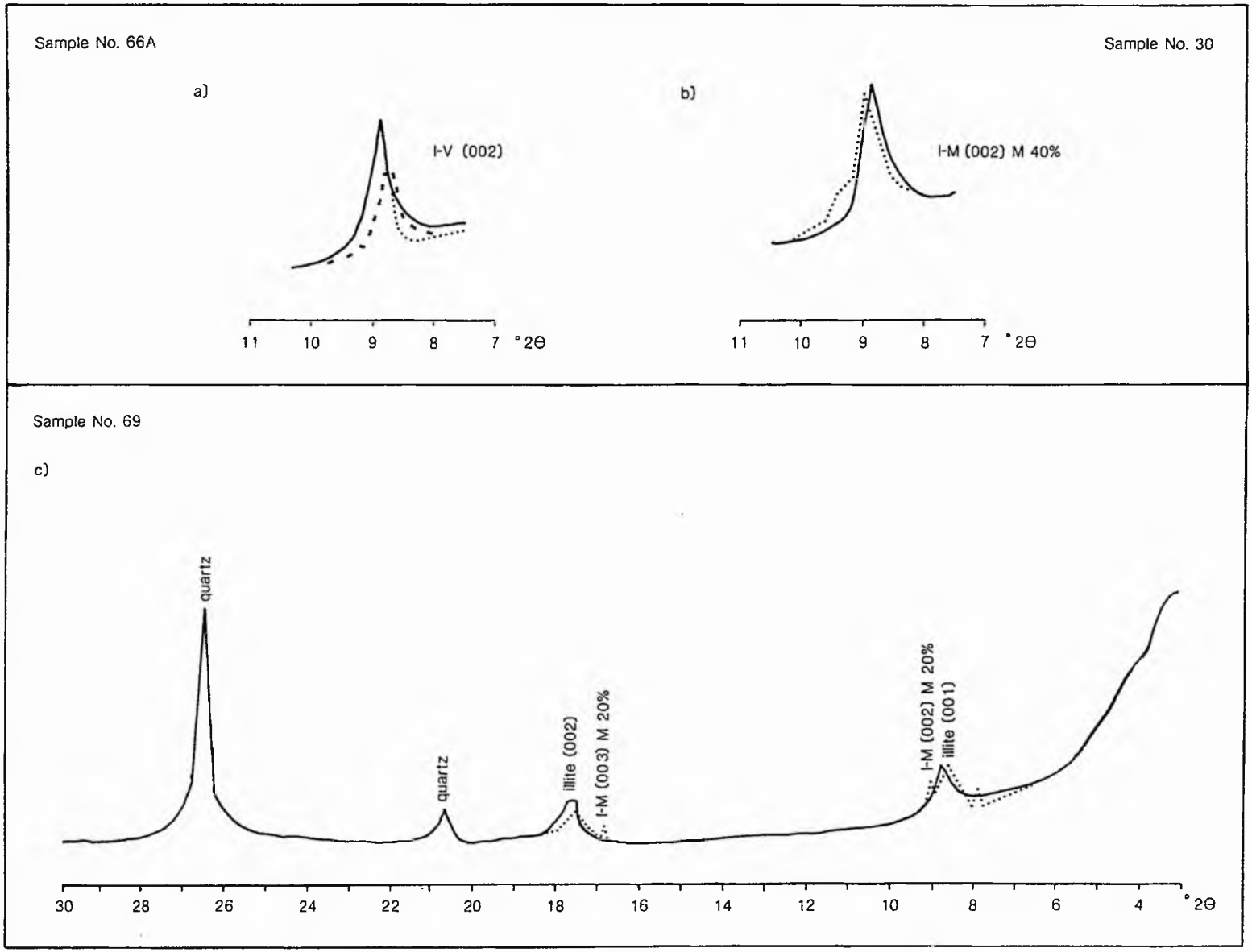


Fig. 1.3.5. Diffractograms of mixed-layers a) illite-vermiculite (I-V), b)illite-montmorillonite (I-M) with 40% M, c) I-M with 20%M. Traces of,— untreated samples, ····· ethylene-glycolated samples.

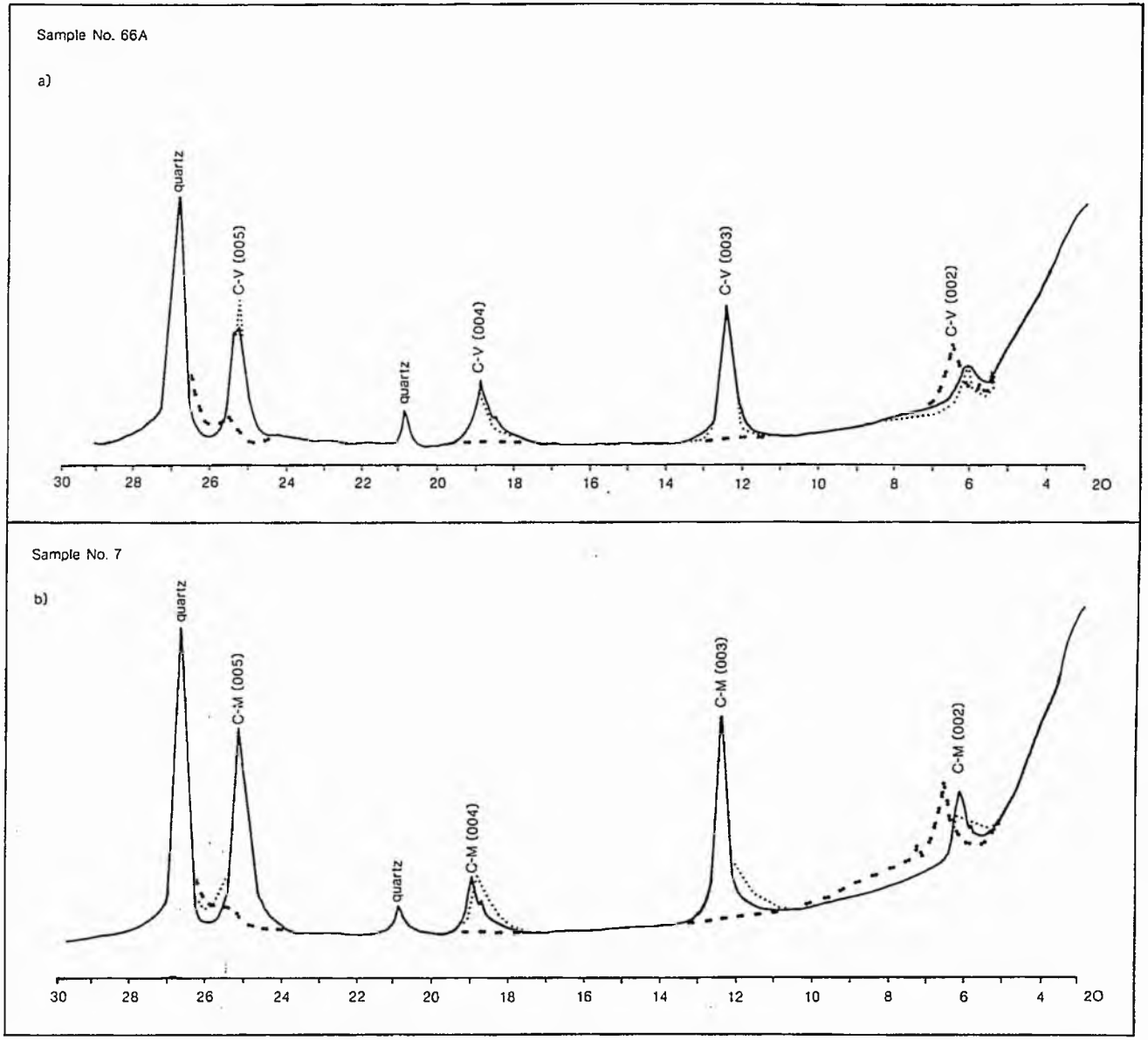


Fig. 1.3.6. Diffractograms of mixed-layers a) chlorite-vermiculite (C-V) b) chlorite-montmorillonite (C-M). Traces of, —— untreated samples, ····· ethylene-glycolated samples, - - - heat treated samples.

simple clay mineral, or to a mechanical mixture of clay minerals. They have a rational series of reflections (Fig 1.3.7) between which there is a regular spacing. Regularly interstratified mixed-layers are true minerals, to which crystal names such as corrensite (chlorite-vermiculite, chlorite-montmorillonite [sensu stricto]) and allevardite (illite-montmorillonite) have been assigned.

Random mixed-layers are random stacks of layers of two or more types. Consequently, the layers do not exhibit an integral series of orders. Reflections are often asymmetric or form broad ill-defined peaks, the limits of which will rely upon the original d-spacing of the two components involved. This is schematically illustrated in Figure 1.3.7. Random mixed-layers are structures, not minerals, and are therefore not usually given names.

Having determined the nature of interstratification from analytical treatments, the d-spacing of the mixed-layers can be expressed as the sum total of the two mineral peaks involved i.e. -

$$d(001)_{AB} = d(001)_A + d(001)_B$$

where AB = mixed-layer e.g. chlorite-montmorillonite

A = chlorite (001) = 14 Å

B = montmorillonite (001) = 17 Å

d(001)AB = 28 Å

Similarly:-

$$(002)AB = (002)_A + d(002)_B \text{ etc}$$

This series of harmonic reflections can also be devised by dividing the (001) basal peak by the order of peak involved.

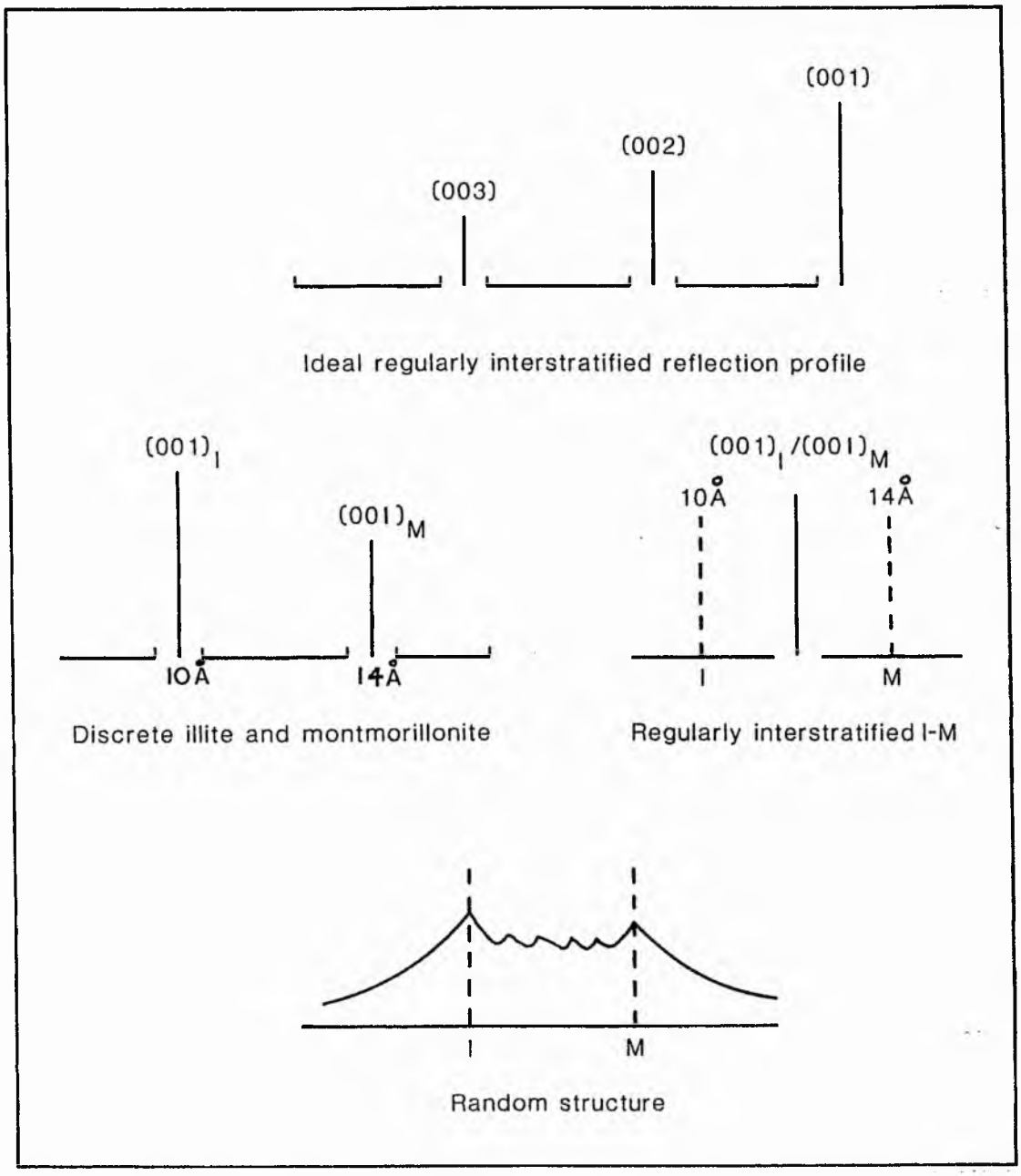


Fig. 1.3.7. Schematic reflection profiles of randomly and regularly interstratified mixed-layer minerals. Illustrated with an example of illite and montmorillonite mixed-layering. Key - I illite, M montmorillonite, I-M mixed-layer illite-montmorillonite.

eg $(001)_{C-M}$ = 28 Å

$(002)_{C-M}$ = 28 Å ÷ 2 = 14 Å

$(003)_{C-M}$ = 28 Å ÷ 3 = 9.3 Å etc

These calculations have to be repeated for ethylene-glycolated and heat-treated samples to obtain accurate identifications of the layers. To assist analyses, a Table (1.3.2) of the behaviour of the (002) basal peak, for the most significant clays and mixed-layer minerals, upon treatments, is included (after Lucas *et al*, 1959).

Consequently, the more regularly interstratified the minerals, the more identical in position the peaks will be to the calculated divisions of the (001) reflections. Nadeau *et al*, (1985), present a cautionary note concerning the XRD identification of I-M series, since differences between random and regular sequences may simply reflect interparticle diffraction effects, which may have resulted from the adsorption of exchangeable cations and water at the interfaces of particles.

**Determination of the degree of interstratification in mixed-layer illite-montmorillonite**

During burial metamorphism of sedimentary piles, the reaction montmorillonite to illite is known to occur (Perry and Hower, 1970 and 1972; Hower *et al*, 1976). Within the Silurian sediments, montmorillonite, randomly and regularly interstratified illite-montmorillonite mixed-layers and illite are present. Consequently, the montmorillonite component of mixed-layer illite-montmorillonite has been determined, so that the transformation from montmorillonite to illite in the Silurian sediments may be

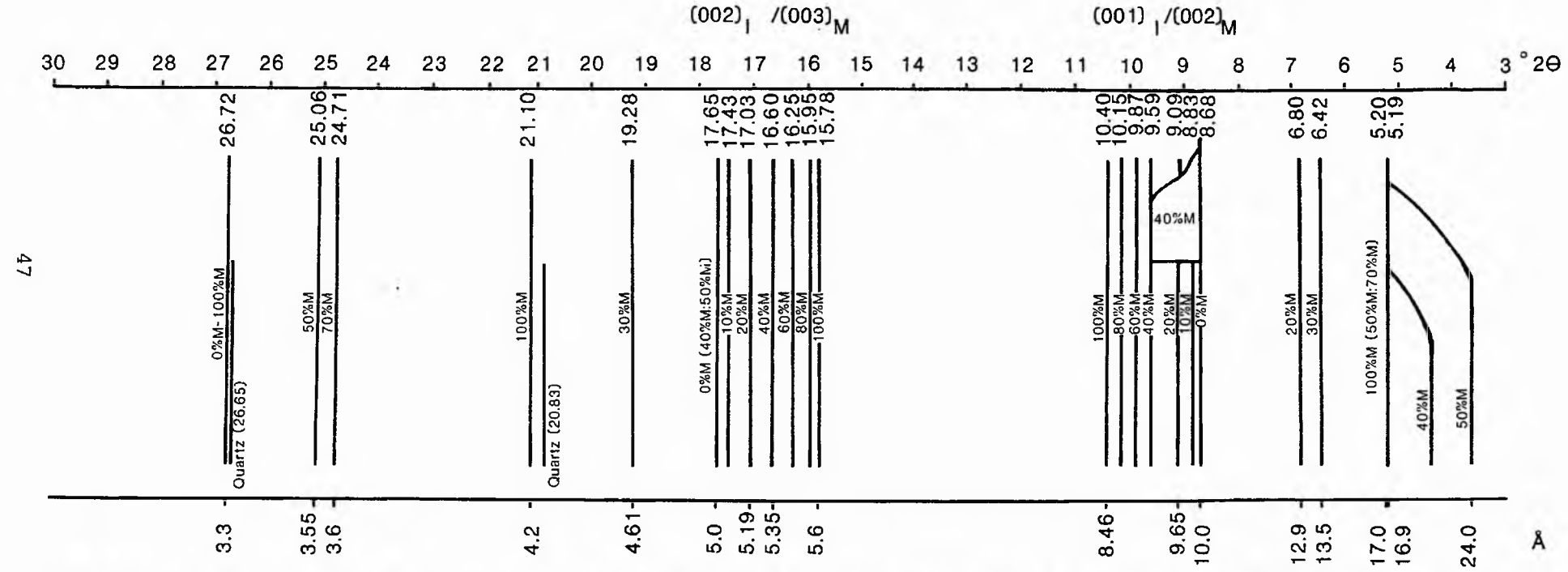


Fig. 1.3.8. Approximate positions in Å and ° 2Θ (CuK∝) of ethylene-glycolated illite-montmorillonite interstratifications. (Compiled from the data of Reynolds and Hower, 1970.) Key - M %montmorillonite interstratified in the illite structure.

monitored. The results of these analyses are presented here, and are discussed further in chapter 1.5.

The illite-montmorillonite ratio was determined according to the method of Reynolds and Hower (1970), using the combined ethylene-glycolated reflections of $(003)_{27}(001)_{10}$ or $(002)_{17}$ at 10.4 to 8.68° 2θ and of $(005)_{27}(003)_{17}$ or $(002)_{10}$ at 15.78-17.65° 2θ. These reflections occur between illite (EG) at 10 Å and montmorillonite (EG) at 16.9 Å (Fig 1.3.8). The method is dependant upon the position of the combined regularly interstratified illite-montmorillonite peak relative to the known peak positions of illite and montmorillonite proper. Between which a graduated scale of percentage interstratification has been established by Reynolds and Hower (1970). All peak positions quoted are for ethylene-glycolated samples. At low angles, divisions between the scales are narrow. The positions of the (002) and (003) illite-montmorillonite peaks were therefore more commonly used to determine the degree of interstratification. For varieties with 40-50% montmorillonite in the illite structure (Fig 1.3.8) the (001) illite-montmorillonite peak is asymmetric towards the low angle, whilst the (002) illite-montmorillonite peak is asymmetric towards the high angle.

Srodon (1980), demonstrated that the ethylene-glycolated montmorillonite reflection may occur between 17 Å and 16.68 Å (ie a variation of 16.9 ± 0.3 Å). This is great enough to account for a 15-20% error in the estimation of the illite-montmorillonite ratio according to the method of Reynolds and Hower (1970). However the application of Srodon's (1980) method fails in rocks such as these, with polymineralic clay assemblages.

Mixed-layer minerals with 5, 10, 20, 30 and 40% montmorillonite

interstratified in the illite structure were found. A full listing of the distribution of these interstratified clay minerals is given in appendix 1.3.2.

In addition to advancing metamorphic conditions, the change in smectite content of the mixed-layer sequences may also reflect the reduction of iron in the sediments (Velde, 1985). If such a chemical change had occurred in I-M, then an associated change in the other phases in the system would be expected. Since the conversion of I-M to illite during burial necessitates $K^+$ fixation (see chapter 1.2). For example, this could be reflected by the loss of kaolinite relative to the growth of chlorite. In the Midland Valley, these phases co-exist (see chapter 1.6). Similar stabilities were demonstrated by Boles and Franks (1979) for the Gulf Coast sediments, where variation in bulk rock chemistry was not anticipated.

### 1.3.5 Conclusions

X-ray diffraction techniques and qualitative clay mineral analyses have established the presence of the following clay minerals in the Silurian sediments of the Midland Valley:-

i) kaolinite
ii) montmorillonite
iii) mixed-layer illite-montmorillonite, with 5-40% interstratified montmorillonite
iv) mixed-layer illite-vermiculite
v) illite
vi) mixed-layer chlorite-montmorillonite
vii) mixed-layer chlorite-vermiculite

viii) chlorite

Furthermore, the analyses have shown that the type of interstratification and the degree of interlayering effects the combined peak position of the mixed-layer minerals.

The petrogenetic significance of these results will be discussed in chapter 1.5.

## Chapter 1.4 Illite crystallinity and $b_o$ spacing

### 1.4.1 Introduction

The mineralogy developed within the Silurian inliers (chapters 1.2; 1.3) is indicative of sub-greenschist facies. The metamorphic grade encountered may be quantified with the aid of illite crystallinity (Kubler, 1968; Weber, 1972) and $b_o$ spacing (Sassi, 1972; Sassi and Scolari, 1974; Fettes *et al*, 1976; Padan *et al*, 1982). These parameters (together with estimates of the degree of mixed layering) were used by Merriman and Roberts (1985), Oliver *et al* (1984) and Roberts and Merriman (1985) to define the relative effects of diagenesis and metamorphism in shales and slates from the British Caledonides. Where:-

i) crystallinity was recorded as the thickness (in mm or in $^{o}2\theta$ of mica crystallites of the 10Å unit cell).

ii) $b_o$ spacing was regarded as a pressure dependant lattice spacing parameter.

### 1.4.2 Illite crystallinity

**Indices**

Three main indices ie the Weaver (1960), the Kubler (1968) and the Weber (1972) indices, have been devised to determine mica crystallinities.

For the Weaver Index (Sharpness Ratio), the ratio of the peak (001) height at 10Å to that at 10.5Å, is measured relative to the distance from the background height. Although this technique is useful at lower grades, with increasing metamorphism the ratio

between the two peaks becomes more difficult to measure as sharpness increases. It is unlikely that accurate measurements could be made consistently throughout the metamorphic range to be investigated. Consequently, this index was not utilized.

Kubler's (1968) and Weber's (1972) indices measure crystallinity as a function of the peak (001) width at half-peak height. Values decrease as peak sharpness and hence metamorphic grade, increases. For the Kubler Index, measurements are made in mm, and are converted into $^{o}2\theta$. Because mm are an absolute measurement, quotation of the Kubler Index as $^{o}2\theta$ enables greater comparability of results between laboratories. For the Weber Index measurements of peak (001) width at half peak height ($Hb_{rel}$) are also made in mm. Values are quoted as ratios relative to the $Hb_{rel}$ for the (100)peak of an external quartz standard. Where:-

$$Hb_{rel} = \frac{Hb\ (001)\ illite}{Hb\ (100)\ quartz} \times 100$$

The boundaries between the different metamorphic zones, are interpreted (Kubler, 1968; Oliver *et al*, 1984) in terms of the Kubler and Weber Indices as:-

| Index | Diagenesis | Anchizone | Epizone |
|---|---|---|---|
| Kubler | >0.43 | 0.43.0.28 | <0.28 |
| Kisch (1980a) | >0.32 (+ low grade anchizone) | 0.35-0.19 | <0.21 |
| Weber | >160 | 160-70 | <70 |

Where diagenesis, anchizone and epizone are approximately equivalent to zeolite, prehnite-pumpellyite and greenschist facies respectively.

**Measurements**

Actual measurements were made on the sedimented samples discussed in chapter 1.3, prior to analytical treatment. Measurements of individual (001) illite peaks were made five times, and the average value taken. Samples were interspersed with analyses of the (100) peak for crushed quartz (also measured 5 times).

Instrumental conditions are the same as those quoted in chapter 1.3.

**Peak Broadening**

The eight factors discussed below, will affect the crystallinity values recorded from each locality. The effects of which will be expressed by broadening of the 10Å peak.

i) Crystallite size: Roberts and Merriman (1985) recognized that the crystallite size may cause line broadening on diffractograms, causing erroneous measurements to be made. The relationship between crystallite size and line broadening is expressed by the equation:-

$$B = K\lambda/nd \cos \theta$$

where K is a constant (0.91)

$\lambda$ = radiation wavelength

n = thickness of crystallites consisting of a stack of n10 Å unit cell

d = unit cell spacing (ie 10 Å)

B = peak width in $^{o}$ 2$\theta$

Roberts and Merriman (1985) found that where n <15, 10 Å peaks were broadened,where n >20 sharp intense peaks were produced, where n >50 (ie <0.16 $\Delta\ ^{o}2\theta$) no reduction in peak width occurred.

ii) The growth of authigenic illite: The growth of illite in sediments and in low grade metamorphic rocks may occur in two ways. Either illite may crystallize from feldspars and montmorillonite during diagenesis, as the direct result of heating. Or, illite may be a degradation product of detrital mica in sediments. Crystallinities measured in the latter instance may have an inherited crystallinity value from the clastic phase. This effect can be minimized (Weber, 1972) by analysing the 2 $\mu$ fraction only. However, Robinson (pers. comm. 1987) found that 0.25 $\mu$ separations still contained the detrital component.

iii) Weathering: weathering of samples can cause mixed-layered illite-montmorillonite to form, the d spacing of which overlaps with and increases the width of, the 10Å illite peak. The effects of weathering were kept to a minimum by analysing only the freshest samples available.

iv) Sedimentation: Nadeau *et al*, (1985) demonstrated that interparticulate diffraction effects from sedimented aggregates of clay particles, can give rise to increased 10Å peak-width thickness if there was a large concentration of <0.1 $\mu$ size fractions in the sediment.

v) Rock composition: Rock composition does affect crystallinity.

Consequently only rocks of the same composition should be compared. Variations are qualified in chapter 1.5.

vi) Retrograde metamorphism. The breakdown of diagenetic/metamorphic illites may occur as a result of retrogressive hydration reactions associated with uplift and cooling. Although it is generally assumed (Johnson *et al*, 1985; Roberts and Merriman, 1985) that maximum illite crystallinity was recorded during burial metamorphism, since compaction and illitization would have reduced the amount of pore-water available for retrograde reactions to occur.

vii) Growth of associated diagenetic/metamorphic minerals: In a sedimentary sequence undergoing burial, metamorphic reactions will involve the conversion of mixed-layer I-M to illite. Whilst in rocks with a suitable bulk composition, paragonite and pyrophyllite will develop. Due to overlapping diffraction peaks, low grade crystallinity values may be due to peak broadening associated with the development of these phases.

viii) Quartz standard: The standard may affect $Hb_{rel}$ crystallinities (Weber, 1972) if the quartz was strained or if it was derived from aluminous shales and cherts (increases (100) $Hb_{rel}$ value of quartz). Furthermore variable quartz peak intensities due either to irregular grain sizes or to the inconsistent use of $\alpha$- or $\beta$-quartz may effect the measurement of $Hb_{rel}$. Weber (1972) recommends the use of quartz from quartzite or from veins. The actual standard used, was derived from a unstrained vein quartz of an independant origin from that used by Weber (1972). Correlation of $Hb_{rel}$ values with those used by

Weber (1972) to define diagenetic, anchizone and epizone conditions must therefore be made with caution.

The effects of these eight factors are quantified later in chapter 1.4, and in chapter 1.5.

In addition to peak broadening, two other factors may affect crystallinity values. Firstly: In North Wales, Roberts and Merriman (1985) found that the crystallinity technique (in pelites) was insensitive to changes in metamorphic grade once biotite was encountered in associated metabasites. At crystallinities of 0.16 $^{o}2\theta$ further increase in mica crystallite size did not result in a significant reduction of the 10Å peak width. The usefulness of crystallinity parameters are therefore limited at higher grades. Secondly: Crystallinity values may preserve more than one record of metamorphism. For example, in North Wales, Roberts and Merriman (1985) recognize weak crystallinities from a deep burial metamorphic event, which have survived later weak deformation. The development of a cleavage would have resulted from the mechanical rotation of existing crystals associated with crenulation. However, the survival of burial metamorphic crystallinities suggests that these domains would have been dispersed so producing a structurally more isotropic medium, and inhibiting the development of cleavage.

### 1.4.3 $b_o$ spacing

$b_o$ measurements were made on the same samples as for illite crystallinity, under the machine conditions stated in chapter 1.3. However, measurement should normally be carried out on randomly oriented samples (D. Robinson pers. comm.). Because of the contribution of expandable phases to low angle peaks in the Silurian

assemblages, actual measurements were made on the (060) illite peak, following Padan *et al*, (1982). The diffractogram was run between 59-63 $^{o}2\theta$, so that the quartz (211) peak could be used as a standard to check for instrumental drift.

There are three factors which could affect the interpretation of the $b_o$ values:-

i) Samples with high quartz, k-feldspar and chlorite contents produce high $b_o$ values (Sassi and Scolari, 1974).

ii) Carbonate-rich samples produce low $b_o$ values (Sassi and Scolari, 1974).

iii) The effects of retrogressive metamorphism on $b_o$ spacing in illite is unknown (Johnson *et al*, 1985).

The effects of these factors are minimized, since the majority of samples analyzed were taken from the most shaley units only. The presence of authigenic chlorite was not believed to significantly effect the results, since the total matrix component was estimated (chapter 1.2) to be $\leqslant$15%.

### 1.4.4 Results

Illite crystallinity measurements from the Silurian sediments range from 80 to 200 $Hb_{rel}$ ($\bar{x}$ = 130), from 6 to 9 mm (Kubler) and from 0.29 to 0.48 $^{o}2\theta$ (fig 1.4.1). $Hb_{rel}$ measurements are compatible with metamorphism in the zeolite to prehnite-pumpellyite facies. Measurements in $^{o}2\theta$ however, are diagnostic of diagenetic conditions. The lack of agreement in metamorphic conditions suggests that

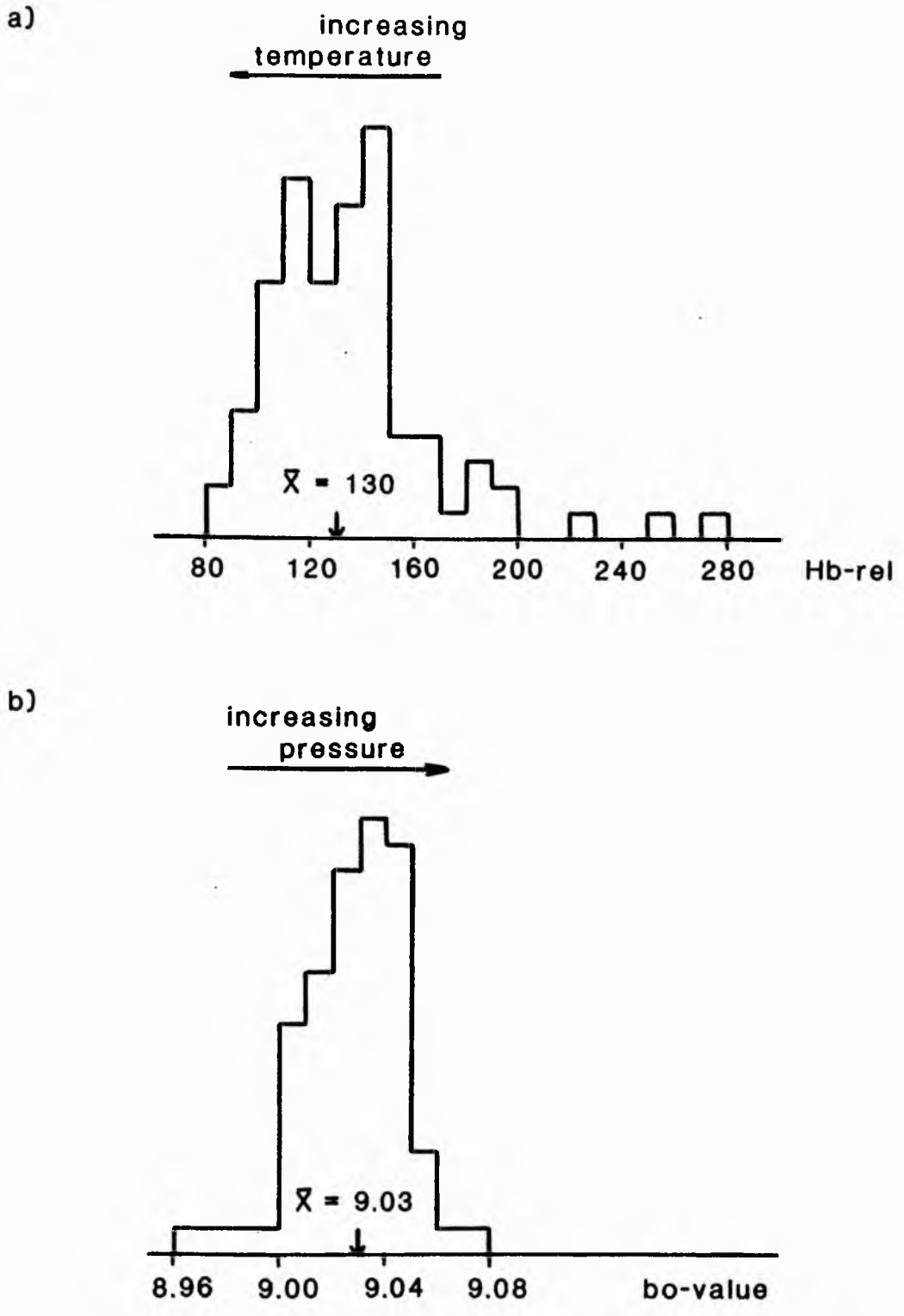


Fig. 1.4.1. Histograms of a) Hb-rel b) bo-values, from Silurian sediments in the Midland Valley of Scotland.

either:-

i) the two indices are not comparable

or

ii) the quartz standard produced erroneously high $Hb_{rel}$ values

Associated $b_o$ values range from 8.96 to 9.08 ($\bar{x}$ = 9.03) and are compatible with metamorphism under sub-Barrovian conditions. Temporal variations in crystallinity and in $b_o$ spacing are discussed in chapter 1.5. Results are summarized in appendix 1.3.2 and in appendix 1.4.1.

## Chapter 1.5 Discussion

### 1.5.1 Aims

To determine the spatial variation in metamorphic conditions across the Silurian inliers of the Midland Valley, with reference to clay mineralogy, illite crystallinity and $b_o$ spacing.

### 1.5.2 Clay mineralogy as indicators of metamorphic grade

Scanning electron microscopy (chapter 1.2) and X-ray diffraction (chapter 1.3) has determined the presence of complex clay mineral associations (chapter 1.3) in the Silurian sediments of the Midland Valley. This mineralogy is quantified below, with respect to:-

i) the relationship between clay mineralogy, lithology and sedimentology.

ii) the percentage montmorillonite interstratified with illite as a function of metamorphic grade: evidence for discrete clay mineral assemblages

**The relationship between clay mineralogy, lithology and sedimentology**

Chlorite, illite, mixed-layered C-M, C-V and for the most part I-M, occur throughout the Silurian geological sequences. Their distribution does not appear to be governed by variable lithological or sedimentological controls.

In the Hagshaw Hills however, mixed-layered I-M is developed at one locality (45 - figure 1.3.1) in an area otherwise characterised by illite (fig 1.5.5). I-M is developed in pelitic facies, whilst illite proper is restricted to more arenaceous horizons. This suggests for the Hagshaw Hills at least, that the development of

illite may have been enhanced in rocks with a higher initial porosity. Similarly, kaolinite is preferentially concentrated in coarse wackes throughout the Midland Valley Silurian.

The development of both kaolinite and montmorillonite is restricted to Llandoverian strata. Since the Llandovery-Wenlock boundary is said (chapter 1.1) to represent a change in deposition, from sedimentary sources in the Llandoverian to igneous sources in the Wenlockian, the distribution of kaolinite and montmorillonite is likely to be related to changing provenance. Similarly R. Fowler (pers. comm., 1983) working in the Girvan district, found that kaolinite was present in those rocks derived from a Llandoverian sedimentary provenance.

The development of mixed-layered I-V is restricted to three localities ie at 50, 58 and 66A (fig 1.3.1). For each of the localities, the lithological characteristics of the sediments and the age of sedimentation is different. In the absence of a unifying factor, it is believed that the development of I-V may reflect crystallization from whole rocks with a restricted chemical composition. Unfortunately this idea was not quantified.

Authigenic kaolinite was not found during SEM examination (chapter 1.2) of the sediments. This tentatively suggests that kaolinite is either a detrital mineral or a weathering product. Even if kaolinite was present as a diagenetic mineral, it is stable over such a wide range of pressures (0-2 kb - Velde, 1977) and temperatures (200 $^{o}$C - Dunoyer de Segonzac, 1970; Kisch, 1981; 0-300 $^{o}$C - Velde, 1977) that it can only be ascribed to the low-grade burial zone. Consequently, kaolinite may not be used as an index mineral for a more restricted PT field. Furthermore, the abundance

of kaolinite in the Silurian inliers, does not decrease as metamorphic grade (crystallinity and $b_o$) increases, therefore the kaolinite is unlikely to be diagenetic.

Although some montmorillonite is shown (SEM - chapter 1.2) to be authigenic, both montmorillonite and kaolinite fail to form part of a recognisable clay mineral assemblage (see below). These minerals commonly occur with well crystallized illite or I-M, and are therefore unlikely to be diagenetic products. The development of kaolinite and montmorillonite however, could have resulted from retrograde reactions associated with uplift (see chapter 1.4), however evidence for this is equivocal.

**Clay Mineral Assemblages**

A close study of appendix 1.3.2 will show that the clay minerals may be divided into the following assemblages:-

Assemblage 1 - Chlorite + illite (M = 0 to 10%)

Assemblage 2a - Chlorite + mixed-layer I-M (M = 10% - 20%)

2b - Mixed-layered C-M + I-M (M = 10% - 20%)

Assemblage 3a - Chlorite + mixed-layered I-M (M = 20% - 30%)

3b - Mixed-layered C-M + I-M (M = 20% - 30%)

Assemblage 4 - Mixed-layered C-V ± chlorite + mixed-layered I-M (M = 30% - 40%)

Assemblage 5 - Mixed-layered C-V + I-V

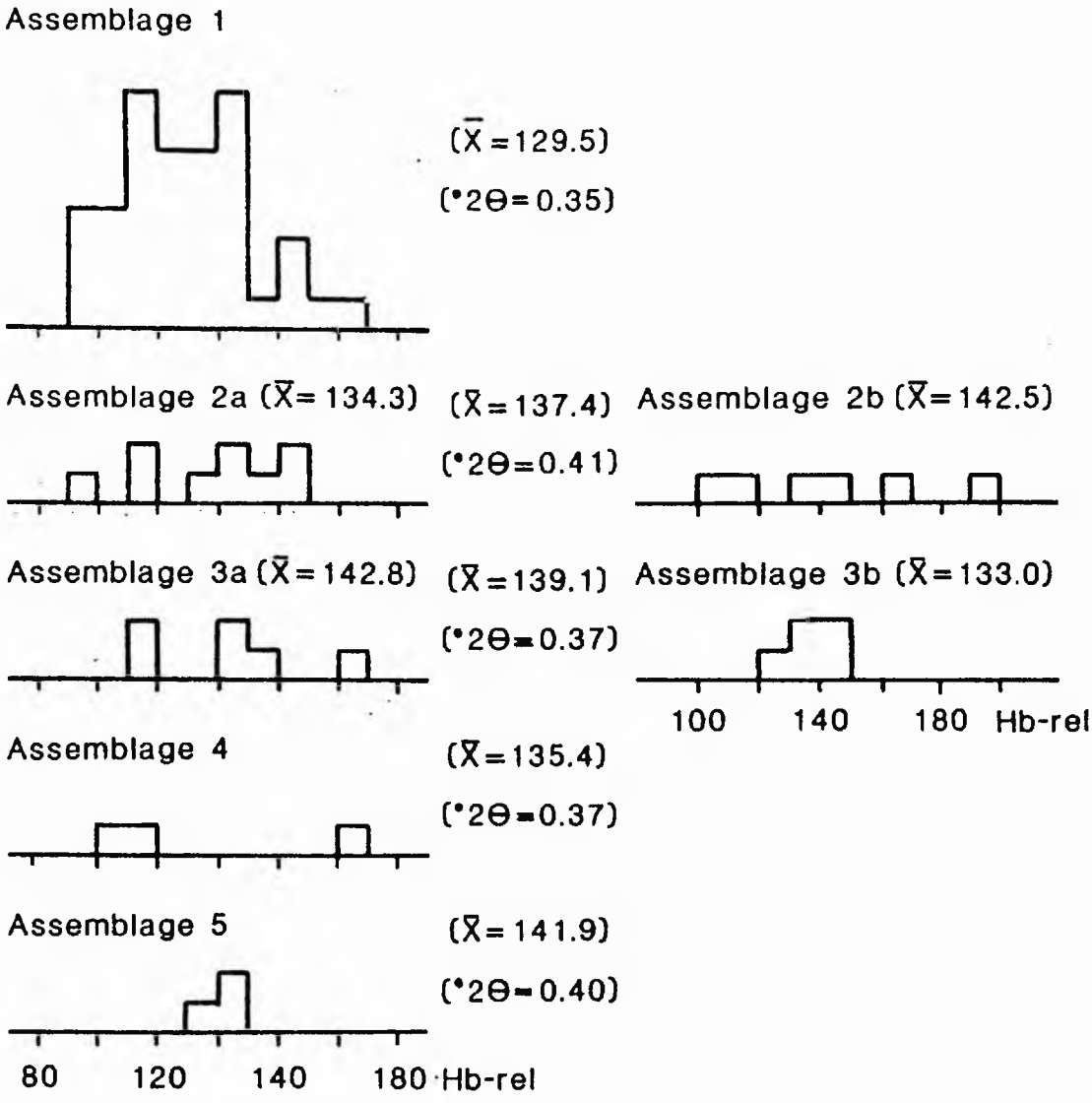


Fig. 1.5.1. Histograms to show Hb-rel values for the different clay mineral assemblages.

where M = the degree of montmorillonite interstratified in the illite structure.

Illite, mixed-layered I-M, chlorite and mixed-layered C-M have been chosen as the key minerals of the authigenic assemblages. The diagenetic origin of illite, mixed-layered I-M and chlorite has already been established from scanning electron microscopy (chapter 1.2). The absence of mixed-layered C-M from recent sediments has led Monnier (1981) to conclude that this mineral is of diagenetic origin.

The major changes in clay-mineralogy occurring from assemblages 5 to 1 are:-

i) the transformation of the expandable phase from 40%M to 0%M
ii) the consistent appearance of chlorite between 30-40%M
iii) the disappearance of mixed-layered C-M between 10-20%M
iv) the increase in chlorite at the expense of mixed-layer C-M

To ensure that these changes represent a progressive transformation with grade, the average illite crystallinity values (fig 1.5.1) of each assemblage have been determined. Comparative $b_o$ values are shown in figure 1.5.2.

$Hb_{rel}$ values increase from 129.5 in Assemblage 1 to 141.9 in Assemblage 5. Sub-assemblages characterized by mixed-layered C-M are of lower and higher crystallinities than the equivalent chlorite-bearing assemblages. $B_o$ values decrease from 9.030 to 9.023 in Assemblages 1 to 5 respectively. Sub-assemblages containing mixed-layer C-M have higher $b_o$ values than the equivalent chlorite-bearing assemblages. Since chlorite does not occur as a stable phase until the 40%M boundary has been passed, the slightly

Assemblage 1

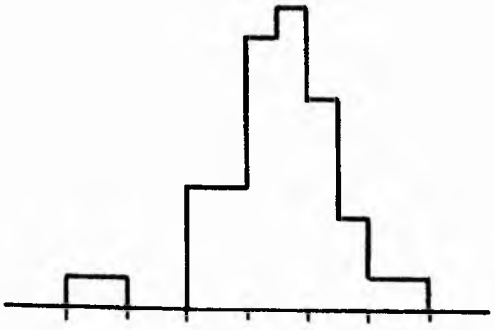

($\bar{X}$=9.03)

Assemblage 2a ($\bar{X}$= 9.026)

Assemblage 2b ($\bar{X}$= 9.027)

($\bar{X}$= 9.026)

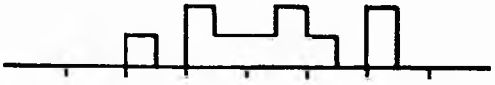

Assemblage 3a ($\bar{X}$= 9.017)

Assemblage 3b ($\bar{X}$= 9.030)

($\bar{X}$=9.024)

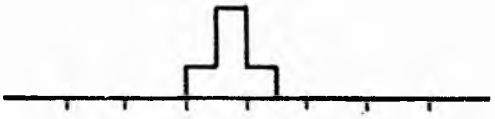

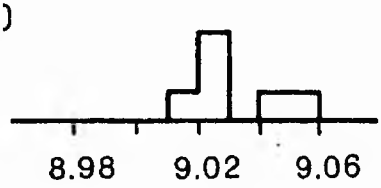


Assemblage 4

($\bar{X}$=9.022)

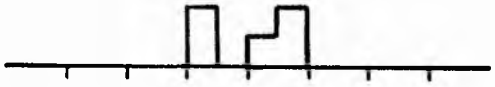

Assemblage 5

($\bar{X}$=9.023)

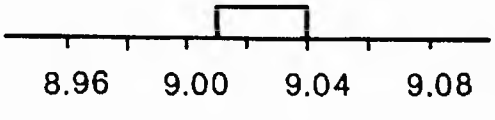


Fig. 1.5.2. Histograms to show bo values for the different clay mineral assemblages.

higher grade shown by the sub-assemblages may be justified if it is more stable at this point than the chlorite-bearing assemblages.

The observed trends in $Hb_{rel}$ and $b_o$ (fig 1.5.3a, b) are consistent with the transformation of mixed-layer illite-montmorillonite (Assemblage 4) to illite proper (Assemblage 1). Furthermore, the relative uniformity of the clay mineral assemblages throughout the Silurian, suggests that there is no appreciable compositional variation in the sediments as a function of age and therefore with depth. The change from I-M to illite must therefore have been caused by progressive metamorphism under increasing temperatures and/or pressures (see below). The appearance of chlorite, and the transformation of mixed-layer C-M to chlorite, occurs synonymously with the decrease in %M in the I-M structures. Consequently this transformation must also have been a function of increasing pressures and/or temperatures during metamorphism.

No attempt has been made to define the $Hb_{rel}$ and $b_o$ values of the various assemblages in terms of the diagenetic, zeolite or prehnite-pumpellyite facies. Instead, all assemblages are attributed to the diagenetic/anchizone in general. This was because calculated standard deviations (table 1.5.1) for average $Hb_{rel}$ and $b_o$ values for the different clay mineral assemblages, covered similar ranges. Consequently, the data may be devoid of petrological significance. The large range of values shown by any one assemblage may be due to:-

i) insufficient samples to characterize any one group

ii) interparticulate diffraction effects; this would have increased $Hb_{rel}$ values therefore giving a poor range.

iii) changes in crystallinity dependant upon the lithology

Table 1.5.1

a) Average $Hb_{rel}$ values for the clay-mineral assemblages

| Assemblages | $\bar{x}$ | $\sigma$ | n |
|---|---|---|---|
| 1 | 129.5 | 21.3 | 47 |
| 2 | 137.4 | 25.8 | 16 |
| 3 | 139.1 | 18.5 | 12 |
| 4 | 135.4 | 32.0 | 3 |
| 5 | 141.9 | 6.4 | 3 |

$\bar{x}$ = mean  $\sigma$ = standard deviation  n = number of samples

b) Average $b_o$-values for the clay-mineral assemblages

| Assemblage | $\bar{x}$ | $\sigma$ | n |
|---|---|---|---|
| 1 | 9.030 | 0.020 | 39 |
| 2 | 9.026 | 0.022 | 15 |
| 3 | 9.024 | 0.013 | 11 |
| 4 | 9.023 | 0.006 | 3 |

Table 1.5.1 Average $Hb_{rel}$ and $b_o$ values for the clay-mineral assemblages

sampled (see earlier).

iv) the contribution from the detrital micas retained in the 2 $\mu$ fraction (D. Robinson pers. com. found that separations of $<0.25\ \mu$ still retain the detrital phase).

v) the inapplicability of the $b_o$ parameter as a changeable factor during low grade metamorphism.

**Pressure and Temperature Conditions**

The pressure and temperature conditions experienced by the Silurian sediments of the Midland Valley, have been estimated by comparison with mineralogical transformations observed elsewhere. Actual values are quoted in section 1.5.3

i) The transformation of I-M to illite

Coombs (1954), ascribed montmorillonite and mixed-layer I-M to the zeolite facies ie P<4 kb, T $\leqslant$200 $^{o}$C. In the Gulf Coast sediments (Burst, 1959) montmorillonite disappeared at about 90 $^{o}$C at a burial depth of 1 km. Elsewhere in the Gulf Coast (Burst, 1969; Perry and Hower, 1970; 1972: Hower *et al*, 1976) montmorillonite gave way to irregularly interstratified I-M at an upper temperature limit of 100-120 $^{o}$C at 2 km. Velde (1977) recognized that regularly interstratified I-M (M $\leqslant$40%) characterized the laumontite zone of the zeolite facies. Pressure and temperature conditions measured from boreholes in the Gulf Coast (Hower *et al*, 1976) indicate that metamorphism occurred at 120 $^{o}$C at 3.7 km. The transformation of I-M to illite, has been recorded at 175 $^{o}$C at a depth of 4 km (Hower *et al*, 1976) and at 225-310 $^{o}$C and 5-7 km (Velde, 1977).

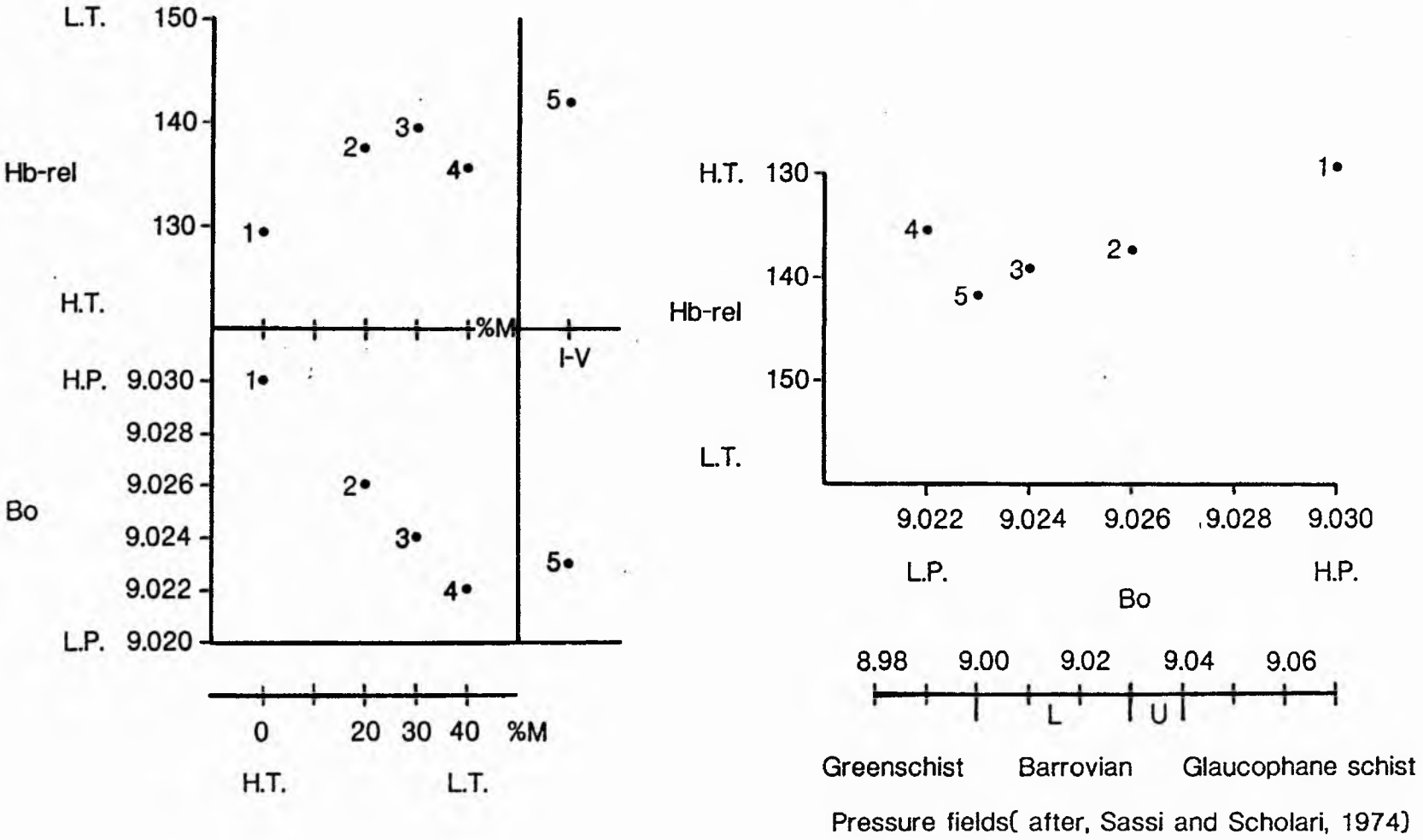


Fig. 1.5.3. Relationship between %M , illite crystallinity and pressure (bo). Numbers 1, 2, 3, 4 and 5 refer to the clay mineral assemblages.

ii) the transformation of C-M to chlorite

Kubler *et al* (1974) and Kisch (1980, b) ascribed mixed-layered chlorite-montmorillonite (corrensite) to the laumontite zone. Seki *et al*, (1969), recognized a lower laumontite zone, where mixed-layered C-M occurred with allevardite (Kubler, 1973), and an upper laumontite zone where chlorite occurred with ordered illite-montmorillonite. In the Gulf Coast sediments (Hower *et al*, 1976) authigenic chlorite- group minerals were not encountered until burial depths exceeded 2.5 km at temperatures greater than about 80 $^{o}$C. Mixed-layered C-M occurred between 2.5 to 3.7 km at temperatures of 80 to 120 $^{o}$C respectively. Beyond this maximum PT range, chlorite occurred as a stable phase.

The documentary evidence sited above recognises the transformation of a disordered C-M + I-M series, to an ordered C + I - M + I series at about 200 $^{o}$C. The identification of comparative clay mineral assemblages in the Silurian sediments suggests that burial metamorphism occurred at similar temperatures. The burial depth at which these transformations occurred, would have been dependent upon the local geothermal gradient in the Midland Valley (see section 1.5.3 for a discussion of burial depths).

**The Conodont Alteration Index**

Epstein *et al*, (1977) found that the colour of the condont animal, darkened in response to increased metamorphic grade. The conodont alteration index (CAI) was devised (op cit) to monitor these colour changes over specific temperature intervals.

Conodonts have been collected from the Silurian inliers at two localities (fig 1.5.4 and 1.5.6) in the Midland Valley:-

i) at Woodland Point, Girvan (Bergstrom, 1980)

ii) at North Esk, Pentlands (Aldridge R J, pers comm, 1983).

At both localities, the conodonts occur with assemblage 2 clay-minerals. CAI values (Aldridge R J pers comm, 1983) of 2 and 2.5 have been recorded from the conodonts at Woodland Point and North Esk, respectively. Indicating metamorphic temperatures of between 60 $^{o}$C and 150 $^{o}$C (Epstein *et al*, 1977). These temperatures are consistent with the metamorphism of assemblage 2 clay-minerals under diagenetic/zeolite facies conditions.

### 1.5.3 Burial metamorphism of the Silurian inliers

In the previous section, it was determined that metamorphism of the Silurian sediments essentially occurred under sub prehnite-pumpellyite facies conditions. In this section, the spatial variation in metamorphic grade is defined from the distribution of $Hb_{rel}$, $b_o$ and clay minerals in the different inliers.

### Local Variations

i) The Pentlands

In the North Esk inlier, isocrysts (Hb-rel), isobars ($b_o$) and clay-mineral assemblages (fig 1.5.4) form linear belts elongated NE-SW.

Clay mineral assemblages (fig 1.5.4a) increase in grade from assemblage 4 in the north-west to assemblage 1 in the south-east. This pattern broadly correlates with a similar increase towards the south-east, shown by the $b_o$ values in figure 1.5.4c. Both trends are

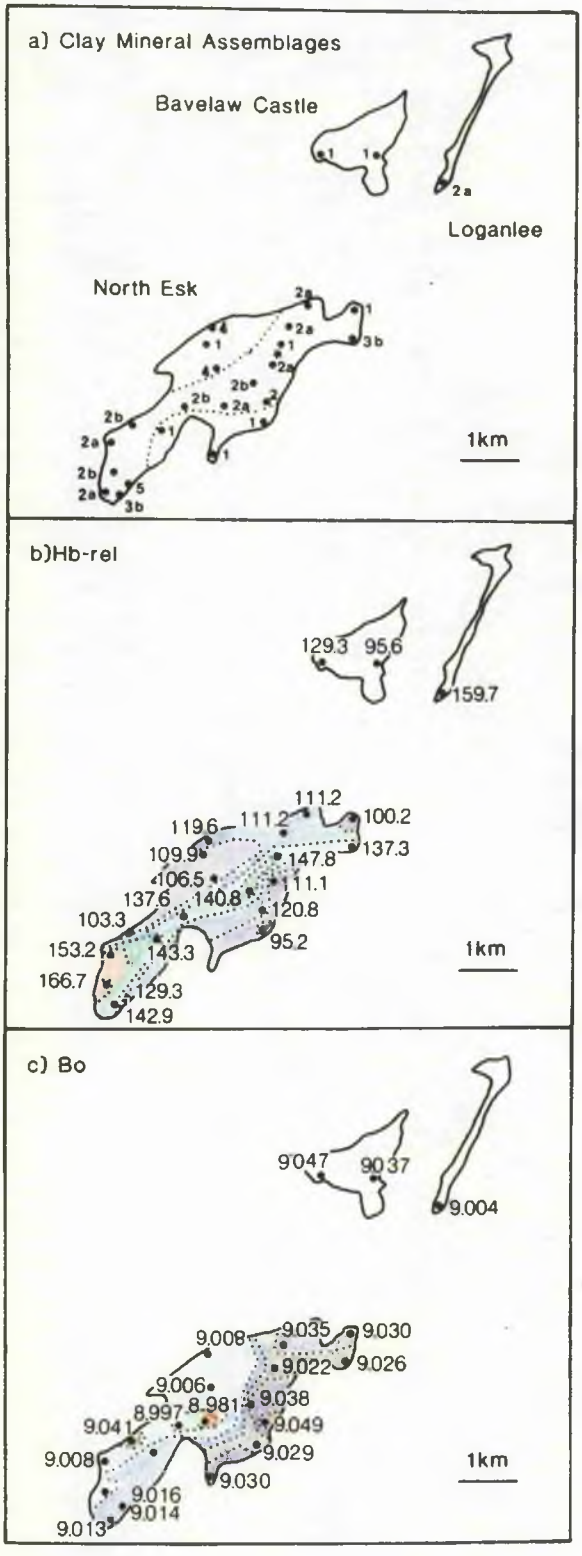


Fig. 1.5.4. Spatial variation of a) clay mineral assemblages b)illite crystallinities and c) bo-values, in the Pentland inliers.

KEY

• localities

* conodont locality

Hb-rel

160
150
140
130
120
100
90

Isocrysts at 10 Hb-rel intervals.

Bo

8.98
8.99
9.00
9.01
9.02
9.03
9.04

Isobars at 0.01 intervals.

consistent with the move from younger to older rocks, suggesting that grade increased with depth and that metamorphism was therefore syn-sedimentary. The textural evidence sited in chapter 1.2, that cementation in Silurian strata was early, is consistent with the proposed syn-sedimentary burial metamorphism.

The trend in $Hb_{rel}$ values (fig 1.5.4b) is inconsistent with those shown by the clay-minerals and by $b_o$ values. Isocrysts (fig 1.5.4b) define two metamorphic highs, symmetrically disposed about a medial low. There are two factors which may have affected a change in $Hb_{rel}$, without significantly altering either the clay mineralogy or the $b_o$ values:-

1 It is possible that high $Hb_{rel}$ values reflect recrystallization in the proximity of ($\geqslant$1 km distance) a 1 m wide dyke. This seems unlikely, since Thomas (1986) determined that illite only ¼ km away from a 10 km diameter granite was unaffected.

2 Several of the high $Hb_{rel}$ values resulted from the sampling of coarse wacke horizons. Detrital illites typically display enhanced crystallinities (see chapter 1.4). Consequently the symmetrical distribution of $Hb_{rel}$ values may only be an apparent feature due to sampling.

All the evidence so far presented, suggests that metamorphism resulted from syn-sedimentary burial. The linear $Hb_{rel}$, $b_o$ and clay-mineral belts however, controversially cut across the Llandovery-Wenlock boundary and across structural trends shown in

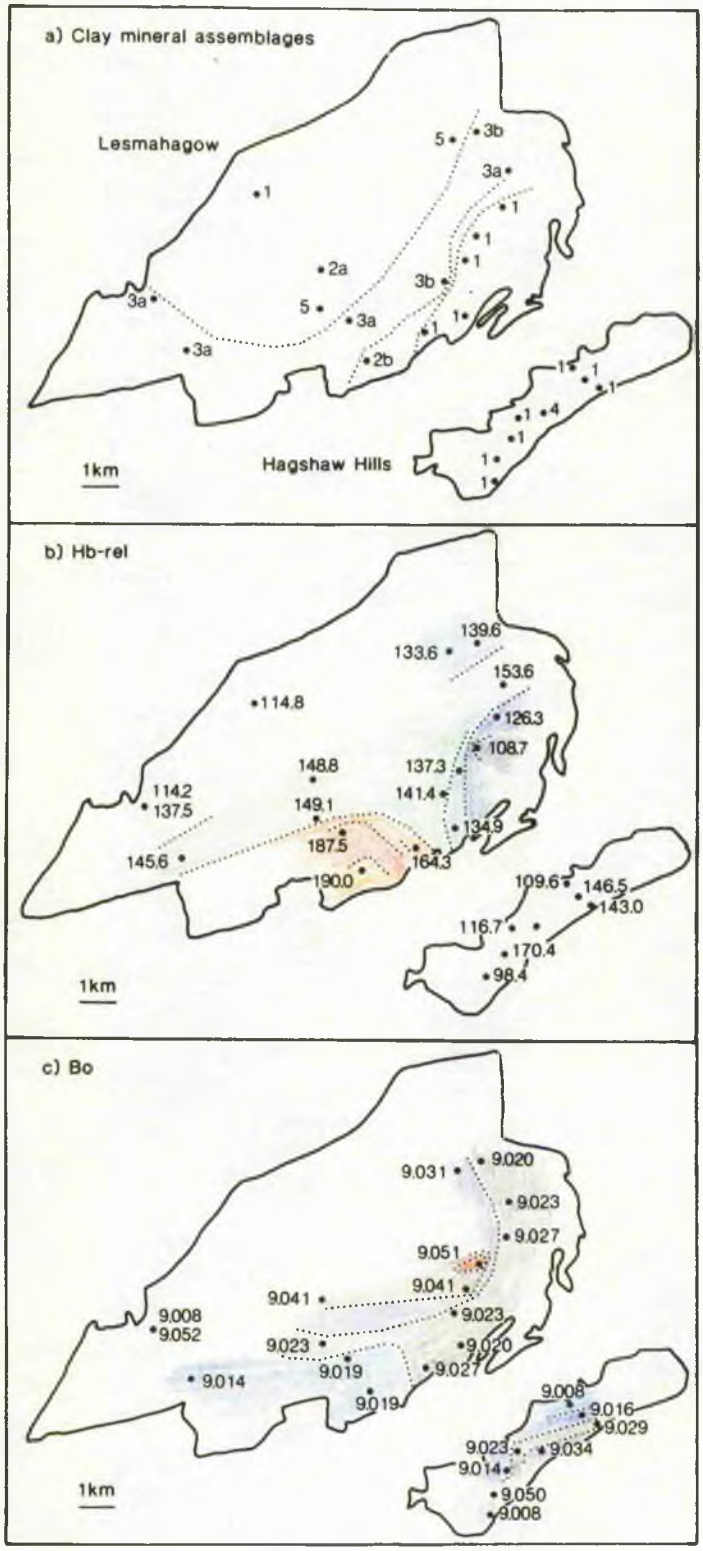


Fig. 1.5.5. Spatial variation of a) clay mineral assemblages b) illite crystallinity and c) Bo-values, in the Lesmahagow and Hagshaw Hills inliers.

KEY

• localities

Hb-rel
190
180
170
160
140
130
120
100

Isocrysts at 10 Hb-rel intervals.

Bo
9.00
9.01
9.02
9.03
9.04
9.05

Isobars at 0.01 bo intervals.

figure 1.1.1. This tentatively suggests that, in addition to syn-sedimentary Silurian metamorphism, the North Esk inlier experienced later Devonian burial metamorphism, along slightly different lines to the Silurian trend. Evidence for this is equivocal and is discussed later in the chapter. However, Roberts and Merriman (1985) found that in the low-grade meta-sediments of North Wales, that early burial metamorphism prevented the rotation of structural domains into the cleavage following weak deformation. Thus in North Wales, and here in the North Esk inlier, syn-sedimentary burial metamorphic phases are preserved.

Insufficient samples were available to categorize metamorphic events at either Bavelaw Castle or Logan Lee. Furthermore, because of the fault bounded nature of:-

a) the northern boundary of the North Esk inlier

b) the eastern boundary of the Logan Lee inlier

c) the south-eastern margins of the Bavelaw Castle inlier, it was impossible to extrapolate from North Esk. Furthermore it was not known whether the inliers were in their present positions at the time of Silurian metamorphism.

ii) The Hagshaw Hills

The Hagshaw Hills inlier is characterized by assemblage 1 clay minerals (fig 1.5.5a). $B_o$ values (fig 1.5.5b) increase from younger to older strata (fig 1.1.1). However this trend, is also consistent with the increasing proximity of the Devonian fold hinge (fig 1.1.1) and with the Devonian reverse fault (fig 1.1.1). Consequently $b_o$ values may reflect either syn-sedimentary burial metamorphism (comparable to that observed at North Esk) or, metamorphism during

Devonian tectonic activity.

$Hb_{rel}$ values increase from south-east to north-west across the inlier, and are inconsistent with both of the above concepts. Increased $Hb_{rel}$ values in the north-western sector of the inlier (fig 1.5.5b) may be due to continued syn-sedimentary burial metamorphism beneath the Upper Devonian basin which developed (Mykura, 1983) between the Lesmahagow and Hagshaw Hill inliers.

iii) Lesmahagow

In the Lesmahagow inlier isocrysts, isobars and clay-mineral assemblages occupy linear zones, parallel to the regional Caledonian trend. Clay-mineral assemblages increase in grade from NW-SE and are accompanied by a decrease in $Hb_{rel}$ values in the eastern half of the inlier. These trends are consistent with a move from younger to older strata, and with increased proximity to the Devonian fold hinge. Metamorphism may therefore be attributed to either syn-sedimentary burial metamorphism or to Devonian deformation. Although textural evidence (chapter 1.2), indicates that early cementation occurred in the Lesmahagow inlier, favouring syn-sedimentary burial metamorphism. In the western half of the inlier, $Hb_{rel}$ values (fig 1.5.5b) decrease towards the north. Increased metamorphic grade in this section may reflect either continued syn-sedimentary burial in this region beneath Devonian cover sequences, or the development of high strains associated with Carboniferous faulting. The presence of Devonian strata to the east of the inlier suggests that Devonian rocks may have covered the entire Silurian sequence. This suggests that the development of regions of high strain were a more probable cause of the

metamorphism. Furthermore, the distributions of $b_o$ values (fig 1.5.5c) indicate that high pressures were not associated either with older strata, or with the Devonian fold axes. Instead, high values are concentrated around late Carboniferous faults (fig 1.1.1) on the limb of the anticline. Suggesting that Carboniferous strain was responsible for some of the metamorphism in the Lesmahagow inlier.

If the faulting affected the crystallinity and $b_o$ values at Lesmahagow, the region must have experienced weak burial followed by later stronger deformation.

iv) Girvan

The distribution of clay-minerals, $Hb_{rel}$ values and $b_o$ values in the Girvan inliers are shown in figure 1.5.6. All regions are dominated by assemblage 1 clay-minerals, suggesting that metamorphism was enhanced in the Girvan region compared to inliers elsewhere. The distribution of $Hb_{rel}$ and $b_o$ values were somewhat variable and therefore contouring was severely restricted (partly because of narrowness of the outcrops). Hence tentative suggestions for the causes of metamorphism could only be made for the larger of the inliers ie the Girvan Main Outcrop.

Clay-mineral assemblages in the Girvan Main Outcrop, increase in grade in the western half of the inlier. This partly reflects the transition from younger to older strata, indicating that clay-mineral transformations occurred during syn-sedimentary burial metamorphism. By analogy with Roberts and Merriman (1985) and with the Pentlands (see previous sections) the distinct lack of cleavage in these isoclinally folded shales (chapter 1.1) suggests that strong burial metamorphism may have preceeded deformation. $Hb_{rel}$ and $b_o$ values

show only slight variations consistent with the transition from older to younger rocks, suggesting that the effects of syn-sedimentary burial metamorphism may have been overprinted.

In the western half of the inlier an elongate zone of poorly crystallized illite separates regions of higher grade to the NW and SE. In the south-east, $Hb_{rel}$ values systematically decrease as strata of older age is encountered. To the north-west the reverse sequence is observed. These latter $Hb_{rel}$ values are inconsistent with the concept of pre-deformation burial metamorphism described previously. Furthermore, the pattern of isocrysts in the north-west, cuts across stratigraphic and structural trends shown in figure 1.1.1. Values may be attributed to continued (post-Silurian) syn-sedimentary burial metamorphism beneath the Devonian basin separating the Graighead inlier and the Girvan Main Outcrop (Mykura, 1983). $B_o$ values in the western half of the Girvan Main Outcrop are difficult to contour. A linear zone of high pressure, co-incident with the poorly crystallized zone described above, is apparent. Both $Hb_{rel}$ and $b_o$ values (linear) parallel the curve of the Camregan Fault (fig 1.1.1.). High $b_o$ values in this region are thought to reflect movements on the Fault.

The eastern half of the Girvan Main Outcrop is characterized by well crystallized illite, displaying moderate $b_o$ values. The $Hb_{rel}$ and $b_o$ values are unlikely to have been generated during syn-sedimentary burial metamorphism, since crystallinities are better than for older strata. The region is isoclinally folded (chapter 1.1) and is bounded by faults to the north and south (fig 1.1.1.). For the most part, the outcrop is $<^1/_3$ km wide. The good $Hb_{rel}$ and $b_o$ values encountered may therefore reflect the high strain placed

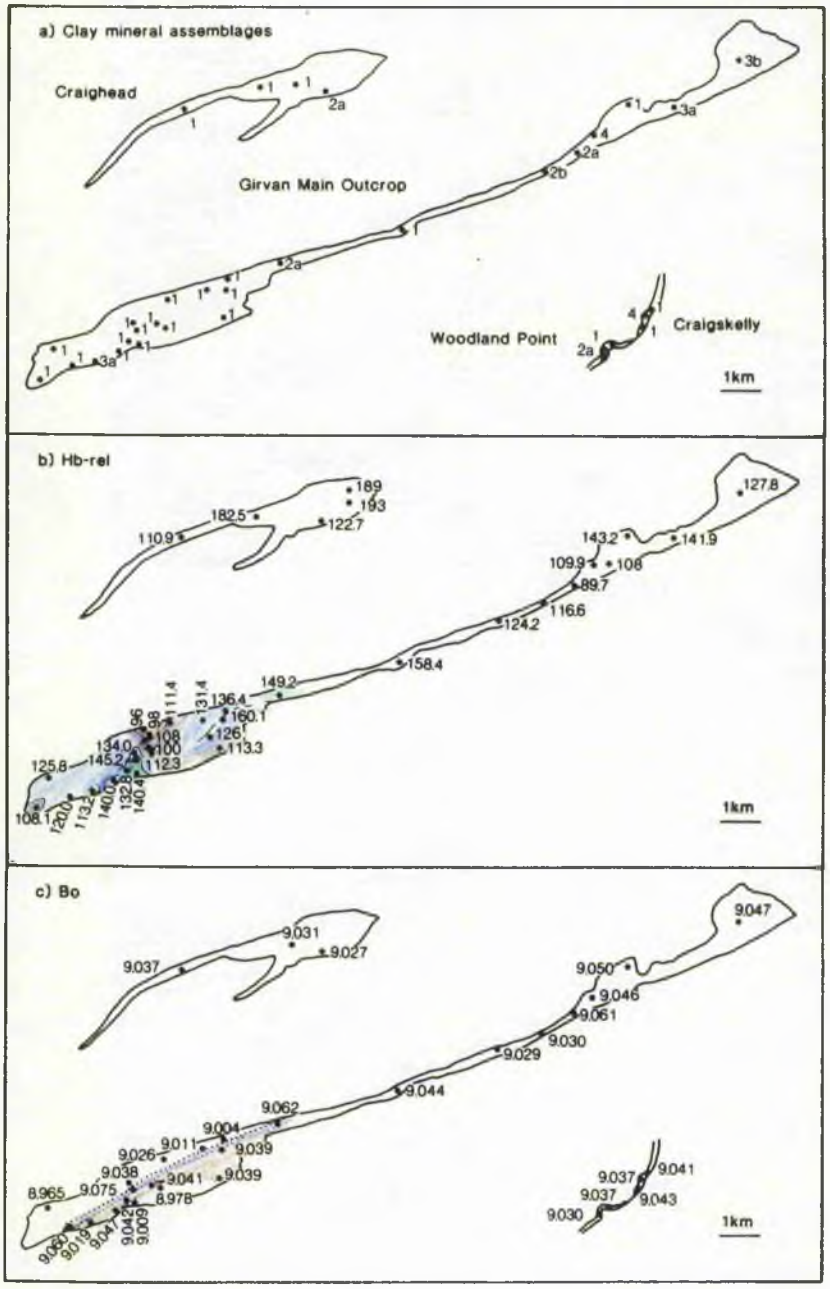


Fig. 1.5.6. Spatial variation of a)clay mineral assemblages b) illite crystallinity and c) bo-values, in the Girvan inliers.

KEY

localities

conodont locality

Hb-rel
140
130
120
110
100
90

Isocrysts at 10 Hb-rel intervals.

Bo
9.03-9.04
9.06-9.07

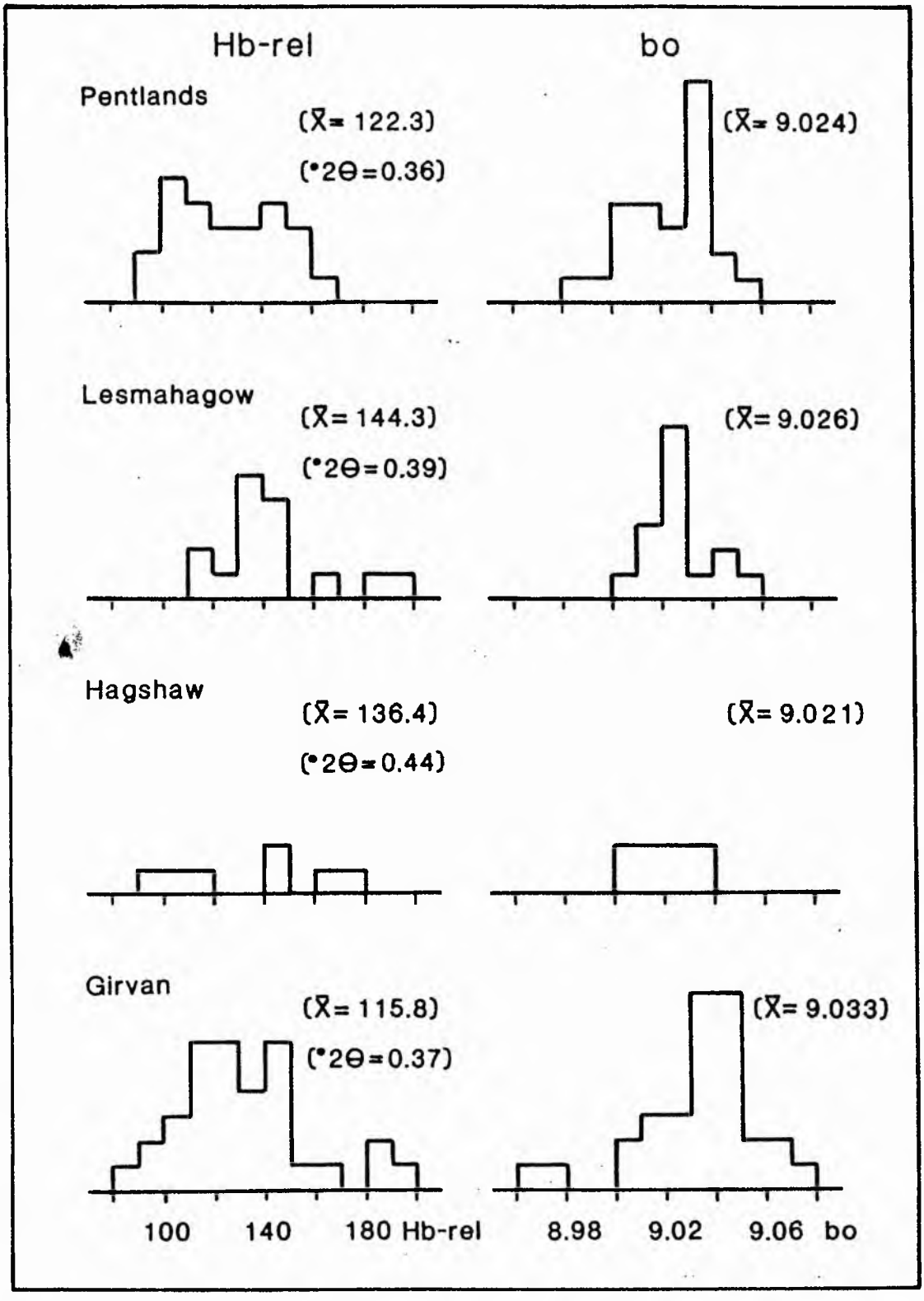


Fig. 1.5.7. Histograms to show the spatial distribution of crystallinity and bo values at each inlier.

upon the rocks in this area.

**Regional Variation**

All the Silurian inliers in the Midland Valley, show evidence (see previous section) of progressive burial metamorphism, which initiated in the Silurian and continued into Devonian times. Deep burial beneath Carboniferous sediments is not envisaged, since the southern Midland Valley was a topographic high of non-deposition (Mykura, 1983) throughout this period.

In addition to the local variation in metamorphic grade seen within the Midland Valley, histograms (fig 1.5.7) compiled from $Hb_{rel}$ and $b_o$ values suggest that the regional grade was different at each inlier. This variation is expressed by a study of the mean $Hb_{rel}$ values at each inlier. The poorest crystallinity is encountered at Lesmahagow ($\bar{x}$ - 144.3); grade increases eastwards to the Pentland Hills ($\bar{x}$ - 122.3), southwards to the Hagshaw Hills ($\bar{x}$ = 136.4) and westwards to Girvan ($\bar{x}$ - 115.8). Since progressive syn-sedimentary burial was the main cause of metamorphism everywhere, the variations above must be a function of either:-

i) variable thickness of Silurian strata

ii) variable thickness of Devonian strata

Both would give variation in the total burial depth.

The maximum thickness of Silurian strata is estimated (Cocks and Toghill, 1973) to be 3 km. The total thickness observed (fig 1.1.2) varies between each inlier (from 1400 m to 2200 m). The greatest accummulation of Silurian strata is to be found at Lesmahagow (fig 1.1.2). The clay mineralogy and illite

crystallinities however, indicate that Lesmahagow suffered the least metamorphism. By comparison, the highest grades of metamorphism are encountered at Girvan, where the Silurian succession is thinnest. The discrepancies between metamorphic grade and the thickness of Silurian sediments necessitates that Devonian strata comprised part of the burial sequence. It is not possible (Mykura, 1983) to determine detailed variations in original thicknesses of Devonian strata in the southern extremities of the Midland Valley. Estimates made by House *et al*, (1977) suggest that the Lower Devonian thinned westwards, from 2200 m in the Pentlands to 0 m in Lanarkshire (a local culmination of 2700 m is observable north-west of the Lesmahagow inlier). In the Girvan district the local thickness of Lower Devonian strata is assumed to be between 800-1600 m (Cameron and Stephenson, 1985). Following Mid Devonian deformation, the deposition of 0-640 m of Upper Devonian sediments occurred between Lesmahagow and the Pentland inliers (Mykura, 1983). Up to 425 m of Upper Devonian sediment was deposited in Ayrshire (Eyles *et al*, 1949). Deposition occurred in two south-easterly orientated basins separated by the tectonically uplifted Lesmahagow inlier.

The total estimated thickness of combined Silurian and Devonian strata is:-

a) Girvan 2300-3400 m

b) Lesmahagow 2200-2650 m

c) Hagshaw 2000 m

d) Pentlands 4100-4700 m

Measurements are for the depth of burial at the base of the sequences. These total thicknesses are in agreement with increased

metamorphic grade away from the Lesmahagow area. Furthermore, it confirms that metamorphism occurred in response to syn-sedimentary burial beneath a combined Siluro-Devonian sequence.

The minimum and maximum burial depths experienced by the Midland Valley Silurian was 2 km and 4.7 km respectively. Assemblage 2 and assemblage 3 are the predominant clay-minerals (chlorite, C-M, I-M where M = 20-30%) developed at 2 km. Whilst assemblage 1 clay-minerals (chlorite, illite M = 0 - 10%) are dominant at 4 km. In the Gulf Coast sediments (see section 1.5.2):-

i) I-M was present at 2 km, at 100-120 $^{o}$C

ii) C-M was present at 2-3 km, at 80-120 $^{o}$C

iii) the transformation of I-M to illite occurred at 4 km, at 175 $^{o}$C

iv) illite occurred at 5-7 km, at 225-310 $^{o}$C.

These transformations are compatible with those observed in the Midland Valley Silurian, and are developed over similar burial depths. The above transformations are consistent with metamorphism under a geothermal gradient of 40-50 $^{o}$C km$^{-1}$. By inference the geothermal gradient during syn-sedimentary burial metamorphism of the Silurian successions, must have equalled 40-50 $^{o}$C km$^{-1}$.

### 1.5.4 Conclusions

The Silurian successions of the Midland Valley experienced sub-prehnite-pumpellyite facies burial metamorphism beneath Siluro-Devonian cover sequences. Local variations in metamorphic grade reflect thinning of the sedimentary successions eastwards and

westwards from the Lesmahagow area. Burial depths varied from 2 to 4.7 km, whilst mineralogical transformations reflect burial under a geothermal gradient of 40-50 $^{o}C\ km^{-1}$.

In view of the relative simplicity of the metamorphic trends (in crystallinty, $b_o$ and clay mineralogy), the metamorphic episode must have been contained within the Midland Valley. Indicating that the Midland Valley had a very different metamorphic history compared to that of the Southern Uplands.

**Scope for further research**

To establish the continuity of metamorphic grade across the Silurian-Devonian boundary.

To investigate the effects of grain size on crystallinity.

# PART TWO

# METAMORPHISM IN THE CARBONIFEROUS VOLCANICS

## Chapter 2.1 Geological Background

### 2.1.1 Aims

The aim of chapter 2.1, is to establish the geological features of the Carboniferous volcanics and associated strata, in the Midland Valley of Scotland. The status of metamorphism in the Carboniferous volcanics, pre completion of this thesis on burial metamorphism, is reviewed. Factors which may have a direct bearing upon burial metamorphic conditions are discussed in detail.

### 2.1.2 Regional Setting (volcanics)

#### i) Occurrence

Igneous strata (fig 2.1.1) (intrusive, extrusive and volcaniclastic) comprises much of the Carboniferous sequence of the Midland Valley of Scotland.

To the west, outcrops in the Campsie Hills, the Kilpatrick Hills, the Renfrewshire Hills and the Lanarkshire Region (Richey *et al's* (1930) Dunlop-Eaglesham-Darvel Uplands) unite to form the extensive Clyde Plateau Lavas (nomenclature after Macdonald, 1975). These lavas continue eastwards subsurface (Hall, 1971) where they overlap, in the Rashiehill borehole (fig 2.1.1), with the westward extension of the Bathgate volcanics (Anderson, 1951). The northern-most extension of the Clyde Plateau Lavas may be seen in the Cleish Hills (fig. 2.1.1).

Smaller lava fields are found in Midlothian (Craiglockhart Hill and Arthur's Seat, Edinburgh), East Lothian (the Garleton Hills) and in Fife (Burntisland Anticline).

Many explosive vents occur. Either:

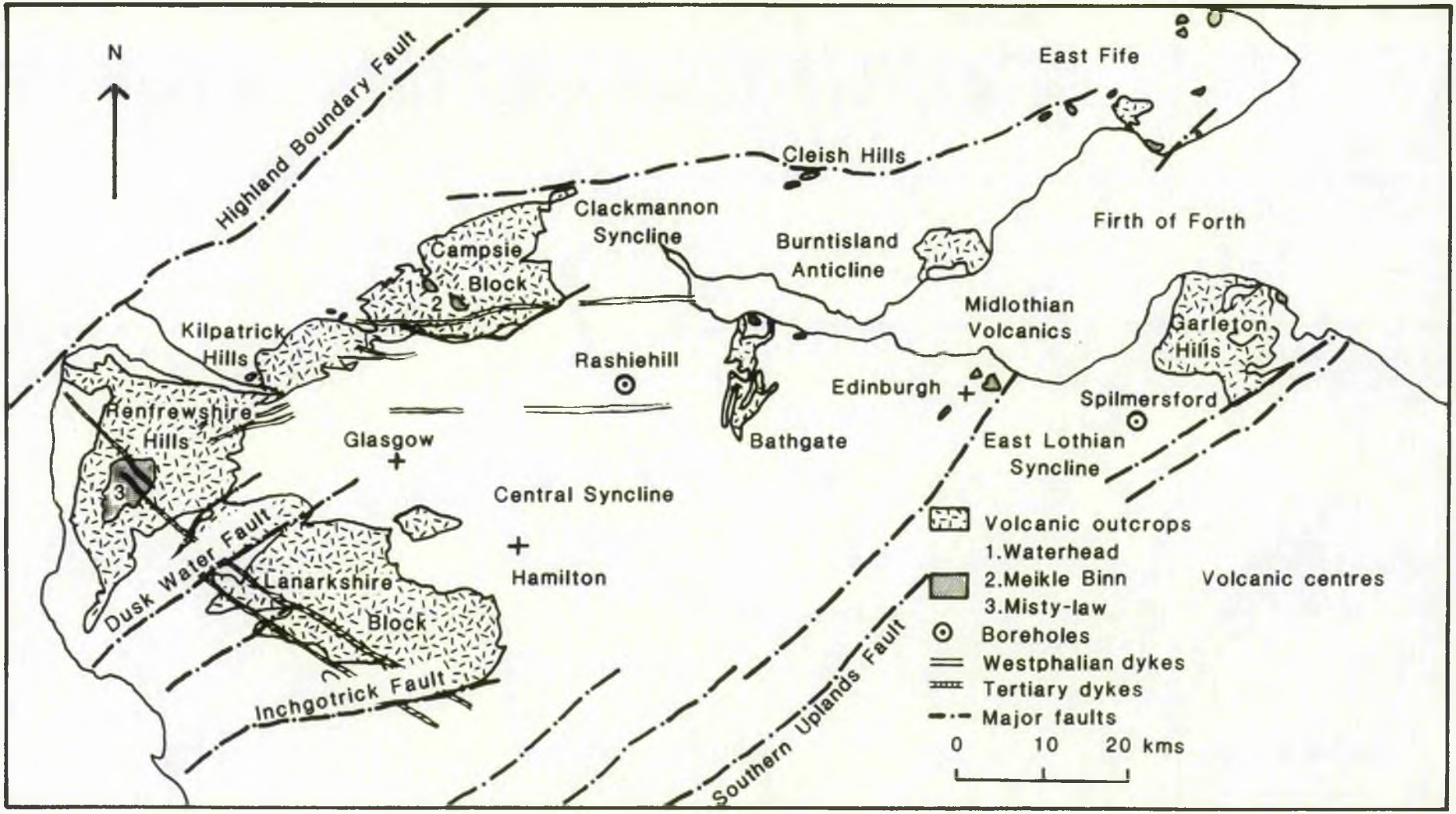


Fig.2.1.1.Distribution of studied Carboniferous volcanics in the Midland Valley,Scotland

a) punctuating the sedimentary sequence, as in East Fife and Ayrshire

or

b) as small centres of eruption within the Clyde Plateau Lavas, such as the Waterhead and Meikle Binn vents of the Campsies, and the Misty Law vent, Ayrshire (fig 2.1.1).

ii) nature and timing of events

Dinantian volcanism in the western Midland Valley was marked by the thick accumulation (<1 km - see part iii) of the Clyde Plateau Lavas. The lavas represent a sequence of flood basalts (Plate 6), which were either extruded directly upon Upper Devonian strata, or were paraconformable with the Calciferous Sandstone Measures (G.S. Sheet 31). Along the southern and western margins of the Campsies, and in the Kilpatrick Hills and Lanarkshire block (fig 2.1.1), the base of the volcanic pile is marked by an accumulation of tuffs. Macdonald (1975), regarded these to be the products of phreato-magmatic activity. Further evidence of pyroclastic activity is rare, occurrences tend to be locally concentrated around the small vents shown in fig 2.1.1. Two major volcanic centres (Macdonald, 1975) occur halfway through the sequence (fig 2.1.1), dividing the pile into an Upper and Lower lava series.

Sedimentary intercalations in the Clyde Plateau Lavas are rare, indicating that volcanism kept pace with regional subsidence and sedimentation. Scoraceous surfaces and reddened-bole testify to both inter-flow and post-eruption subaerial weathering.

Outliers of Calciferous Sandstone age (in the Campsies) and of Limestone Group and Limestone Coal age (Lanarkshire Block) indicate

Plate 6: Typical flood basalt scenery in the Clyde Plateau Lavas. Photograph taken looking eastwards over Loch Humphrey. Individual flow units dip southwards. Overlay: - - fault bounded margin of area; - mineralogical isograds parallel contours (see text, chapter 2.2 for explanations of mineral zones).

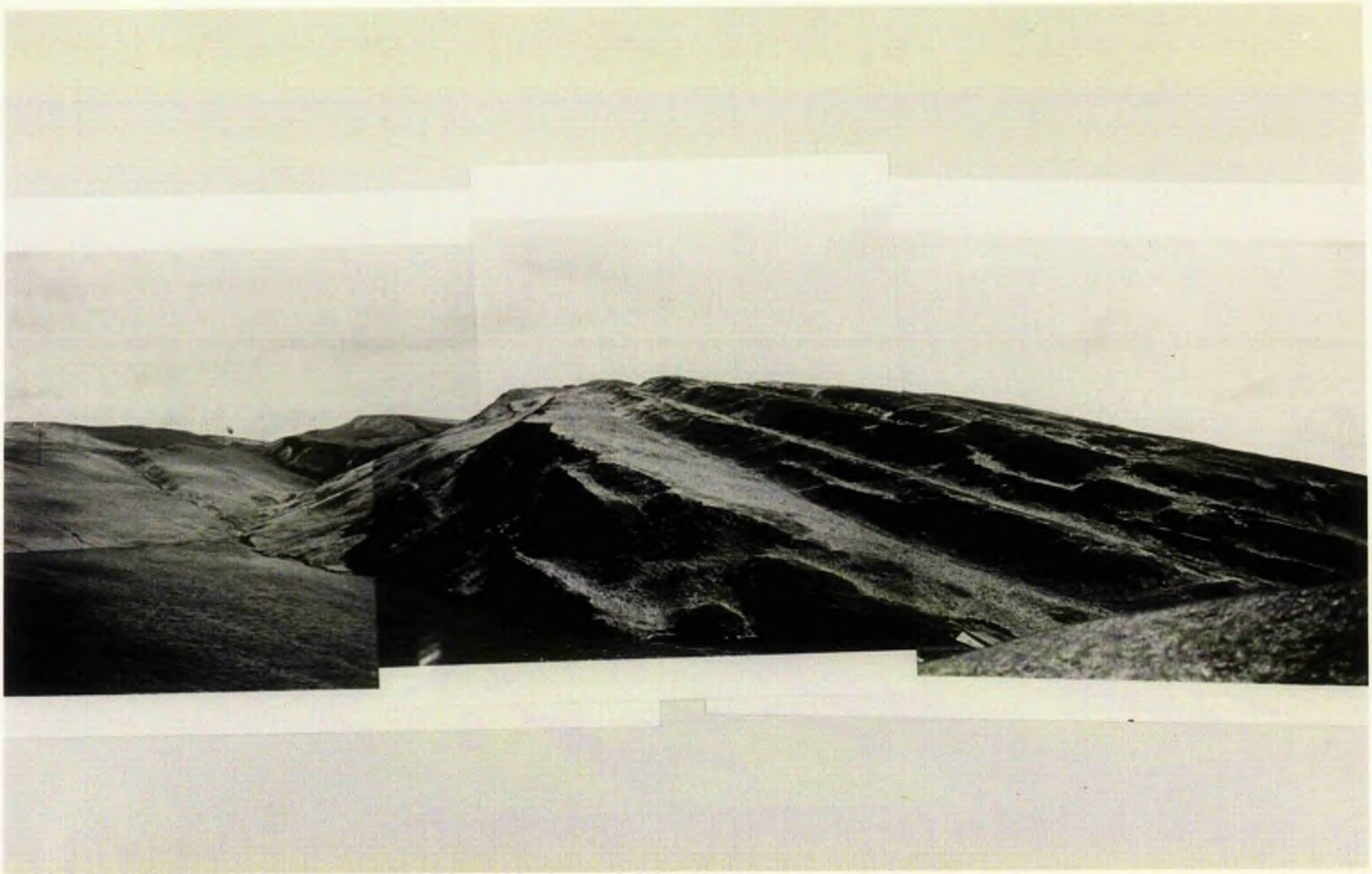

that the Clyde Plateau Lavas were transgressed by variable thicknesses of strata.

In the eastern Midland Valley, Dinantian volcanism (Cameron and Stephenson, 1985) occurred in Midlothian and in the Garleton Hills. At Burntisland and in the Bathgate Hills, volcanism continued into the Upper Limestone Group. Sedimentary intercalations (G.S. Sheets 31; 32; 33; 40), demonstrate that volcanism occurred at different times in geographically distinct areas (see figure 2.1.2). Intercalations are common at Bathgate (fig. 2.1.1), suggesting that there was a marked failure of volcanic output with time.

By Passage Group times, volcanism was concentrated at small vents in Ayrshire and Fife. Here the products of volcanism were essentially pyroclastic. Francis and Hopgood (1970) regarded the deposits to be the result of Surtseyan type activity.

Three intrusive episodes are recognized in the Midland Valley.

a) a series of NE-SW trending Dinantian dykes. Seen,
   1) at outcrop in the base of the Renfrewshire volcanics; where Richey *et al,* (1930) believed them to be the conduits through which the lava pile was fed.
   2) swarms associated with the Misty law and Meikle Binn (fig 2.1.1) volcanic centres (Richey, 1939)

b) a suite of alkali-olivine dolerite sills, comagmatic (Francis 1983) with the extrusive rocks (290-313 Ma, de Souza, 1979). The most volumetrically significant episode of intrusion occurred during late Westphalian/early Stephanian times, when a suite of E-W trending quartz-dolerite dykes and sills were emplaced. Although the dykes mainly outcrop in the sedimentary sequences of the eastern Midland Valley, several extend westwards to the

Clyde Plateau Lavas.

c) a series of NW-SE aligned dykes, which traverse the Clyde Plateau Lavas to the south of the Clyde. These dykes are associated with the Tertiary magmatism of Mull (59.5 ± 2.9 Ma, Evans *et al*, 1973).

iii) **Penecontemperaneous sedimentation and strata thicknesses.**

Continuous deposition occurred throughout the Carboniferous of the Midland Valley. Sediments accummulated in the two major basins of the Central Coalfield and East Lothian (fig 2.1.1). Barriers between basins were formed by penecontemperaneous volcanism.

The earliest sediments are the playa lake and fluvial deposits (George *et al*, 1976) of the Calciferous Sandstone Measures. Open marine conditions were introduced during the Lower Limestone Group, and continued into the Upper Limestone Group. A hiatus in marine sedimentation is marked by the intervening deltaic Limestone Coal Group. Isopachytes (Goodlet, 1957) for the Limestone Series indicate that much thinning of sediments occurred over volcanic areas. This pattern of sedimentation is characteristic of the later formations also. The Passage Group and the Lower, Middle and Upper Coal Measures, represent a return to deltaic conditions.

Details of the sedimentary successions, as recorded by MacGregor (1930; 1960), are given in figure 2.1.2; together with the present-day thickness of sedimentary and volcanic rocks. Estimates of sedimentary thicknesses are given in the works of Freshney (1961), George *et al*, (1976), Ramsbottom *et al*, (1978), Francis (1983) and Cameron and Stephenson (1985). Volcanic thicknesses are given by MacGregor and MacGregor (1961), Mitchell and Mykura (1962), Davies

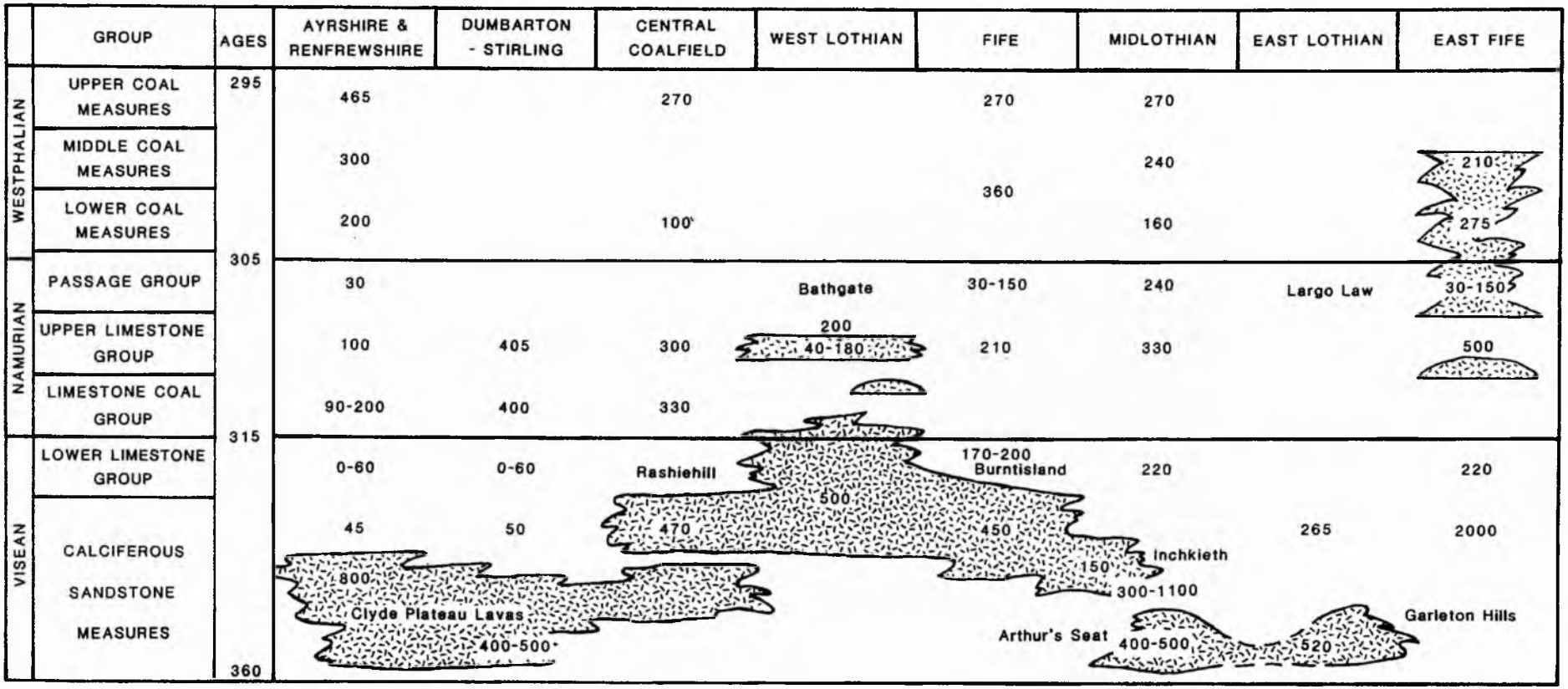


Fig.2.1.2. Stratigraphic thickness variations of Midland Valley volcanics and sedimentary formations

Thicknesses quoted in metres (see text for references : dates, after de Souza,1979). Volcanics

(1936), Hall (1973), Alomari (1980), Francis (1983) and Davidson *et al*, (1984).

### 2.1.3 Igneous Petrology

The Carboniferous volcanics are composed of associated macro- and micro-porphyritic basalt. Field terms (table 2.1.1), dependant upon the size and type of the main phenocryst(s), were devised by MacGregor (1928). Macdonald (1975) and MacDonald and Whyte (1981) applied modern basalt terminology (table 2.1.1) to MacGregor's (1928) categories. Basically:-

i) Jedburgh and Markle basalts are equivalent to hawaiites,

ii) Dunsapie and Dalmeny basalts are equivalent to 'true basalt'

iii) Hillhouse basalts are equivalent to basanites

iv) Craiglockhart basalts are equivalent to ankaramites.

Numbers i) to iii) represent a temporal succession. Furthermore, basalts from each geographically distinct area, have a distinctive magmatic lineage (Macdonald, 1975) recognized in terms of silica undersaturation, Fe/Mg ratio, $Na_2O/K_2O$ ratios and $TiO_2$ and $P_2O_5$ content. In addition, each geographically distinct area retained its own distinctive trace element chemistry (Macdonald, 1980) over periods of up to 50 Ma.

In addition to these more basic rocks of the Midland Valley, there is a wide range of associated nepheline- and/or hypersthene-normative intermediate lavas of Dinantian age in the Clyde Plateau Lavas.

Table 2.1.1

| Basalt type of MacGregor (1928) | Phenocrysts | | Chemical classification of Macdonald (1975) | Type locality |
|---|---|---|---|---|
| | abundant | sometimes present in lesser amounts | | |
| Macroporphyritic (phenocrysts >2 mm) | | | | |
| Markle | plag | ±ol, Fe-oxide | plag ±ol ±Fe-oxides-phyric basalts, basaltic hawaiites or hawaiites | Markle Quarry, East Lothian (flow) |
| Dunsapie | plag+ ol + cpx | ±Fe-oxide | ol-cpx-plag-Fe-oxides-phyric basaltic hawaiites, or ol-cpx-plag-phyric basalts | Dunsapie Hill, Edinburgh (vent intrusion) |
| Craig-lockhart | ol + cpx | | Ankaramite | Craiglockhart Hill, Edinburgh (flow) |
| Microporphyritic (phenocrysts <2 mm) | | | | |
| Jedburgh | plag | ±ol, Fe-oxide | plag ±ol ±Fe-oxides-phyric (basaltic) hawaiites, (occasionally basalt) | Little Caldon, Stirlingshire plug . Also in Jedburgh area |
| Dalmeny | ol | ±cpx, plag | ol±cpx-phyric basalt | Dalmeny Church, West Lothian (flow) |
| Hillhouse | ol + cpx | | ol-cpx-phyric basalt (rarely basanite) | Hillhouse Quarry, West Lothian (sill) |

plag - plagioclase ol - olivine cpx - clinopyroxene

Table Nomenclature of basic igneous rocks of Carboniferous age in the Midland Valley

### 2.1.4 Previous references to metamorphism in the Carboniferous Volcanics

During the Carboniferous the Midland Valley of Scotland was too far removed from the centre of Hercynian tectonics to have suffered regional dynamothermal metamorphism. Metamorphism within the Midland Valley must therefore be attributed to burial to hydrothermal activity or to contact against cooling igneous bodies.

Until now, burial metamorphism in the Midland Valley volcanics has been referred to loosely as 'alteration', (eg calcite, chlorite, quartz, chalcedony, haematite and clays) from veins, amygdales and scoriaceous surfaces of basalt. These minerals are generally considered (MacDonald and Whyte, 1981; Cameron and Stephenson, 1985) to be the result of widespread deuteric alteration of lavas immediately after eruption. Or, they form part of metasomatic zones surrounding intrusions (eg at Meikle Binn and Dungoil, Campsies - Whyte and MacDonald, 1974). The same minerals have been recorded in thin-section, infilling interstices and replacing mafic minerals (olivine in particular) (MacGregor and MacGregor, 1961).

Similarly, altered lavas have been recorded from boreholes (Anderson, 1951; McAdam, 1974); rhyolites show evidence of silicification, whilst basalts are albitized, chloritized, hydrated or carbonated (MacDonald, 1973). There is even evidence (Goswami, 1963) for post-magmatic or late-stage oxidation ($Fe^{3+}$ of lavas could not be explained by primary iron ore contents alone).

Evidence from the Rashiehill borehole, Stirlingshire (fig. 2.1.1), (Anderson, 1951) that alteration is most intense in the deepest flows, suggests a relationship between the intensity of alteration and burial depth. However, the change in the degree of

alteration also corresponds with the move from upper Dalmeny and Dunsapie lavas, to lower Jedburgh and Markle lavas. This suggests that alteration may also be a function of the mineralogy and geochemistry of a particular lava type. Such relationships are discussed further in chapter 2.2.

At Spilmersford borehole (fig 2.1.1), McAdam (1974) established that such alteration, for the East Lothians at least, predated neighbouring unaltered sill or dyke intrusion, confirming that 'alteration' was a separate event. However, should the dyke have been impermeable, a similar alteration pattern would have arisen.

In addition to the aforementioned secondary minerals, numerous zeolites (eg stilbite, heulandite and analcime) and related minerals (eg prehnite and apophyllite) have been recorded (Heddle, 1901; Goodchild, 1903), from the Clyde Plateau Lavas in particular. Cameron and Stephenson (1985) believe the zeolites to be a product of hydration, penecontemperaneous with lava extrusion. However, the association of zeolites in the Kilpatrick Hills with feldspathic mugearites and with Markle and Jedburgh type basalts only (Grabham, 1925), suggests that this is unlikely.

Observations of zeolites from basic rocks in Ireland (Walker 1950, 1960a) and from Iceland (Walker, 1960b) and from volcaniclastic rocks in New Zealand (Coombs *et al*, 1959; Boles and Coombs 1975, 1977; Houghton 1982; Sameshima 1978, 1986) have led to the following discoveries.

1 That zeolitization was late in respect to the main volcanic episode.
2 That individual zeolites species predominate in successive zones

which cut across the lava stratigraphy and as such represent isograds parallel to the ancient landsurface.

3 That lava thicknesses of some 200 m, with empty vesicles, overlies amygdale-bearing lavas, providing a blanket zone within which zeolites cannot develop because of too low temperature.

Evidence from Midland Valley

a) boreholes 1 - 'alteration' predates and is unrelated to intrusion

2 - increase in the intensity of 'alteration' with depth

and from

b) the Kilpatricks - zeolites essentially developed in feldspathic rocks, suggest much of what has previously been described as 'alteration' by various researchers, is in fact burial metamorphism.

Effects of contact metamorphism are most clearly seen in Carboniferous sediments. Low grade thermal alteration of sediments has resulted in the production of a local rock-type, known as white-trap, composed of kaolinite, chlorite, amorphous silica and carbonate. The alteration process (Mykura, 1965) is caused by the reaction of materials with gases distilled from heated pore-waters of carbonaceous sediment during intrusion.

In the lava piles, contact metamorphism by dykes is rarely observed, since insufficient time has lapsed to allow for cooling of the lavas before the numerous dykes were intruded. Chilled margins are best displayed where Tertiary dykes are intruded into

Carboniferous Volcanics eg at Loanhead Quarry, Beith (locality CV69, appendix 2.2.1).

### 2.1.5 Structure

The Midland Valley, is a graben developed in association with the Upper Palaeozoic rift systems of Scandinavia and America (Francis, 1978a), along lines determined during the Lower Palaeozoic (Kennedy, 1958; George, 1960). Three distinct structural episodes effected the Carboniferous sequence within the graben.

The earliest event (Dinantian to Lower Westphalian) is characterized by NE-SW trending faults parallel to the marginal graben faults (fig 2.1.1) eg the Dusk Water and Inchgotrick Faults. In the eastern Midland Valley, deformation is characterized by the development of the syn- sedimentary folds of the Clackmannan and Midlothian synclines (Hall, 1973). Here, angular unconformities separating the Passage Group from underlying strata suggest that this early tectonic phase should be further divided into a pre- and post-Namurian episode. In the western Midland Valley, syn-sedimentary movement on major faults (Francis, 1978a) similarly affected sedimentation. Lateral thickness variations of 75-100 m across faults are recorded (Francis, 1978a). The Inchgotrick and Dusk Water Faults (fig 2.1.1) also acted as barriers to the spread of volcanics (Hall, 1973), causing ponding of the Clyde Plateau Lavas eastwards towards the Central Coalfield (Richey *et al*, 1930). Similar faults are also thought (White and MacDonald, 1974; Francis, 1978b) to have controlled the location of eruption throughout the period.

The second structural phase of the Carboniferous is

characterized by the development of E-W faults. This event is dated at pre 295 Ma (de Souza, 1979), since many of the faults in the eastern Midland Valley have 295 Ma old quartz-dolerite sills intruded along their course.

Evidence for a third structural phase is described from boreholes (Anderson, 1951), where NW-SE aligned faults occur.

### 2.1.6 Geophysics

Geophysical work has been undertaken in the Midland Valley, mainly aimed at determining

i) the character, thickness and sub-surface expression of the lavas
ii) the presence of intrusive bodies deeper in the crust
iii) the deep structure of the Midland Valley.

i) Borehole logging at Rashiehill (Anderson, 1963) and Spilmersford (Allsop, 1974) determined the lithology and extent of alteration at depth. Hall and Dagley (1970) related high frequency magmatic anomalies to the subsurface expressions of Carboniferous lavas and sills. Consequently, Hall (1971 and 1973) used seismic reflections to determine the westward thinning of lavas from 470 m in the vicinity of Rashiehill to zero at a distance of 1.5 km, and to observe similar thicknesses variations (of up to 1 km) across NE-SW trending faults. Estimations of thicknesses within the Clyde Plateau from seismic surveys indicate the presence of 500 m of lava in the Medox area (fig 2.1.1) (Davidson *et al*, 1984) and of 900 m beneath sediments to the south of the Campsie Fault (Cotton, 1968). Magnetic

surveys (Alomari, 1980) south of the Campsie Fault however, suggest that thicknesses of lava are nearer to 500 m. Such problems arise in interpreting the thickness of the volcanics in the Midland Valley because the lavas are not very different in their seismic velocity from the surrounding sediments (J.J. Doody, personal communication 1985). This is presumably because the lavas are so altered, and because of the high dyke density in the sediments.

ii) Geophysical evidence has revealed the presence of three major intrusions, concealed beneath the Carboniferous rocks of the Midland Valley. In the Campsies, magnetic anomalies (Cotton, 1968) located a gabbroic intrusion underlying the volcanics in the vicinity of the Meikle Binn or Waterhead vents. However, there are so many contributors to gravity anomalies in the western Midland Valley, that any gravity interpretations must be viewed with caution (J.J. Doody, personal communication, 1984).

Further east, gravity anomalies have been located beneath sediments at Bathgate and Hamilton (fig 2.1.1) (Alomari, 1980; Davidson *et al*, 1984). At Hamilton the presence of a gravity low (+4 mgal, Davidson *et al* 1984) devoid of any magnetic expression (Alomari, 1980) suggests that the anomaly is related to an acid igneous intrusion. At Bathgate, a gravity high (+24 mgal) corresponds with an area of high density. The source of the anomaly is believed to be (Davidson *et al*, 1984) an ultrabasic pluton.

iii) Hall *et al*, (1984), determined that the Carboniferous basins sit upon a reflective lower crust with velocities of 5-7 $km^{s-1}$. Seismic velocities (Vp) of 3.0-3.7 $km^{s-1}$ and of 4.0-5.5 $km^{s-1}$ (Davidson *et*

*al*, 1984) have been recorded from:-

a) the Carboniferous and Upper Devonian sediments

b) the Lower Devonian and Lower Palaeozoic sediments

Immediately below these, rocks with P-wave velocities (Vp) of 6.0-6.1 $km^{s-1}$ (Davidson *et al*, 1984) are recorded. Seismic velocities correlate closely with those of LISPB layer 2 (~6.4 $km^{s-1}$, Bamford *et al*, 1977). The presence of granulitic rocks in Carboniferous diatrems (Upton *et al*, 1984) indicate that these P-waves arise from 1000 Ma old basement (Watson, 1983) underlying the Midland Valley.

### 2.1.7 Conclusions

Major faults controlled the locus and thickness of igneous and sedimentary rocks throughout the Carboniferous. Volcanism was characterized by the early effusion of flood basalts in the Clyde Plateau Lavas and Garleton Hills, and by later more explosive activity in Fife. The distinctive composition of the lavas implies long lasting heterogeneity of the underlying mantle from which basaltic magmas were derived by variable degrees of partial melting at variable levels in the mantle. There is evidence for widespread zeolitization in the volcanics which has been loosely described as alteration and has been attributed to deuteric action immediately after eruption. No interpretation has been made in terms of low grade metamorphism.

## Chapter 2.2

## Hydrothermal Alteration in Carboniferous Midland Valley Lavas.

### 2.2.1 Aims

1 To characterize the styles of hydrothermal alteration experienced in the Carboniferous Volcanics of the Midland Valley.

2 To determine the regional distribution of hydrothermal alteration styles.

### 2.2.2 Introduction

This study has recognised three hydrothermal alteration styles in the Carboniferous volcanics of the Midland Valley, Scotland. The different alterations constitute:-

i) greenstones

ii) amygdale assemblages

iii) palaeo-geothermal plumes

The evidence presented below shows that several geographically distinct areas may have experienced more than one kind of hydrothermal activity. Field evidence for the characterization of the alteration styles is discussed below. Reference is made, wherever possible, to the development of similar examples of hydrothermal alteration elsewhere in the world.

### 2.2.3 The greenstones

Greenstone alteration is a characteristic feature of the eastern Midland Valley. The localities are shown in figure 2.2.1 and

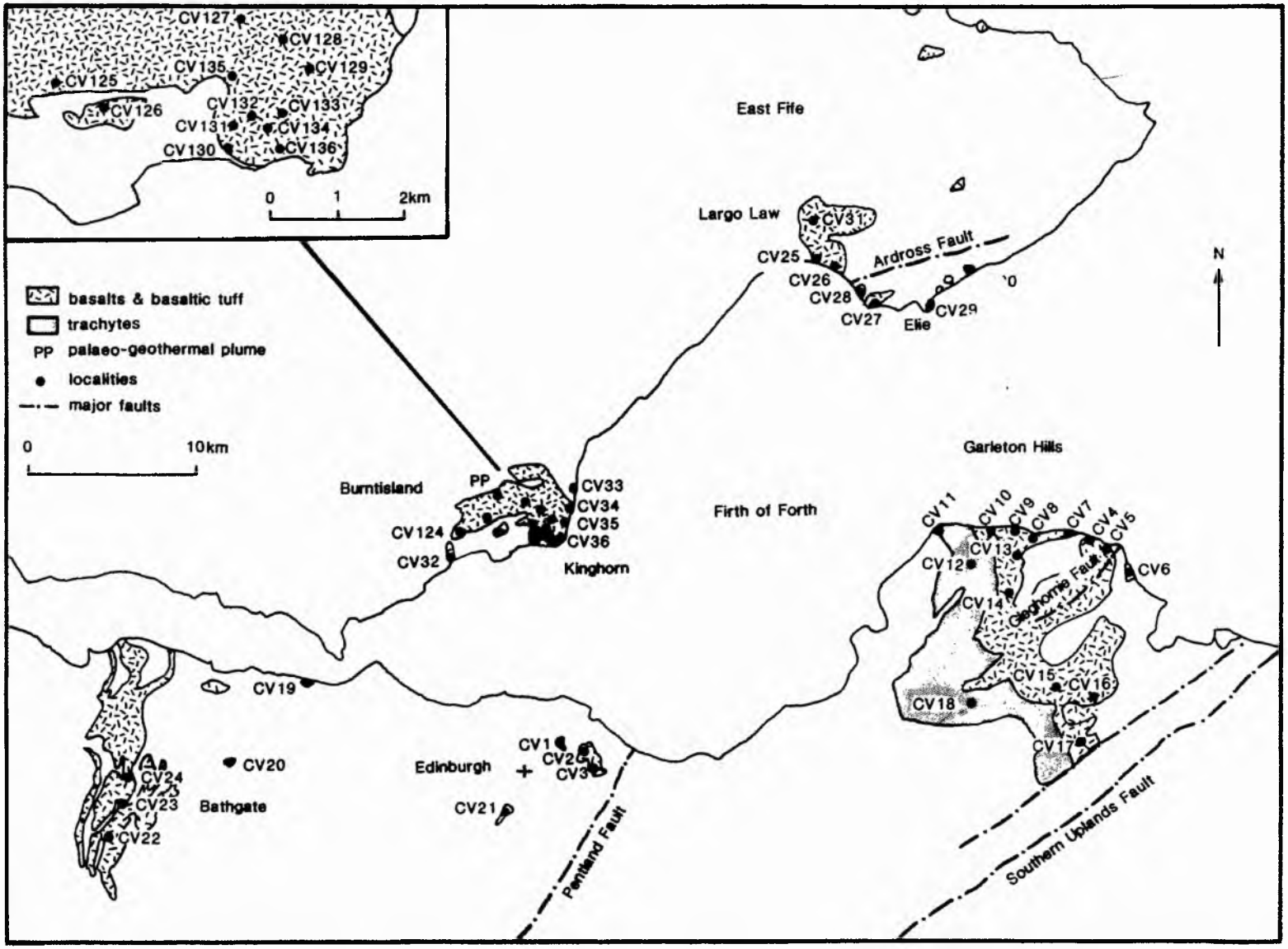


**Fig.2.2.1. Sample localities in the eastern Midland Valley.**

are listed in appendix 2.2.1.

This style of hydrothermal alteration owes its name to the intense green colouration imparted to tuffs, agglomerate and associated basalt, by the development of chlorite. Chloritic alteration is presumed to be the product of exchange between the volcanics and the surrounding fluids. These may have been:-

i) meteoric; reddened bole is developed at several localities eg CV7, Fig 2.2.1, indicating that a long period of subaerial weathering post-dated the extrusion of the volcanics. Meteoric water (and/or seawater, following later submersion) must therefore have entered the system after extrusion and cooling.

ii) magmatic (discussed later)

iii) seawater; given that the Clyde Plateau Lavas represent a vast subaerial accummulation of volcanics which are devoid of greenstones, and that the eastern Midland Valley volcanics have extensive greenstones, but were periodically submerged by the sea (chapter 2.1), it seems likely that the presence of seawater was a major factor to the development of the greenstones. Fluid sources during greenstone alteration are discussed further in chapter 2.6.

Calcification is important during greenstone alteration. Products (of several generations) occur as cements in agglomerate (Plate 7a) and as druzy vein filling material. At Kinghorn, North Berwick and Dunbar (Fig 2.2.1) vein calcite is associated with quartz and barytes. Such gangue assemblages, suggest that the minerals were derived from metasomatic fluids associated with vent intrusion, as

does:-

i) abundant evidence for forceful vein intrusion (evidence for, and causes of hydrofracturing are discussed further in chapter 2.7).

ii) the net increase in veining towards vents.

At localities eg CV33 (see Fig 2.2.1), where the volcanics interdigitate with marine sediments, there is a noticeable increase in mineralization at the base of the greenstone units. This suggests that many veins owe their origin to the expulsion of volatiles from the wet sediments beneath.

**2.2.4 Amygdale assemblages**

2.2.4.1 Introduction

Amygdales in basalt are commonly infilled with hydrated minerals plus quartz and calcite. Heddle (1924) provided extensive documentation of the distribution of zeolite species in the Carboniferous Volcanics of the Midland Valley in particular. Zeolite distributions in fossil geothermal areas were recorded by Walker (1951; 1960), Coombs (1954; 1971), Coombs *et al*, (1959) Miyashiro and Shido (1970), Jolly (1970), Boles and Coombs (1975) and others. These researchers showed that zeolites:-

i) show consistent variations in amygdular assemblages

ii) provide direct evidence of hydrothermal alteration

iii) form distinctive zones as a function of progressive burial metamorphism.

Table 2.2.1a

| Name | Formula | Crystal System |
|---|---|---|
| Analcime | $Na_2(Al_2Si_4)O_{12}\cdot 2H_2O$ | Cubic |
| Chabazite* | $Ca(Al_2Si_4)O_{12}\cdot 6H_2O$ | Hexagonal-Trigonal |
| Ferrierite* | $(NaK)_4Mg_2(Al_6Si_{30})O_{72}(OH)_2\cdot 18H_2O$ | Orthorhombic |
| Gmelinite* | $(Na_2Ca)(Al_2Si_4)O_{12}\cdot 6H_2O$ | Trigonal |
| Gonnardite* | $Na_2Ca[(AlSi)_5O_{10}]_2\cdot 6H_2O$ | Monoclinic |
| Heulandite | $CaNa_2(Al_2Si_7)O_{18}\cdot 6H_2O$ | Monoclinic |
| Laumontite | $Ca(Al_2Si_4)O_{12}\cdot 4H_2O$ | Monoclinic |
| Mesolite | $Na_2CA_2[(Al_2Si_3)O_{10}]_3\cdot 8H_2O$ | Mono + Tri-clinic " |
| Mordenite* | $(Na_2K_2Ca)(Al_2Si_{10})O_{24}\cdot 7H_2O$ | Orthorhombic |
| Natrolite | $Na_2(Al_2Si_3)O_{10}\cdot 2H_2O$ | Orthorhombic |
| Stilbite | $(CaNa_2K_2)(Al_2Si_7)O_{18}\cdot 7H_2O$ | Monoclinic |
| Thomsonite | $NaCa_2[(AlSi_5)O_{10}]_2\cdot 6H_2O$ | Orthorhombic |
| Wairakite | $Ca(AlSi_2O_6).H_2O$ | Monoclinic |
| Apophyllite | $KCa_4(Si_4O_{10})_2F\cdot 8H_2O$ | Tetragonal |
| Prehnite | $Ca_2Al_2Si_3O_{10}(OH)_2$ | Orthorhombic |

Table 2.2.1b

| Name | Formula | Crystal System | Reference |
|---|---|---|---|
| Brewsterite | $SrBa[Al_4Si_{12}O_{32}]\cdot 10H_2O$ | Monoclinic | Heddle 1901; 1924 |
| Edingtonite | $Ba_2[Al_4Si_6O_{20}]\cdot 8H_2O$ | Tetragonal | " " " |
| Harmotome | $Ba_2[Al_4Si_{12}O_{32}]\cdot 12H_2O$ | Monoclinic | " " " |
| Phillipsite | $(Ca_{0.5}NaK)_6[Al_6Si_{10}O_{32}]\cdot 12H_2O$ | Monoclinic | " " " |

Table 2.1. Amygdale minerals of the Midland Valley Carboniferous: a) collected by L J Evans b) collected by Heddle (1901; 1924); * denotes new zeolite occurrences.

In this section, the lateral distribution of zeolites in the eastern Midland Valley and in the Clyde Plateau Lavas are considered. Associated vein assemblages are also discussed and their relationship to the amygdular assemblages determined.

2.2.4.2 Identification of hydrous silicates

Euhedral hydrous silicates were identified in the field by their crystal topologies (Plates 8, 9, 10). Where this was not possible, crystals in amygdales and veins were handpicked and subjected to X-ray diffraction. This was carried out according to the conditions listed in chapter 1.3. Identification was made by reference to the powder diffraction files. The results of this study were used as an aid in subsequent field-work and in the optical study (chapter 2.3) of the same samples. Several species have been identified upon the basis of microprobe analyses (chapter 2.4) only. Table 2.2.1(a), comprises a list of those hydrous silicates found. This includes six new (* - see table 2.2.1) zeolite occurrences in the Midland Valley of Scotland. Table 2.2.1(b), are additional species collected by Heddle (1903), that were not found during preparation of this thesis.

2.2.4.3 General characteristics of amygdular horizons.

Basalt flows are composed of a middle massive layer (MML) and of an upper and lower amygdaloidal layer (UAL and LAL, respectively; Walker, 1972) (Plate 7b). In the field, alteration is dominant in the UAL and LAL; undoubtedly, because of enhanced permeability and porosity controls in these horizons. [Porosity and permeability as factors limiting the extent of hydrothermal alteration are discussed

Plate 7A: Photograph of calcite cemented greenstone agglomerate. Bottom left, consolidated ash. Top right, basaltic clasts traversed by late calcite veins. (CV10 Garleton Hills)

Plate 7B: Photograph of lava tube in metabasalt infilled with early platy heulandite (heu) and late druzy quartz (qtz). (CV97 Gargunnock Hills, The Campsies)


OLYMPUS

in chapter 2.7. Whilst, alteration in the MML is discussed in chapter 2.3].

In general, there is a relationship between the size of an amygdale and the number of infilling layers. Usually the smaller amygdales have one layer; larger amygdales have as many as four layers. By comparing the infill sequence of the large amygdales with those of the small amygdales, it is obvious that the small amygdales were infilled first. Larger amygdales must therefore have been progressively infilled, and reflect either:-

i) changing saturation levels in one hydrothermal fluid with time

or

ii) the introduction of several hydrothermal fluids of contrasting composition

Evidence of fluctuations in supply are provided by initially half-filled vesicles or geodes. Most of which, have been filled in a subsequent hydrothermal episode. Precipitates are predominantly sodic (eg analcime, natrolite) or calcic (eg laumontite, heulandite). This is probably related to the breakdown of igneous feldspars in the MML (chapter 2.3).

Crystal precipitation was initiated at amygdale and/or vein walls. Successive generations progressively infill the voids. Terms such as 'early' or 'late' used throughout the text, therefore refer to relative positions in the crystallization sequence. That is:-

i) early; precipitates from initial fluids, that have crystallized

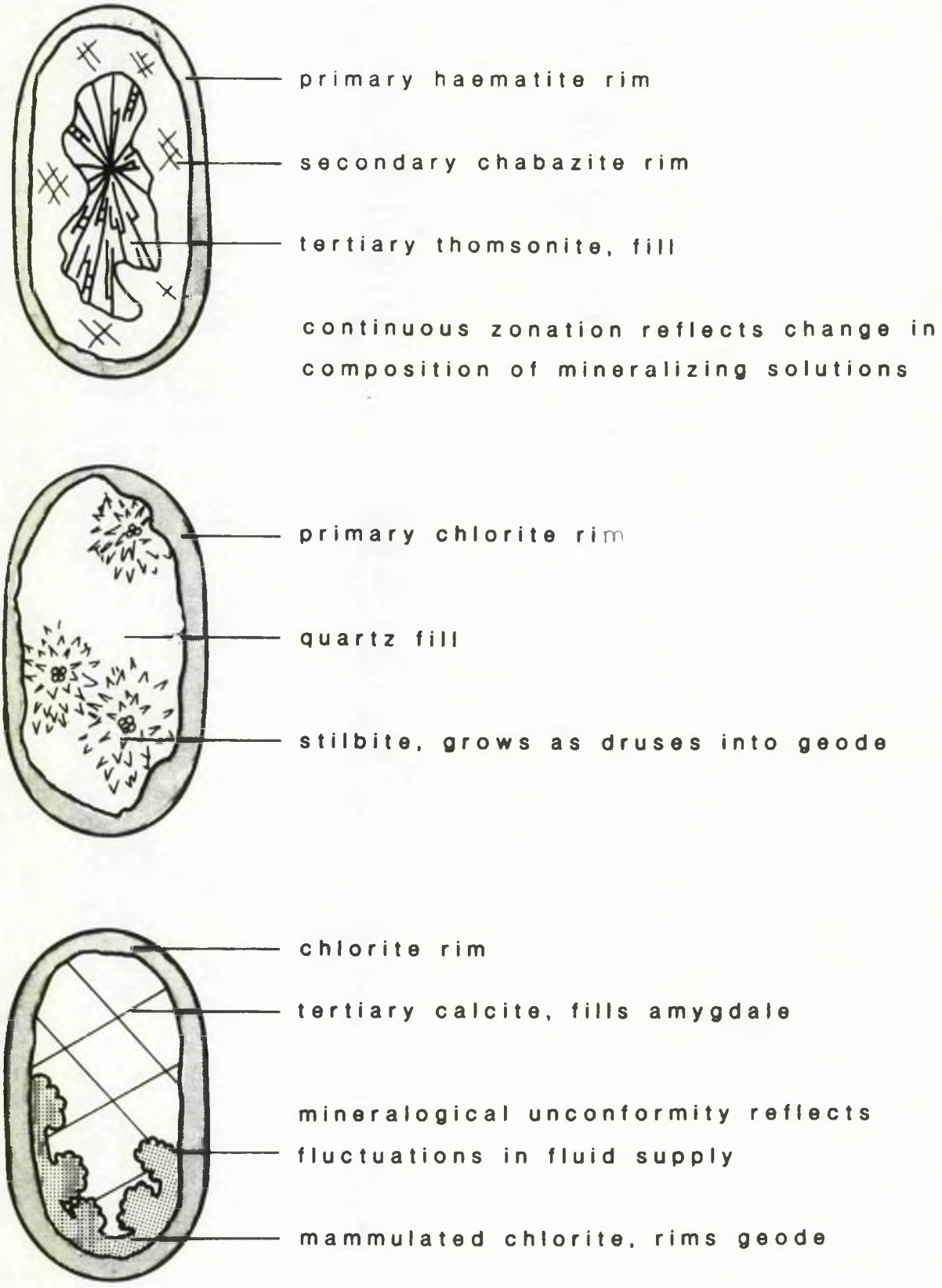


Fig.2.2.2. Representative amygdale infill sequences

around the rim of a void.

ii) late; precipitates from evolved or from second generation fluids, that have crystallized in the core of voids.

Examples are illustrated in Fig 2.2.2.

2.2.4.4 Vein systems

At several horizons amygdaloidal assemblages are cut by vertical vein systems bearing less hydrous zeolite species. The majority of the veins penetrate along cooling joints in the basalt. Several veins display antitaxial features (Durney and Ramsay, 1973), characteristic of syntectonic growth. Identical zeolite species are usually contained in both vein systems. The veins extend upwards from a region where the vein material occurs as the dominant amygdale filling. For example, in the Kilpatricks (Fig 2.1.1):-

i) basalt with amygdaloidal natrolite, is overlain by basalt with amygdaloidal analcime plus vein natrolite.

ii) basalt with amygdaloidal analcime, is overlain by basalt with amygdaloidal quartz and chlorite, plus vein analcime

Likely origins of the vein and amygdale systems are discussed below.

2.2.4.5 Porosity and Permeability

Amygdale and vein assemblages reflect initial rock porosity and permeability. For example, it is suggested in

a) chapters 2.2 and 2.3; that the extent of alteration was related to variations in permeability/porosity within individual flows or flow units

b) chapter 2.6; higher water:rock ratios in tuffs enhance zeoliti-

zation at shallower burial depths than in basalts.

Vein systems

In the metavolcanics of the Midland Valley less hydrous (higher temperature) zeolites have been found to be stable in veins, whilst more hydrous phases (lower temperature) occur in amygdales. For example, at Burntisland (chapter 2.2), natrolite occupies veins whilst analcime occurs in amygdales at the same stratigraphic level. The origin of the veins is problematical, since vein assemblages occur at all levels within the volcanics. Consequently, variations in $P_{load}$ or variations in bulk composition between the vein and the adjacent amygdaloidal region, are discounted as a possible cause of the anomally.

The distribution of vein and amygdale assemblages may be accounted for in three ways:-

i) As a result of temperature variations. This would require that vein minerals were precipitated from metamorphic fluids which were, either driven-off from intrusive bodies or were liberated during dehydration reactions at greater depths. The former, was envisaged by Walker (1960b) to account for zeolitization in the basalts of eastern Iceland. Under such conditions, fluids in amygdaloidal regions would have been intergranular; hence $P_{lith} = P_{fluid}$.

ii) As a result of higher fluid/rock ratios in the veins. According to Houghton (1982), this could lead to chemical differences in the fluids of the two environments.

iii) As a result of variations in $P_{H_2O}$ during metamorphism, due to chemical dilution of the fluid phase. Thus whereas $P_{fluid} = P_{load}$ during metamorphism, $P_{H_2O}$ may be less than $P_{fluid}$. The the most likely varient would have been the differing chemical potential ($\mu$) of $\mu CO_2/\mu H_2O$

The chemical potential (or molar free energy) of an ideal gas is related to pressure (P) by the following equation:-

$$\mu = \mu^{\ominus} + RT \, \text{Ln} \, P.$$

Where $\mu^{\ominus}$ = $\mu$ at unit P

R = gas constant

T = absolute temperature

However it is unlikely that variable $\mu CO_2/\mu H_2O$ ratios were responsible for variations in $P_{fluid}$ in the Midland Valley. It was demonstrated in chapter 2.2 that there were a sparcity of clay-carbonate assemblages in the zeolite sequences. Thompson (1971a) suggests that this reflects a consistently low value of $\mu CO_2$ throughout amygdular hydrothermal alteration.

Point (i) has established that fluid (?) in amygdular regions was under lithostatic pressure ($P_{lith} = P_{fluid}$). However, Houghton (1982) demonstrated that at shallow burial depths, major fractures are open to the surface, so that fluid contained in veins was under hydrostatic pressure ($P_{hyd} = {}^{1}/_{3} P_{lith}$). Thus higher fluid pressures

in amygdales may have favoured the formation of more hydrous species, under conditions where less hydrous phases were stable in veins.

The factors responsible for crystallization can be derived by comparing equations for the chemical potential of vein and amygdale mineral growth under hydrostatic and lithostatic pressures, respectively. A general equation for a vein crystal growing in a fluid under hydrostatic pressure ($P_h$), as determined by Everett (1961) is given below:-

$$\mu = \mu (P_h) + V^s \sigma (\delta A/\delta V)$$

where $V^s$ = molar volume of solid

$\sigma$ = interfacial energy between solid and liquid

A = area of interface

V = volume of solid

This may be compared with Yardley's (1975) equation for crystal growth under lithostatic ($P\varrho$) conditions.

$$\mu = \mu + w + V^s \sigma (\delta A/\delta V) + E$$

where w is dependant upon surface tension ($\sigma$), local stress deviation, and $\Delta P_h - P_\varrho$, E = energy.

In the latter instance, pore fluids are intergranular, and hence the surface of all the crystals will be in equilibrium with the adjacent fluid. Movement of material into the vesicles will therefore have resulted from a potential ($\mu$) gradient operating between the vesicle and the groundmass fluid. This was defined by

Yardley (1975), as:-

$$\delta\mu/\delta x = (\mu_m - \mu_v)/x$$

where $\mu_m$ = $\mu$ of groundmass grain

$\mu_v$ = $\mu$ of vein grain

x = distance between grains

However, considering that zeolitization requires progressive dehydration reaction, liberated water must have moved along grain boundaries and generally upwards to lower $P_{fluid}$. Any vesicles would have been filled by fluid under confining conditions of $P_{fluid} = P_{lith}$.

1 Fluid motion would have been governed by:-

i) diffusion through crystal lattices
ii) interstitial or porosity flow
iii) fracture flow

Petrographic evidence for diffusion is sited in chapter 2.3. Briefly: flow was concentrated in fractures; alteration haloes were developed in the adjacent metabasalts and reflected exchanging fluid: rock reactions. (see chapter 2.6 for further discussion). The chemical potential ($\mu$) of the two areas would have been different, therefore material would have diffused from the vein to the wall-rock to eliminate the potential ($\mu$) gradient. Fyfe *et al*, (1978), define the flux (J) of material (i) across a plane perpendicular to the

direction of mass transfer as:-

$$J_i = D_i \, (dc_i/dx)_t \ cm^2 \ s^{-i}$$

Where dc/dx = a concentration gradient. This is proportional to a potential gradient ($d\mu/dx$) across the plane.

where $D_i$ = the diffusion co-efficient

t = time

x = mole fraction of component i

The equation shows that flow was controlled by the chemical potential of the fluid and by the length of time that channel-ways were open. By inference, zeolitization (although self-propagating exothermic reactions) must have been controlled by the relative rates of fluid access.

Interstitial/porosity flow occurred through macro-pore (vesicles) and micro-pore (along intergranular boundaries) spaces. The effectiveness of the process varies as a function of:-

i) pressure; this reduces grain boundary volume through compaction

ii) time; progressive sealing of pore spaces due to precipitation from fluids.

Both variables reduce pore volume (porosity) and the degree of

Table 2.2.3

| Rock Type | Region | k ($cm^2$) | Reference |
|---|---|---|---|
| Dense rhyolite | Opsidian Dome, | $10^{-8}$ to $10^{-12}$ | Eichelberger |
| Vesicular rhyodacite | California | $0.2 \times 10^{-8}$ | *et al.*, 1986 |
| Vesicular basalt | Oahu, Hawaii | $10^{-6}$ | Cheng & |
| Vesicular basalt | Wairakei, New Zealand | $10^{-10}$ | Minkowycz, 1977 |
| Bedded tuff | unspecified | $10^{-10}$ to $10^{-12}$ | Norton & Knapp, |
| Welded tuff | unspecified | $<2 \times 10^{-16}$ | 1977 |

Table 2.2.3 Permeability measurements (k) in volcanic rocks.

interconnection between pores (permeability).

Fracture flow reflects fluid movement along veins under the physiochemical conditions to be established in section 2. For hydraulic fracture to occur however, $P_{hyd}$ must exceed the tensile strength ($\sigma 3$) of the rock.

The total porosity of the rock (Norton and Knapp, 1977) is a function of fracture flow, diffusion porosity and residual pore space. Permeability, however is governed by the abundance and geometry of continuous flow channels. Measurements of permeability (k) must also take into account the temperature (T) and the viscosity ($\eta$) of the fluid involved, such that:-

$$k = (Q/A)n(dp/ds)^{-1} \qquad \text{after Fyfe } et\ al,\ 1978$$

Where Q equals the volume of fluid which passes with time through an area (A) in the direction of the pressure gradient (dp/ds). Measurements are quoted in Darcies D, where 1D = 1 $cm^3\ s^{-1}\ cm^{-2}$ at 1 bar $cm^{-1}$; T = 20 $^oC$.

Representative permeability measurements in certain volcanic rocks are presented in table 2.2.3. These values may be compared with permeability measurements in fractures. Toulmin and Clark (1967) considered that in a dense rock, (where $k = 10^{-5}D$), $k = 3 \times 10^3 D$ in a 1 $\mu$ fracture and K = 3000 D in a 1 mm fracture. The data suggests that fractures significantly increase the flow of hydrothermal fluids in volcanics.

2.2.4.6 Amygdale assemblages of the eastern Midland Valley

Amygdale assemblages are developed in four geographically

distinct regions (Fig 2.2.1) of the eastern Midland Valley:-

i) Bathgate

ii) Burntisland (and East Fife)

iii) Arthur's Seat and Craiglockhart Hill, Edinburgh

iv) the Garleton Hills

Sampled localities are shown on figure 2.2.1, and are listed in appendix 2.2.1. Zeolite distributions are presented in figure 2.2.3. Eight of Heddle's (1924) localities are incorporated on the map; the remainder represent new zeolite occurrences in the Midland Valley.

The following paragraphs describe the amygdale assemblages from the regions listed above. Explanations of the small scale features are given. The overall significance of the amygdale assemblages to hydrothermal alteration will be discussed later in the chapter.

**Bathgate**

Evidence for hydrothermal alteration in the Bathgate Volcanics is limited. Basalts are generally fresh, although green 'spots' related to chlorite crystallization (confirmed by microprobe analyses - chapter 2.4) may occur.

Vesicular and/or amygdaloidal horizons are present; neither are abundant. Amygdales and veins contain quartz and/or calcite. Vein mineralization (at CV22 and CV24) can be directly related to the proximity of quartz-dolorite sills and dykes. Since amygdale horizons are rare, it is impossible to determine whether their contents:-

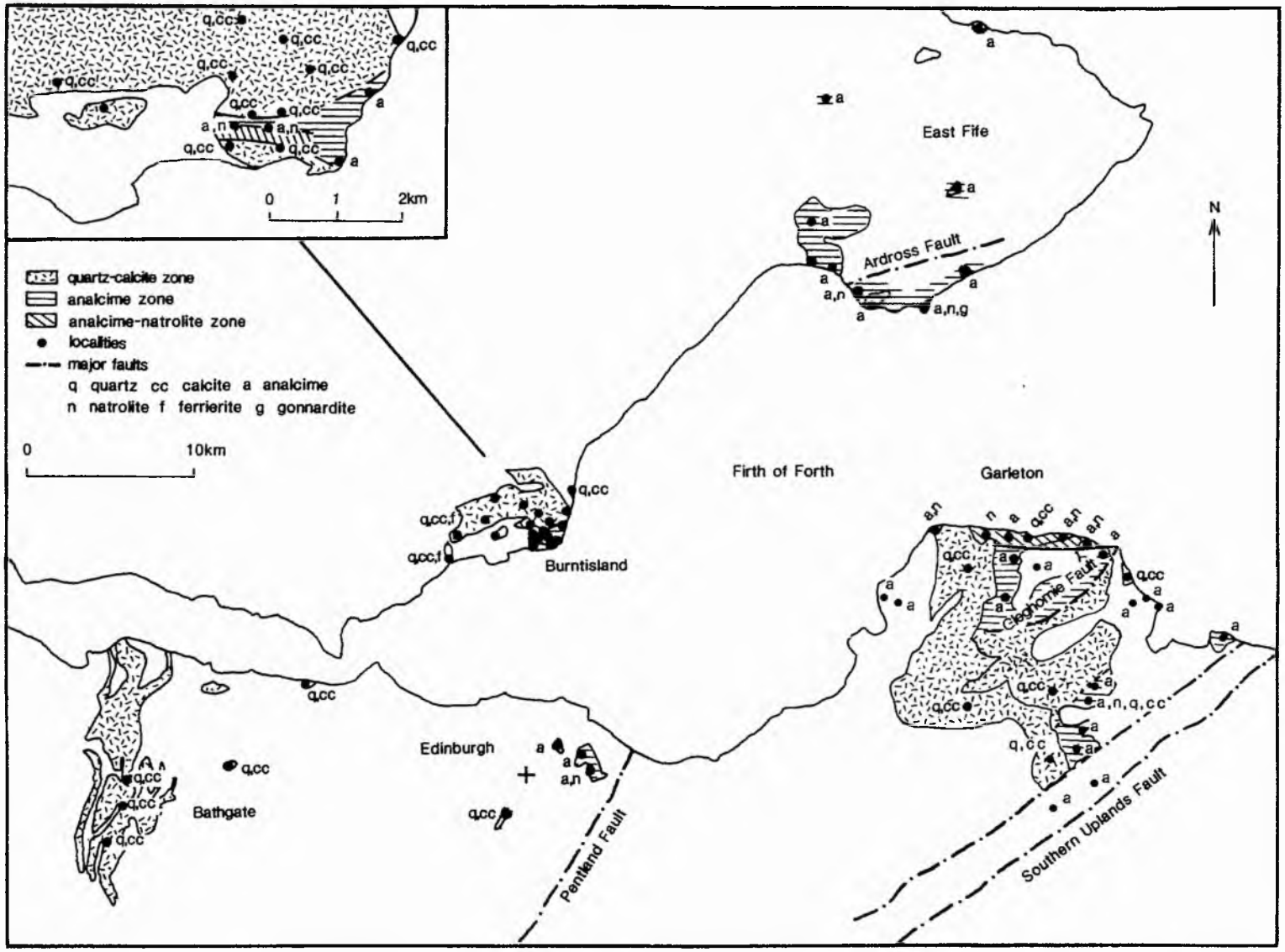


Fig.2.2.3. Mineral zones in the Carboniferous volcanics of the eastern Midland Valley, Scotland.

i) were also precipitated from mineralizing solutions associated with intrusion

ii) represent intergranular pore fluids

Products of the different types of hydrothermal alteration (see introduction) in the Bathgate Volcanics, cannot be distinguished.

Generally clay products predominate in regions of low-grade alteration. For example, in eastern Iceland (Walker 1960b) clays are associated with quartz/calcite - and analcime-bearing volcanics. At Bathgate (and in unzeolitized and analcime-bearing volcanics elsewhere in the eastern Midland Valley) chlorite is present, suggesting that temperatures were high. Sill and dyke intensities in these regions are also exceedingly great. It is therefore believed that the presence of chlorite in the basalts is a contact effect associated with intrusion.

**Burntisland (and East Fife)**

Greenstone alteration (section 2.2.4) predominates at Burntisland and in East Fife. Closer examination however, reveals that greenstone alteration was overprinted by zeolitic amygdale assemblages. Since greenstone characteristics such as veining, decrease with increased height in the volcanic pile, and are abruptly truncated by highly analcimitized metabasalt. The distribution of zeolites in the East Fife volcanics is shown in figure 2.2.3. At Burntisland, evidence for the over- printing is most obvious, and this enables a four-fold division of the volcanic pile (Fig 2.2.4). This sequence comprises:-

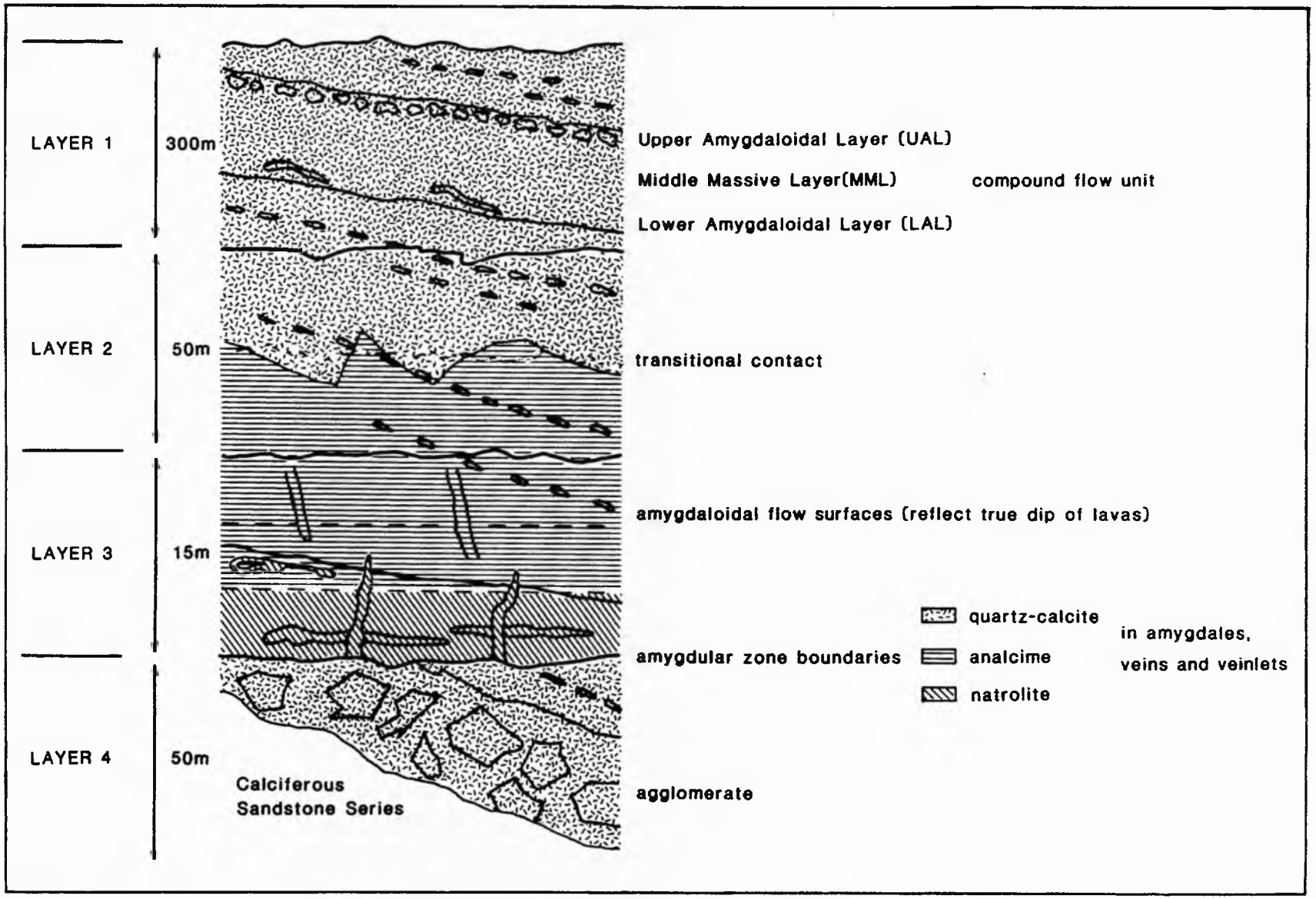


Fig.2.2.4. Schematic representation of Burntisland amygdale divisions.

Layer 4: a lowermost zone of intense greenstone alteration (50 m wide)

Layer 3: a 15-20 m wide zone of analcimitized metabasalt extending along the cliff section inland of Pettycur Bay to the shore at Kinghorn (Fig 2.2.1). The zone has sharp contacts (within 1 m) with the adjacent greenstone alteration and dips to the NW at a slight angular discordance to the dip of the lava pile. These differential angles suggest that the zone must be a secondary feature post-dating regional tilting of the area.

To the north of Pettycur Bay, the analcimitized metabasalt layer cuts across two compound lava flows. The MML of these flows are composed of phaneritic light grey basalt, akin in character to dolerite. However, well developed $UAL_s$ and $LAL_s$ indicate that the rocks are lava flows. The characteristics of these flows are similar in description to Pietursson's 'Grey Stage Lavas' of Iceland. Walker (1960, b) reflected on this, and attributed their colouration and freshness to the development of zeolitic alteration.

Amygdale and vein assemblages in the meta-basalt layer are characterized by analcime and natrolite. The lowermost 5 m of the layer is characterized by abundant bladed natrolite, infilling major veins (<3 cm wide), amygdales and veinlets (adjoining contiguous cavities). Natrolite also forms clusters of alteration throughout the basalt groundmass. Within the central portions of the layer, natrolite is less abundant. It occurs as hair-like needles lining amygdales and is accompanied by abundant late (see section 2.2.4.3 for definition) analcime. In the uppermost 5 m of the layer natrolite is absent. Reduced amounts of analcime are present in amygdales,

together with minor amounts of late calcite. In this region vein analcime, perpendicular to alteration horizons in the analcimitized meta-basalt layer, are developed.

Layer 2: represents a transitional contact between the fresh basalt layer above and greenstone alteration below. Alteration in this second greenstone layer is concentrated in the $UAL_s$ and $LAL_s$ of the flows, and shows a marked decrease in development perpendicular to the surfaces of individual lava flows.

Layer 1: comprises 300 m of unaltered basalt. Amygdales are infilled with quartz.

Layers 1-4 reflect two types of hydrothermal alteration:-

i) associated with greenstones (developed in Layers 4, 2 and 1)

ii) associated with amygdale assemblages (developed in Layers 3, 2 and 1)

Greenstone characteristics decrease in intensity with increased height in the volcanic pile. It has already been established (2.2.3) that seawater was a probable fluid source. However, if seawater was the cause of alteration, then the importance of seawater as a reacting medium, must also have decreased with height in the volcanic pile. This is likely to have occurred since the Burntisland area rapidly became subaerial (see chapter 2.1). Furthermore, alteration horizons perpendicular to lava flow surfaces, establish the early origin of greenstone alteration with respect to zeolitization. Metamorphic differentiation in the MML, UAL and LAL, is attributed to enhanced permeability contrasts with increased distance from the

fluid source. However, such permeability contrasts could also be governed by burial metamorphic gradients (discussed later in the chapter).

Successive amygdale assemblages (quartz-analcime-heulandite-laumontite) were used by Walker (1960 b) to define burial metamorphic profiles in eastern Iceland. In the eastern Midland Valley amygdales form zones which are discordant to the lava stratigraphy. This establishes the late age of zeolitization in the volcanic history of Burntisland. These sequences are interpreted in burial metamorphic terms later in the chapter. Significantly, the zeolite zone of Burntisland is suspended above the base of the lava pile. Similar observations were made by Walker (1951) in the Garron Plateau Lavas of Ireland. In both regions, the suspended base of the zeolite zone reflects the area of greatest heat accumulation, during the exothermic hydration of glass and igneous minerals. Adjacent to this region, the zeolitized zone would have cooled by conduction to the surface and the floor of the pile.

Analyses of vein ferrierite and amygdular thomsonite intergrown with gonnardite (Fig 2.2.3) were made from the quartz-calcite and analcime-natrolite zones respectively. These minerals cannot be reconciled with the regional burial metamorphic scheme advocated here to explain the hydrothermal alteration of the Burntisland Volcanics. These zeolites are highly hydrated varieties, which are all recorded in close proximity to vent intrusions; and are believed to have formed under circumstances similar to those developed in the palaeo-geothermal plumes (see section 2.2.5).

**The Edinburgh District**

In the Edinburgh district, representatives of unzeolitized, analcime and analcime-natrolite zone minerals occur in Craiglockhart Hill, Calton Hill and Arthur's Seat respectively.

At Craiglockhart Hill, amygdale and vein assemblages bear quartz; whilst at Calton Hill, calcite cemented tuffs are traversed by analcime veins. At Arthur's Seat, amygdaloidal and vein quartz decrease in abundance away from intrusive centres. Hence, they are likely to have been precipitated from fluids associated with intrusion. Analcime and natrolite have been collected (by Heddle, 1924) from amygdales and vesicles in the Westphalian dolerite sill of the Salisbury Craig.

**The Garleton Hills**

Hydrothermal alteration in the Garleton Hills is characterized by:-

i) greenstone alteration at the base of the volcanic pile
ii) amygdale divisions comparable to those at Burntisland.

Along the northern coastal section, natrolite veins and amygdaloidal analcime are present in basalt and basaltic tuff. Natrolite has not been encountered inland, although analcime (± quartz) is present in amygdales as far south as the Gleghornie Fault(Fig 2.2.3). These assemblages have not been observed south of the Gleghornie Fault. Instead amygdales and veins are infilled with quartz, calcite and chlorite. However, McAdam and Tulloch (1985) and Davies *et al*, (1986) recorded amygdular, vein and matrix analcime ±

natrolite from localities along the south-eastern margins of the Garleton Hills and from vents along the east coast. This data has been incorporated on figure 2.2.3. Amygdales in trachytes (mark the western edge of the Garleton Volcanics - Fig 2.2.3), are infilled with quartz and calcite only; veins are occupied by haematite.

It is clearly shown in figure 2.2.4, that the amygdales occupy zones which cut across the lava stratigraphy. Furthermore, it appears, from the distribution of the zones, that the amygdale assemblages have been displaced across the Gleghornie Fault (of Calciferous Sandstone age Fig 22B).

The lack of amygdaloidal variation shown by the trachytes, suggests that either:-

i) the trachytes were chemically distinct and do not favour zeolite production; there is no evidence to prove or disprove this theory.

ii) the amygdale assemblages were developed in the basalts and basaltic tuff before the extrusion of the trachytes. The base of the trachytes would then represent a mineralogical unconformity comparable to that observed by Aguirre *et al* (1978), where mineralogical breaks coincide with regional unconformities due to the sealing of each unit after its particular metamorphic episode.

iii) the trachytes are impermeable

However, later in the chapter, it will be shown that it was necessary for the entire volcanic (and sedimentary) thickness to have been developed before analcime-natrolite zeolitization could have

Table 2.2.2

| Amygdale Mineral | Abundance |
|---|---|
| Analcime | 27.7% |
| Calcite | 25.8% |
| Quartz | 18.3% |
| Heulandite | 14.2% |
| Thomsonite | 13.3% |
| Natrolite | 10.8% |
| Stilbite | 10.8% |
| Prehnite | 8.3% |
| Laumonite | 7.5% |
| Chabazite | 4.2% |
| Apophyllite | 1.7% |
| Mordenite | <1% |
| Gonnardite | <1% |
| Mesolite | <1% |
| Gmelinite | <1% |
| Ferrierite | <1% |

Table 2.2.2 Relative abundance of amygdale minerals in the Clyde Plateau Lavas (Abudance in amygdale)

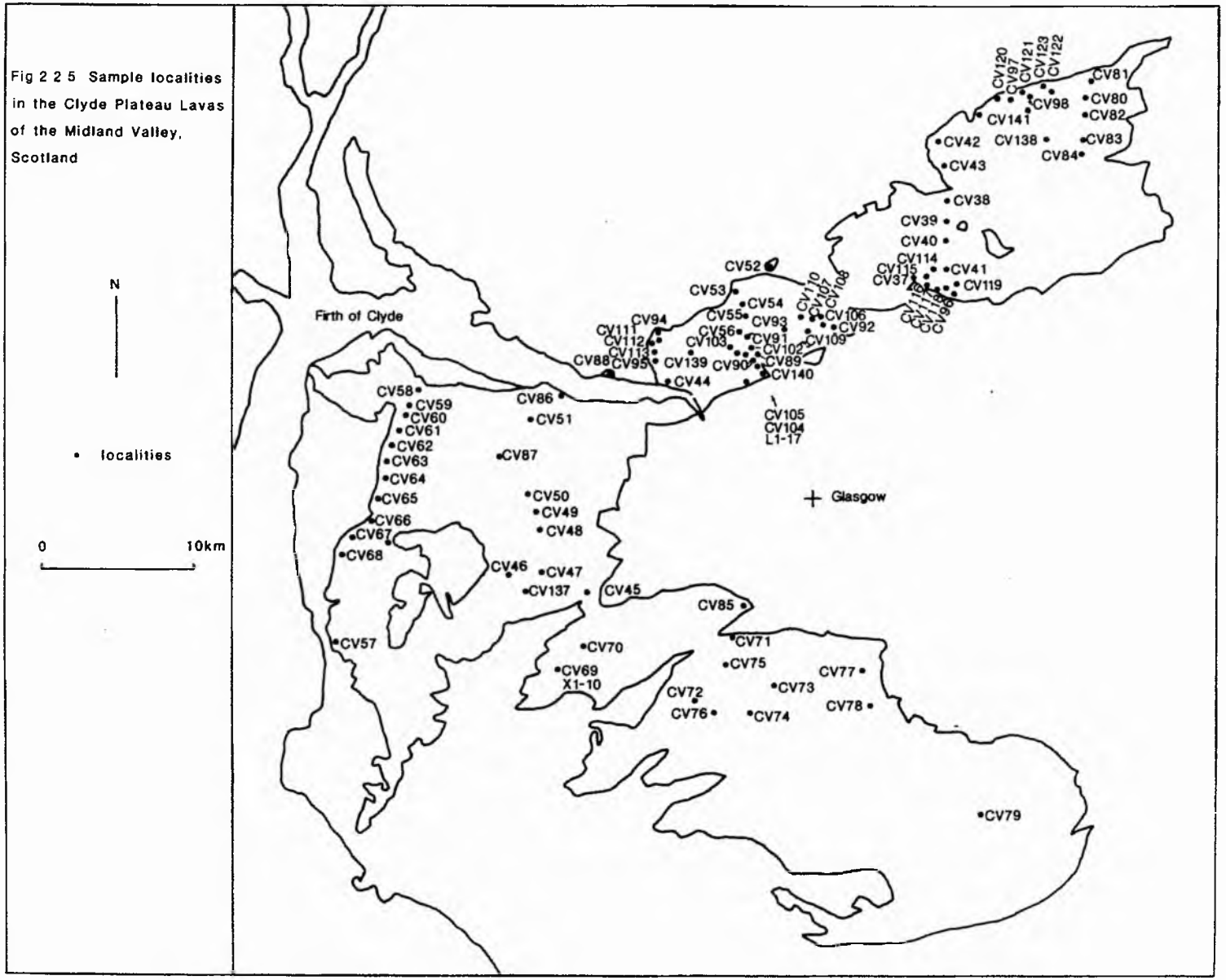
Fig 2 2 5 Sample localities in the Clyde Plateau Lavas of the Midland Valley, Scotland
N
• localities
0
10km
Firth of Clyde
Glasgow
CV120
CV97
CV121
CV123
CV122
CV81
CV98
CV80
CV141
CV82
CV42
CV138
CV83
CV84
CV43
CV38
CV39
CV40
CV114
CV115
CV41
CV37
CV119
CV52
CV53
CV54
CV55
CV93
CV106
CV92
CV56
CV91
CV103
CV102
CV109
CV111
CV94
CV112
CV113
CV88
CV95
CV139
CV90
CV89
CV140
CV44
CV58
CV59
CV60
CV61
CV62
CV63
CV64
CV65
CV66
CV67
CV68
CV86
CV51
CV87
CV105
CV104
L1-17
CV50
CV49
CV48
CV46
CV47
CV137
CV45
CV85
CV71
CV75
CV77
CV73
CV72
CV76
CV74
CV78
CV57
CV70
CV69
X1-10
CV79

proceeded.

2.2.4.6 Amygdale assemblages of the Clyde Plateau Lavas

Hydrous silicates have been collected from the localities shown in figure 2.2.5 and listed in appendix 2.2.1. Table 2.2.2 comprises a list of those found in the Clyde Plateau Lavas, together with their relative abundances. The distribution of these species are shown in figure 2.2.6. Additional localities shown on figure 2.2.6 are from field observations of amygdale and vein assemblages for which no collection was made. Representative cross-sections through the zeolitized Clyde Plateau Lavas are given in figure 2.2.8. These are discussed below, in order of decreasing stratigraphic position in the volcanic pile.

**Laumontite**

Laumontite occurs as pink vitreous columnar crystals or as white opaque botryoids in amygdales and veins in the Clyde Plateau Lavas.

The most extensive development, is seen along the northern edge of the Campsies, where a 7 m wide zone of amygdaloidal laumontite (+/- late quartz), extends laterally for 5 km. Laumontite crystallization is suspended @ 5 m above the base of the pile. No zeolites have been recorded below this level. Suspended zeolite zones have also been recorded from Burntisland (see - section 2.2.4.4) and from the Garron Plateau, Ireland (Walker, 1960a).

Above this zone, amygdaloidal laumontite is associated with late heulandite and/or stilbite. Along the western edge of the Kilpatrick Hills (Fig 2.2.6) this association has been found in the

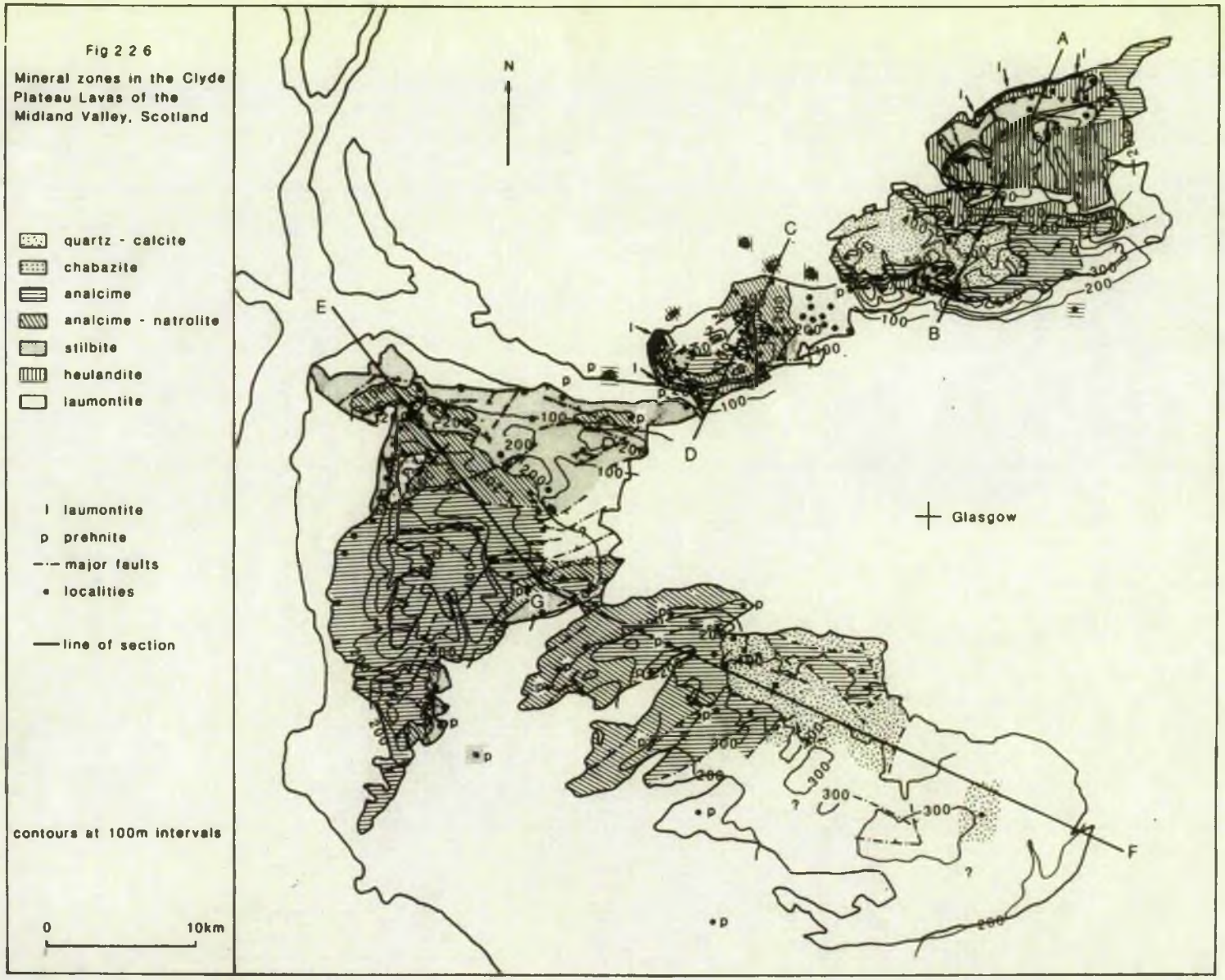
Fig 2 2 6
Mineral zones in the Clyde Plateau Lavas of the Midland Valley, Scotland
quartz - calcite
chabazite
analcime
analcime - natrolite
stilbite
heulandite
laumontite
l laumontite
p prehnite
major faults
localities
line of section
contours at 100m intervals
0
10km
N
Glasgow
A
B
C
D
E
F
G

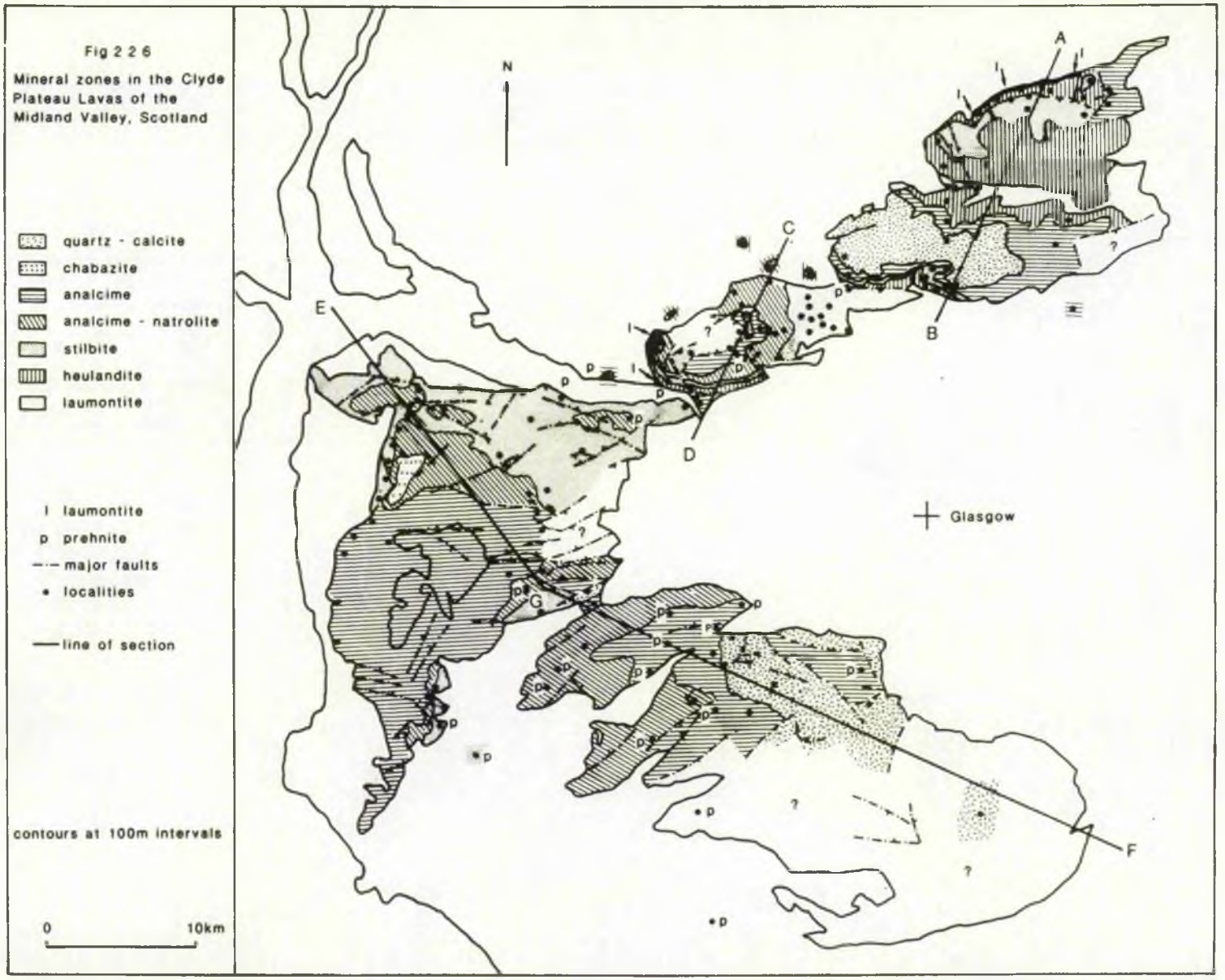
Fig 2 2 6
Mineral zones in the Clyde Plateau Lavas of the Midland Valley, Scotland
quartz - calcite
chabazite
analcime
analcime - natrolite
stilbite
heulandite
laumontite
l laumontite
p prehnite
major faults
localities
line of section
contours at 100m intervals
0
10km
N
A
B
C
D
E
F
G
Glasgow

Plate 8A: Photograph of spherulitic quartz, retrieved from veinlets in metabasalt. Arrow points to haematite trails growing along partings within the quartz.

Plate 8B: Photograph of botryoidal prehnite growing on vitreous acicular thomsonite.


2 cm

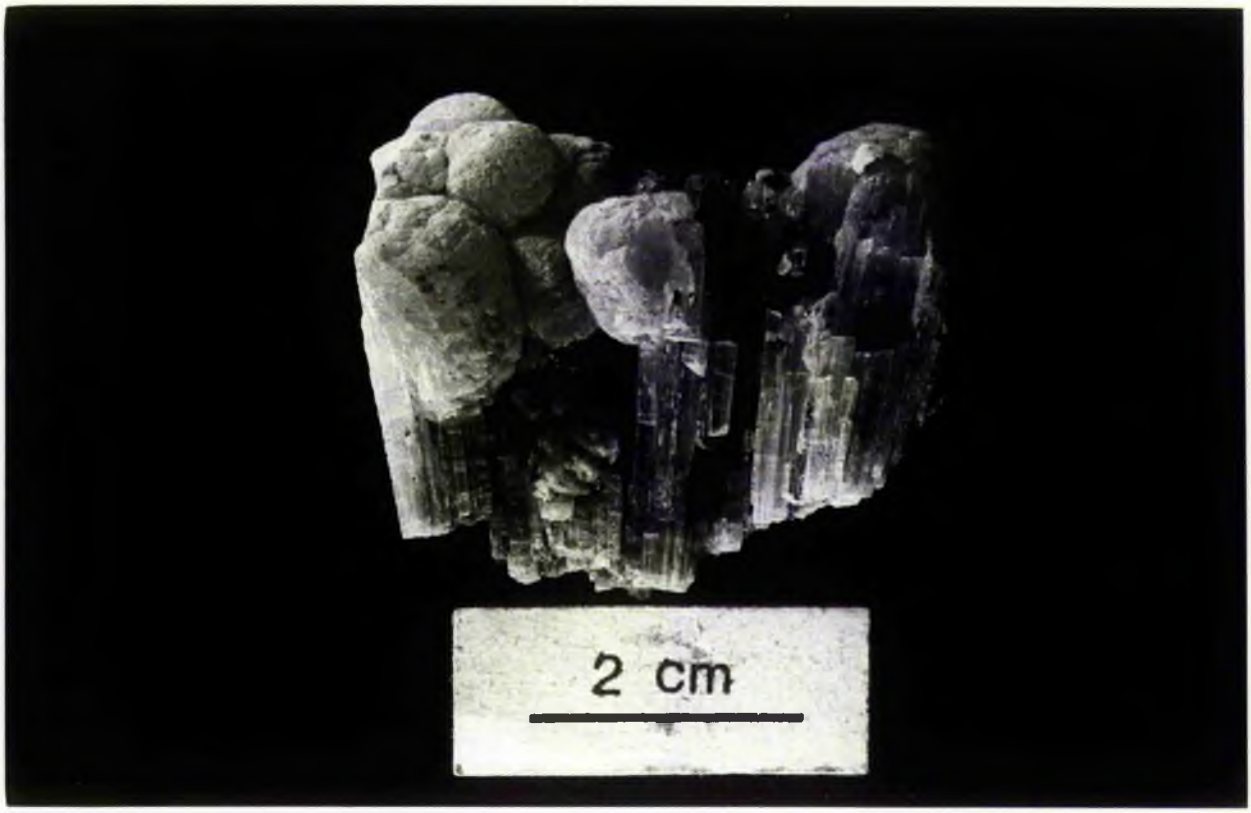
2 cm

UAL of one flow near the base of the pile. Heddle (1924) described amygdaloidal laumontite-heulandite assemblages from three localities south of the Clyde (appendix 2.2). These have not been confirmed during this study; the data is however incorporated in figure 2.2.6.

To the south-east of the Misty Law vent (Fig 2.2.1), laumontite veins are encountered in analcime and analcime-natrolite amygdaloidal horizons. Laumontite veins also surround a vent at Milngavie (Fig 2.2.6). The restriction of laumontite to veins, and the distribution of these veins around the vents suggest that laumontite represents a low grade hydrothermal contact aureole (Fig 2.2.6). A similar laumontite-bearing aureole surrounding the Cullins intrusive complex Skye, was described by King (1977).

**Heulandite**

Vitreous brick-red coffin shaped crystals of heulandite occupy amygdales and veins in basalt, the distribution of which indicates a major zone of variable thickness (150 m maximum). This zone outcrops in the north and west Campsies, in the north and west Kilpatricks, and along the northern edge of the Renfrewshire Block (Fig 2.2.6).

Heulandite is accompanied in amygdales by a variety of hydrous silicates; associated minerals are listed in table 2.2.3. Their textural relationships are discussed below.

i) laumontite; predates heulandite in amygdales
(see previous page)

ii) quartz; grows upon amygdular heulandite (Plate 2.2.1 c) at the base of the heulandite zone.

iii) stilbite ± mordenite; stilbite postdates heulandite

Plate 9A: Photograph of late isositetrahedral analcime crystals. Centre left, associated early acicular thomsonite.

Plate 9B: Photograph of opaque radial natrolite clusters.

10mm

10mm

in amygdales and veins. In one amygdale (locality CV81) white radial fibres of mordenite form a tertiary zeolite filling. This is the only reported occurrence of mordenite in the Midland Valley. In Iceland (Walker, 1960 (b)) mordenite is commonly associated with stilbite in tholeiitic basalts. Heulandite-stilbite±mordenite associations overlie amygdales containing heulandite-quartz.

iv) analcime; towards the top of the heulandite zone late analcime accompanies heulandite in amygdales.

In the field, zeolitization seems to be most enchanced in the heulandite zone well above the base of the lava pile as in Antrim (Walker, 1960a).

**Stilbite**

Sheaf-like aggregates of stilbite are extensively developed in the Campsies and along the western edge of the Kilpatricks (Fig 2.2.6). To the south of the Clyde, stilbite occurs sporadically along the northern and western ridges bounding the Renfrewshire Block. Stilbite forms a zone which is always seen to overlie heulandite.

Stilbite first appears in the heulandite zone as late precipitates in veins and amygdales. Amygdales at the top of the stilbite zone are essentially composed of stilbite alone. Although late precipitates of chabazite, ferrierite, mordenite, analcime or quartz are known to occur.

Stilbite crystals show considerable colour variation. Crystals

Plate 10A: Photograph of vitreous silbite sheafs growing on quartz in a geode.

Plate 10B: Photograph of vitreous coffin-shaped heulandite crystals growing into a geode.


2 cm


10mm

are white in the Campsies, pink in Renfrewshire and red in the Kilpatricks. The colouration is thought to reflect different concentrations of haematite inclusions and hence variable oxidation states in the hydrothermal fluids.

**Natrolite**

Natrolite has been recorded (Fig 2.2.6) from localities in the Campsies, the Kilpatricks, the Renfrewshire Block and from peripheral areas in the Lanarkshire Block. Crystals may be prismatic or form fine acicular radial masses. Changes in topology, comparable with those seen in the eastern Midland Valley (section 2.2.4.5) are observed with depth in the natrolite zone. Natrolite either occurs on its own or in association with late analcime. Textural relationships are discussed in detail in section 2.2.4.5.

Natrolite has not been found in veins or amygdales with either laumontite, heulandite or stilbite. However, amygdaloidal natrolite always occurs in a zone directly overlying amygdaloidal stilbite.

**Analcime**

Zoned icositetrahedral analcime crystals are predominantly developed in amygdales and veins to the south of the Clyde. Minor outcrops occur in the Campsies and in the Kilpatricks (Fig 2.2.6).

Associated amygdaloidal minerals include heulandite-stilbite, natrolite, quartz, thomsonite and chabazite. The textural relationships of the first three minerals have already been discussed. Quartz post-dates analcime in amygdales towards the top of the analcime zone in localities north of the Clyde. In a small area surrounding Milngavie (Fig 2.2.11) quartz has not been

encountered. Here thomsonite postdates amygdaloidal analcime. Late amygdaloidal thomsonite is developed with analcime in the Renfrewshire Block (Fig 2.2.6). Chabazite precipitation sometimes intervenes between analcime and thomsonite. Amygdaloidal analcime-quartz assemblages are not developed south of the Clyde.

**Chabazite**

With the aid of X-ray diffraction and from microprobe analyses, chabazite has been recorded from

i) the south-west Campsies, as primary precipitates in amygdales with later thomsonite
ii) the western margins of the Renfrewshire Hills, as secondary precipitates with primary amygdaloidal stilbite

The latter relationship is discussed in greater detail later in the chapter.

**Thomsonite**

Thomsonite has been recorded from amygdales in the Renfrewshire Hills (fig 2.2.6), postdating either analcime or chabazite. Thomsonite is more commonly found in veins in prehnitized basalt; this association is discussed in section 2.2.6.

In the Kilpatrick Hills, amygdaloidal quartz-calcite assemblages overlie the amygdaloidal analcime zone (Fig 2.2.6).

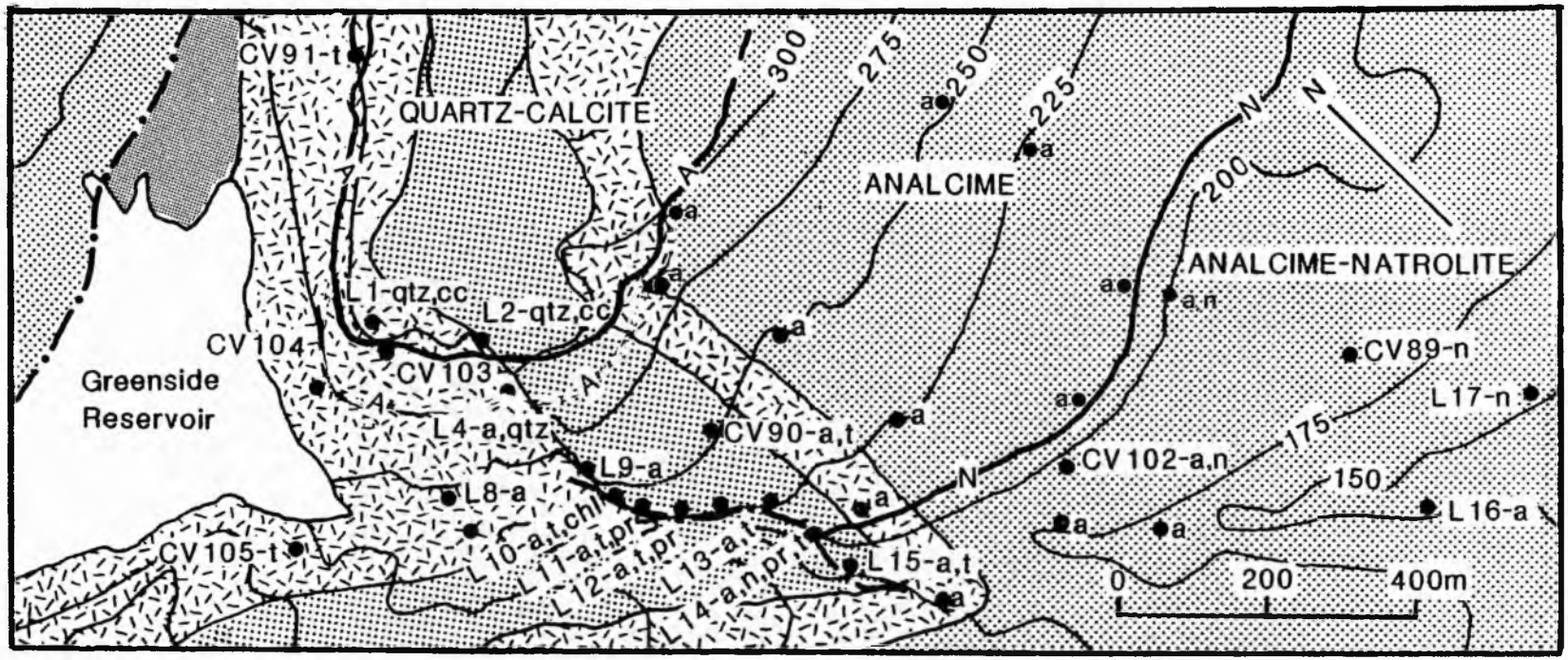


Fig.2.2.7. 1:50 000 map of Cochno zeolite zones, the Kilpatricks. contours at 25m intervals ● localities —·— major faults —A—A— Isograd for the first appearance of analcime —N—N— Isograd for the first appearance of natrolite basaltic tuff Jedburgh basalt Markle basalt a-analcime n-natrolite t-thomsonite pr-prehnite chl-chlorite qtz-quartz cc-calcite

### 2.2.4.7 Discussion of amygdale assemblages in the Midland Valley

On the scale of an exposure, it has been demonstrated (section 2.2.4) that amygdaloidal minerals occupy zones, which succeed one another in an orderly vertical fashion. Figure 2.2.4, indicates that the zeolite zones cut across the lava stratigraphy. In the eastern Midland Valley the zeolite zones dip towards the west. In the Clyde Plateau Lavas, the zones dip southwards north of the Clyde, whilst to the south of the Clyde the zones dip to the east and to the west. Detailed mapping in the Kilpatricks (Fig 2.2.7) has shown that locally the zeolite zones lie parallel to the contours. Here lavas dip 10 $^{o}$SE, thus emphasizing the lateness of the zeolitization with respect to the main volcanic episode. It has been inferred (Walker, 1960b) in eastern Iceland that the zeolite zones reflect post-tilting isograds, parallel to the ancient landsurface. Cross-sections (Fig 2.2.8 a, b) through the zeolitization lavas of the Clyde Plateau and of the eastern Midland Valley, reflect similar features.

The sequence of zones developed are listed in Fig 2.2.9. The upper half of this orderly succession is recorded in the eastern Midland Valley. In the Clyde Plateau Lavas the entire sequence is seen. In most places (see figs 2.2.3 and 2.2.6) a quartz-calcite zone conformably succeeds the analcime zone. In the Renfrewshire Hills (Fig 2.2.6) the analcime zone is succeeded by a thomsonite-chabazite zone. In eastern Iceland, Walker (1960b) recognized the thomsonite-chabazite zone in tholeiitic lavas only. Such magmatic affinities are not present in the Carboniferous volcanics of the Midland Valley (Cameron and Stephenson, 1985).

In the Campsies and in the Renfrewshire Hills, sub-assemblages

have also been mapped (Fig 2.2.6), because of distributive overlap between zeolite species.

Coombs (1954), Coombs *et al,* (1959) and Walker (1960a; 1960b) attribute zeolitization to burial metamorphism. Estimates of the depth relationships of the various zones, were established in Ireland and eastern Iceland by Walker (1960a; 1960b). Walker (1951) indicated from the distribution of chabazite habits in the Garron Plateau, Co Antrim, that the zeolite zones cut the interbasalt horizon and therefore zeolitization did not take place until the bulk of the lavas had erupted; a minimum thickness of 200 m would have been required before the process started. Further evidence from Iceland (Walker, 1960b) indicated that a blanket zone some 180-275 m thick, existed at the top of the pile, where no zeolites formed due to too low a temperature. Analcime and laumontite are the diagnostic amygdale minerals most frequently collected from zeolitized basalts in the world. The contact of the base of the analcime zone with the top of the laumontite zone has been reported at a burial depth of 1000 m in Iceland (Walker, 1960b; Kristmannsdottir and Tomasson, 1978), New Zealand (Sameshima, 1978) and India (Sukheswala *et al,* 1974) and at 1600 m in Puerto Rico (Jolly, 1970). The relative positions of the heulandite and/or stilbite zones in these regions varies by 100s and/or 1000s of metres.

The zones developed in the Carboniferous Volcanics of the Midland Valley are directly comparable to those seen (Walker, 1960a) in the Tertiary Antrim basalts (Fig 2.2.9). Depth relations of the various zones are better know from E Iceland (Walker, 1960b) (Fig 2.2.9). The Midland Valley zones are compared with the above in figure 2.2.9. The figure shows that in order to obtain the necessary

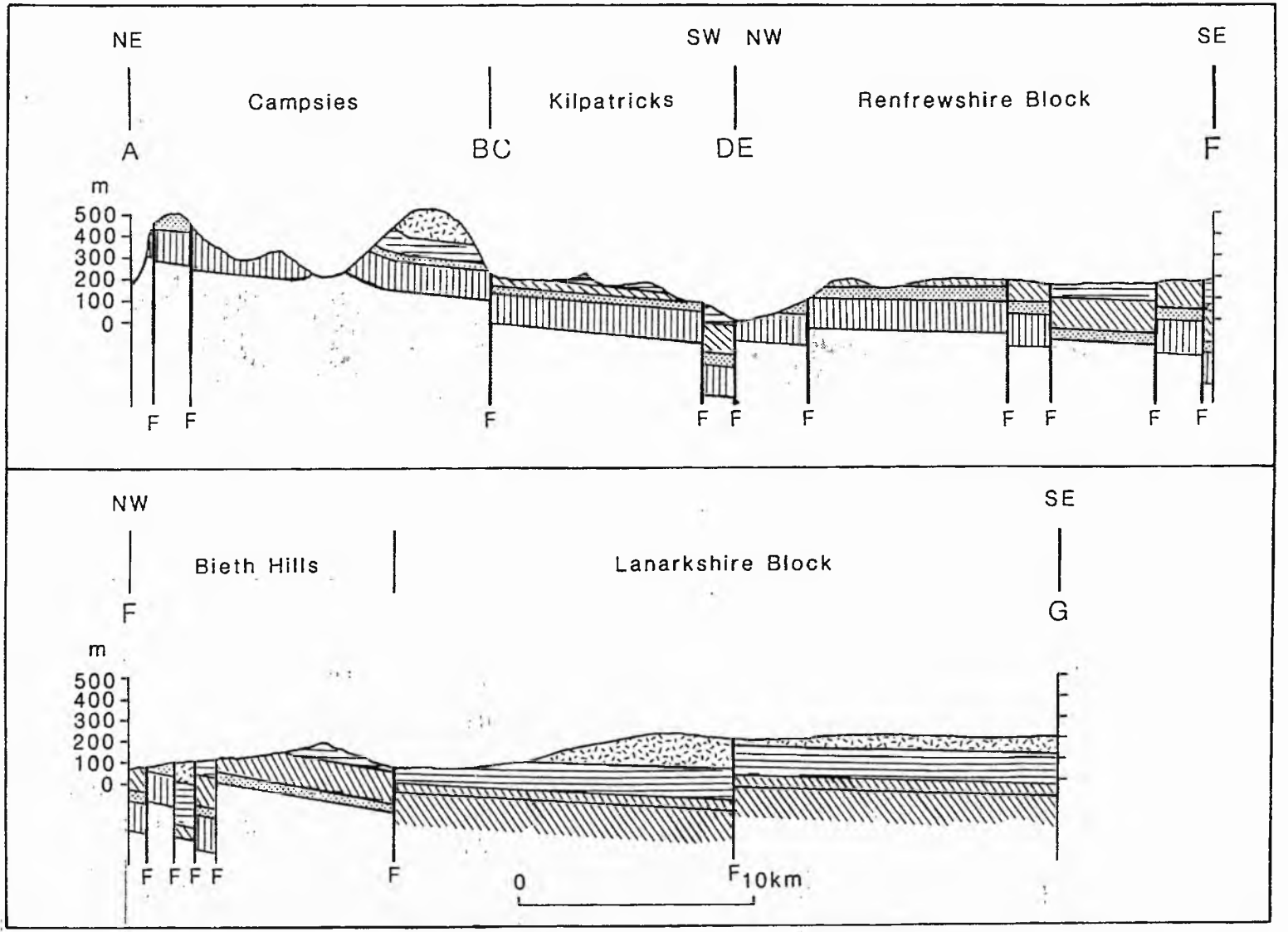


Fig 2.2.8 Cross-sections through the mineral zones of the Clyde Plateau Lavas Key quartz-calcite, analcime, analcime-natrolite, stilbite, heulandite, laumontite, F fault
Lines of sections shown on Fig 2.2.6

metamorphic conditions, the base of the volcanics have to be buried to a depth of:-

i) 900 m in the eastern Midland Valley.

ii) 1300-1500 m in the Clyde Plateau Lavas.

In all instances the volcanic thicknesses (Fig 2.2.9; see chapter 2.2) alone are insufficient to produce the metamorphic conditions. This necessitates that the volcanics were buried beneath a complementary thickness (Fig 2.2.9; see chapter 2.1) of sediments. Consequently:-

**In Bathgate:** the volcanics can never have been buried sufficiently for zeolitization to have occurred; the empty vesicles recorded in the upper 50 m of the volcanics must be a primary feature.

**In Garleton:** the trachytes and sediments need to have overlain the whole sequence for the basalts and basaltic tuff to have experienced burial metamorphism. Therefore, the inception of zeolitization was much later than the evidence provided by the Gleghornie Fault (see page 126-127).

**In Edinburgh and Burntisland:** some 150 m of sediment need to have been removed by erosion.

**In East Fife:** although only 500-600 m of sediment overlie the volcanics in the immediate viscinity of Largo Law and Elie, throughout the area the sedimentary sequence is known to be 2 km thick (see chapter 2.1).

**In the Clyde Plateau Lavas:** substantial thicknesses (500-900 m, Fig

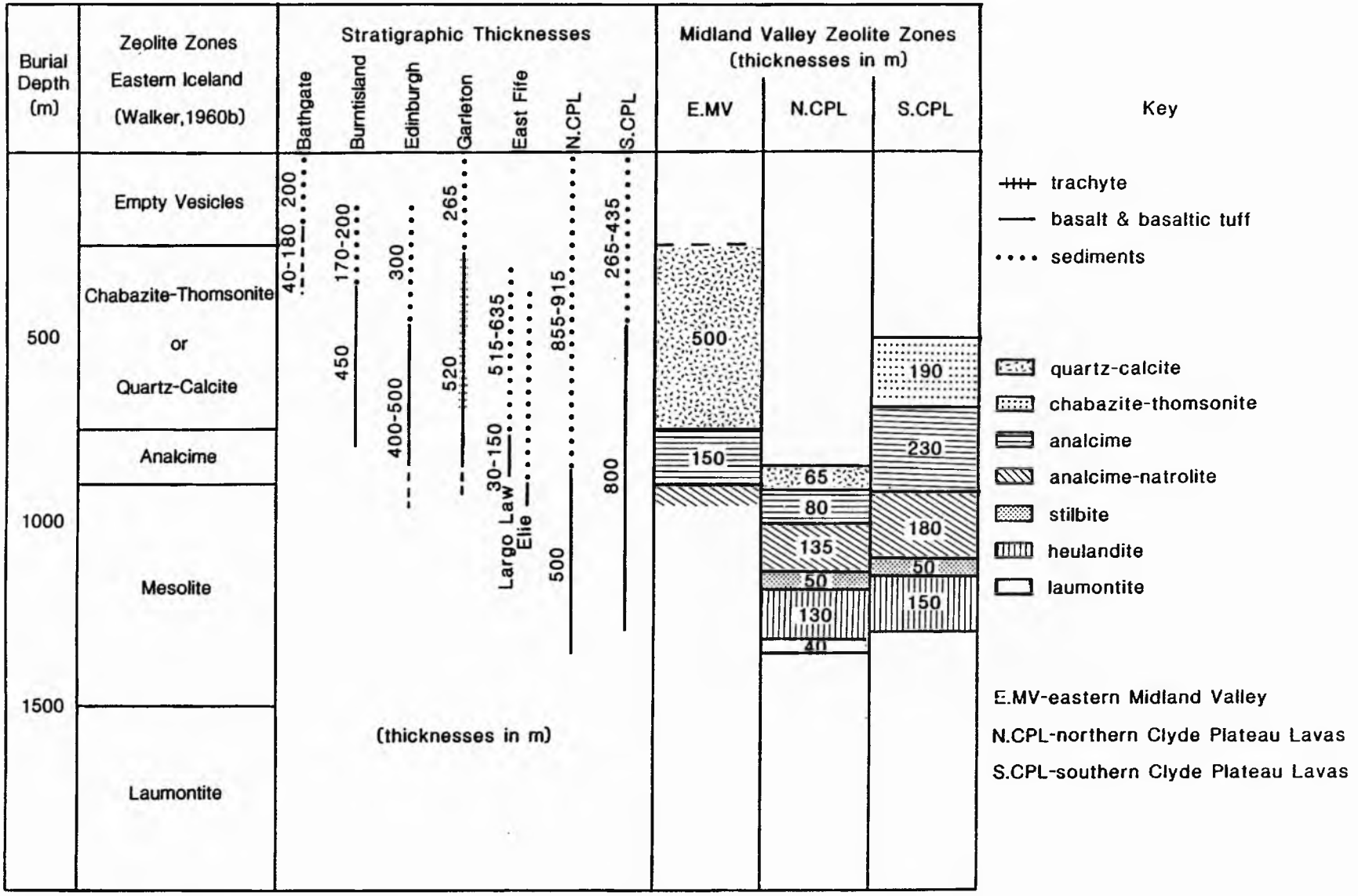


Fig.2.2.9. Comparative burial metamorphic zeolite zones for the Midland Valley and eastern Iceland.

2.2.9) of Carboniferous sediment must have been deposited upon the volcanics, following the cessation of volcanic activity. From the evidence provided, the zeolite zones must reflect progressive burial beneath volcanic and sedimentary accummulations. Zones in the Clyde Plateau Lavas dip towards the SE in the Renfrewshire, Kilpatrick and Campsie Hills. Whilst in the Beith Hills and in the Lanarkshire Block the zones dip towards the NE and SW. These regional dips reflect progressive sedimentary overlap from the Central and Ayrshire Basins towards the volcanic areas.

Sources of heat and mineralizing solutions are discussed in chapters 2.4 and 2.7.

### 2.2.5 Palaeo-geothermal Plumes

Steep-sided zones (plumes) of hydrothermal activity have been recognised at seven localities (Fig 2.2.10; table 2.2.4) in the Carboniferous Volcanics of the Midland Valley. The observations made are from quarries or road-cuttings, where blasting has provided large fresh exposures. It is therefore possible that more plumes occur throughout the lavas, but the quality of exposure on moorland tops, is such that they have not been recognised. The general characteristics of these plumes are outlined below.

#### Plume Characteristics

Hydrothermal activity in palaeo-geothermal plumes is expressed as steep-sided zones of essentially monomineralic alteration. The zones are some 1-15 m wide. Wall-rock contacts with regional zeolitized basalt are sharp, and are often visible on quarry walls. The distinct absence of plume aureoles (excluding Langbank and Beith)

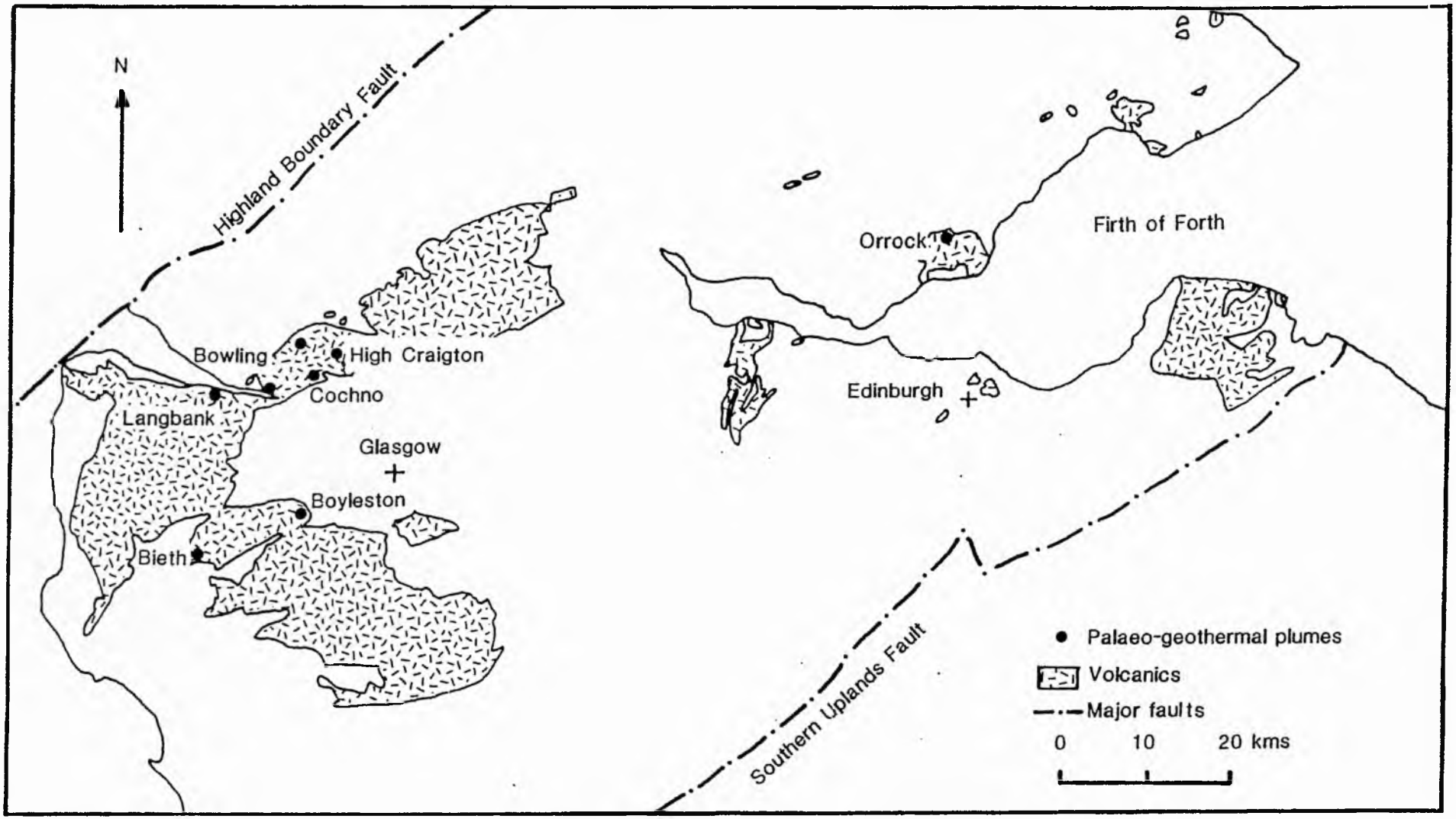


Fig.2.2.10.Distribution of palaeo-geothermal plumes within the Midland Valley Carboniferous , Scotland.

Table 2.2.4

| Locality | Grid Reference |
|---|---|
| Bowling Quarry, the Kilpatricks | NS 443 739 |
| Boyleston Quarry, Barrhead | NS 492 598 |
| Cochno road cutting, Kilpatricks | NS 479 748 |
| Langbank road cutting, Port Glasgow | NS 369 735 |
| Loanhead Quarry, Bieth | NS 358 555 |
| Orrock Quarry, Burntisland | NS 237 907 |
| High Craigton Quarry, Milngavie | NS 526 769 |

Table 2.2.4 Midland Valley geothermal plumes in Carboniferous Volcanics.

indicates that a steep geothermal gradient must be invoked to explain the plumes. Map interpretation, indicates that these near vertical plumes cut across or are cut by the horizontal regional zeolite zones.

Within the palaeo-geothermal plumes, alteration is complete. Lava flows are only recognized by virtue of the fact that weathered surfaces have been haematized. Individual flow units (UAL, MML, LAL; see section 2.2.4.3 for definition) are completely destroyed.

The metabasalt in handspecimen has two textural forms. The least common texture is that of orbicular poorly defined concentric zones, within which replacement by epidote has occurred. More commonly the metabasalt forms light grey pseudohexagonal clusters, with radial partitions culminating at a central point (plate 11); replacement is by prehnite. The presence of epidote and prehnite in these rocks has been confirmed by X-ray diffraction, thin-section analyses and microprobe analyses.

At Langbank (Fig 2.2.10), the prehnitized metadomain (as described above) is only 1 m wide. Beyond this zone, prehnite is patchily distributed throughout anomalously zeolitized basalt. Zeolite species present include analcime, stilbite and heulandite. These minerals are also characteristic of the regional zeolite zone. However, zeolite productivity decreases rapidly away from the palaeo-geothermal plume, to a more 'normal' level of zeolitization in the surrounding metabasalt (no prehnite recorded here). This anomalous zeolite productivity is believed to represent a low temperature hydrothermal aureole surrounding the prehnitized geothermal plume. The data from Langbank suggests that either:-

Plate 11A: Photograph of prehnitized metabasalt. Consisting of paeudo-hexagonal clusters of prehnite, which extend into amygdales (top left).

Plate 11B: Cross-section through botryoidal prehnite extending into a vein. Note the textural similarities between plate 11A and 11B.

10mm

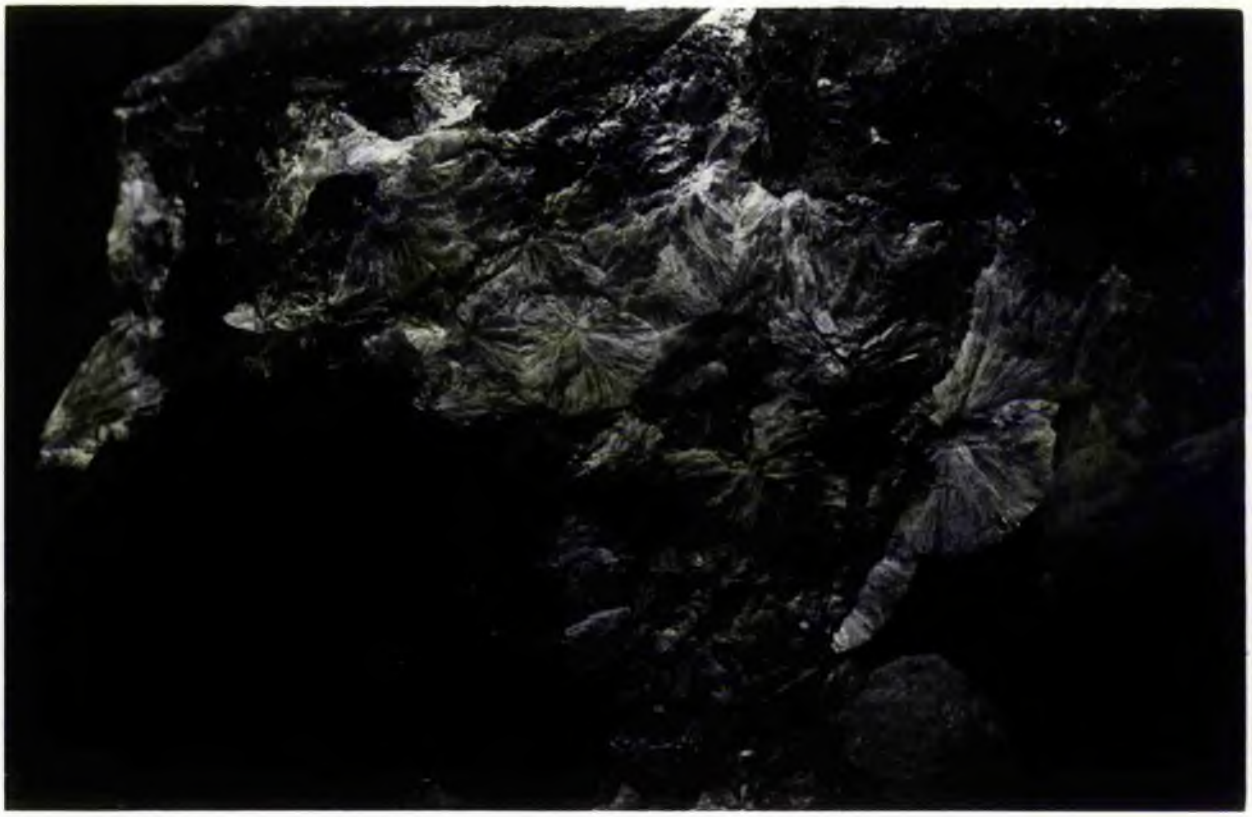

15mm

i) a structurally higher level in a palaeo-geothermal plume is viewed, as compared to structurally lower levels seen elsewhere. Such vertical differentiation of minerals in geothermal areas has been observed by Kristmannsdottir and Tomasson (1978).

ii) temperatures were not as high in other regions

iii) a fluctuating heat flow existed which was not maintained for sufficient duration to allow for extensive prehnitization.

At Beith (Fig 2.2.10) a major palaeo-geothermal plume associated with a Tertiary dyke (see chapter 2.1), is developed within the regional analcime-natrolite zeolite zone. A sketch map of the study area is presented in Fig 2.2.11. There are four aureole zones surrounding the Tertiary dyke. With increasing distance from the contact, these are:-

i) a 1 m wide zone of carbonate metasomatism, characterized by the contact metamorphic mineral rankinite. (Rankinite is also encountered at CV63, CV84 and CV65 in association with the Tertiary dyke outcrops). The basalt shows extensive replacement by calcite and epidote. Geodes are infilled with thomsonite.

ii) a 6 m wide epidote contact aureole. Individual flow units are destroyed, although haematite veins testify to flow boundaries. Localities nearest to the dyke are veined with calcite.

Plate 12A: Photograph of hydrothermally altered basalt from Beith quarry, in the Clyde Plateau Lavas. The dark band is the haematized flow top.

Plate 12B: Photograph of hydrothermally altered metabasalt from the Icelandic rift zone, Krafla.

iii) a 20 m wide zone of light grey basalt showing flow characteristics and phenocrystic textures. Amygdales and veins are infilled with prehnite, which decrease in abundance away from the dyke. At most localities, prehnite is overgrown by thomsonite, which is present throughout the zone. In some handspecimens, thomsonite needles are seen to pseudomorph the plagioclase phenocrysts

iv) a 4 m wide zone of orbicular green and/or grey metabasalt (plate 12a) disects zone (iii). The texture developed is similar in character to the hydrothermally altered basalt (plate 12b) seen in Icelandic rift zones (personal observations). The metabasalt is infact composed of prehnite; epidote and hydrogrossular have been recorded from voids. The margins of the zone show evidence of hydrofracture. It is likely that increased fluid pressure surrounding the dyke caused fracturing and hence fluid flow into the area (this is discussed further in chapter 2.7).

The boundaries of all the zones are vertical and sharp; in plan (Fig 2.2.11), the zones are parallel to the dyke margins.

**Classification**

The presence of essentially monomineralic metadomains within the Midland Valley volcanics, implies the existence of confined zones where extensive element mobility occurred under high water-rock ratios. Since the metadomains cut across the sub-horizontal zeolite zones, and can be traced vertically through the volcanic pile, fluid movement must have occurred in a plume of hot rising water. Bevins

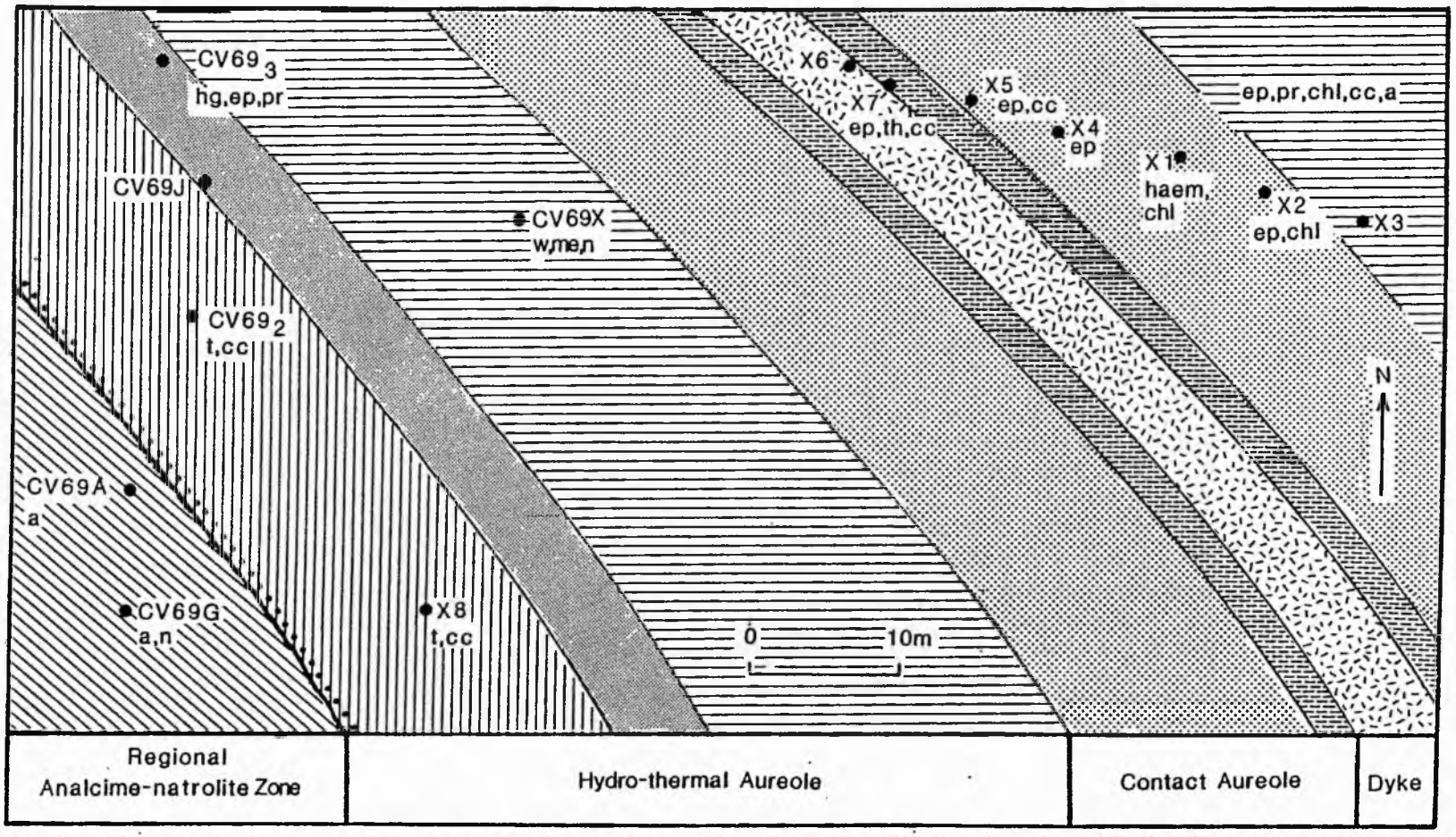


Fig.2.2.11. Simplified sketch map of Belth palaeo-geothermal plume. ● localities: • • • westward extent of hydro-thermal aureole : a-analcime n-natrolite t-thomsonite pr-prehnite ep-epidote hg-hydro-grossular. w-wairakite me-mesolite haem-haematite chl-chlorite cc-calcite
Tertiary dyke : Alteration Zones :: carbonate metasomatism epidote prehnite-thomsonite prehnite-epidote thomsonite analcime-natrolite

(1985), described a similar example of metadomains from central Wales.

Saturated solutions precipitated thomsonite and prehnite. In the Midland Valley, thomsonite is more frequently recorded from palaeo-geothermal plumes, than from the regional zeolite zones. Evarts and Schiffman (1983), similarly noted that in modern systems, thomsonite was more abundant in geothermal fields than in the burial metamorphic environment. With the possible exclusion of Langbank no vertical zonation of hydrothermal minerals within the palaeo-geothermal plumes is apparent. However all the plumes examined exist at the same stratigraphic level ie within the analcime or analcime-natrolite zones. Similar assemblages have been recorded at comparable levels (c 750 m depth, at 250 $^{o}$C) in the geothermal plumes of central Iceland (Kristmannsdottir and Tomasson, 1978), where a geothermal gradient of 30 $^{o}$C/km is encountered.

**Plume Mechanics**

Plume mechanics are discussed in greater detail in chapter 2.7. Only those points that are obvious from field relationships are discussed here.

For the plumes to function, there are three necessary requirements:-

i) a heat source

ii) a fluid source

iii) channelways for fluid circulation

**Heat Sources:** Bowling and Milngavie palaeo-geothermal plumes are disposed about Dinantian vents; whilst at Beith, Langbank and Orrock

hydrothermal activity is associated with the proximity to sills and dykes. The diameter of individual palaeo-geothermal plumes is governed by the size of the associated igneous body.

At Cochno and Boyleston, igneous bodies are not exposed and geophysical evidence for their presence is lacking. A possible source of heat (decarbonation of organic matter) for the Boyleston plume is discussed in chapter 2.6. . It is doubtful that this explanation can be extended to cover palaeo-geothermal activity at Cochno.

**Fluid Sources:** Fluids may comprise pore-water expelled from the under- and over-lying sediments; or circulation may involve seawater. In some plumes, evidence of hydrofracture associated with magma intrusion, suggests a relationship to increased fluid pressures.

**Channelways:** An indication of the pattern of fluid circulation is given by the distribution of metadomains within the plumes. On the scale of an exposure, channelways for fluid movement are provided by lava flow boundaries and by vertical joint planes and fractures. In both instances, higher temperature assemblages crystallize along these planes, and decrease in abundance away from them.

**Timing of Palaeo-geothermal Events**

At Cochno and Bowling, high temperature metadomain assemblages (thomsonite and prehnite) crystallized from saturated solutions before minerals of the regional zeolite zone. These plumes must have developed during the Dinantian, before regional zeolitization occurred and possibly before the bulk of the lavas were extruded.

Hydrothermal activity is likely to have been associated with 'feeder dykes' to the lavas (see chapter 2.1).

Elsewhere metadomains are imprinted upon the regional burial metamorphic zones. Such overprinting of fabrics, necessitates that a long period of 'cool' groundwater percolation predated the high temperature geothermal systems. At Orrock and Langbank, plume development is clearly associated with the intrusion of Westphalian (290 Ma; de Souza, 1979) quartz-dolerite dykes and sills. The Beith palaeo-geothermal plume developed in association with the Tertiary dyke phases (59.5 Ma, Evans *et al*, 1973) of Mull.

### 2.2.6 Conclusions

1 Three styles of hydrothermal alteration have been recognised in the Carboniferous Volcanics of the Midland Valley. These are:-

i) early greenstone alteration, involving exchange between volcanics and (sea)-water.

ii) late regional burial metamorphism in the zeolite facies; expressed by amygdale and vein assemblages.

iii) palaeo-geothermal plume alteration.

2 Hydrothermal alteration is distributed as follows:-

i) greenstone alteration is confined to vents or to the basal accummulations of volcanic piles, in the eastern Midland Valley.

ii) burial metamorphism is developed in the Clyde Plateau Lavas and in the eastern Midland Valley. The intensity of alteration decreases towards the Central and

Ayrshire Synclines ie higher in the stratigraphic sequences.

iii) palaeo-geothermal plumes are localized and reflect areas of particularly high heat production.

## Chapter 2.3 Petrography

### 2.3.1 Aims

Three types of hydrothermal alteration (greenstone, regional burial metamorphic and palaeo-geothermal plume) have been recognized in the Midland Valley, on the basis of field-mapping (chapter 2.2). In chapter 2.3. , petrographic observations are recorded, to:-

i) determine the extent of alteration exhibited by relict igneous assemblages
ii) characterize metamorphic assemblages
iii) correlate thin-section assemblages with field assemblages (chapter 2.2).

### 2.3.2 Introduction

One hundred and fifty eight thin-sections of basalt (see chapter 2.3 for nomenclature), mugearite, trachyte and basaltic tuff, were examined in order to determine the petrographic characteristics of the alteration styles.

An initial survey of the relict mineralogy was undertaken, to determine:-

i) the original mineralogy of the lavas and tuffs
ii) which minerals were most readily effected by metamorphism
iii) the effects of hydrothermal alteration in the different lava types.

The chapter is essentially concerned with the metamorphic

Plate 13A: Photomicrograph of plagioclase showing rim replacement textures. Coronas are infilled with chlorite and sericite.

Plate 13B: Photomicrograph of plagioclase phenocryst showing patches of incipient albite crystallization. Dusty speckles are of sphene. Veins, amygdales and groundmass laths show similar replacement by albite.

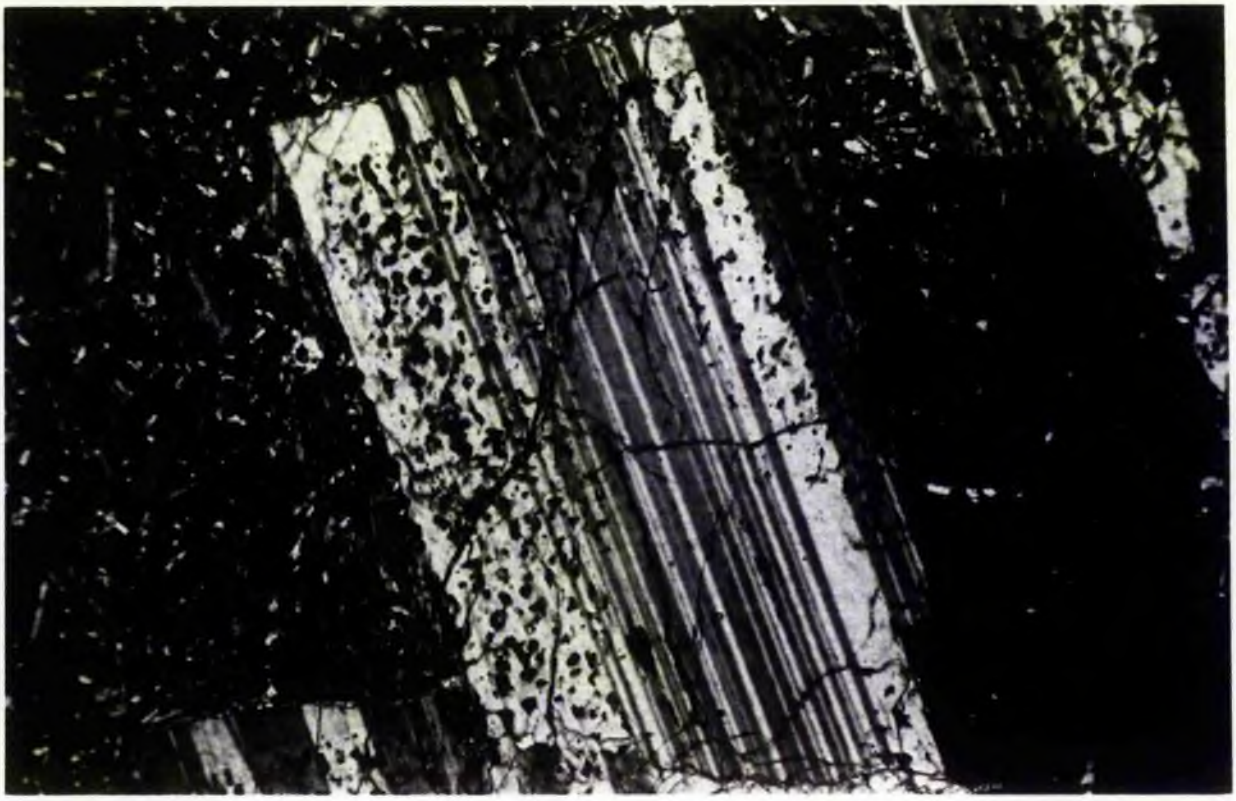

50μ

50μ

petrography of the regional burial zones and with alteration in the palaeo-geothermal plumes. The main petrographic characteristics of the greenstone alteration are compatible with those observed under 'Relatively unaltered basalt'. The greenstones also show features characteristic of regional burial metamorphism; these details are discussed during petrographic analysis of the regional burial zones.

Mineral chemistries and petrological discussions are dealt with in chapter 2.4.

### 2.3.3 The Relict Mineralogy

Listed above (table 2.3.1) are those primary igneous minerals that occur in relict assemblages in thin-section. Observations made are regardless of alteration state; since, in plane light all thin-sections retain their original textures (porphyritic, amygdaloidal, trachytic), so that a fairly good approximation can be made of the original phases.

Only apatite and biotite have experienced little or no alteration during low-grade metamorphism. Magnetite is commonly converted to haematite or sphene; whilst pyroxene (augite and titan-augite) is replaced by a mixture of iron oxide and chlorite (chlorophaeite), calcite or sphene. Plagioclases are saussuritized, albitized or chloritized. Of the 75% altered, total albitization affects only 55%, the remainder show only partial albitization along cracks and cleavages in minerals (plates 13; 14). Glass (perlitic textures were not observed) and olivine are nearly always altered. The presence of glass is inferred by chlorite, chlorophaeite and analcime in the interstices between minerals (plate 15a); and olivine by reddish brown iddingsite and green chlorophaeite. Zeolitic

Table 2.3.1

| Mineral Phase | % Present* | % Altered* |
|---|---|---|
| Magnetite | 92% | 30% |
| Glass | 92% | 95% |
| Orthoclase<br>Plagioclase Feldspar<br>Oligoclase | 91% | 75% |
| Olivine | 88% | 95% |
| Pyroxene (clino-) | 87% | 52% |
| Apatite | 53% | 6% |
| Biotite | 4% | 0% |

Table 2.3.1 Percentage of total thin-sections containing a given phase and percentage of those reconstituted by low grade metamorphism * based on 158 thin-sections.

Table 2.3.2

| Rock Type | | Markle (M) | Jedburgh | Dalmeny | Tuff | Dunsapie (M) | Hill-house | Craig-lockhart (M) | Trachyte + Mugearite |
|---|---|---|---|---|---|---|---|---|---|
| Abundance in T/S* | | 31% | 21% | 12% | 10% | 6% | 4% | 3% | 3% |
| Relict Minerals | Magnetite | 37% | 33% | 32% | 27% | 40% | - | - | - |
| | Glass | 100% | 97% | 89% | 93% | 100% | 71% | 60% | 100% |
| | Feldspar | 86% | 82% | 74% | 53% | 80% | 14% | 20% | 40% |
| | Olivine | 98% | 94% | 84% | 53% | 90% | 86% | 100% | 100% |
| | Pyroxene (clino) | 57% | 55% | 63% | 47% | 10% | 43% | - | 50% |
| | Apatite | 8% | - | - | - | 10% | - | - | - |
| | Biotite | - | - | - | - | - | - | - | - |

Table 2.3.2 Percentage of volcanic types described in thin section and relationship between the type of volcanic rock and the percentage of altered primary phases * based on 158 thin-sections (M) = macroporphyritic basalt.

Plate 14A: Photomicrograph of albitized plagioclase phenocryst sitting in opaque analcimitized metabasalt.

Plate 14B: Enlargement of plate 14A, to show fasicule bundles of albite.

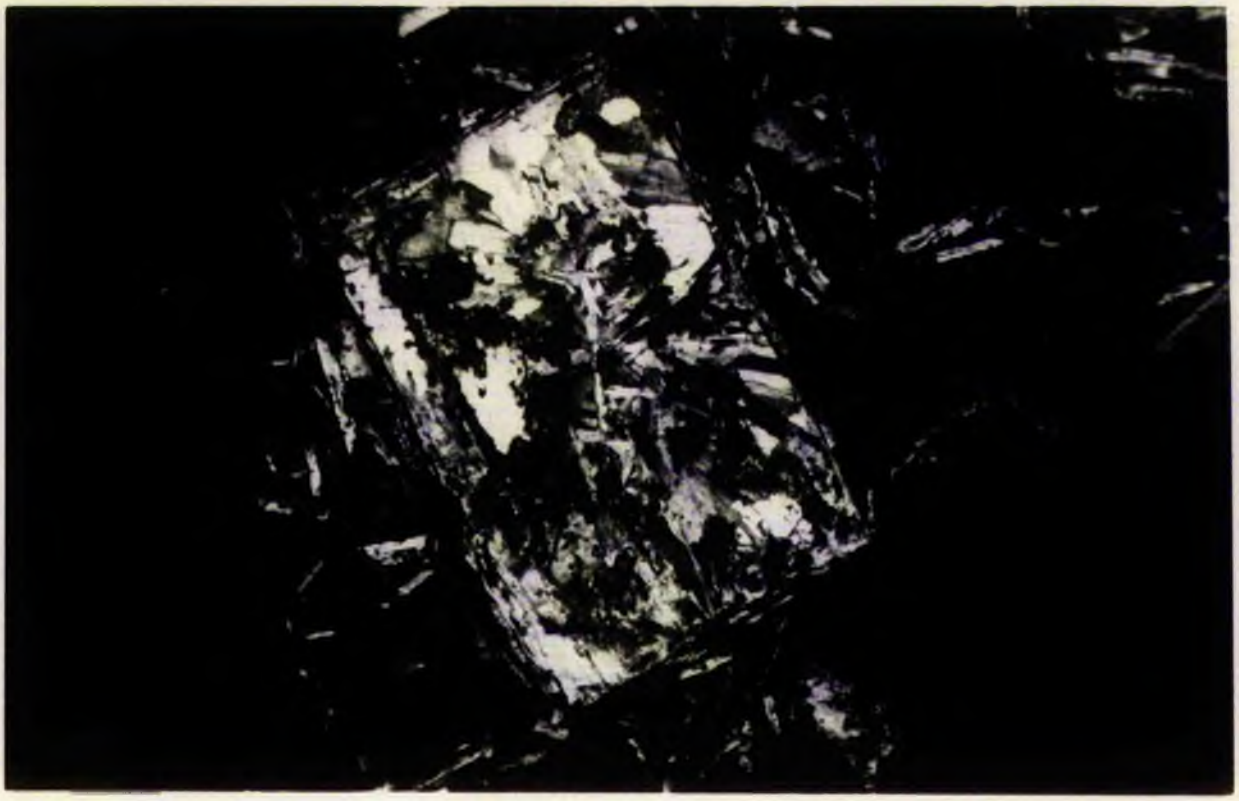

50μ

20μ

replacements (and associated minerals) are discussed later in the chapter.

The relationship between the type of volcanic rock and the percentage of altered primary phases is shown in table 2.3.2. Relict minerals in Markle, Jedburgh, Dunsapie and Dalmeny-type basalts are more altered than those in mugearites, trachytes and tuff, which in turn are more altered than those in Craiglockhart and Hillhouse type basalts. Furthermore, for any given mineral (excluding clinopyroxene in Dalmeny type basalts) the percentage alteration is greater in the macroporphyritic (eg Markle) as opposed to the associated microporphyritic (eg Jedburgh) environment. If this phenomenon was attributed to permeability contrasts between phaneritic and aphanitic basalt, alteration would be greater in the microporphyritic variety. Since microporphyritic lavas have a higher surface area, thereby yielding a greater grain boundary driving force for reaction (Vernon, 1979) and allowing easier intergranular diffusion or passage of intergranular fluids. This may be observed within single flows in the Midland Valley, where relict minerals in the UAL* or LAL* have experienced greater alteration than those in the MML* (* abbreviations are defined in chapter 2.2). Macro- and micro-porphyritic lavas eg Markle and Jedburgh, are compositionally similar, and do not show a predominance of jointing/veining in one variety as opposed to the other. Variation in the extent of alteration between macro- and micro-porphyritic lavas is therefore attributed to either:-

i) an increase in volatiles in macroporphyritic lavas. This would have reduced viscosity and enhanced the development of aa-type

Table 2.3.3

| Amygdale and vein minerals | Minerals that pseudomorph relict igneous phase +/or replace whole-rock. |
|---|---|
| albite | albite |
| analcime | analcime |
| calcite | chlorite |
| chabazite | epidote |
| chlorite | haematite |
| epidote | laumontite |
| ferrierite | natrolite |
| gmelinite | prehnite |
| gonnardite | sphene |
| haematite | |
| heulandite | |
| hydrogrossular | |
| laumontite | |
| mesolite | |
| natrolite | |
| prehnite | |
| quartz | |
| sphene | |
| stilbite | |
| thomsonite | |
| wairakite | |

Table 2.3.3 Products of hydrothermal alteration.

Plate 15A: Photomicrograph to show the interstitital growth of radial chlorite, from glass (plane-light).

Plate 15B: Photomicrograph of prehnitized (bottom) and analcimitized (top) metabasalt. The alteration front cuts the amygdale margin transversally (see overlay).

50μ

50μ

lavas. This should effectively have increased the proportion of cracks in the lavas. Surfaces of many flows show evidence for autobrecciation, however this is not a feature restricted to macroporphyritic lavas.

ii) the increased proportions (ie sizes) of crystals within macroporphyritic lavas. This would have increased viscosity abruptly (McBirney, 1984), so that upon extrusion macro- and microporphyritic lavas would have had different rheological properties. This may have led to differences in primary interconnecting pore-spaces, which the hydrothermal alteration exploited.

Within the basalts a decrease in the extent of relict mineral alteration is observed. From:-

i) Markle - Dunsapie - Craiglockhart type basalts (macroporphyritic)

ii) Jedburgh - Dalmeny - Hillhouse type basalts (micro-porphyritic).

These trends indicate that alteration is dominant in feldspar phyric basalts, and decreases as the proportion of feldspar in phenocrysts and groundmass becomes subordinate to olivine and pyroxene crystals. Hence Ca-plagioclase-rich basalts are altered to albite and/or analcime rich metabasalts, thereby releasing CaAl to the hydrothermal fluid to form zeolites.

**2.3.4 The Mineralogy**

Table 2.3.3, forms a comprehensive list of those minerals developed as a direct result of hydrothermal alteration

Plate 16A: Photomicrograph of analcimitzed metabasalt in plane-light. Analcime is characteristically dusty, and replaces the groundmass and felspar phenocryst, as well as growing into amygdales. The centre of the amygdale is infilled with natrolite radials.

Plate 16B: Photomicrograph, as above, taken in cross-polars.

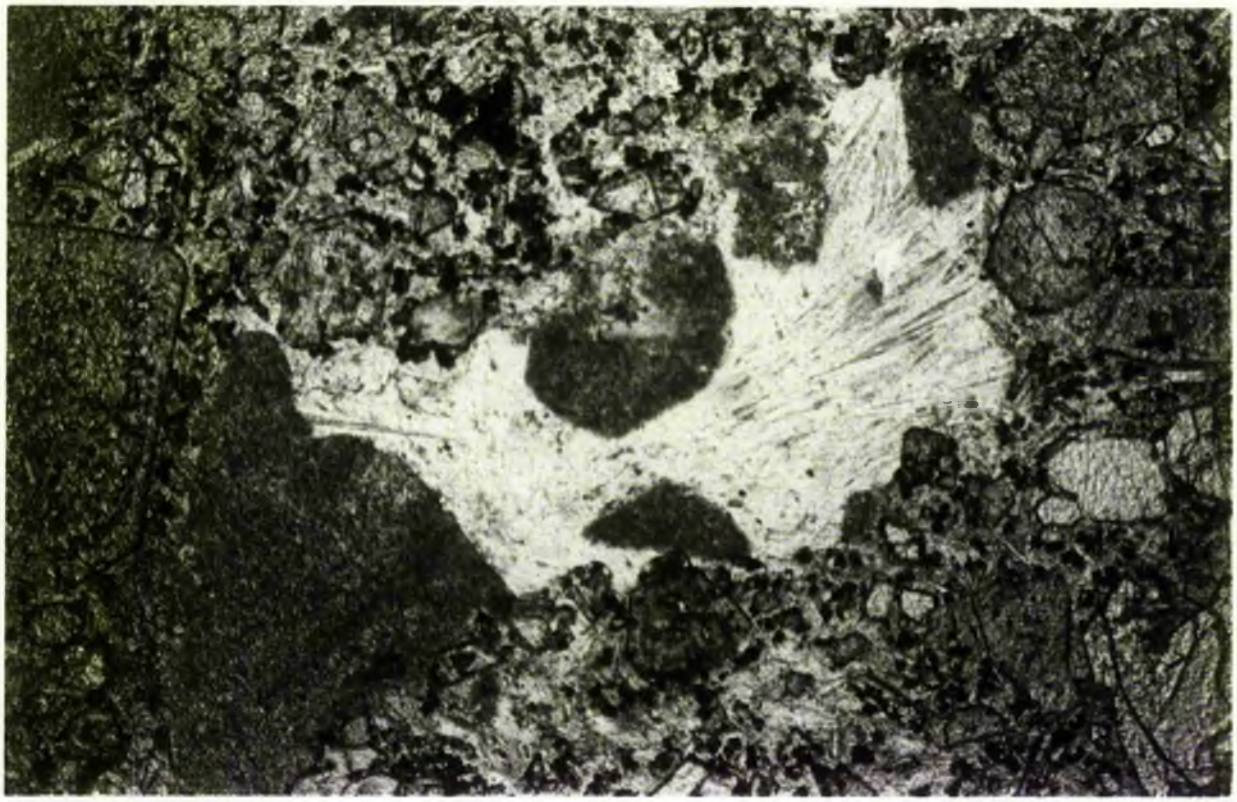

50μ

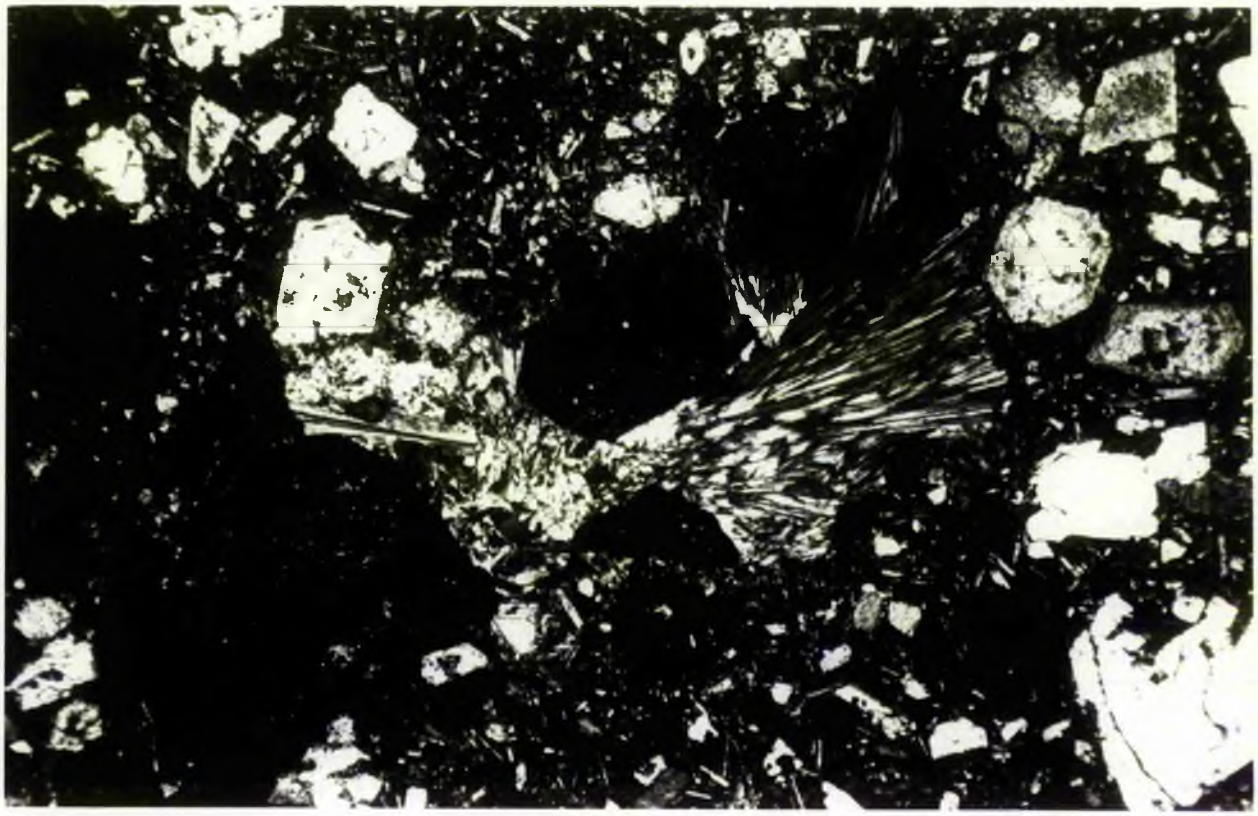

50μ

(non-specific). In addition to those minerals listed, relict igneous phases also persist.

A distinction can be made between those minerals that pseudomorph relict igneous phases and those minerals that occupy amygdales and veins. The former principally concerns albite, analcime, laumontite, prehnite, haematite and sphene; and less commonly natrolite (plates 13-19). The latter concerns the aforementioned, plus heulandite, stilbite,thomsonite, chabazite and quartz (plates 13-19). These minerals may also be found in amygdales and veins (plates 16; A; 20-21).

Amygdaloidal minerals either show

i) equant euhedral crystal habits (plates 16; 20-22)
ii) pseudohexagonal radial clusters (plates: 17; 20; 21; 23)

It is important to remember that analcime, natrolite and laumontite are the only zeolites to replace igneous phases (including glass) in the basalt. Whilst, the CaAl-zeolites are more commonly restricted to amygdales.

### 2.3.5 Metamorphic petrology of the burial zones

Field mapping has established seven burial-related amygdale zones (see chapter 2.2, fig. 2.2.9) in the Midland Valley. Petrological evidence however, demonstrates that the zonal minerals (exoluding analcime, natrolite and laumontite) are restricted to the amygdale and vein environments. Consequently, petrological observations of matrix alteration, have defined only three burial zones. These are characterized by:-

Plate 17A: Photomicrograph of icositetrahedral analcime projecting into amygdale from analcimitized metabasalt. Within the amygdale, late radial natrolite is seen to grow upon early analcime.

Plate 17B: Photomicrograph of pseudomorphed felsapr phenocryst in analcimitized metabasalt. The left-hand side of the crystal is replaced by natrolite, and right-hand side by analcime.

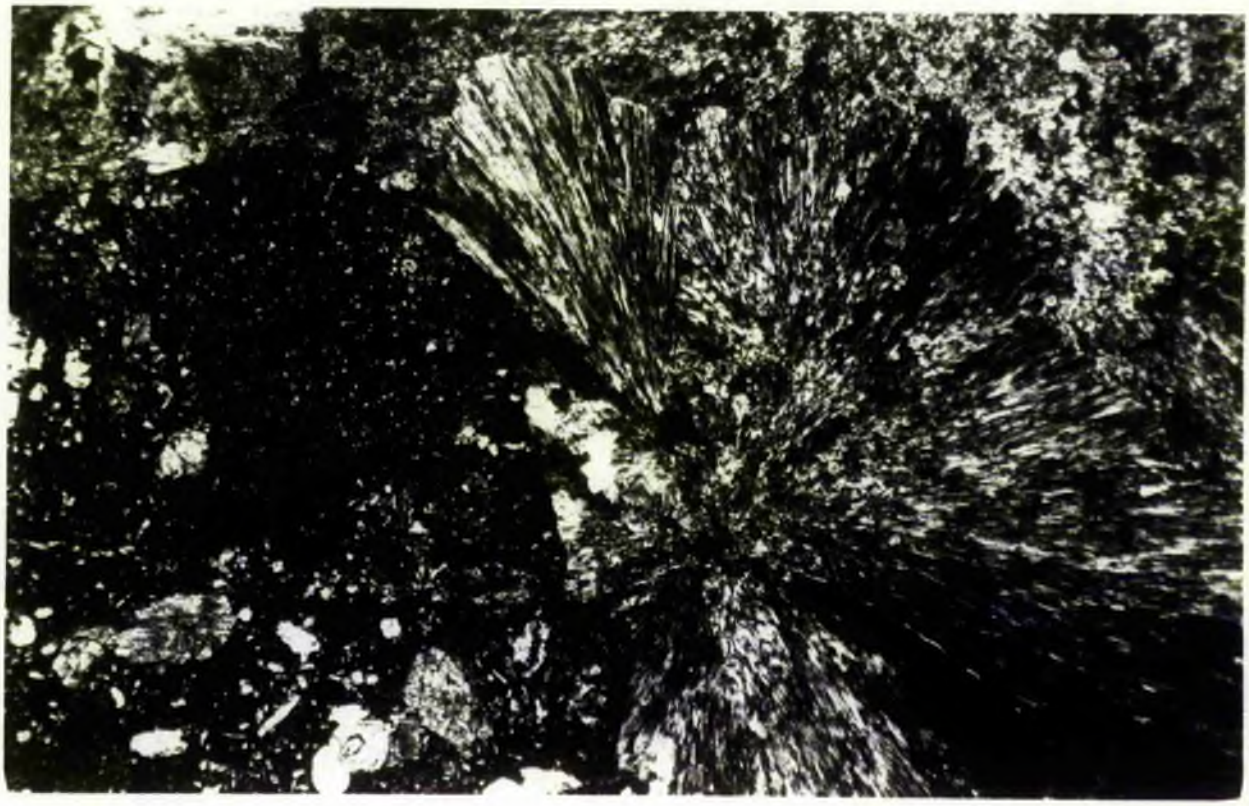

50μ

50μ

i) relatively unaltered basalt

ii) analcimitized and/or albitized metabasalt

iii) laumontized and/or albitized metabasalt

The petrological characteristics of these zones are discussed below. The relationship of these zones to the seven zones established during field mapping are discussed at the end of this section.

**Relatively unaltered basalt**

The basalt in this zone is characterized by fresh plagioclase, pyroxene and apatite. Olivine and glass are pseudomorphed by chlorite.

Amygdale and vein assemblages consist of chlorite, quartz and calcite.

**Analcimitized metabasalt**

Analcime is present in the matrix in zones where thomsonite-chabazite, analcime, analcime-natrolite, stilbite and heulandite predominate in amygdales and veins.

The extent of alteration in the analcimitized metabasalt:-

i) varies significantly, depending upon the availability of fluids and upon the basalt permeability (see chapter 2.2; section 2.2.4).

ii) increases with burial depth, as defined by the distribution of zones in chapter 2.2.

Below the top of the stilbite zone, the degree of reconstitution

Plate 18A: Photomicrograph of laumontized metabasalt, in plane-light. The opaque mineralogy preserves the primary igneous textures.

Plate 18B: Photomicrograph, as above, under cross-polars. Relict igneous textures are difficult to observe, and are incompletely replaced by aggregates of radiating laumontite. Sphene and opaque ores form inclusions in laumontite.

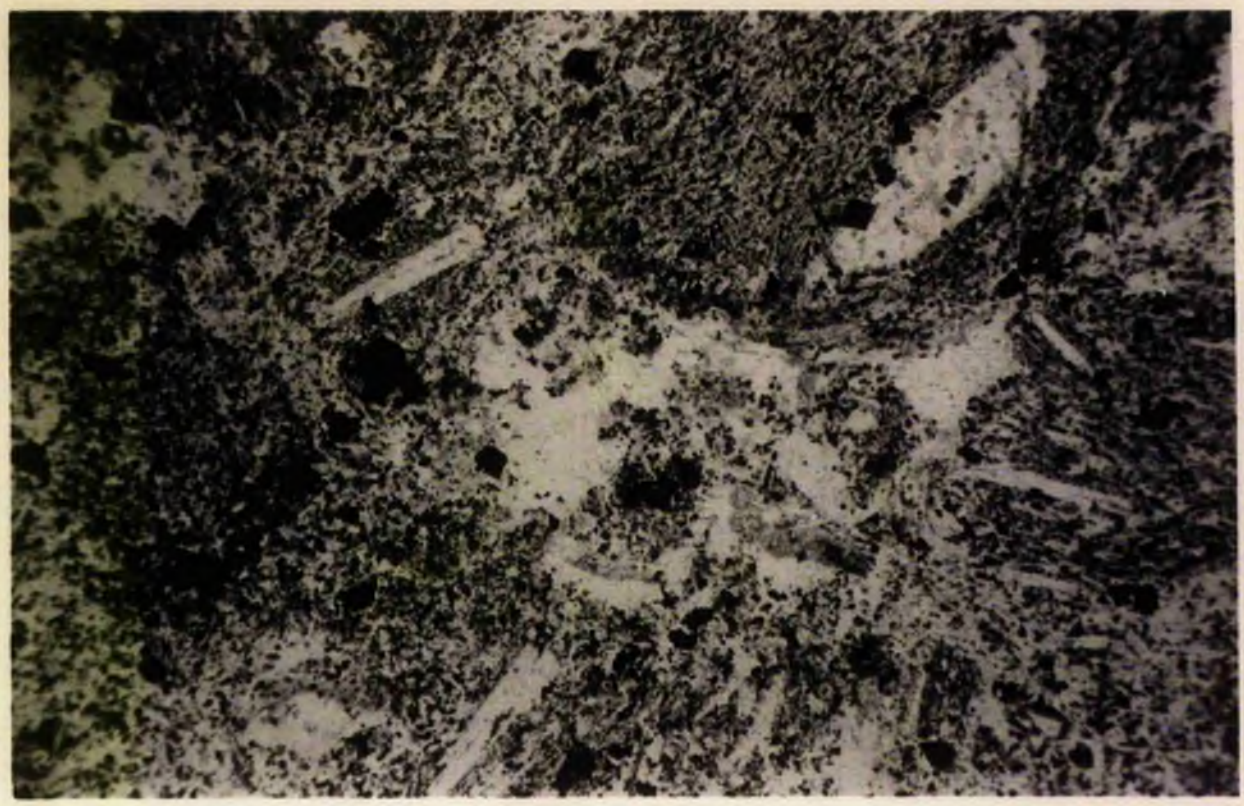

50μ

50μ

changes dramatically. This line has been chose as an arbitrary divide, to describe the alteration characteristics in the analcimitized metabasalt.

i) The upper division: The igneous mineralogy is characterized by fresh apatite. Chlorite variably replaces olivine, glass, plagioclase and pyroxene, but is seldom encountered in amygdale rims. Feldspars are more commonly albitized. Initial replacement is concentrated around rims (plate 13) and along cracks in the crystals (plate 13). In such sections analcime and albite appear to be in contact and therefore are in (meta-)stable co-existence. Locally in analcimitized sections, where vein or amygdular quartz is present, feldspars are saussuritized. This suggests that albite is unstable in the presence of analcime plus quartz (Thompson, 1971b). Replacement by analcime is variable, and may be encountered in the groundmass, pseudomorphing feldspars and infilling amygdales and veins.

Following the appearance of natrolite, feldspars are completely albitized (replacement by analcime and natrolite is sometimes also encountered - plate 17). Where feldspars are completely albitized:-

a) haematite is present and coats relict crystals, amygdales and clasts.

b) magnetite is pseudomorphed by sphene (sphene also occurs as anhedral inclusions in albitized feldspars; plate 14)

c) pyroxene pseudomorphs may be zoned from sphene cores to chlorite rims; this probably reflects initial variation from titan-augite to augite.

ii) The lower division: The matrix metamorphic mineralogy is characterized by sphene - chlorite - albite - analcime - haematite ±

Plate 19A: Photomicrograph of partially pseudomorped pyroxene in analcimitized metabasalt. The pyroxene is in its extinction position; replacement is by prehnite.

Plate 19B: Photomicrograph of prehnitized metabasalt. Sphene and opaque ores form inclusions in prehnite.

50μ

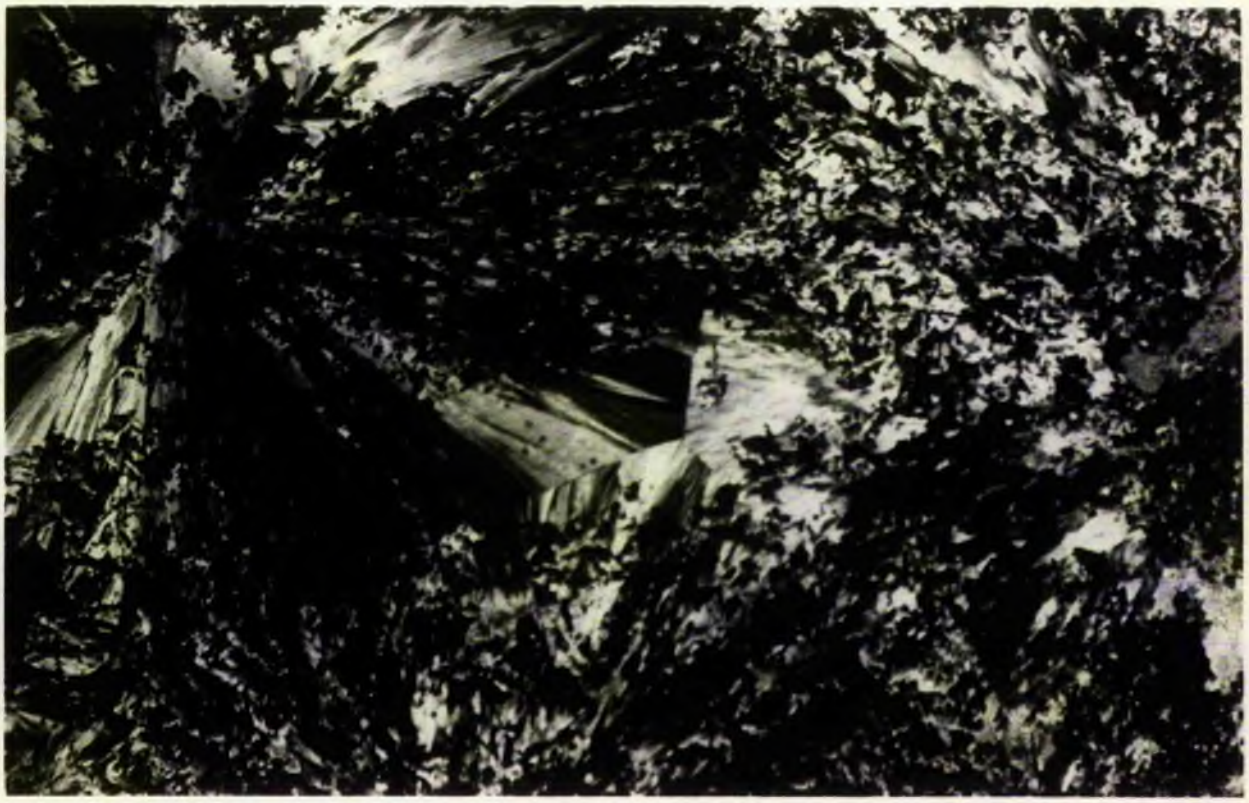

50μ

amygdaloidal quartz, stilbite and heulandite. These minerals replace the relict mineralogy in a similar fashion to that described in the upper divide. The main feature of the lower divide, is that analcimitized metabasalt is essentially confined to the middle massive layer (MML) of lavas flows. In the upper and lower amygdaloidal layers (UAL; LAL), Ca-feldspars are pseudomorphed by simply twinned albite. In several sections, small areas of incipient albite recrystallization (plate 24) destroy the relict igneous textures.

**Laumontized metabasalt**

Laumontized metabasalt is characterized by the assemblage, laumontite - albite - sphene - chlorite - haematite. In the MML, laumontite is restricted to veins. Feldspars are pseudomorphed by albite; whilst the groundmass and mafic minerals are replaced by chlorite and/or sphene. In the UAL, relict igneous textures are visible in plane-polarized light only (plate 18a), and are picked out by interstitial chlorite and/or haematite. Under crossed polars (plate 18b) the metabasalt is composed of polygonal granoblastic laumontite. Sphene, chlorite and haematite form inclusions within the laumontite.

### 2.3.6 Metamorphic petrology of the palaeo-geothermal plumes

Metamorphism is essentially monomineralic within the intense regions of palaeo-geothermal plume alteration. The metabasalt, is composed of polygonal granoblastic prehnite (plate 19). Original igneous textures are visible in plane light only. Epidote and

Plate 20A: Photomicrograph of early opaque icositetrahedral analcime overgrown by late prehnite.

Plate 20B: Photomicrograph of amygdular laumontite.

50μ

50μ

hydrogrossular (plate 22) may crystallize in veins cutting prehnitized metabasalt.

At a distance from the centre of alteration, prehnite either pseudomorphs pyroxene (plate 19), or is restricted to veins which cut the analcimitized and/or albitized metabasalt (plate 25). Igneous textures in these rocks are well preserved.

Field evidence (chapter 2.2; eg at Boyleston see fig 2.2.10 for location) has already established that prehnitization +/- calcification, may both pre- and post-date zeolitization. Textural evidence, shows that early analcime (plate 25) is unstable in the presence of later calcite. However, where calcite was precipitated prior to prehnite and prior to analcime (plate 21), analcime is apparently stable.

### 2.3.7 Discussion

Alteration (metamorphism) in the burial zones and in the palaeo-geothermal plumes, has been described as hydrothermal. This is because:-

1 Alteration is characterized by hydrous mineral species.

2 Rim reaction textures (plate 13) are an initial feature of alteration and promotes the idea of an intergranular fluid attacking the igneous silicates.

3 In the burial zones, the extent of alteration is limited by permeability contrasts (see chapter 2.2) within individual flows, suggesting that the availability of fluid was an important factor during metamorphism.

4 The hydrous mineralogy commonly develops polygonal granoblastic textures, or are euhedral. These textures, in the absence of

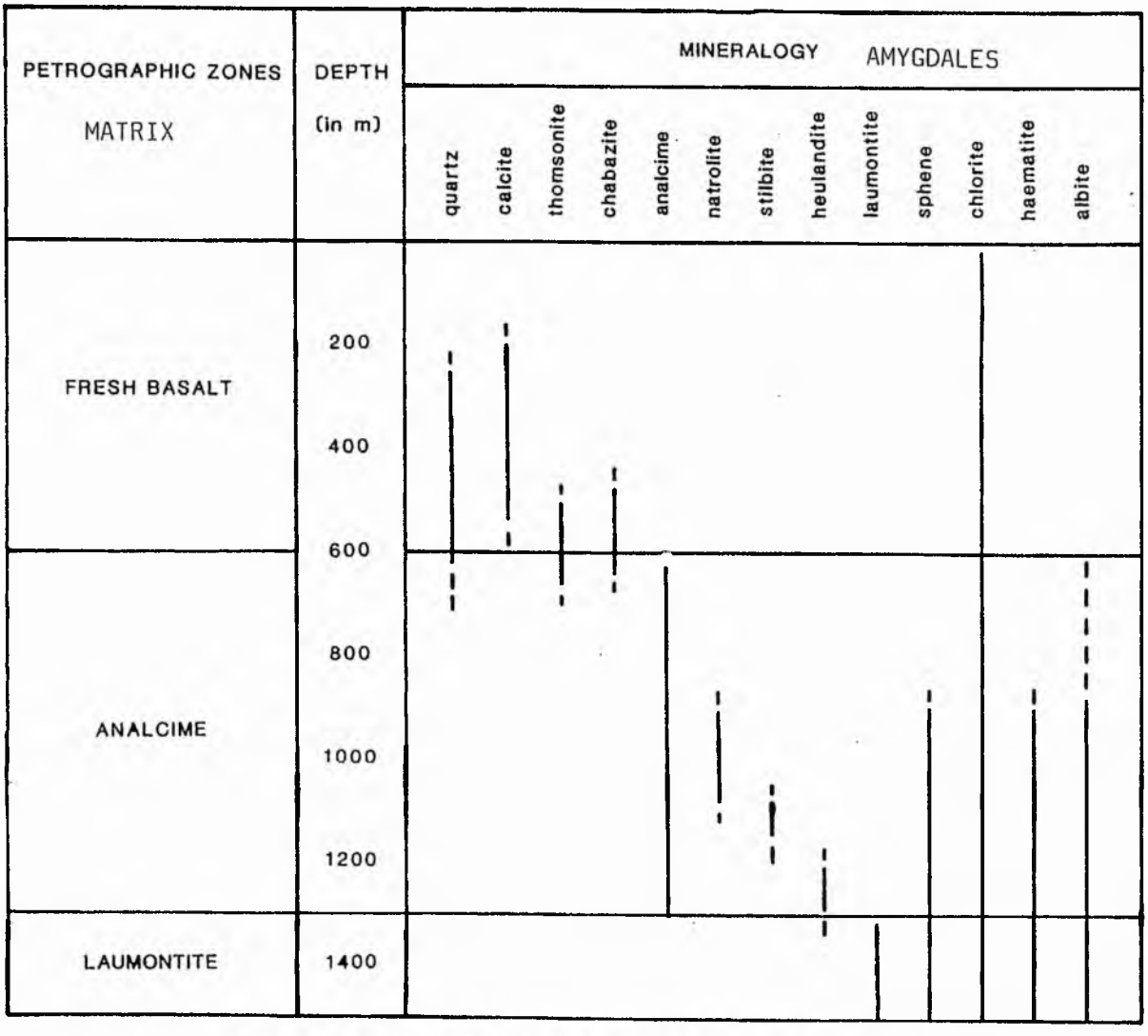


Table 2.3.4. Progressive mineral changes with burial depth.

Plate 21A: Photomicrograph of analcimitized metabasalt. Amygdales infilled with chlorite, calcite and idiomorphic sphene.

Plate 21B: Photomicrograph of acicular prehnite bows growing into geode.

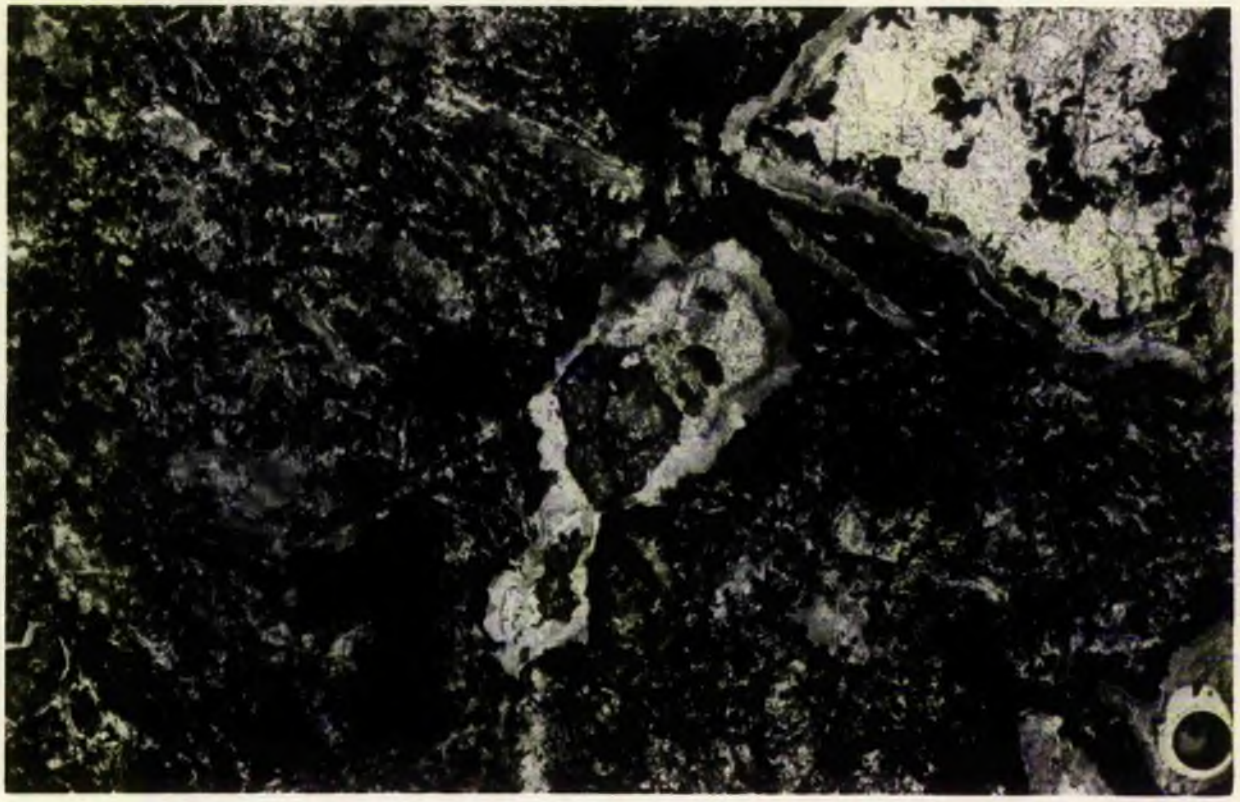

50μ

50μ

Plate 22A: Photomicrograph of amygdular stilbite, heulandite and quartz, growing tangentially from analcimitized metabasalt. Haematite coats the amygdale rim and heulandite crystals. The stilbite is seen to actively replace heulandite.

Plate 22B: Photomicrograph of prehnitized metabasalt. The dark areas characterize replacement by epidote. Top centre, equant partially isotropic hydro-grossular grows into geode. Bottom centre early icositetrahedral analcime has been pseudomorphed by calcite.

50μ

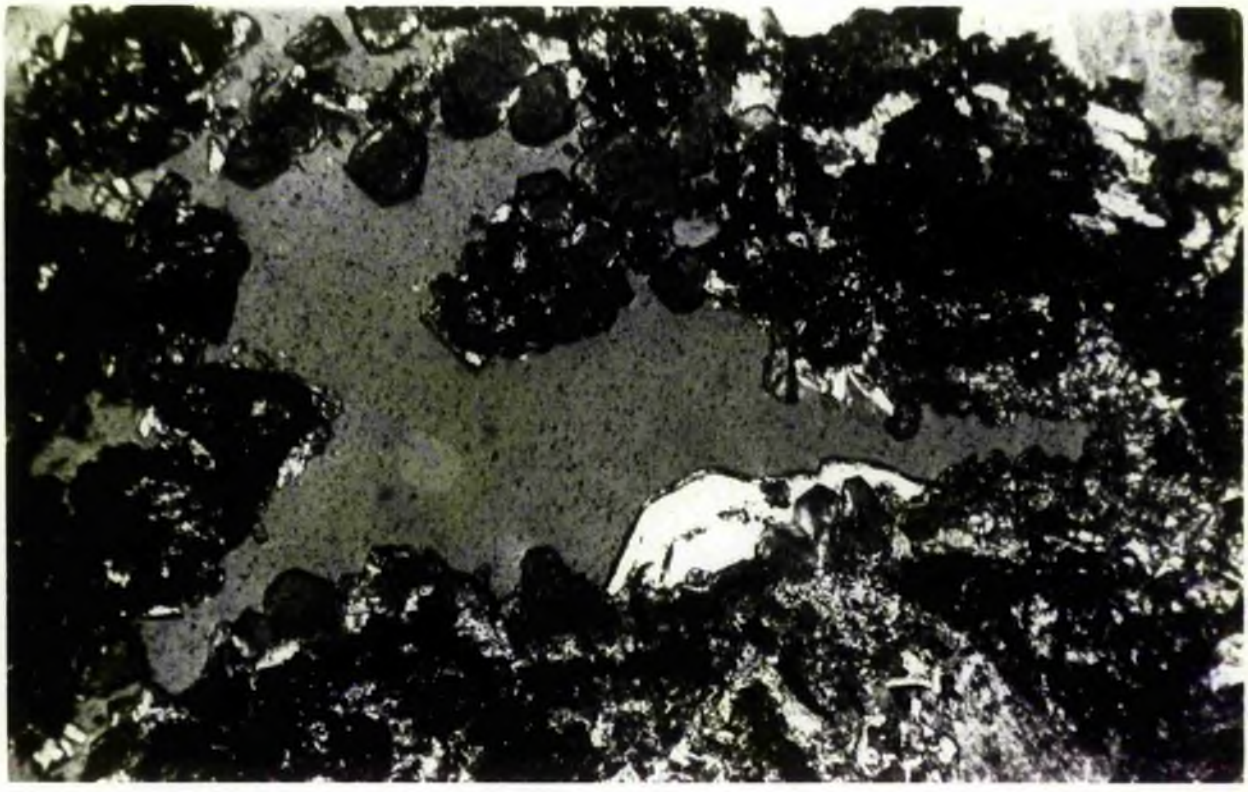

50μ

regional fabrics, represent stable mineral boundaries generated by thermal metamorphism in the absence of an effective strain.

The mineralogy of the burial zones, constitutes a recognisable and progressive change in assemblages. This can be correlated with (table 2.3.4) burial depth, as defined in chapter 2.2. The persistence of igneous textures and igneous minerals indicates that it is not possible to assume that an entire thin-section (or hand-specimen) was in total phase equilibrium. However, there is a remarkable degree of uniformity among the reaction products, suggesting that metastability was attained locally.

The progressive alteration of relict minerals suggests that reactions at low-grade involved the hydration of an initially anhydrous igneous mineralogy. The metamorphic mineralogy reflects progressive metamorphism since reactions involving the conversion of analcime to laumontite (see chapter 2.4), involved the dehydration of hydrated assemblages formed at lower grades (see chapter 2.4). Reaction textures between analcime and laumontite have not been observed in the Midland Valley.

The hydrous mineralogy developed, provides a key to the nature of the hydrothermal fluid. During burial metamorphism, the conversion of analcime to natrolite to laumontite necessitates that early fluids were sodic, and became increasingly calcic as alteration progressed. Amygdale and vein minerals eg heulandite, stilbite, thomsonite and chabazite, are essentially calcic (microprobe data is presented in chapter 2.4). The restriction of calcic-zeolites to these environments, suggests that the amygdale assemblages reflect a second flushing of the metabasalts by Ca-fluids liberated during advanced alteration of the igneous silicates. Criteria for these

Plate 23A: Photomicrograph of spherulitic vein ferrierite in basalt.

Plate 23B: Photomicrograph of spherulitic stilbite and quartz growing into geode in analcimitized metabasalt.

50μ

50μ

Plate 24A: Photomicrograph of prehnite, showing optical continuity between occurrences in a vein and a pseudomorph. The prehnite is in analcimitized metabasalt.

Plate 24B: Photomicrograph of analcime (centre), calcite (tangential) and prehnite. The calcite replaces analcime.

50μ

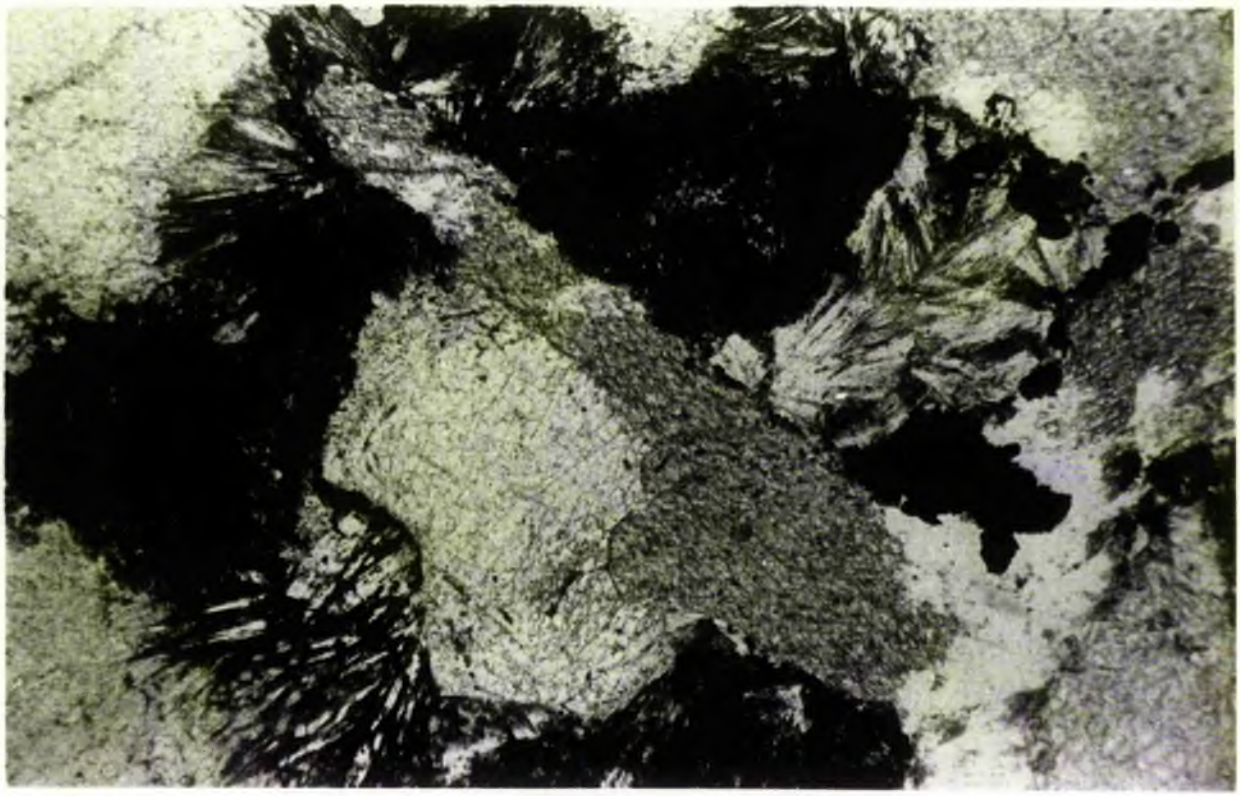

50μ

events are discussed further in chapter 2.4.

The hydrous mineralogy of the palaeo-geothermal plumes indicates that the metabasalts experienced intense Ca-metasomatism.

### 2.3.8 Conclusions

1 Alteration of relict igneous assemblages is enhanced in the amygdaloidal layers of individual flows, due to inherant permeability contrasts. Alteration increases with burial depth and with metamorphic grade.

2 A study of the matrix petrography reveals 3 burial metamorphic environments, characterized by the following assemblages.

i) quartz-calcite-chlorite

ii) analcime ± albite ± sphene ± chlorite ± haematite ± amygdaloidal quartz ± natrolite ± thomsonite ± chabazite ± stilbite ± heulandite.

iii) laumontite-albite-sphene-chlorite-haematite

Although not all areas have a laumontite zone beneath the analcime zone.

Palaeo-geothermal plumes are characterized by the assemblages:- prehnite ± sphene ± haematite ± albite ± hydrogrossular ± epidote ± chlorite

3 Thin-section assemblages and field assemblages are correlated in table 2.3.4. Thin-section analysis shows that the analcime zone should truly encompass the thomsonite-chabazite, analcime, analcime-natrolite, stilbite and heulandite amygdale zones described in chapter 2.2.

## Chapter 2.4 Mineral Chemistry

### 2.4.1 Aims

1 To establish pressure and temperature conditions of the metamorphism from mineral chemistries.

2 To establish the composition of the fluid phase.

### 2.4.2 Introduction

In this chapter the chemistry of the zeolites and of associated minerals (described in chapter 2.2 and 2.3) are determined from microprobe analyses. Comparison is made with mineral chemistries from similar hydrothermally altered regions. Particular reference is made to low grade metamorphic sequences in Iceland, New Zealand and the British paratectonic Caledonides.

### 2.4.3 Mineral Chemistry

1 Methods

Measurements were made, using a JEOL Superprobe 733. An operating current of $10^{-9}$ nA at 15 kV was utilized. Beam width varied from 1 $\mu$ for feldspars, to 10-20 $\mu$ for the hydrated silicates.

Difficulties were encountered for the determination of alkaline elements, especially sodium. Variation is attributed to the loss of weakly bonded elements in the vacuum chamber. This resulted from partial volatilization, associated with the heat of the electron beam. A small increase in the count rates arose due to this phenomenon, and was expressed by high $Al_2O_3$ and $SiO_2$ values. Several totals greater than 100% were observed for feldspars because of

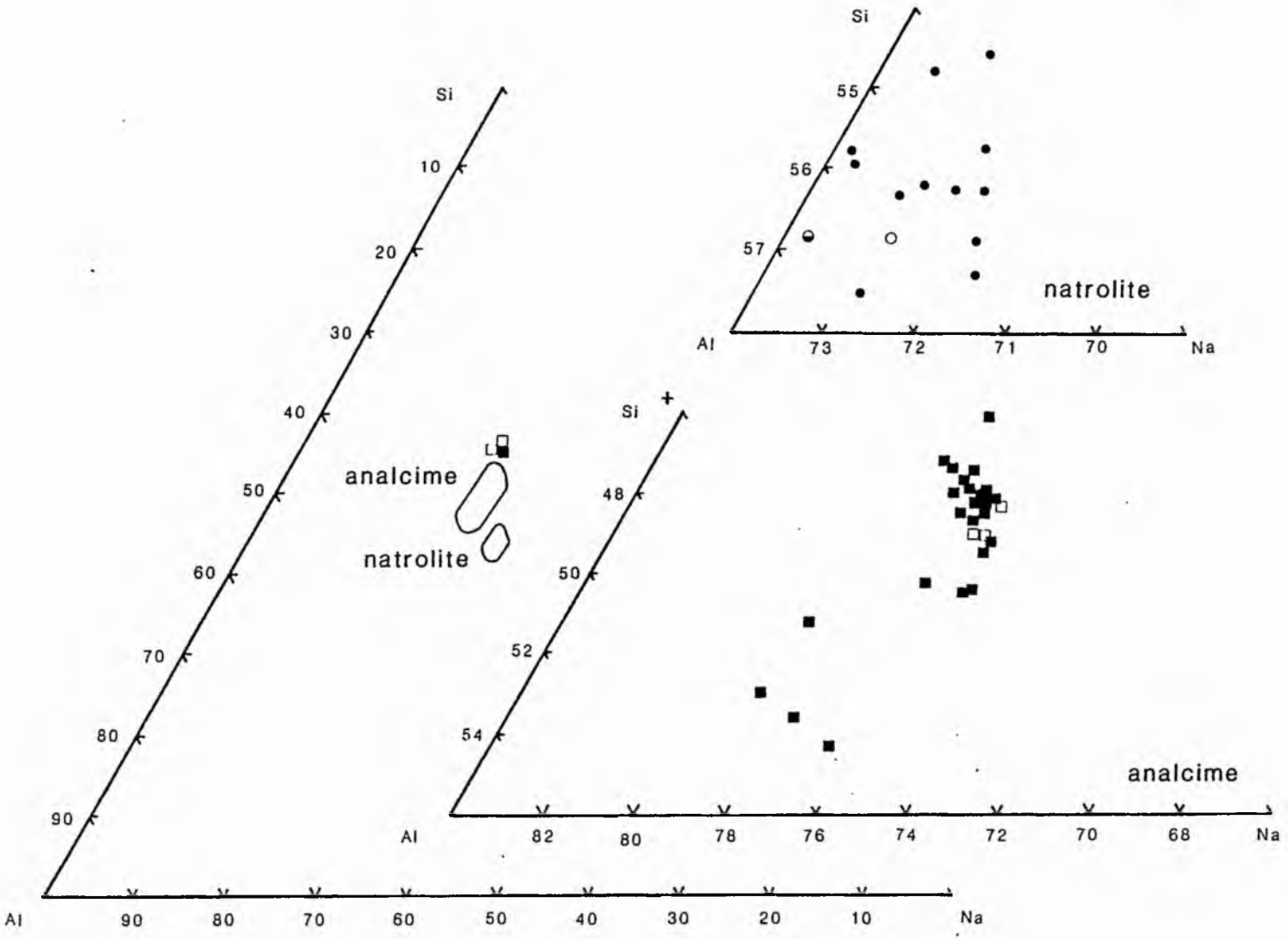


Fig.2.4.1. Analcime and natrolite plotted in terms of Si ,Al and Na cation proportions. Natrolite -● this study, ○ after Iijima and Harada(1969), ◒ after Houghton(1982). Analcime - ■ this study, □ after Coombs and Whetten(1967).

Na-volatilization. In these instances a moving 10-20 $\mu$ beam was used. The total water content of hydrated mineral species was determined by difference.

To avoid sample disintegration during analayses, a wide beam (10-20 $\mu$) was used on hydrated species, and the beam moved after every 10 second count.

Calibration was monitored relative to individual standards (appendix 2.4.17). Detection limits were ±1% at the 50% concentration level, and ±2% at the 15% concentration level. Standards with <15% concentration level were not used.

The back-scatter facility was used to select areas for analysis in crystals where compostional variation was not expressed optically.

**Analcime $Na_2 (Al_2Si_4)O_{12} \quad 2H_2O$**

Twenty-six analcime analyses are presented in figure 2.4.1. Chemical formulae (appendix 2.4.1) are recalculated upon the basis of the anhydrous cell contents ie 6 oxygens.

Microprobe analyses (appendix 2.4.1) indicate that analcime is an Na-silicate, containing as much as <11 wt% $H_2O$. According to Deer *et al*, (1962) analcime is usually characterized by <9.6 wt% $H_2O$. The apparantly high water contents described here for analcime, and from associated hydrous silicates in the Midland Valley, are due to devolitization under the electron beam. The major oxides in analcime show variations (appendix 2.4.1) as great as <8 wt%. A plot of these oxides in terms of cation proportions however (fig 2.4.1a), shows that analcime crystallized over a fairly restricted range of compositions.

An enlargement of the compositional field (fig 2.4.1c) shows

that Na occupies 20-24% of the unit cell. Variation is attributed to small amounts (<0.3 atoms) of $Ca^{2+}$ and/or $K^{+}$ substituting for Na. The main substitution in analcime (fig 2.4.1c) is of Si $\rightleftharpoons$ $Al^{3+}$. Substitution of NaSi $\rightleftharpoons$ CaAl must also occur, since fig 2.4.1c shows that % Na decreases with Si, as $Al^{3+}$ and $Ca^{2+}$ increases. The latter substitution is necessary in order to maintain the charge balance (Deer *et al*, 1962).

Analcime analyses on figure 2.4.1c, form two groupings:-

GROUP 1 - a tight cluster, characterized by high Si values

GROUP 2 - a broad scatter, characterized by low Si values

Correlation with field (chapter 2.2) and petrographic (chapter 2.3) studies, indicate that the analcime of group 1 are unaccompanied by zeolites in the paragenesis. Analcimes of group 2 occur with and are pre-dated in the amygdale crystallization sequence, by natrolite (chapter 2.2). Intergrowths of the two species are sometimes encountered. These associations suggest that group 2 analyses characterize higher grade assemblages. Since amygdular natrolite occurs (chapter 2.2) at deeper burial depths than amygdular analcime. Hence, Si depletion is a function of increased temperature; this relationship was established by Saha (1961) during experimental investigations in the system $NaAlSiO_4$-$NaAlSi_3O_8$ - $H_2O$. Temperature dependant variations in Si (1.90-2.07 atoms) of burial metamorphic analcime, were also reported by Coombs and Whetten (1967), who also noticed that Si content of analcime varied in relation to a $Na^{+}$ and to a $SiO_2$. Variations in Si are therefore of no significance as a geothermometer.

### 2.4.4 The Zeolites

**Natrolite $Na_2$ $(Al_2Si_3)O_{10}$ $2H_2O$**

Twelve natrolite analyses are presented in figure 2.4.1. Chemical formulae (appendix 2.4.2) are recalculated upon the basis of 80 oxygens.

Compositional variation is minimal, and is essentially restricted to $Al^{3+} \rightleftharpoons Si$ substitution.

Variation in Na is encountered, but is restricted to <2 atoms. The variation may be due to volitization during analysis. However several natrolites with low Na values, contain <0.5 $Ca^{2+}$ atoms, suggesting that $Ca^{2+}$ is substituting for Na in the unit cell. Part of the X-site (see appendix 2.4.2) may be filled by Sr (<0.2 atoms). There is no evidence (fig 2.4.1) that the presence of $Ca^{2+}$ is due to the substitution of NaSi $\rightleftharpoons$ CaAl, as in analcime. Substitution is therefore of Na $\rightleftharpoons$ 2Ca or Sr. However, this requires Al $\rightleftharpoons$ Si substitution to balance.

Natrolite analyses obtained from Hawaiian (Iijima and Harada, 1969) and from New Zealand (Houghton, 1982) metavolcanics are compatible (fig 2.4.1) with Midland Valley analyses.

**Thomsonite Na $Ca_2$ $[(AlSi_5)O_{10}]_2$ 6 $H_2O$**

Seventeen thomsonite analyses are plotted in figure 2.4.2. Chemical formulae (appendix 2.4.3) are recalculated upon the basis of 80 oxygens.

Thomsonite (fig 2.4.2) shows minor compositional variation. Substitution is essentially of $Ca^{2+} \rightleftharpoons$ Na (Al $\rightleftharpoons$ Si). The compositional range shown (fig 2.4.2) is compatible with thomsonite from the thomsonite-chabazite burial metamorphic zone of eastern

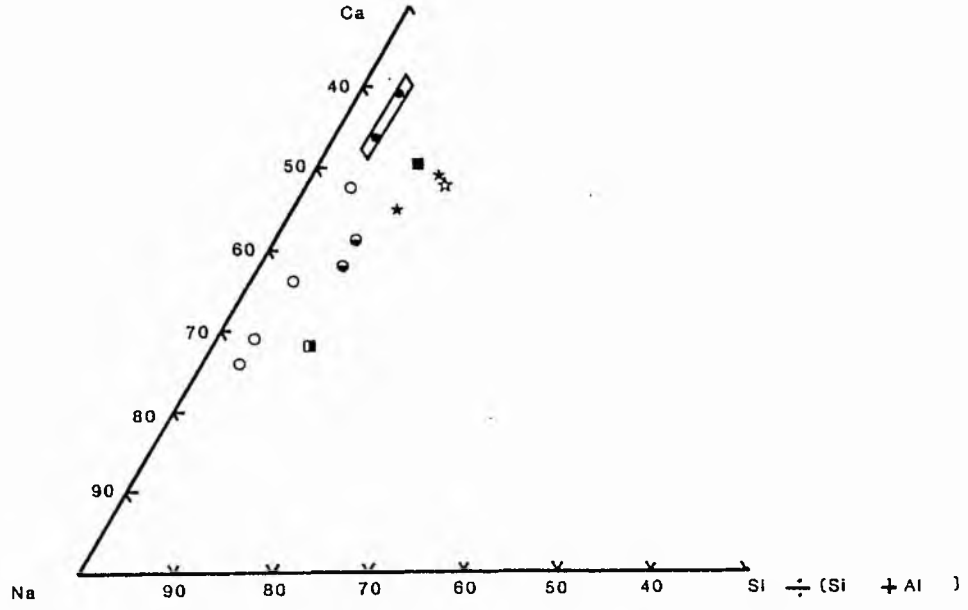


Fig. 2.4.2. The Na,Ca zeolites plotted in terms of Ca , Na and Si ÷ (Si + Al ) cation proportions. Rectangle - compositional field of thomsonite, this study: ● thomsonite, after Hey (1932). Gonnardite - ○ this study, ◒ after Hey (1932). Gmelinite - ■ this study, ◨ after Smith et al. (1916). Mesolite - ★ this study, ☆ after Sukheswala et al. (1974).

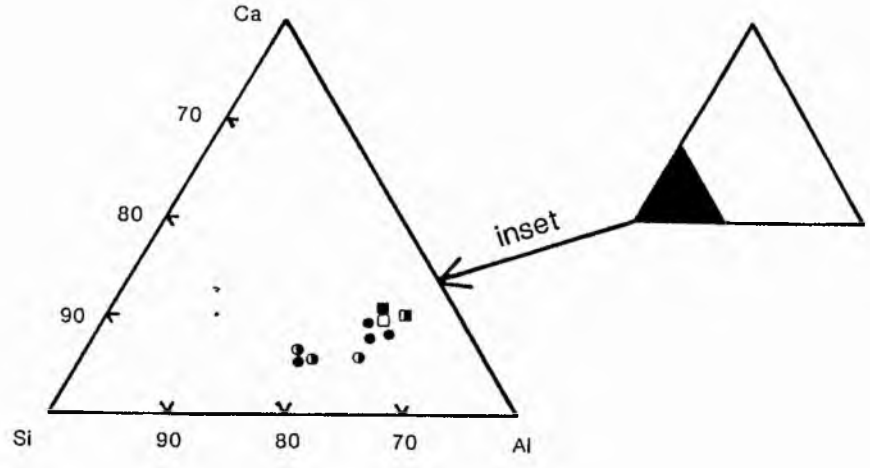


Fig. 2.4.3. Representative heulandite and stilbite analyses, plotted in terms of Si Al and Ca cation proportions. Circles, heulandite - ● after Houghton (1982), ◑ after Boles and Coombs (1975). Squares, stilbite - ■ after Houghton (1982), ◨ after Gschwind and Brandenberger (1932), □ after Novacek (1936).

Iceland (Hey, 1932).

**Gonnardite $Na_2$ Ca $[(AlSi)_5O_{10}]_2$ 6 $H_2O$**

Four analyses of gonnardite, intergrown with thomsonite, are presented in figure 2.4.2. Chemical formulae (appendix 2.4.4) are recalculated upon the basis of 80 oxygens.

Gonnardite (fig 2.4.2) shows substantial Ca:Na (of Al:Si) variation. Comparible observations were made by Meixner *et al*, (1956) and by Hey (1932). Midland Valley analyses contain appreciable Fe (<1.77 atoms) and $Mg^{2+}$ (<1.85 atoms) in the unit cell.

**Mesolite $Na_2$ $Ca_2$ $[Al_6$ $Si_9$ $O_{30}]$ 8 $H_2O$**

Two mesolite analyses are represented in figure 2.4.2, together with one comparative analysis from zeolitized volcanics in the Deccan Plateau, India (after Sukheswala *et al*, 1974). Chemical formulae (appendix 2.4.5) are recalculated upon the basis of 30 oxygens.

Mesolite shows (fig 2.4.2) minor compositional variation, related to the substitution of Si $\rightleftharpoons$ Al and Na $\rightleftharpoons$ Ca.

**Gmelinite $(Na_2Ca)(Al_2Si_4)O_{12}$ 6 $H_2O$**

One gmelinite analysis is presented in figure 2.4.2, together with one comparative analysis from the gmelinite zone of Antrim (after Smith *et al*, 1916). Gmelinite (appendix 2.4.5) is recalculated upon the basis of 48 oxygens.

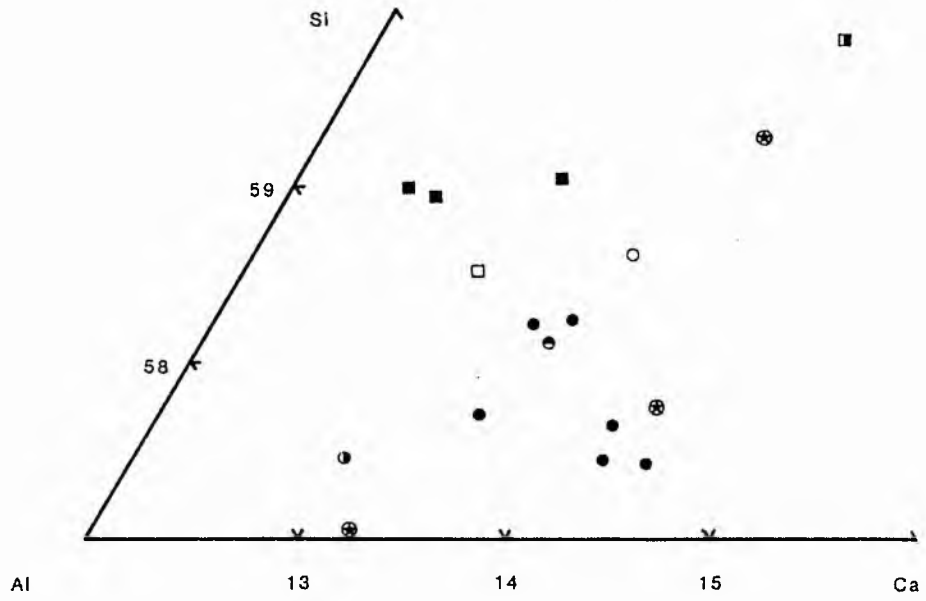


Fig. 2.4.4. Laumontite and wairakite plotted in terms of Si ,Al and Ca cation proportions. Circles - laumontite, ● this study, ○ after Sukheswala (1974), ◑ after Coombs (1952) ⊛ after Houghton (1982). Leonhardite - ⊖ after Coombs (1952). Squares - wairakite, ■ this study, □ after Steiner (1955), ◨ after Kristmannsdottir (1981).

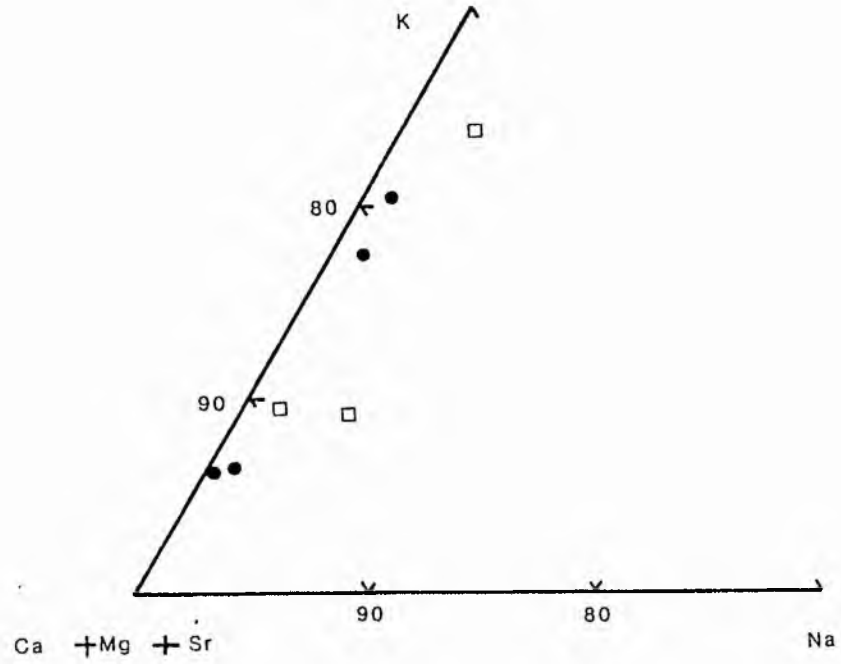


Fig. 2.4.5. Chabazite plotted in terms of Ca +Mg +Sr ,K and Na cation proportions. Circles - this study. Squares - after Passaglia (1970).

Ca-zeolites

Included in this group, are the minerals heulandite [$(Ca, Na_2)(Al_2Si_7)O_{18}$ 6 $H_2O$] and stilbite [$(Ca, Na_2, K_2)(Al_2Si_7)O_{18}$ 7 $H_2O$]. Analyses of these minerals have not been obtained, since during sample preparation, the zeolites were always removed from polished thin-section surfaces. Representative analyses have been selected from the data of Deer *et al* (1962) and from Houghton (1982), and have been plotted on figure 2.4.3, to show the main substitutions.

Laumontite $Ca(Al_2Si_4)O_{12}$ 4 $H_2O$

Six laumontite analyses are presented in figure 2.4.4. Chemical formulae (appendix 2.4.6) are recalculated upon the basis of 48 oxygens.

The laumontite unit cell is essentially composed of Si, $Al^{3+}$ and $Ca^{2+}$. Minor amounts of $K^+$, Na and Sr occur; with $K^+$ = 0.24 to 0.38 atoms in four of the analyses. These cations are believed to substitute for $Ca^{2+}$ in the X-site. One analysis (CF93[54]) has an appreciable quantity of Fe. Henderson and Glass (1933) demonstrated that Fe isomorphously replaces $Al^{3+}$ in the structure.

The main trend developed in fig 2.4.4, between laumontite analyses in zeolitized volcanics from the Midland Valley, New Zealand (Coombs, 1952; Houghton 1982) and India (Sukheswala *et al*, 1974), indicates that Si $\rightleftharpoons$ Al substitution occurred at fairly constant (13.0 to 14.5%) $Ca^{2+}$ values. Three analyses (plotting in the bottom right-hand corner) show an increase in $Al^{3+}$, suggesting that substitution of the type NaSi $\rightleftharpoons$ CaAl also occurred.

Wairakite $Ca[AlSi_2O_6]\ H_2O$

Wairakite has been identified at two localities in the Midland Valley. At CV69 (GR: NS 358 555) wairakite is mantled by analcime; whilst at CV93 (GR: NS 526 769) wairakite is associated with laumontite.

Analyses are presented in figure 2.4.4. Chemical formulae (appendix 2.4.7) are recalculated upon the basis of 6 oxygens. Compositions lie close to the ideal end member, $Ca\ [AlSi_2O_6]\ H_2O$.

Figure 2.4.4, demonstrates that wairakite Si: $Al^{3+}$ ratios are fairly constant. The main substitution in wairakite is therefore of the type $Ca \rightleftharpoons 2Na$ (plus associated Al:Si).

Comparative analyses from Krafla, Iceland (Kristmannedottir, 1981) and from Wairakei, New Zealand (Steiner, 1955) have been plotted in figure 2.4.4. Only those analyses from Wairakei, are directly comparable with those of the Midland Valley. Rocks of Wairakei, are compositionally similar to plagioclase-rhyolites (Steiner, 1955), whilst those of the Midland Valley are hawaiites (chapter 2.1). Abundant wairakite analyses from Japan (Aoki and Minato, 1980) fall outside the compositional range shown in figure 2.4.4; these are typically enriched in $Ca^{2+}$ and $Al^{3+}$ relative to Midland Valley varieties. The wide range in wairakite chemical compositions has been interpreted by Aoki and Minato (1980) as evidence for continuous solid solution in the analcime-wairakite series.

Chabazite $Ca\ (Al_2Si_4)O_{12}\ 6\ H_2O$

Four chabazite analyses are presented in figure 2.4.5. Chemical formulae (appendix 2.4.7) are recalculated upon the basis of

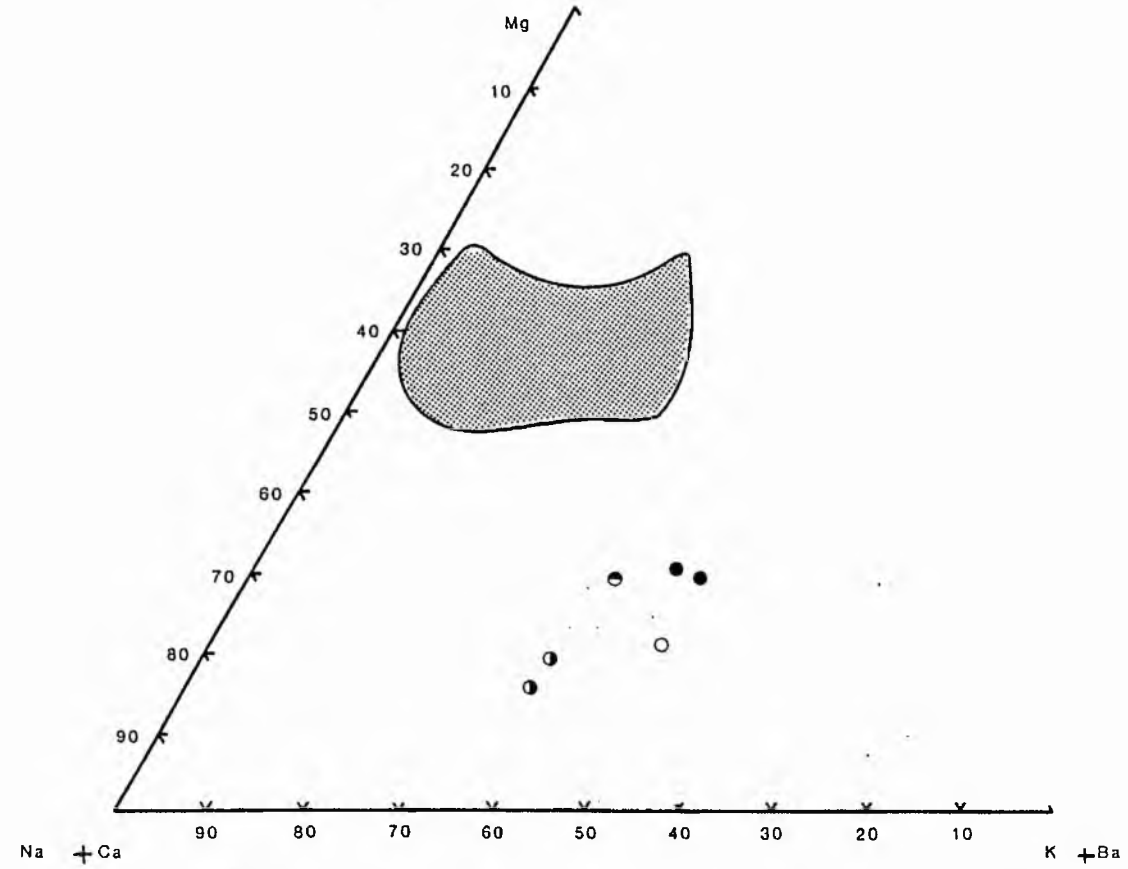


Fig. 2.4.6. Ferrierite plotted in terms of Mg , Na + Ca and K + Ba cation proportions. Symbols - ● this study. ◑ after Wise et al. (1969), ○ after Wise and Tschermich (1976), ◓ after Yajima and Nakamura (1971). Stippled area, after Sameshima (1986).

72 oxygens. Coombs *et al* (1959), described extremely variable chabazite compositions. Midland Valley chabazites show the following range:-

$(Ca\ Na_2K_2)_{5.76-6.62}\ Al_{11.80-12.31}\ Si_{23.62-23.90}\ O_{72}\ 36\ H_2O$

Figure 2.4.5 demonstrates that this variation can be largely attributed to the substitution of $Ca^{2+} \rightleftharpoons K^{+}$. With minor substitution of $Mg^{2+}$, Na and Sr occurring in the X-site.

Minor substitution of Al + Fe $\rightleftharpoons$ Si also occurs.

Low silica chabazite varieties, such as those found in the Midland Valley, are characteristically developed in basic rocks. Comparison in figure 2.4.5, is made with analyses 12, 13 and 14 of Passaglia (1970). Chabazites in the basic volcanics of Italy (Passaglia, 1970), Hawaii (Iijima and Harada, 1969) and in the volcaniclastics of Auckland, New Zealand (Sameshima, 1978) are all Na enriched, with respect to those in the Midland Valley.

**Ferrierite $(Na\ K)_4\ Mg_2\ (Al_6\ Si_{30})O_{72}\ (OH)_2\ 18H_2O$**

Two ferrierite analyses are presented in figure 2.4.6. Chemical formulae (appendix 2.4.8) are recalculated upon the basis of 72 oxygens, the anhydrous cell contents.

Midland Valley ferrierites show the following compositional range:-

$(Na,\ K)_{2.82-3.12}\ Mg_{1.27-1.39}\ Al_{5.46-5.52}\ Si_{30.22-30.43}\ O_{72}\ (OH)_2\ 18_2O$

Chemical investigation of the 21 previously recorded ferrierites in the world (Sameshima, 1986) demonstrated that atomic variation was related to the substitution of:-

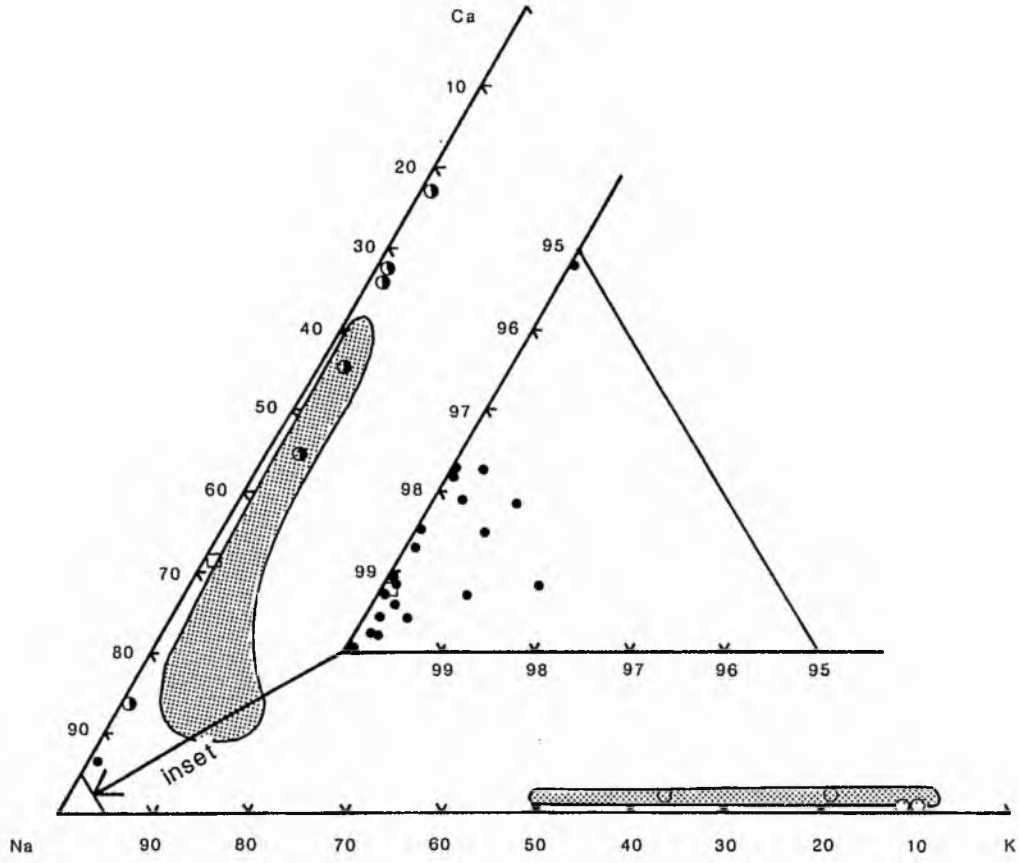


Fig. 2.4.7. Felspar plotted in terms of Ca , Na and K cation proportions. Circles, this study - ○ k - spar, ◑ plagioclase, ● albite. Plagioclase □ after Kuniyoshi and Liou (1976). Stippled fields, after Boles and Coombs (1975).

i) Si (Na, K $\rightleftharpoons$ Al (Ca, Mg)

ii) 2Si $\rightleftharpoons$ Mg

The majority of the ferrierite analyses reported in Sameshima (1986), plot within the stippled field in figure 2.4.6. These ferrierites are mainly reported to occur in basalts in association with heulandite, clinoptilolite and mordenite. Midland Valley ferrierites occur in heulanditized basalts, or surrounding vents in the analcime-natrolite zone. These analyses (fig 2.4.6) have closer affinities with ferrierite (± heulandite, ± quartz) in andesites (Wise *et al*, 1969; Wise and Tschernich, 1976; Yajima and Nakamura, 1971).

### 2.4.5 Associated minerals

#### Feldspar

Thirty-four feldspar analyses are presented in figure 2.4.7. Chemical formulae (appendices 2.4.9; 2.4.10; 2.4.11) are recalculated upon the basis of 32 oxygens, following Deer *et al* (1980).

The analyses define three groups (fig 2.4.7) characterized by:-

| | |
|---|---|
| i) K-spar, with | Or = 62 - 91 |
| ii) plagioclase, with | An = 15 - 78 |
| iii) albite, with | Ab = 90 - 100 |

#### K-spar K $AlSi_3O_8$

The K-spars are restricted to Markle and Jedburgh type meta-basalts (nomenclature after MacGregor, 1928) and to associated trachy-andesites. Bevins and Rowbotham (1983), similarly described rare K-feldspar from low grade metavolcanics in Wales. The

feldspars are believed to reflect (described in chapter 2.3) phases that have escaped metamorphism, and reflect the formation of basalt from a highly evolved magma.

Two analyses (CV69(1) and CV28(1)) possibly conform to adularia (?); $Or_{90}$ $An_9$ $Ab_1$, as defined by Deer *et al*, (1962). Identification of the polymorph could not be confirmed by X-ray diffraction because of the small particle size. According to Deer *et al's*, (1962) definition the polymorph could equally be ascribed to orthoclase. However, it is believed to be adularia (?) because BaO contents are typically 0.5 to 0.7 wt% (1 wt% in orthoclase); CaO <0.05% (2 wt% in orthoclase); FeO and MgO values are correspondingly low; only minor substitution of Na for $K^+$ occurs in the unit cell.

Midland Valley adularia (?) occurs in the analcime zone. Investigations by Coombs *et al*, (1959) and Utada (1965; in Miyashiro and Shido, 1970), associate adularia with the higher grades of the zeolite facies ie within heulandite and laumontite zones. The stability of adularia in low grade metamorphism (Munha *et al*, 1980) may be lowered (T >145 $^oC$) in the presence of excess ($K^+$ saturated) seawater in rocks poor in primary Fe-Mg phases. Sheet silicate analyses (this chapter) show that $K^+$ fixation did not play a major role in the development of clay-chlorite mineralogies in the Midland Valley. It is therefore unlikely that Carboniferous seawaters would have been sufficiently depleted in $K^+$ to have inhibited the development of adularia (?).

Adularia is also common in rocks of high initial permeability and in active geothermal areas such as Iceland (Browne, 1978). The two analyses obtained from the Midland Valley are from within the palaeo-geothermal plumes (for further references - see chapter 2.2

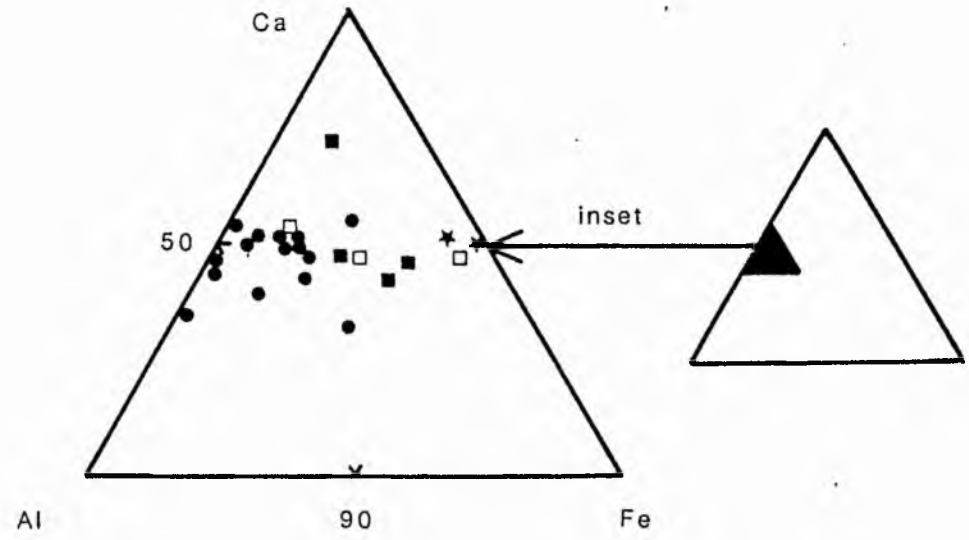


Fig. 2.4.8. Prehnite plotted in terms of Ca, Aland Fe cation proportions. Symbols - ● this study, □ after Tulloch (1979), ■ after Boles and Coombs (1977), ✶ after Bevins (1985).

and 2.6).

Plagioclase $Ca\ Al_2Si_2O_8$

Plagioclase analyses (An 44-87) were only obtained from basalts and tuffs in the quartz-calcite zone and from the least altered areas of the analcime zone. An contents vary from 44-50, 50-70 and 70-87, reflecting the presence of andesine, labradorite and bytownite respectively (figure 2.4.7). The wide range of An displayed is believed to be a function of the original basalt chemistry in unmetamorphosed volcanics.

Albite $NaAlSi_3O_8$

70% of the analyses obtained (appendix 2.4.9) show albite compositions, with Ab 90-100.Si deficiencies and corresponding $Al^{3+}$ enrichments for certain samples, testify to $Al^{3+} \rightleftharpoons Si$ substitution.

Albite analyses characterized feldspar compositions in the zeolitized Carboniferous volcanics of the Midland Valley. Albite as a secondary phase in low grade metabasalts has also been described by Boles and Coombs (1975), Coombs *et al* (1976), Kuniyoshi and Liou (1976), Oliver and Leggett (1980) and Bevins and Rowbotham (1983).

Prehnite $Ca_2Al\ [AlSi_3O_{10}]\ (OH)_2$

Eighteen prehnite analyses are presented in figure 2.4.8. Chemical formulae (appendix 2.4.12) are recalculated upon the basis of 22 oxygens.

Figure 2.4.8 demonstrates that substitution is essentially of the kind $Fe^{tot3+} \rightleftharpoons Al^{3+}$, with $Fe^{tot3+}$ replacing 0 to <3% of this unit cell. Two analyses (CV69(16); CV69(20)) show substitutions as

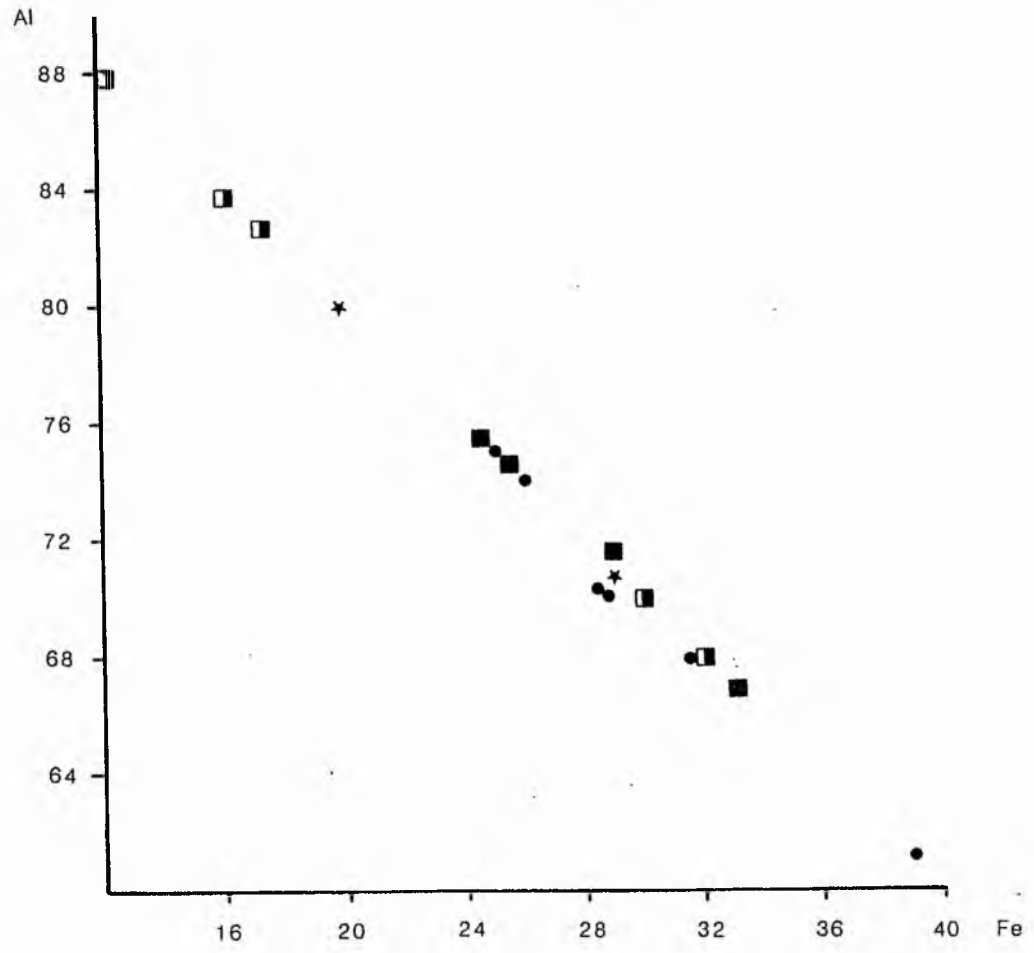


Fig. 2.4.9. Epidote plotted in terms of Al and Fe cation proportions, where 100 x (Fe$^{3+}$ / Fe + Al ). Symbols - ● this study, ◨ after Coombs et al. (1976), ■ after Coombs et al. (1977) ✱ after Bevins and Rowbotham (1983).

great as 18.5% and 23.5% respectively. Analyses are taken from amygdaloidal/vein prehnite, and from prehnite replacements after feldspar and pyroxene. Variation in the degree of $Fe^{tot3+}$ substitution however, is irrespective of precursor compositions.

Bevins and Rowbotham (1983) and Oliver and Leggett (1980) described prehnites with 0 to 8.23% and 0 to 5.5% iron variation. Boles and Coombs (1977) and Tulloch (1979) report prehnites enriched in $Fe^{tot3+}$ (fig 2.4.8) relative to Midland Valley analyses. Surdam (1969) and Kuniyoshi and Liou (1976b) related prehnite $Fe^{tot3+}$ enrichments, in a zeolite ($Fe^{tot3+}$ <0.6%) to prehnite-pumpellyite ($Fe^{tot3+}$ = 5-8%) facies tuff sequence to increasing metamorphic grade. The range (0-6.4%) shown by Midland Valley prehnites, must therefore reflect the temperature dependence of Fe == Al substitutions.

Epidote $Ca_2Fe^{3+}Al_2Si_3O_{12}(OH)$

Six epidote analyses are presented in figure 2.4.9. Chemical formulae (appendix 2.4.13) are recalculated upon the basis of 12 oxygens. It is assumed that all iron is present as $Fe^{3+}$, following Deer *et al* (1962).

The boundary between the two end members clinozoisite and epidote, is arbitrarily limited to clinozoisite = 0-10% $Fe^{3+}$, following Miyashiro and Seki (1958). Midland Valley epidotes are therefore divided into pistacite (Ps = 11-14%) and clinozoisite (Ps = 9.2-9.6%) varieties. Fig 2.4.9, demonstrates that $Fe^{3+}$ substitutes for $Al^{3+}$, and is limited to 1:2. Mineral compositions therefore lie close to the $Ca_2Fe^{3+}Al_2Si_3O_{12}(OH)$ end-member.

In Figure 2.4.9, Midland Valley analyses plot over a comparable

range with pistacitic epidote from the pumpellyite-actinolite facies of Switzerland (Coombs *et al*, (1976) and from the prehnite-pumpellyite facies of New Zealand (Coombs *et al*, 1977). The data suggests that $Fe^{3+}$ substitution is not definitive of metamorphic grade. However, within a particular facies, Coombs *et al*, (1976; 1977), Miyashiro and Seki (1958) and Bevins and Rowbotham (1983), found that:-

i) epidotes formed at lower temperatures plotted closer to the Fe end-member

ii) epidotes formed at higher temperatures were Fe-poor, and showed a wide range of $Al^{3+} = Fe^{3+}$ substitutions

This suggests that pistacitic epidotes in the Midland Valley may have crystallized at lower temperatures relative to clinozoisite. However, the minerals are not compositionally zoned with respect to falling temperatures. Furthermore, the overlap (fig 2.4.9) shown by epidotes from different facies indicates that crystal-chemical restrictions on $Al^{3+} = Fe^{3+}$ substitution at low temperatures are not stringent. Variation is therefore attributed to the tendancy for increased $f_{O_2}$ (due to the disassociation of water from the zeolites), and for the increased availability of additional $Ca_2Al_3Si_3O_{12}(OH)$ components, with advancing metamorphism.

**Garnet $Ca_3Al_2Si_2O_8$ $(SiO_4)1-m$ $(OH)4m$**

Zoned hydro-garnets (confirmed by X-ray diffraction) are present at Beith palaeo-geothermal plume. Analyses are presented in figure 2.4.10. Chemical formulae (appendix 2.4.14) are recalculated

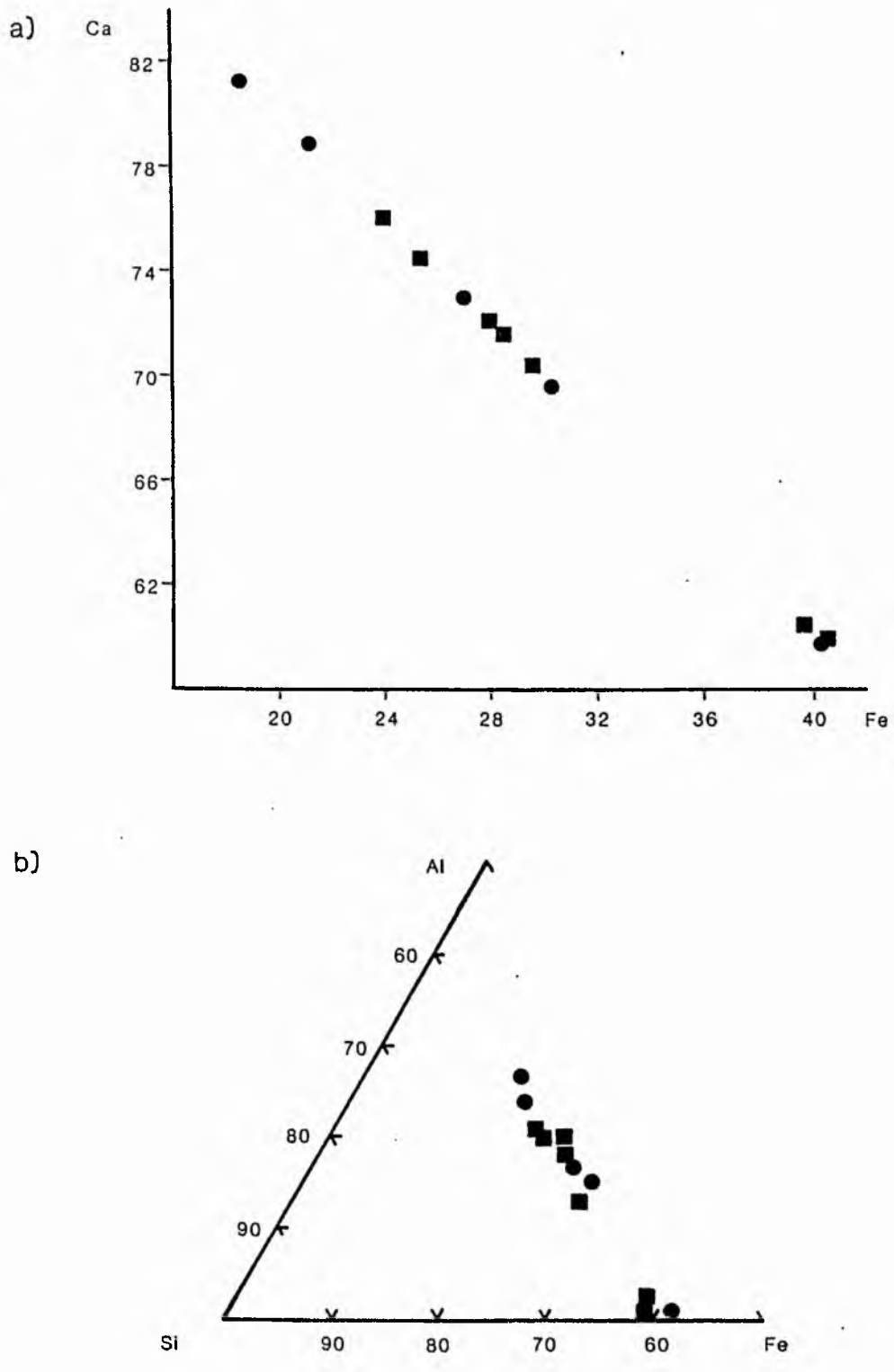


Fig. 2.4.10. Hydro - grossular plotted in terms of a) Ca and Fe b) Al , Si and Fe cation proportions. Symbols - ● this study, ■ after Coombs et al. (1977).

upon the basis of 32 oxygens.

A plot (fig 2.4.10a) in terms of $Ca^{2+}$, $Fe^{tot3+}$ cation proportions indicates that the garnets show solid-solution in the compositional range grossular to andradite. Distinction between the two, is placed at the andradite >28 wt% $Fe_2O_3{}^{tot}$ boundary (ie 3.44% $Fe^{tot}$), following Peters (1965). Although Deer *et al* (1982) have andradite analyses with $Fe_2O_3{}^{tot}$ = 19 wt%. Midland Valley analyses (fig 2.4.14b) have water contents in the range 0.4 to 17 wt%, thus warranting (Deer *et al*, 1982) the addition of the prefix 'hydro'.

Midland Valley garnets are zoned from hydro-grossular towards hydro-andradite, reflecting an increase in Si and $Ca^{2+}$ in the core and an increase in $H_2O^+$ and $Fe^{tot3+}$ at the rim. Mantling of the garnets by more hydrous phases suggests a retrograde origin for the zonation. Yoder (1950) determined that the $SiO_2$ content of garnet increased proportionally to temperature. By comparison, the associated increase in Si in the less hydrous cores of the Midland Valley garnets, supports the lower temperature origin of the mantles.

Primarily, the availability of excess Mg, $Ca^{2+}$ and $Fe^{3+}$ (from whole-rock alteration) in moderately oxidized metabasalt allowed garnet (?), as well as the more common epidote and prehnite, to crystallize in the palaeo-geothermal areas. Both andradite and grossular rich garnets may form over variable pressure, temperature and $f_{O_2}$ conditions (Liou, 1974), their stabilities being extended to lower temperatures at low $\mu$ $CO_2$. However, apart from the chemical variation described above, further evidence for temperature variation in the palaeo-geothermal plumes is equivocal. By comparison with Coombs *et al*, (1977), the co-existence of Fe-poor prehnite, Al-rich epidote and increased Fe/Mg ratios in palaeo-geothermal plume

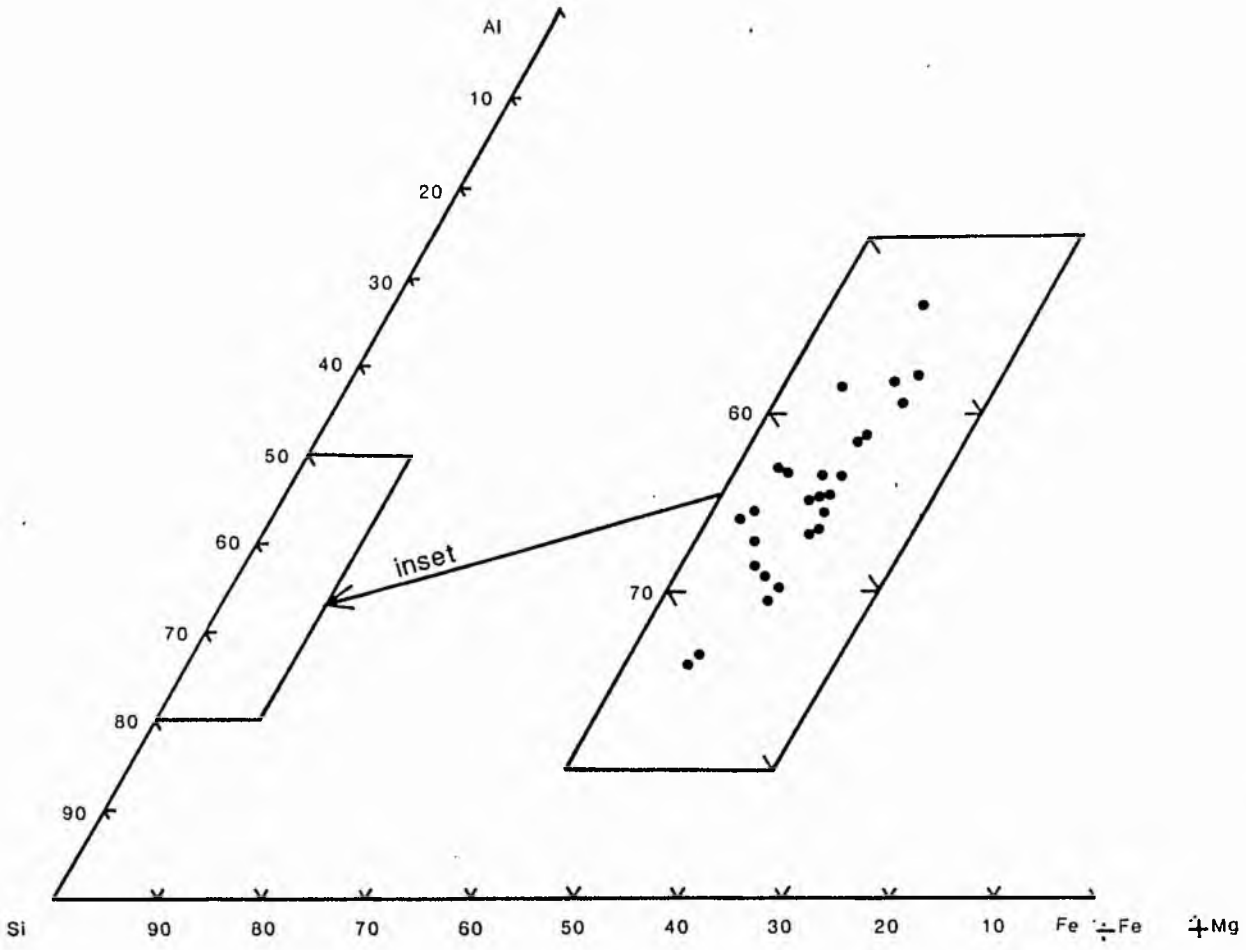


Fig. 2.4.11. Chlorite plotted in terms of Si , Al and Fe ÷ (Fe + Mg ).

chlorites, suggests that at constant temperatures decreasing $f_{O_2}$ could produce the hydro-grossular-rich mantles observed.

Chlorite

Twenty-six analyses are presented in figures 2.4.11 and 2.4.12. Chemical formulae (appendix 2.4.15) are recalculated upon the basis of 28 oxygens.

Chlorite group minerals show (appendix 2.4.15) appreciable variation in $SiO_2$, $Al_2O_3$, $Fe^{tot}$ and MgO wt%. A plot of these in terms of cation proportions (fig 2.4.11 - 2.4.12) shows that this variation may be attributed to

i) Si $=$ Al substitution

ii) Fe $=$ Mg substitution

$Fe^{tot}$ however occupies <6% of the available Fe and Mg sites (fig 2.4.11). Indicating that in order to full-fill stochiometric conditions in $Mg^{2+}$ deficient chlorites, both $Fe^{tot+}$ and $Al^{3+}$ substitution for $Mg^{2+}$ must have occurred. Compositions (fig 2.4.12) fall in the chemical range (Hey, 1954) of brunsvigite, diabantite, pycnochlorite and penninite.

Analysed chlorites from the Midland Valley are compatible with (fig 2.4.12) chlorites in prehnite-pumpellyite facies metabasalts from the Southern Uplands (Oliver and Leggett, 1980) the Welsh Basin (Bevins and Rowbotham, 1983) and from Southern New Zealand (Coombs *et al*, 1977). Bevins and Rowbotham (1983) found that for the Welsh Basin, compositional variation was with respect to $SiO_2$ rather than

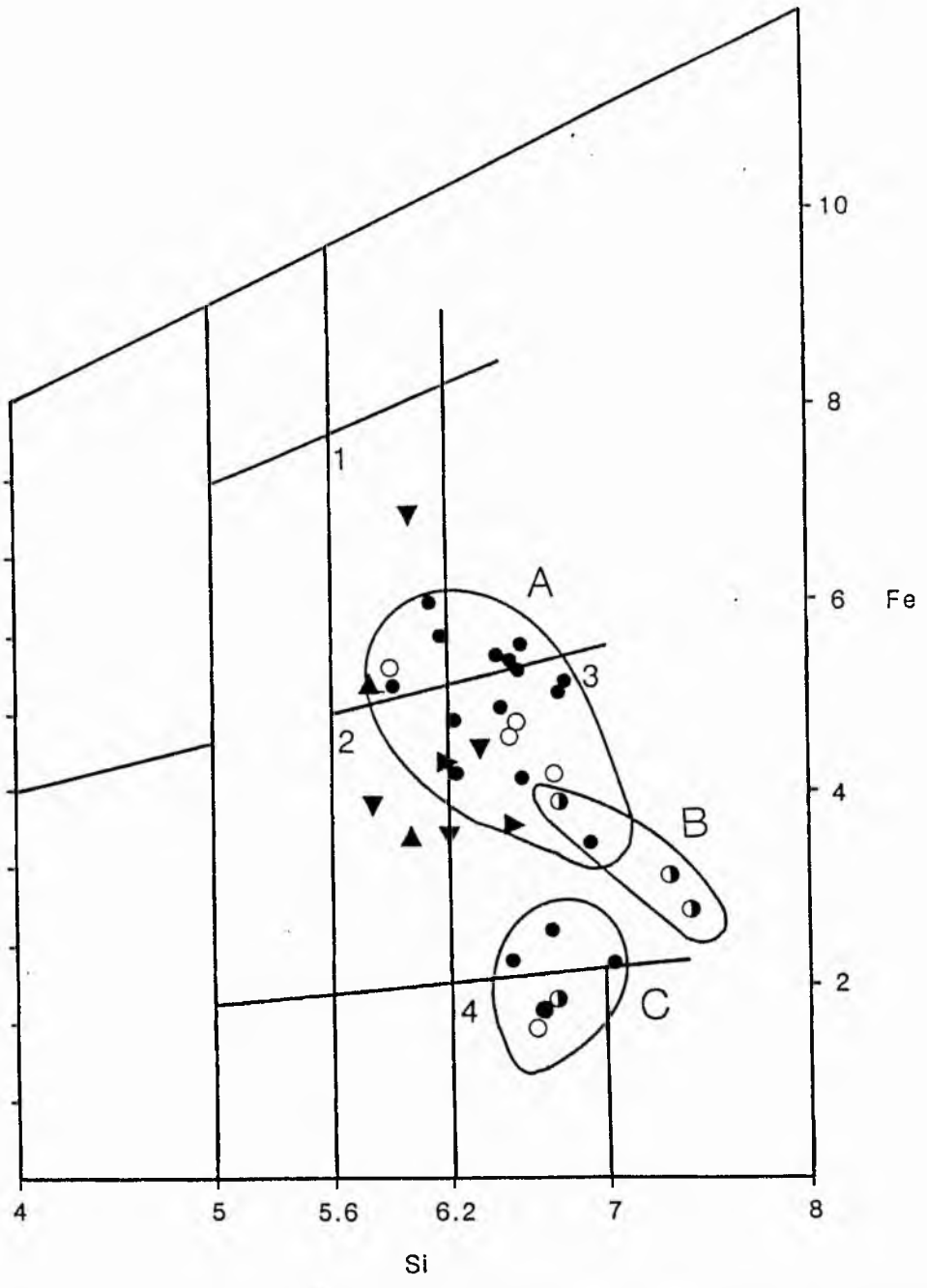


Fig. 2.4.12. Chlorite plotted in terms of Fe and Si cation proportions, according to the classification scheme of Hey(1954). FIELDS: 1-brunsvigite, 2-pycnochlorite, 3-diabantite, . 4-penninite, A-chlorite from analcime and analcime-natrolite burial metamorphic zones, B-chlorite from heulandite and stilbite burial metamorphic zones, C-chlorite from regions where the effect of burial metamorphism has been overprinted by palaeo-geothermal plume activity.Symbols - ▲ after Coombs et al (1977), ▶ after Oliver and Leggett (1980), ▼ after Bevins and Rowbotham (1983), Circles, this study - ● chlorite from the analcime burial zone, ○ chlorite from the analcime-natrolite burial zone, ◑ chlorite from the heulandite and stilbite burial zones.

to FeO. Furthermore, analyses from all three regions are slightly depleted in $SiO_2$ relative to zeolite facies chlorites from the Midland Valley, thus suggesting that silica activity was greater at lower grades. With the exclusion of the Welsh Basin analyses, chlorite compositions also vary with respect to FeO, reflecting fluctuations in FeO supply with time. The distribution of Fe-rich chlorites in the analcime and natrolite burial zones and of Fe-poor chlorite in the heulandite and stilbite burial zones (fig 2.4.12) suggests that the supply of FeO decreased with increased burial depth.

Chlorites from geographically separated palaeo-geothermal plumes, are compositionally distinct (fig 2.4.12) from chlorites grown during burial metamorphism. Compositions, border the diabantite and penninite fields.

**Sphene**

Sphene occurs as a replacement mineral in feldspars, metamorphosed in the analcime to laumontite zones of the zeolite facies. Chemical analyses are presented in figure 2.4.13 and in appendix 2.4.16. Due to uncertainties in the determination of the $Fe^{2+}/Fe^{3+}$ ratio, chemical formulae were re-calculated assuming 4 Si cations in the unit cell (following Coombs *et al*, 1976).

Analyses show that minor amounts of barium, strontium and sodium, presumably liberated from decomposed feldspars, were partitioned into the calcium site. The main replacement (figure 2.4.13) was of Al and Fe for Ti. Similar substitutions, leading in particular to an enrichment with respect to Al was noted by Higgins and Ribbe (1976). This substitution is thought by Boles and Coombs

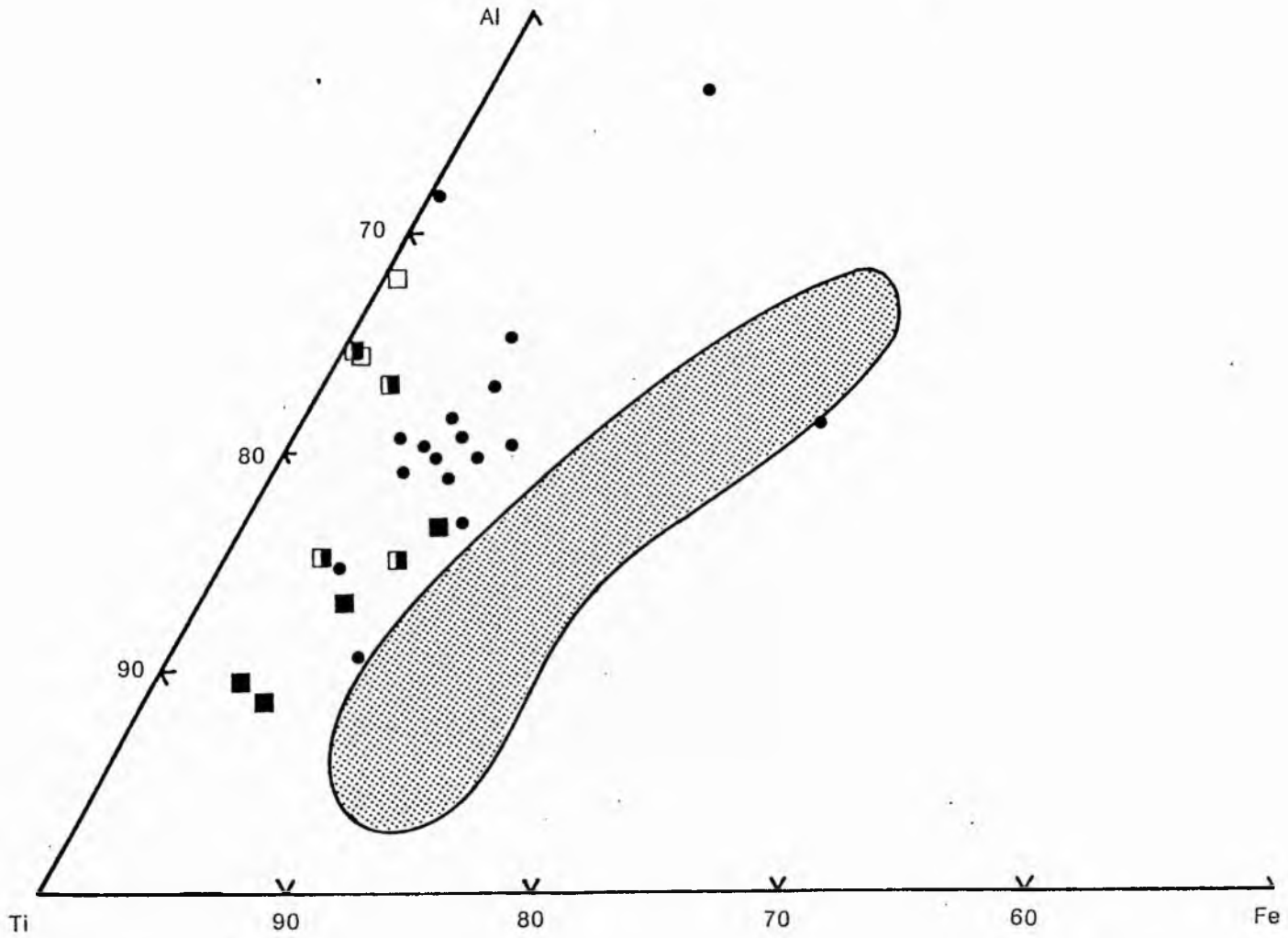


Fig. 2.4.13. Sphene plotted in terms of Al, Fe and Ti cation proportions. Symbols - ● this study, □ after Tulloch (1979), ◨ after Boles and Coombs (1977), ■ after Bevins (1985). Stippled area, after Oliver and Leggett (1980).

(1977) to be typical of sphenes from low grade burial metamorphic terrains. Compositions of sphenes from the Midland Valley are compatible with analysed samples reported by Boles and Coombs (1977), Tulloch (1979) and Bevins and Rowbotham (1983). With one exception, Midland Valley analyses are depleted in Fe relative to the sphene analyses reported by Oliver and Leggett (1980) from the Southern Uplands. The exceptional analysis is different from those replacing feldspar since the sphene formed a discrete crystal in the groundmass, and is likely to be a pseudomorph after ilmenite, rutile or titan augite.

### 2.4.6 Metamorphic facies

The Carboniferous metavolcanics of the Midland Valley are characterized by the assemblage albite - chlorite - sphene - prehnite - haematite - zeolite ± epidote ± hydrogrossular. The crystallization of these minerals in the absence of pumpellyite, actinolite or lawsonite, characterizes metamorphism in the zeolite facies as defined by Coombs (1954).

### 2.4.7 Metamorphic conditions

Mineralogical observations pertinent to the discussion of metamorphic conditions in the Midland Valley are considered below, with reference to:-

i) metamorphic pressures
ii) metamorphic temperatures
iii) the composition of the fluid phase
iv) $X_{CO_2}$ in the fluid phase

v) oxygen fugacity

**Metamorphic pressures**

The absence of lawsonite from metamorphic assemblages necessitates that pressures during zeolite facies metamorphism, did not exceed 4 kb (Liou *et al*, 1985). However, the development of lawsonite might not be relevant in these bulk rock compositions. Pressure maxima may be estimated from the burial depths determined in Chapter 2.2. Maximum burial was attained in laumontite grade metavolcanics; where burial depths of 1300 m are equivalent to $P_{lith}$ = 0.36 kb. Within the zeolite zones, zeolitization begins at an approximate burial depth of 500 m; and the transition between the analcime and the analcime-natrolite zones was encountered at 900 m. These burial depths impose pressure constraints of 0.14 kb and 0.25 kb respectively. By comparison with burial depths in figure 2.2.9, the transformation of heulandite to laumontite should occur at 0.30 kb. However Thompson (1971b) determined that this reaction occurred at 2 kb $P_{H_2O}$ (where $P_{H_2O} = P_{Lith}$).

Pressures within the palaeo-geothermal plumes are constrained by the experimental evidence of Liou *et al*, (1983). These researchers determined that the assemblage epidote-hydrogrossular-prehnite was only stable at 6 km over a very narrow temperature range (see below). Estimated pressures are not in agreement with pressures ($\leqslant$120 bars) determined from fluid inclusion analyses in chapter 2.5.

The stratigraphic evidence provided indicates that for $<$1.5 km burial depth, pressures are equivalent to $<$0.45 kb. Suggesting that monitored experimental transformations (eg Thompson, 1971b; Liou *et al*, 1983) occurred under a metastable state and thus resulting

pressure determinations have no application in zeolite facies metabasalts.

**Metamorphic temperatures**

The upper temperature of the zeolite facies is encountered in the palaeo-geothermal plumes. Independent experimental evidence for crystallization at $P_{fluid}$ = 2 kb, indicates that for

a) hydrogrossular to form, T = <420 °C (Hsu, 1980)

b) epidote-garnet- prehnite stability, T = 360 ± 30 °C (Liou *et al*, 1983)

c) the non-development of rutile (from sphene), T <350 °C (Schulling and Vink, 1976).

These temperatures are compatible with homogenization temperatures (chapter 2.5) in palaeo-geothermal thomsonite and prehnite.

The crystallization of rankinite in carbonated metabasalt immediately adjacent to the Tertiary dykes, indicates that contact metamorphism occurred at 1000 °C (Winkler, 1976).

The lower temperature limit of the zeolite facies is not defined. The contemperaneous appearance of natrolite with sphene indicates that at a burial depth of 900 m ($P_{lith}$ = 0.25 kb) temperatures (experimental) of 220 ± 20 °C (Schulling and Vink, 1976) were encountered. Fluid inclusion (chapter 2.5) and stable isotope (chapter 2.6) evidence however indicates that temperatures of 140 ± 30 °C were more realistic at this burial depth.

Conditions within the zeolite zones are limited by zeolite-zeolite dehydration reactions.

For example:-

i) $Na(Al\ Si_2)O_6\ \ H_2O + SiO_2 = Na\ AlSi_3O_8 + H_2O$ at 130 ° ± 10 °C

Thompson 1971b)

analcime + quartz = albite + water

ii) $CaAl_2Si_7O_{18}\ 6\ H_2O = CaAl_2Si_4O_{12}\ 4H_2O + 3SiO_2 + 2H_2O$ at 180 °C

(Liou *et al*, 1985)

heulandite = laumontite + quartz + water.

These reactions were used by Coombs (1958) to subdivide the zeolite facies. This division is realistic in terms of thin-section analysis in the Midland Valley (chapter 2.3). (Metamorphic reactions are discussed further in the following section). The different temperatures quoted on the previous page must indicate that the reactions may occur at different depths and under different pressures. This is certainly true in the Midland Valley, where the top of the laumontite zone is encountered at different levels north and south of the Clyde.

**Composition of the fluid phase**

The fluid chemistry will be a function of the initial fluid composition and of the interactions between the initial fluid and the host rock. Freezing point depressions measured from inclusions (chapter 2.5) indicate that the fluid was composed of a saline brine (>13.24 wt% NaCl equivalents). Seawater is likely to have been the initial fluid; however measured seawater salinities (see chapter 2.6) are composed of <3 wt% NaCl equivalents, therefore considerable salinity enhancements occurred (see chapter 2.5).

Initial alteration is characterized (chapter 2.3) by the breakdown of plagioclase (anorthite) to form albite and/or analcime

in the analcime zone. These transformations are characterized by:-

i) $CaAl_2Si_2O_8 + 4\ SiO_2 + 2Na = 2Na\ AlSi_3O_8 + Ca^{2+}$

(anorthite) (quartz) (albite)

ii) $Ca\ Al_2Si_2O_8 + 2SiO_2 + 2H_2O + 2Na = 2Na(AlSi_2)O_6 \cdot H_2O + Ca^{2+}$

(anorthite) (quartz) (analcime)

iii) $3CaAl_2Si_2O_8 + 13SiO_2 + 14H_2O + 2Na + CO_2 =$

(anorthite) (quartz)

$NaAlSi_3O_8 + Na(AlSi_2)O_6 \cdot H_2O$

(albite) (analcime)

$+ Ca(Al_2Si_7)O_{18} \cdot 6H_2O + Ca(Al_2Si_7)O_{18} \cdot 7H_2O$

(heulandite) (stilbite)

+ CaCO

The breakdown of anorthite to form either analcime or albite, requires the introduction of Si, Na and $H_2O$. Igneous plagioclases however, are labradorite, therefore the addition of excess Na may not be necessary. Both Na and $H_2O$ may have been obtained directly from seawater. Bischoff and Dickson (1975) found that the silica activity (aSi) of seawater in contact with hot (200 $^{o}$C) volcanic glass, rose

rapidly to near-saturation with respect to amorphous silica. Consequently, excess silica in the Midland Valley may also have been derived from seawater. Furthermore, prolonged contact of high aSi seawater with the glassy lining of vesicles in adjacent basalt may have favoured the formation of quartz in amygdales.

The transformation of quartz - analcime - natrolite and of stilbite - heulandite - laumontite (chapter 2.2) occurred in the Midland Valley with increased burial depth. Coombs *et al* (1959) and Miyashiro and Shido (1970), for similar amygdale sequences, found that these transformations reflect crystallization under conditions of decreasing aSi. Decreased aSi in the Midland Valley is related to increased distances from the seawater/basalt interface. Silica ratios of analysed analcimes and chlorites also indicate that aSi declined with increasing metamorphic grade.

The reaction (see below) of heulandite to laumontite and of stilbite to laumontite at depth, liberates $SiO_2$ and $H_2O$ with advancing metamorphic grade.

i) $Ca(Al_2Si_7)O_{18}\cdot 6H_2O \longrightarrow Ca(Al_2Si_4)O_{12}\cdot 4H_2O + 3SiO_2 + 2H_2O$

(heulandite) (laumontite) (quartz)

ii) $Ca(Al_2Si_7)O_{18}\cdot 7H_2O \longrightarrow Ca(Al_2Si_4)O_{12}\cdot 4H_2O + 3SiO_2 + 3H_2O$

(stilbite) (laumontite) (quartz)

The production of stilbite, heulandite and laumontite reflects the transformation of essentially Na-assemblages to Ca-assemblages with increasing depth. Mineralogical variations must reflect local gradients in $aNa^{+}/aCa^{2+}$. These gradients may be a product of either

varying initial fluid compositions or of varying degrees of equilibration of the fluid with pre-existing solid phases. The composition of fluid inclusions (chapter 2.5) suggests that the initial Na-fluid was uniform. The degree of equilibrium between pre-existing solid phases and the fluid, is a function of:-

1 Porosity and permeability contrasts (chapter 2.7) within the metavolcanics. The $aNa^{+}/aCa^{2+}$ ratio will be related to the effectiveness of the flow mechanism (diffusion, porosity or fracture flow - chapter 2.7). This is witnessed (chapter 2.3) by the retention of lower grade (?) Na-assemblages in the MMLs* of individual flows, relative to the development of higher grade (?) Ca-assemblages in the UALs* or LALs* (* where MML = Middle Massive Layer, UAL and LAL = Upper and Lower Amygdaloidal Layers respectively).
2 The degree of metamorphism attained with increasing dT/dP; with advancing grade, more Ca was released (eg from anorthite) to the fluid to form the Ca-zeolites.

**$XCO_2$ in the fluid**

The $XCO_2$ of the fluid is an important variable limiting the crystallization of the zeolites. The absence of clay-carbonate assemblages in the zeolite zones and in the palaeo-geothermal plumes, indicates (Thompson, 1971a; Houghton, 1982) that $XCO_2$ was consistently low. Although concentrations were high enough to prevent the crystallization of pumpellyite (assuming that PT conditions were appropriate), despite the presence of epidote and garnet (Coombs *et al*, 1976; 1977).

The ubiquitous occurrence of sphene indicates that $P_{CO_2}$ <50 bars (Schulling and Vink, 1976; Coombs *et al*, 1976) for $P_{fluid}$ = 2 kb. At Beith palaeo-geothermal plume, estimates in the region of $P_{CO_2}$ = 30-40 bars (Thompson, 1971a) are compatible with the formation of prehnite from zeolites plus calcite at $P_{fluid}$ = 2 kb. The presence of rankinite in carbonated metabasalt indicates that maximum $P_{CO_2}$ = 0.3 kb (Winkler, 1976) were encountered adjacent to the Tertiary dyke.

Oxygen fugacity ($f_{O_2}$)

The exact value for the partial pressure of $O_2$ in the metamorphic fluid in the Midland Valley is unknown. The occurrence of haematite in the zeolite zones and in the palaeo-geothermal plumes indicates a relatively high $f_{O_2}$ value. Miyashiro (1973) determined that for $P_{H_2O}$ = 2 kb and < 400 °C, haematite would crystallize at $PO_2 < 10^{-10}$ bars.

2.4.8 Conclusions

1 Mineral assemblages characterize metamorphism in the zeolite facies, under conditions of a) $P_{fluid}$ = 200-400 (?) bars at 200 °C

b) $P_{fluid}$ = <120 bars at 350-420 °C, for the zeolite zones and palaeo-geothermal plumes respectively.

2 In addition to pressure and temperature variables, the composition of the fluid phase was governed by aSi, aNa, aCa, $XCO_2$ ($P_{CO_2}$ <50 bars) and $f_{O_2}$ ($P_{O_2}$ <$10^{-10}$ bars).

## Chapter 2.5 Fluid Inclusion Studies

### 2.5.1. Aims

Fluid inclusion studies were preformed to determine the pressure and temperature conditions during

a) regional burial metamorphism and

b) palaeo-geothermal alteration (see chapter 2.2).

### 2.5.2 Introduction

Fluid inclusions are droplets of liquid trapped during crystal growth. The fluid itself may have been a low-density vapour phase or an aqueous fluid containing solutes, with which the mineral was in contact or from which the mineral may have grown. Shrinkage of this fluid phase during cooling, necessitates that two-phase or multi-phase inclusions develop at room temperature. The inclusions may be heated until these phases homogenize to form a single phase once more. At this temperature (known as the homogenization temperature or as Th$^{o}$C - see section 2.5.5) the single phase reflects the state of the trapped material at the time of trapping. The determination of Th$^{o}$C for the hydrothermal minerals in the Carboniferous lavas of the Midland Valley can therefore provide realistic data for comparision with temperature estimates from mineral chemistry data (chapter 2.4) and from stable isotope data (chapter 2.6).

### 2.5.3 Choice of material

Material for analysis was selected (fig 2.5.0) from mineral pseudomorphs, from veins and from hydrothermal alteration envelopes

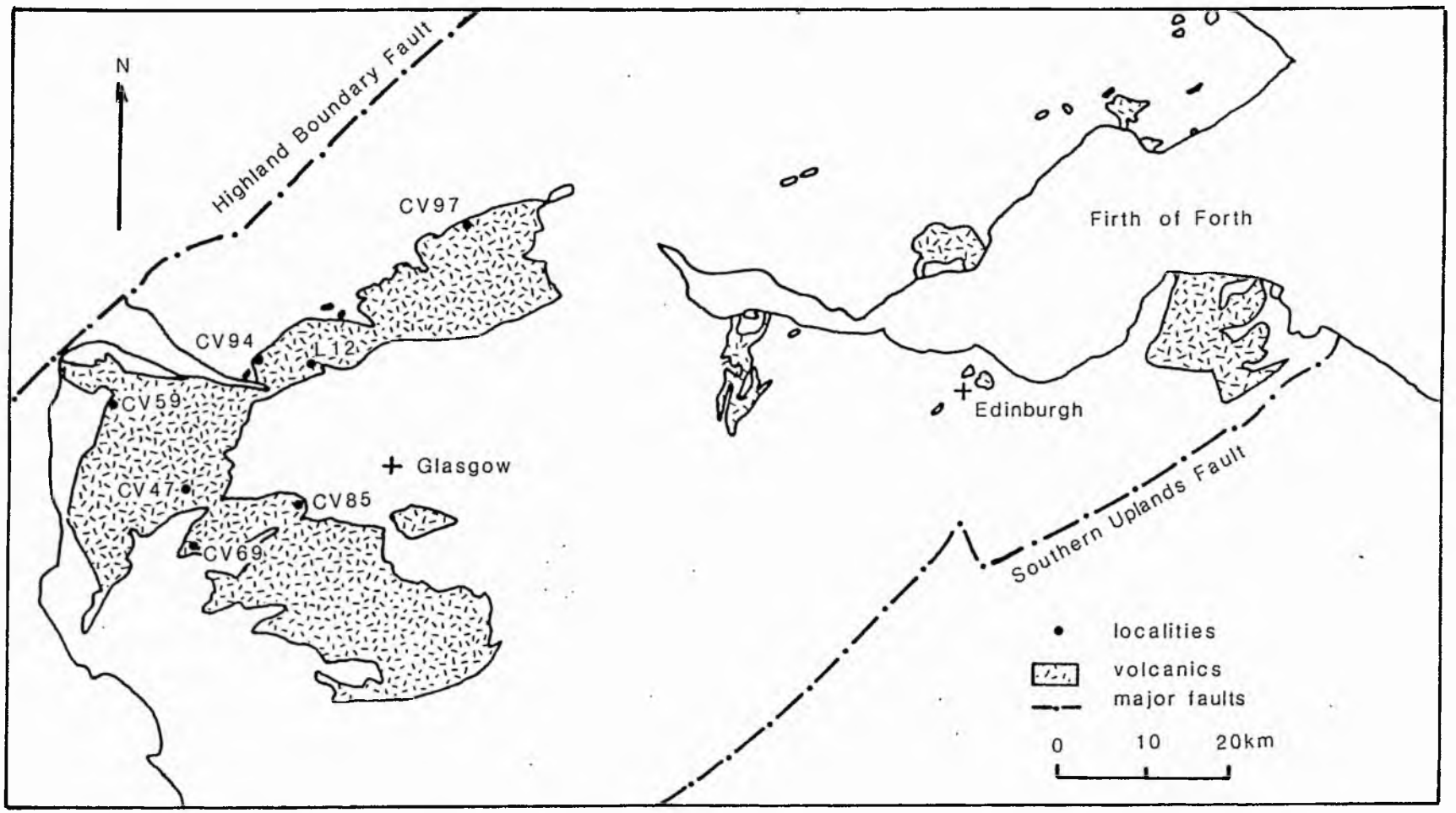


Fig. 2.5.0. Locality map for fluid inclusion data.

in metabasalt, where phaneritic, transparent crystals were developed.

Hydrothermal minerals in the Carboniferous lavas of the Midland Valley, are characterized by zeolites, analcime and prehnite (see chapter 2.2, 2.3 and 2.4). Such minerals are usually disregarded for fluid inclusion studies because they are often well-cleaved and are therefore susceptible to leakage and necking down. However, these minerals were utilized because:-

i) there was a sparcity of quartz and calcite in the assemblages.

ii) these minerals were paragenetically related (see chapter 2.4).

Care was taken in the selection, such that minerals were not strained or deformed and had not been subjected to temperatures above the formation temperature of the inclusions. (ie crystals in proximity to intrusions were not examined).

Multiple stages of zeolite deposition have been recognized (see chapter 2.2) in the Midland Valley lavas. Consequently, representative zeolites were chosen, where possible, from each burial zone. Thermometric analyses were undertaken on analcime, natrolite and heulandite in the analcime zone (as defined from thin-section analysis - chapter 2.3); and upon laumontite in the laumontite zone. In the palaeo-geothermal plumes, the thermometric character of the two minerals, thomsonite and prehnite, was investigated.

### 2.5.4 Optical examination

Prior to thermometric analyses, initial examination of fluid inclusions was caried out using all (158) the ordinary thin-sections available and 30 double-polished wafers, with a standard optical microscope. The following parameters were determined:-

i) overall inclusion abundance

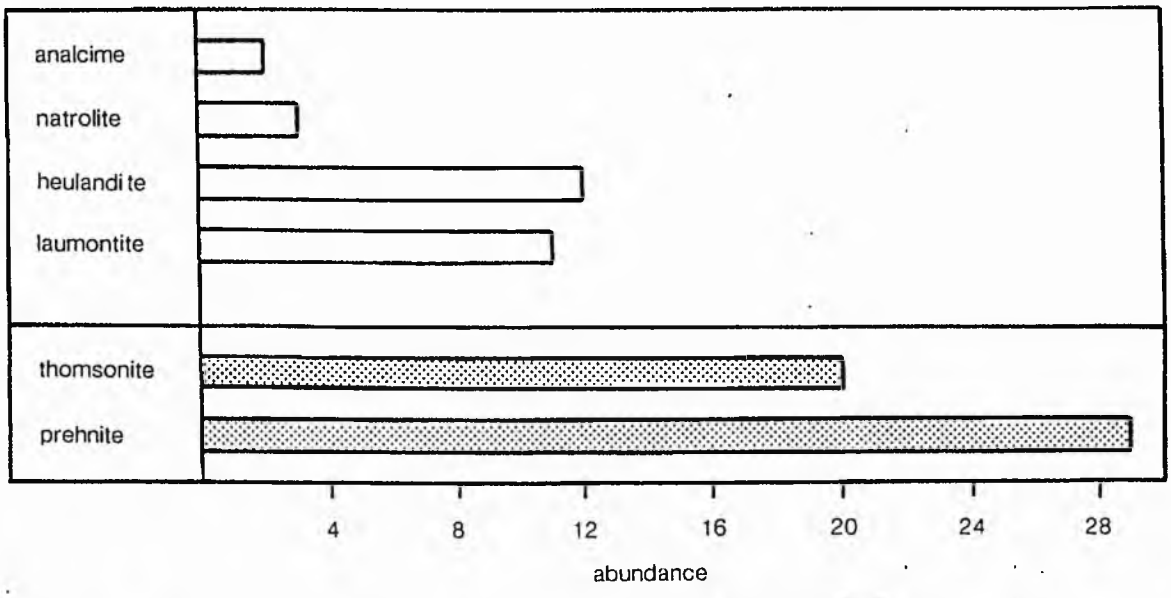


Fig. 2.5.1. Histograms to illustrate inclusion abundance in different host minerals. ▭ amygdale minerals (burial related) ▨ palaeo-geothermal plume minerals. Abundance based upon mean number of inclusions in a half field of view at X430 magnification.

| inclusion type | degree of fill (F) max | min | examples | abbreviations |
|---|---|---|---|---|
| monophase liquid | 1.00 | | | L |
| liquid-rich, 2 phase | 0.95 | 0.80 | | L + V |
| vapour-rich, 2 phase | 0.70 | 0.50 | | V + L |
| monophase vapour | | 0.00 | | V |
| multiphase solid | variable | | | S + L + V |

Fig. 2.5.2. Classification scheme for fluid inclusions in Carboniferous metabasalt of the Midland Valley.

ii) internal nature of inclusions

iii) type of inclusions

i) overall inclusion abundance.

Abundance was based upon the mean number of inclusions (30 to 5$\mu$ diameter) in several half fields of view at x430 magnification. Crystal terminations noticeably contained fewer inclusions than more massive areas. This was presumably related to a decrease in precipitation rates. Thus in order to ensure that the inclusion density was representative, the entire area of a thin-section was examined. The mean density of inclusions encountered in each mineral phase was determined for about 100 half-field of view measurements on each sample, and the results plotted on the histogram in fig 2.5.1.

For the sequential metamorphic series (chapter 2.2) analcime, natrolite, heulandite and laumontite, a consistent increase in inclusion abundance relative to increasing burial depth was noted. Furthermore, inclusion abundance in the burial terrains was clearly subordinate to the inclusion content of palaeo-geothermal thomsonite and prehnite. These increases in fluid inclusion abundance were taken to be a function of the progressive increase in the degree of hydrothermal activity associated with the different burial zones and with the palaeo-geothermal plumes.

ii) internal nature of inclusions

Five inclusion types (fig 2.5.2) were observed in the hydrothermal minerals. Identification was dependant upon the recognition of vapour (V), liquid (L) and solid (S) phases, at room temperature. A classification scheme based upon such observations is

presented in figure 2.5.2. Inclusions were essentially classified according to the volumetric proportions of L and V present and upon the absence/presence of a solid phase. Visual estimates of the degree of fill (F) were made by comparision with the figures of Shepherd *et al*, (1985).

The degree of fill (F) was determined merely to categorize inclusion types, and not as an aid in determining density and pressure measurements (see Shepard *et al*, 1985). Accurate determinations of F could not be made because:-

i) of irregularities in inclusion shape

ii) the area could only be assumed to equal the volume of an inclusion, when the inclusion was itself flattened; such instances were rare.

In nature L-, V+L-, L+V- and S+L+V-type inclusions were found in the hydrothermal minerals of the regional burial zones. In the palaeo-geothermal plume minerals investigated, all five categories of inclusion (described in fig 2.5.2) were present. The inclusions found in each mineral may have had a multiplicity of origins. Whereby, discreet episodes of capture were witnessed by variable phase ratios within the inclusions. The speculative origins of the different inclusion types are discussed briefly below, and are qualified further in sections 2.5.6 and 2.5.7.

For the minerals of the regional burial zones, different types of inclusions may have resulted from either:-

a) sequential trapping of a homogeneous or inhomogeneous fluid under variable fluid pressures and temperatures,

b) with pressure decreases associated with uplift, leading to partial or complete decrepitation (Roeder, 1984) or,

c) to boiling at each uplift stage.

In addition, boiling, necking down, leakage, fracturing and later refilling, may have resulted in the entrapment of different proportions of fluid, leading to variable phase ratios.

These principals may equally be applied to the origin of inclusions in the palaeo-geothermal minerals. Boiling however may have been an important mechanism for the production of variable inclusion types. It has already been noted above that boiling may provide variable phase ratios in L+V- and V+L- type inclusions. Furthermore, the existence of single phase L- or V-type inclusions, in accordance with proof of simultaneous entrapment, may indicate boiling. Increased salinity, leading to the production of daughter/solid phases is also a feature of boiling (Roedder, 1984).

(iii) type of inclusions

Primary, secondary and pseudo-secondary inclusions were recognized in prehnite, analcime and associated zeolites. A comprehensive paragenetic classification of the different generations was not possible, because of the extremely small (<5$\mu$) secondary inclusion size.

All inclusions examined in the course of this study were either formed in isolation or were contained within crystal growth planes. However, since size alone is not a prefuntary for determining inclusion type, all inclusions studied were regarded as secondary until it could be proved otherwise.

Plate 25A: Photomicrograph of fluid inclusions (1-11) in thomsonite at Tf = -76.6 °C.

Plate 25B: Photomicrograph of fluid inclusions (1-11) in thomsonite at Tf = -37.2 °C.

5μ

### 2.5.5. Methodology

Methodology involves the consideration of:-

i) sample preparation and machine conditions

ii) the freezing procedure

iii) the heating procedure.

i) sample preparation and machine conditions

Heating and freezing measurements were carried out on 50-100$\mu$ doubly-polished wafers, using a calibrated Linkam TH600 inclusion stage. The apparatus yielded a measurable range of -180 $^{o}$C to plus 600 $^{o}$C, with a resolution of ±0.1 $^{o}$C at -180 to +200 $^{o}$C, and ±1 $^{o}$C at temperatures in excess of +200 $^{o}$C. Shepherd (1981) quoted equipment accuracy to be +/-1.4%.

The calibration, using standards with known melting temperatures, was determined by J. Kinnaird (pers. comm., 1984). Differences between measured temperatures and known melting temperatures were smaller than the melting temperature variation due to standard impurities. Accuracy of the low temperature measurements (<0 $^{o}$C) = +/- 0.05 $^{o}$C, whilst accuracy of the high temperature measurements (+100 $^{o}$C) = +/- 0.5 $^{o}$C (Shepherd, 1981).

Variable heating/freezing rates (generally <10 $^{o}$C/min) were utilized throughout this study. Near phase transitions a heating rate of <1 $^{o}$C/min was employed to ensure equilibrium conditions.

Inclusion measurements were made in triplicate to ensure accuracy of thermometric data.

ii) the freezing procedure

Freezing measurements enable:-

i) the approximate composition of the fluid phase to be known

Plate 26A: Photomicrograph of fluid inclusions (1-11) in thomsonite at Tf = -34.7 °C.

Plate 26B: Photomicrograph of fluid inclusions (1-11) in thomsonite at Tf = -33.2 °C. The temperature was held constant to allow one single large ice-crystal to grow.

Plate 26C: Photomicrograph of fluid inclusions (1-11) in thomsonite at room temperature.

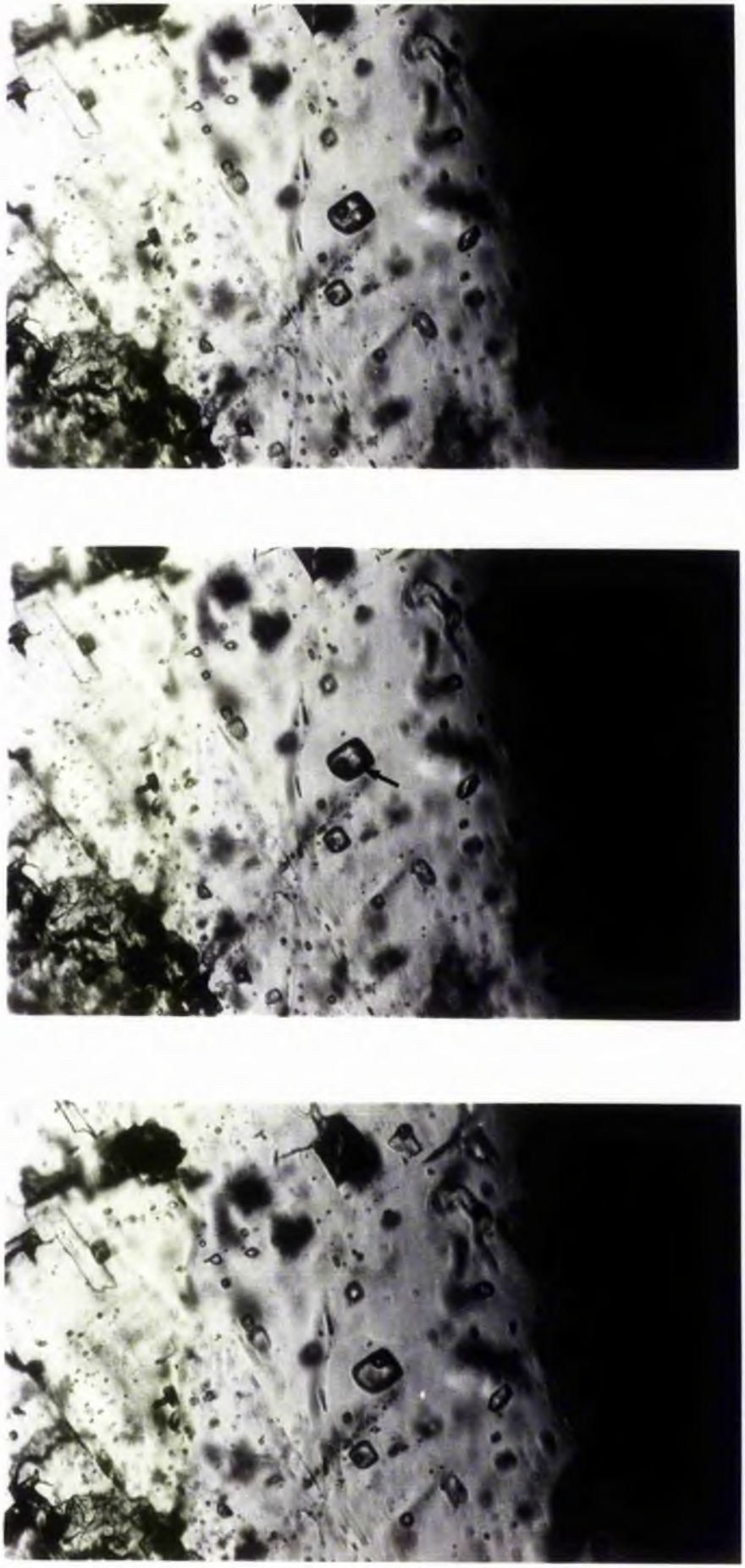

10μ

ii) the amount of dissolved salt to be determined

During freezing, fluid in inclusions is supercooled and forms ice crystals well below its eutectic temperature (Te). The temperature of first ice melting, during gradual warming of the inclusion, occurs at a measurement equivalent to that of the eutectic temperature for a given salt solution. The concentration of this salt solution may be expressed as a wt% NaCl equivalent, and is determined at the temperature of last ice melting (Tlm). The homogenization temperature (Th) requires that the salinity be known (Potter, 1977) so that the relevant density isochore can be used for the pressure corrections (see sections 2.5.6 and 2.5.7).

Te was not recorded here, because of the difficulties in observation. Measurements were restricted to $T_{lm}$ and were obtained during the following procedure.

Fluid inclusions were frozen by the passage of coolant gas ($N_2$) through the apparatus. Fairly quick flow was vital, to overcome the effects of supercooling. Although flow was quick, it was not so rapid as to enable the inclusion to stretch and to encur subsequent leakage. Leakage would have expressed itself as variable and irrepeatable $T_{lms}$ on warming. Following freezing, the temperature was allowed to rise at a controlled rate (see above), so that the $T_{lm}$ might be observed. Plates 25 and 26 show a sequence of inclusions taken from Tn (temperature of nucleation or freezing) at -76.6 $^{o}C$, upon heating to room temperature. Observation of final melting was made easier by allowing a single large ice crystal to grow (plate 26B). This was achieved by holding the temperature for a few seconds, below the $T_{lm}$.

For all samples, freezing measurements were undertaken first,

Plate 27A: Photomicrograph of L+V and V+L-type secondary inclusion trails in laumontite at room temperature.

Plate 27B: Photomicrograph of above inclusions at 151.5 $^{o}$C.

Plate 27C: Photomicrograph of above inclusions at 153.6 $^{o}$C. Note the small amount of liquid remaining in the tip of the central inclusion.

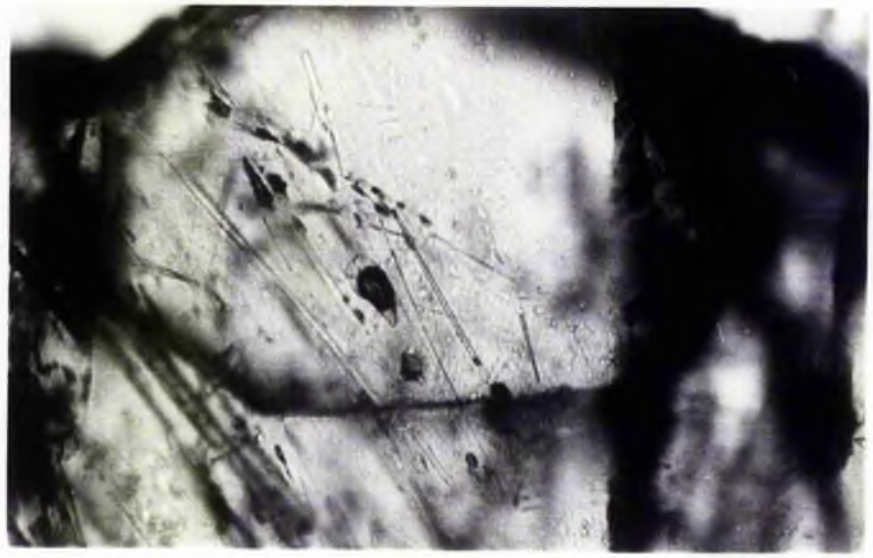

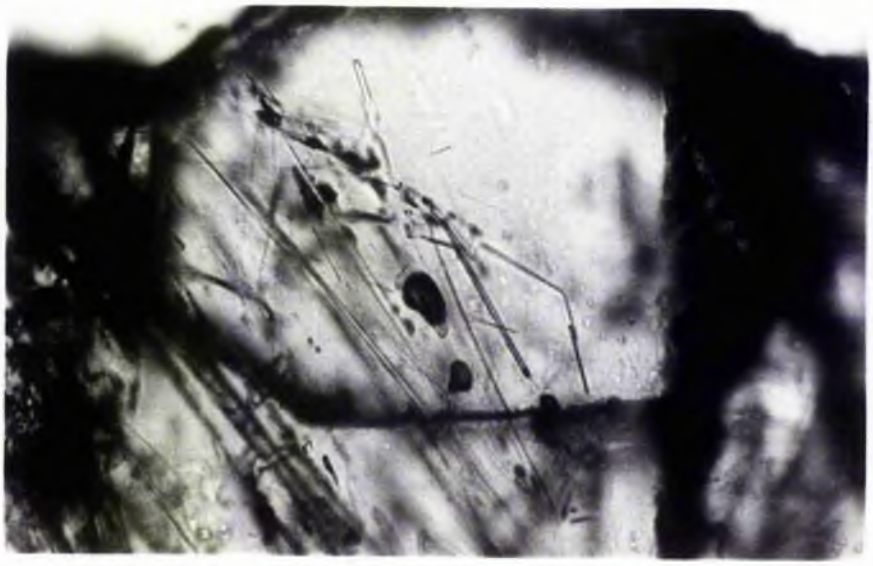

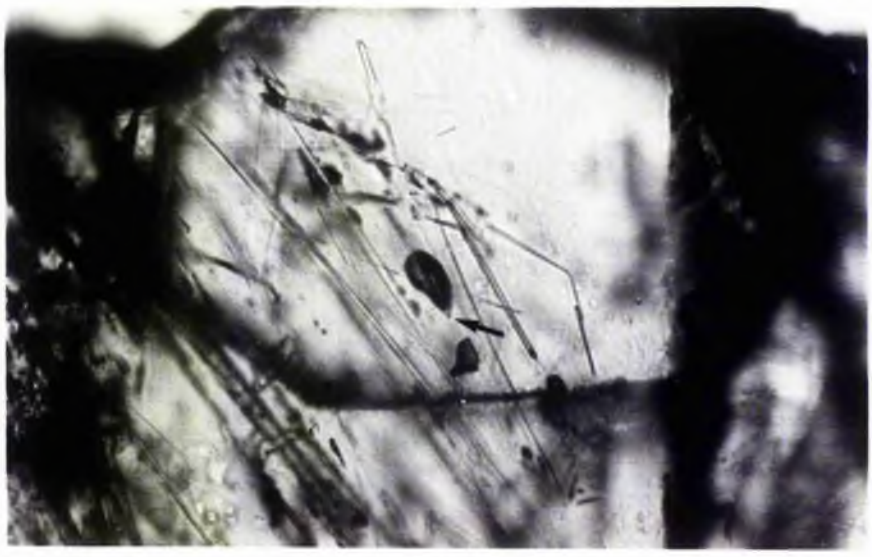

10μ

because of the possibility of decrepitation during heating.

iii) the heating procedure

Heating homogenized the components of an inclusion to a single phase at a temperature assumed to be equivalent to the minimum temperature of trapping ie the homogenization temperature (Th).

Inclusions homogenized either to the liquid, or occasionally to the vapour phase. In the former, smooth gradual heating resulted in the reduction in size and eventual disappearance of the vapour bubble (Plate 27). Upon homogenization to the vapour phase, the vapour bubble expanded until it filled the inclusion (plate 27). In the latter, anomalous Th values were attributed to errors that arose due to difficulties in distinguishing the dark rim of the bubble from the dark rim of the inclusion.

In thomsonite and prehnite, daughter minerals occurred. These persisted on heating even after homogenization of the vapour and liquid phases. Further heating was required for the dissolution of these phases. The temperatures of solid dissolution was known at Ts.

**2.5.6 Results of Thermometry**

Thermometric data was obtained from 2-phase vapour-rich, 2-phase liquid-rich and multiphase-solid inclusions.

1 Freezing measurements and salinities

Because of the effects of supercooling, ice crystallized in inclusions below known eutectic temperatures. Observed freezing temperatures ranged between -29.6 $^{o}$C to -89.3 $^{o}$C for the amygdaloidal minerals, and between -41.2 $^{o}$C to -122 $^{o}$C for the palaeogeothermal plume minerals. During gradual warming the final ice melting

temperature ($T_{lm}$) ranged between:-

i) -31.1 °C to -0.4 °C for L+V-type inclusions

ii) -16.6 °C to -21.1 °C for V+L-type inclusions

iii) -22.3 °C to -29.4 °C for S+L+V-type inclusions

These $T_{lms}$ are equivalent to salinities (Clynne and Potter, 1977) of 31.7 to 0 wt% NaCl for (i), 2.3 to 0 wt% for (ii) and 37.5 to 56.0 wt% for (iii). Where salinity was estimated from:-

a) the depression of the freezing point ie $T_{lm}$, for L+V- and V+L-type inclusions, and

b) the NaCl solubility curves of Shepherd *et al*, (1985 - figure 4.5)

In those L+V-type inclusions with salinities greater than 23.3 wt% ($T_{lm}$ -20.8 °C) hydro-halite ($NaCl \cdot 2H_2O$) was observed by virtue of its strong positive relief and biefringence. Hydrohalite may melt incongruously, up to temperatures of +4 °C (Roedder, 1984). Observed $T_{lms}$ in some inclusions, of >0 °C may therefore reflect melting of the hydrohalite phase, rather than melting of a persistant ice crystal. For V+L-type inclusions the occurrence of ice (?) at temperatures in excess of 0 °C, may reflect the presence of a $CO_2$ or $CH_4$ clathrate. Although $CO_2$ clathrates usually homogeneize between +8 to +10 °C whilst $CH_4$ clathrates homogeneize at temperatures greater than +10 °C (Roedder, 1984).

2 Composition

Upon freezing, two fluid phase compositions have been recognized:-

i) 2-phase water-rich inclusions of variable salinity

ii) methane-water-rich inclusions

In 2-phase water-rich inclusions, first ice-melting

temperatures were difficult to observe. Those observed, were below the eutectics for the $NaCl-CaCl_2$ system (Te = -52 $^{o}C$ Borisenko, 1977; Crawford, 1981). Additional cations such as $Ca^{2+}$ +/- $Mg^{2+}$ must therefore be present (Clynne and Potter, 1977). Furthermore, the majority of inclusions in thomsonite turned dark brown on freezing due to the formation of a $CaCl_2$ hydrate indicating (Shephard *et al*, 1985) the presence of $Ca^{2+}$. Because the eutectics were not observed, it was impossible to identify other saline solutions.

In the methane-water inclusions, cooling of the inclusions below the critical temperature for $CH_4$ (-82.45 $^{o}C$, Hollister and Burruss, 1975) led to the separation of the methane into a liquid and gaseous phase. These phases rehomogenized upon warming, at temperatures above the critical point for methane suggesting the presence of higher hydrocarbons or $CO_2$ in the inclusions (Islam and Hesse, 1983).

In the Midland Valley Carboniferous, methane-rich inclusions are encountered in laumontite in the laumontite zone, and in thomsonsite in the palaeo-geothermal plumes. The inclusions co-exist with water-rich inclusions. In the analcime zone water-rich inclusions only occur. A similar distribution was recognized by Mullis (1979) and by Islam and Hesse (1983), correlating:-

i) $CH_4$- and $H_2O$-rich inclusions with the late diagenetic zones

ii) $H_2O$- ± $CH_4$ ± $CO_2$-rich inclusions with the anchizone

iii) $CO_2$-$H_2O$-rich inclusions with the epizone.

3 Heating measurements

Homogenization temperatures in fluid inclusions from the zeolite zones and from the palaeo-geothermal plumes are summarized in

Table 2.5.1

| | Mineral | Homogenization Temperature (Th°C) | | |
|---|---|---|---|---|
| | | L+V type inclusions | S+L+V-type inclusions (Ts°C) | V+L-type inclusions |
| Amygdale Zones | Analcime | 123 - 176 °C<br>210 - 308 °C | -<br>307 °C | -<br>- |
| ↓ | Natrolite | 261 - 331 °C | - | 322-347 °C |
| | Heulandite | 88 - 178 °C<br>220 - 302 °C | -<br>- | -<br>360 °C |
| Increasing burial depth | Laumonite | 231 - 310 °C | 368 - 372 °C | 305 - 405 °C |
| Palaeo-geothermal Minerals | Thomsonite | 184 - 295 °C<br>350 - 414 °C | -<br>352 - 493 °C | -<br>477 °C |
| | Prehnite | 88 - 224 °C<br>379 - 449 °C | -<br>389 - 459 °C | -<br>- |

Table 2.5.1 Homogenization temperatures encountered in L+V-, V+L- and S+L+V-type inclusions in amygdular and palaeo-geothermal minerals.

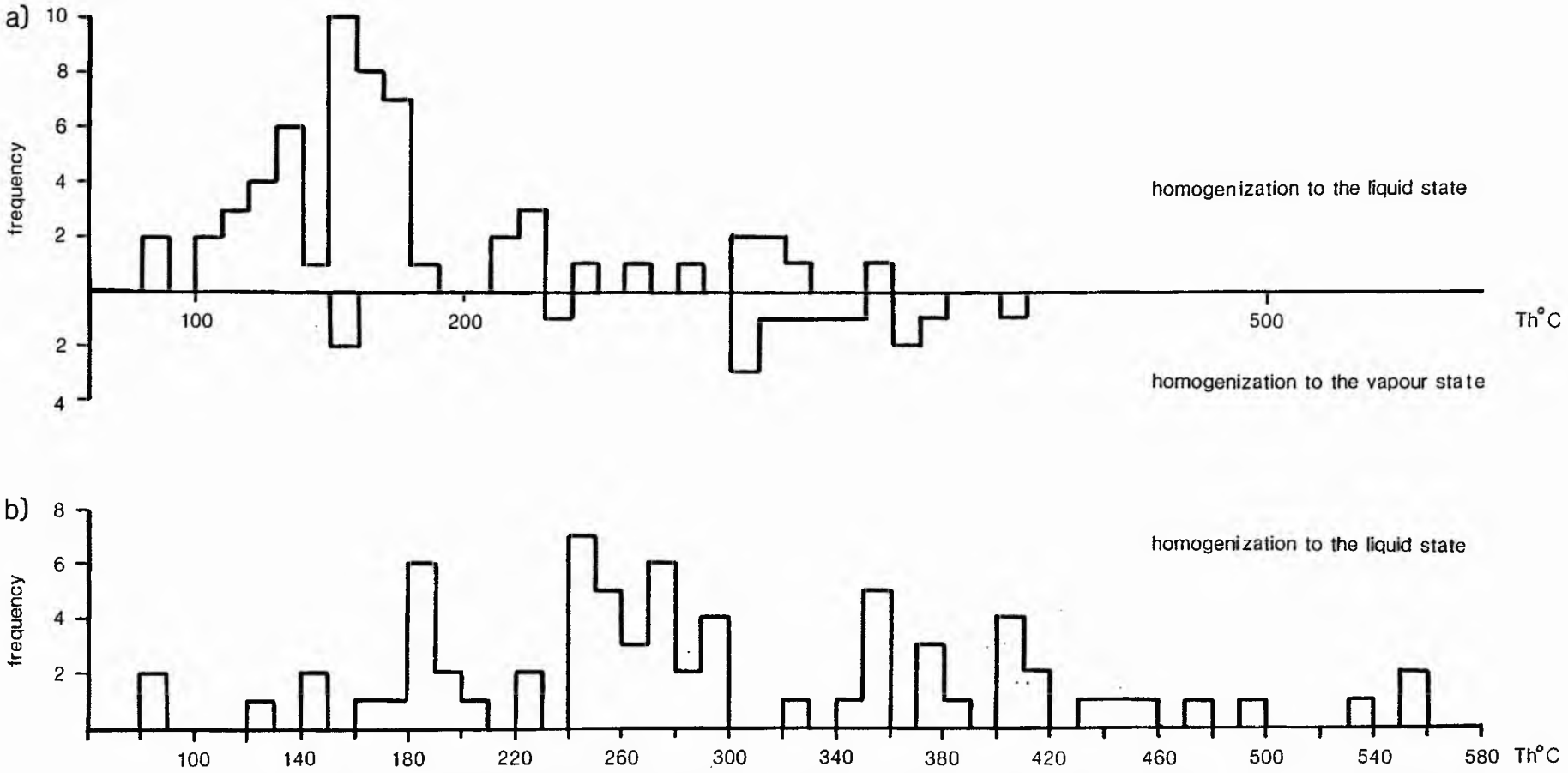


Fig. 2.5.3. Range of homogenization temperatures (Th°C) in a) burial related amygdale and vein minerals, b) palaeo-geothermal plume mineral associations.

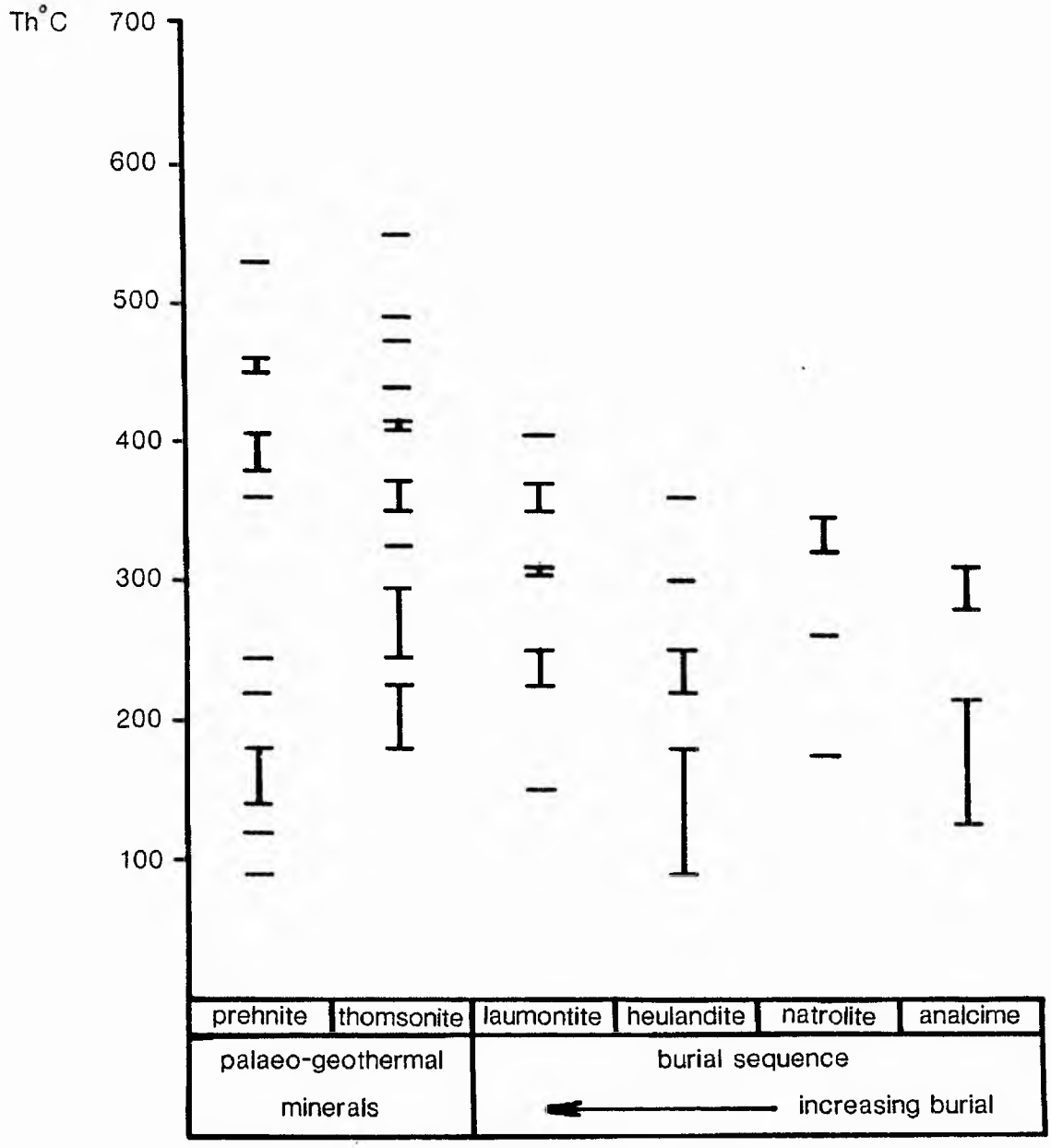


Fig. 2.5.6. Spatial variation in homogenization temperatures (Th°C).

figure 2.5.3 and as histograms and in figures 2.5.4 and 2.5.5 as Th vs salinity plots. (see also Appendix 2.5.1) Interpretations of the latter two diagrams are given in section 2.5.7.

The majority of inclusions observed, homogenized to the liquid phase, without prior decrepitation. For every mineral (excluding natrolite and laumontite) homogenization occurred over two temperature intervals (table 2.5.1). For example, L+V-type inclusions in analcime and in heulandite (both minerals of the analcime zone - see chapter 2.3) homogenized between 88-178 $^{o}$C and between 210-308 $^{o}$C. In the analcime zone, maximum honogenization temperatures equal to 360 $^{o}$C were encountered. Whilst in the laumontite zone, maximum Th = 405 $^{o}$C. Homogenization temperatures in the three amygdale divisions of the analcime zone (ie in analcime, natrolite and heulandite) and in the laumontite zone showed gross overlap. This may reflect that in any division, the temperatures of fluid entrapment were not restricted to the time of maximum heating, For example, lowered temperatures could reflect lateral movement of water after the fluid had been trapped. However, figure 2.5.6 shows an increase in maximum Th $^{o}$C with increased burial depth. In the palaeo-geothermal plumes homogenization temperatures in thomsonite and prehnite again show significant overlap, with maximum Th = 493 $^{o}$C.

Those inclusions that homogenized at the lower temperature ranges shown in table 2.5.1, consist of L+V-types only. At higher temperatures L+V-type inclusions are associated with V+L- and/or S+L+V-type inclusions over compatible temperature intervals. (The reasons for such associations are discussed in section 2.5.7 below). Solid dissolution temperatures ranged between 307-372 $^{o}$C in the

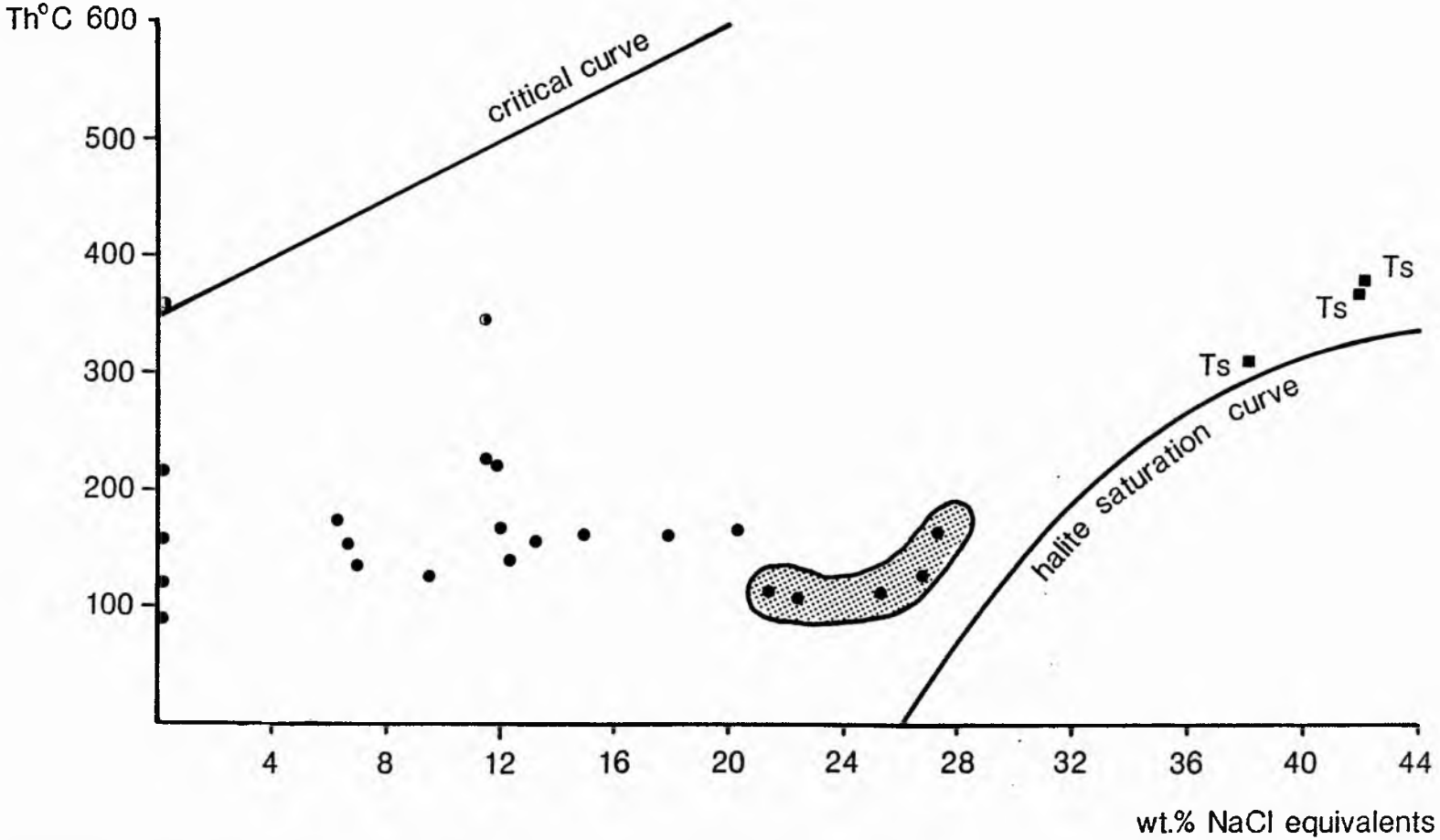


Fig. 2.5.4. Th vs salinity plots for fluid inclusions in burial related amygdale and vein minerals. Symbols - • L+V-type inclusions, ◗ V+L-type inclusions, ■ S+L+V-type inclusions,. Ts - temperature of solid dissolution. Stippled area, field of methane-rich inclusions.

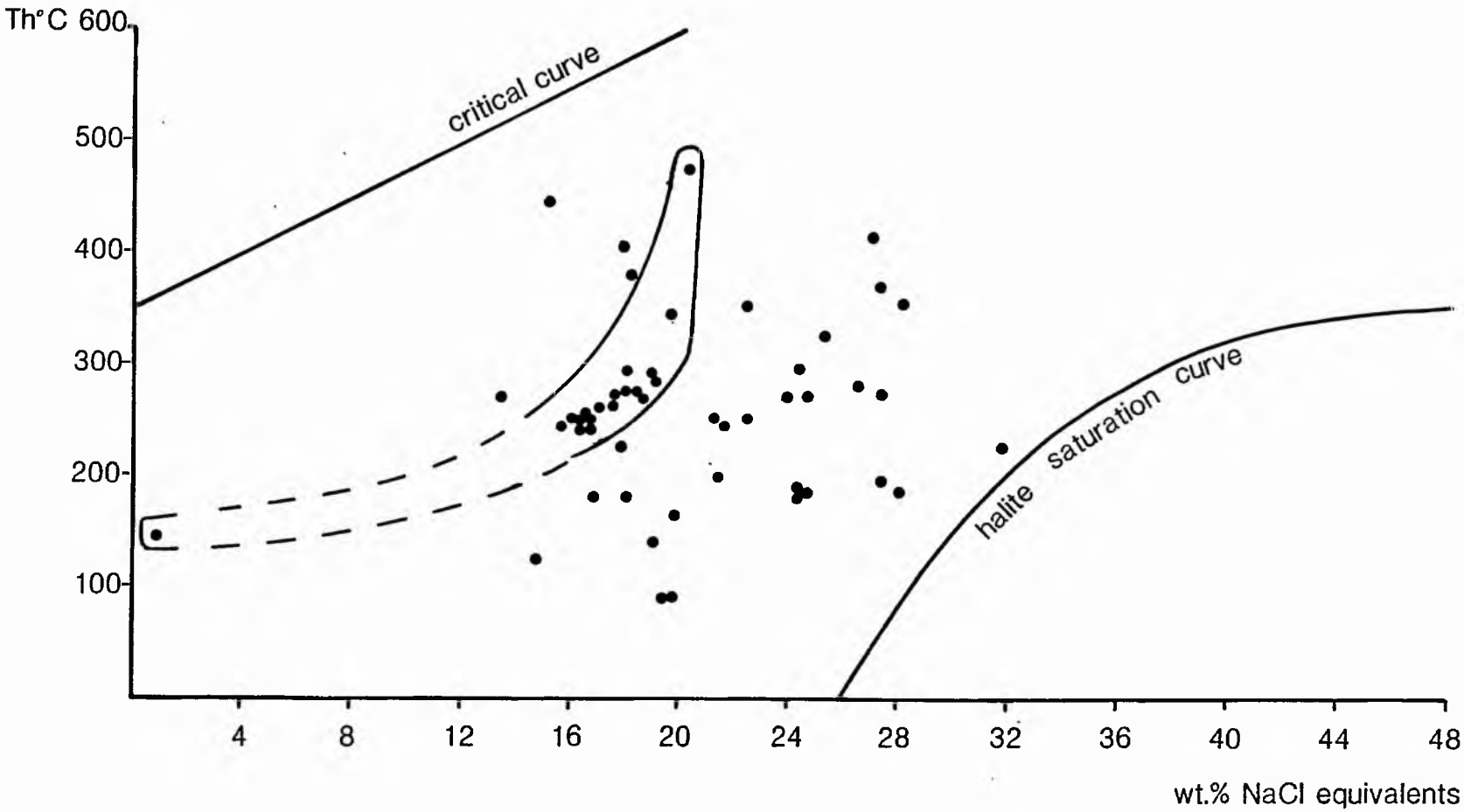


Fig. 2.5.5. Th vs salinity plots for fluid inclusions in palaeo-geothermal minerals. • L+V-type inclusions. Circled area, field of dilute salt solutions.

zeolite zones and between 352-493 °C in the palaeo-geothermal plumes.

### 2.5.7 Discussion

#### 1 Interpretation of thermometric data

The thermometric data is discussed below, with reference to:-

a) Fluid inclusions in the zeolite zones

b) Fluid inclusions in the palaeo-geothermal plumes.

Interpretations were made difficult because:-

i) it was impossible to establish the paragenetic history of the inclusions.

ii) several alternative explanations could be proposed to explain the fluid inclusion trends and groupings on the Th vs salinity plots (figures 2.5.4 and 2.5.5).

**Fluid inclusions in the zeolite zones**

In the zeolite zones the following types of inclusions have been encountered ie L, L+V, V+L and S+L+V. Thermometric measurements are available for the latter three types. Plotted on figure 2.5.3a these measurements record a Th peak in the analcime zone at 150 °C. Insufficient data was available to characterize temperatures in the laumontite zone where inclusions homogenized at <230 °C.

Paired data sets (Th and salinity) were available for a limited number of measurements (essentially L+V-type inclusions). On figure 2.5.4, two vertical arrays at constant salinities (0 wt% NaCl equiv.; 12 wt% NaCl equiv.) are shown. Measurements were taken from inclusions within analcime, natrolite and heulandite in the analcime zone. Consequently the vertical arrays are unlikely to signify leakage or necking down, which gave way to variable phase ratios

within individual crystals. For all the inclusions in the arrays, paired V+L- and L+V-type inclusions homogenized at constant temperatures; salinity measurments were not available. However such an association of inclusions homogenizing over similar temperatures ranges may possibly be indicative of the co-existence of vapour and liquid over the same temperature ranges (Alderton and Rankin, 1983) ie of boiling. The arrays may be representative of sequential boiling, possibly associated with uplift towards the end of the Dinantian (chapter 2.1), when renewed magmatic activity occurred beneath the Campsie and Renfrewshire volcanic areas. Unfortunately there are insufficient V+L-type inclusions plotted on the Th vs salinity diagram (fig 2.5.4) to establish their relationship to L+V- and S+L-V- type inclusions.

The main trend on figure 2.5.4 is one of increased salinity with rising temperature. Although, at salinities <20 wt% NaCl equiv., the trend is somewhat isothermal. Consideration of this trend and of the unpaired data presented in Appendix 2.5.1, suggests three alternative explanations to account for the origin of the fluids:-

a) The presence of both L-rich and V-rich inclusions suggest that at the time of growth of the host crystals, the hydrothermal fluids were boiling. The low abundance of associated V+L- and L+V-type inclusions however, must indicate that if boiling occurred, it was of limited development.

b) L+V-type inclusions may have been a precursor to V+L-type inclusions liberated during boiling. The unmixing of an earlier fluid may have resulted from pressure release. This could have been effected by a change from a lithostatic to a hydrostatic pressure

regime during fracturing of the rock (see chapter 2.2 for discussion of pressure regimes). Brecciated veins and whole-rock (chapter 2.2) testify to explosive degassing, possibly associated with this change from a lithostatic to a hydrostatic environment. It seems unlikely however, that boiling was restricted to the vein environment, since different inclusion types +/or abundances are not encountered between the veins and the groundmass material. This suggests that fracture allowed for the lateral spread of boiling fluids. Supporting the discussion in chapters 2.2 (section 2.2.4.6) and 2.7 that fracture significantly increased and concentrated the flow of hydrothermal fluids in the volcanics. The development of more saline concentrates (S+L+V-type inclusions) is consistent with prolonged boiling of these earlier fluids during fracturing.

At 20 wt% NaCl equiv., the inclusions show (fig 2.5.4) a decrease in homogenization temperature, accompanied by the separation of an immiscible $CH_4$-rich fluid. Separation is invoked, because no water-rich inclusions of comparable salinity or Th co-exist. Such a decrease in Th, was noted by Alderton and Rankin (1983) to follow boiling, as a result of decompressive cooling upon the release of water vapour. Furthermore, Mullis (1979) recognized that in the Swiss Alps, under isothermal conditions (similar to those established in the zeolite zones of the Midland Valley) $CH_4$ was liberated following a sudden pressure drop. By comparison this suggests that fracturing occurred in the zeolite zones of the Midland Valley at about 170 $^{o}$C involving the circulation of fluids with c20 wt% NaCl equiv. The associated pressure release may have resulted in boiling and lateral movement of the hydrothermal fluid and to the release of a $CH_4$ fluid.

c) The earliest fluids may have been the most saline, with progressive dilution of trends resulting from the mixing and dilution with cooler groundwater. Stable isotope data (chapter 2.6) confirms that groundwater had a role to play during hydrothermal alteration.

In all probability inclusions in the zeolite zones, reflect a combination of the processes discussed in b) and c). L+V-type inclusions are the most abundant and their low homogenization temperatures suggest the presence of a large volume of cool water (groundwater(?)). Whilst variable salinities and associated V+L-type inclusions suggest periodic boiling. V+L- and L+V-type inclusions are associated with L-type inclusions. Yermakov (1965) determined the upper temperature of formation of L-type inclusions to be $\leqslant$70 $^{o}$C. However, Roedder (1984) states that L-type inclusions can form above this temperature and exist in the metastable state at Th $\leqslant$170 $^{o}$C. The association of V+L- and L+V-type inclusions with L-type inclusions at 170 $^{o}$C has been determined by Alderton and Rankin (1983) to reflect the transition between meteoric hydrothermal and a cool supergene groundwater regime.

**Fluid inclusions in the palaeo-geothermal plumes**

All five fluid inclusion types described in figure 2.5.2 were found in thomsonite and prehnite. Thermometric data is available (appendix 2.5.1) for L+V-, V+L- and S+L+V-type inclusions. Table 2.5.1 indicates that between 350-450 $^{o}$C, those inclusions in thomsonite and prehnite homogenized over a similar temperature range. Such an association denotes boiling, but its significance could not be determined since paired (Th and salinity) measurements were available for L+V-type inclusions only.

Figure 2.5.3b demonstrates that the majority of fluid inclusions in the palaeo-geothermal minerals, homogenized between 180 to 420 °C. Comparative Th (220-340 °C) have been obtained (Belkin *et al*, 1985) from quartz in geothermal wells in Tuscany. Whilst the majority of homogenization temperatures in the analcime zone (fig 2.5.3a) ranged between 100 to 190 °C. Fluid inclusion data from the palaeo-geothermal plumes indicate that the majority of hydrothermal minerals investigated were precipitated from fluids hotter than those contained in the surrounding rocks. Fluid inclusion evidence therefore testifies to an actual change in the thermal regime of the zeolite zones surrounding the palaeo-geothermal plumes.

L+V-type inclusions in prehnite homogenized between 88-224 °C and between 379-449 °C at salinities of 14-19 wt% NaCl equiv. These values expressed on a Th vs salinity diagram (fig 2.5.5), plotted as a vertical array. This trend would be consistent with leakage and/or necking down. Variable phase ratios or cracks leading from those inclusions analysed were not observed in the polished wafers. Furthermore, not all the analyses were taken from the same wafer. This suggests that the trend must reflect conditions in the palaeo-geothermal prehnite, other than necking or leakage. The restricted salinities in the prehnite inclusions, suggest that cooling occurred either:-

a) as a result of the dissipation of heat from the hydrothermal fluid itself.

b) by mixing with a cooler fluid of the same salinity.

At 88-170 °C L+V-type inclusions in prehnite, co-exist with L-type. Such fluid inclusion associations at these temperatures represent the possible transition between supergene groundwater, with the same

salinity (14-19 wt% NaCl equiv.) as that found in the high temperature inclusions. This suggests that the hottest waters may infact have been superheated groundwater.

Inclusions in thomsonite are divided into two groups on figure 2.5.5 ie

a) inclusions with 14-19 wt% NaCl equiv.

b) inclusions with >19 wt% NaCl equiv.

The restricted salinities of group (a) suggest that thomsonite was compatible with development from the same fluid as prehnite. In the handspecimen (chapter 2.2) prehnite was observed to grown first, followed by the later precipitation of thomsonite. Prehnite was obtained from the central hotter (?) part of the plume, whilst thomsonite was collected from peripheral cooler (?) areas. Assuming that prehnite was precipitated during the hydrothermal peak (low temperature inclusions merely represent late capture), then it appears that the initial Th in thomsonite (c200 $^{o}$C) was lower than the initial Th in prehnite (c350 $^{o}$C). Inclusions in thomsonite may therefore be indicative of a temperature decrease in the peripheral regions of the plume.

Inclusions in group (b) show a trend (fig 2.5.5) of increased salinity with increased Th. S+L+V, V+L and L+V- type inclusions homogenize over the same temperature interval. This suggests that either a high temperature saline fluid mixed with a cooler less saline fluid, or that boiling of a 14-19 wt% NaCl equiv. solution occurred. The sharp drop in temperatures observed between group (a) or group (b) at 19 wt% NaCl equiv., followed by the development of high temperature saline solutions, and to the release of $CH_4$-rich solutions suggest that boiling may have occurred and was associated

Table 2.5.2

| Mineral | Tt°C L+V type inclusions only | Pt = Phy'd (bars) | depth of boiling (m) |
|---|---|---|---|
| Analcime | 123 - 176<br>210 - 308 | 1.9 - 7.4<br>17.8 - 91.9 | 8.4 - 66<br>177 - 1056 |
| Natrolite | 261 - 331 | 43.8 - 119.1 | 470 - 1416 |
| Heulandite | 88 - 178<br>220 - 302 | 0.7 - 9.4<br>21.7 - 80 | -3.5 - 86.2<br>219 - 907 |
| Laumontite | 231 - 310 | 26.1 - 91.9 | 269 - 1056 |
| Thomsonite | 184 - 295<br>350 - 414 | 9.4 - 69.4<br>⩽120 | 86 - 776<br>⩽1500 |
| Prehnite | 88 - 224<br>368 - 449 | 0.7 - 21.7<br>⩽120 | -3.5 - 219<br>⩽1500 |

Table 2.5.2 Temperature of trapping (Tt), pressure at time of trapping (Pt) and depth of boiling in L+V-type inclusions under hydrostatic conditions. P hy'd = hydrostatic pressure.

with the release of pressure during fracturing.

## 2 Pressure Corrections

Fluid inclusions trapped in hydrothermal minerals in the Midland Valley occur in vein and amygdale environments in the same rock; where pressure conditions were hydrostatic in the former and lithostatic in the latter (see chapter 2.2). The thermometric measurements quoted so far however, do not taken into account the effects of pressure or of salinity at the time of trapping. The pressure correction therefore has to be applied. This is infact a temperature correction which must be added to Th to obtain Tt (temperature of trapping). It has been so called, because pressure controls the density of the fluids and hence the magnitude of the pressure correction.

Tables 2.5.2 and 2.5.3 comprise a list of Tt, Pt (pressure at the time of trapping) and burial depths experienced in the amygdale zones and in the palaeo-geothermal plumes, under hydrostatic and lithostatic conditions respectively. To minimize errors in the pressure correction, temperatures were determined at salinities of 10 wt% NaCl equiv., following Roedder (1984).

For those fluid inclusions trapped during boiling ie under hydrostatic conditions, Th = Tt therefore no pressure correction was required. Estimates of the depth at which boiling occurred and associated hydrostatic pressures were determined visually from the figures and tables of Haas (1971). The information regarding depth of boiling (table 2.5.2) suggests that many fractures in the analcime and in the palaeo-geothermal plumes, were open to the surface, where fluids may have expressed themselves as thermal springs.

Table 2.5.3

| Mineral | Tt°C L+V-type inclusions | Pt = Plith (bars) | Maximum burial depth (m) |
|---|---|---|---|
| Analcime | 123 - 200<br>235 - 328 | 274 | 1000 |
| Natrolite | 291 - 355 | 328 | 1195 |
| Heulandite | 88 - 208<br>260 - 327 | 377 | 1375 |
| Laumontite | 271 - 345 | 388 | 1415 |

Table 2.5.3 Temperature of trapping (Tt), pressure at time of trapping (Pt) and maximum burial depths of L+V-type inclusions under lithostatic conditions in the amygdale zones.

In the majority of inclusions (ie those under lithostatic pressure) a vapour bubble would not have developed until the pressure and temperature had dropped below the Tt. In this instance, independant evidence of burial depth and hence pressure at the time of trapping (chapter 2.2; table 2.5.3) for 10 wt% NaCl equiv. solutions, were used to calculate the pressure correction. Estimates were made visually from the figures of Potter (1977). Corrections have only been made (table 2.5.3) and are only valid for those inclusions which homogenized to the vapour phase.

Lithostatic pressure was calculated from the following equation:-

$P_{lith}$ = depth (km) x density of overburden gm $cm^{-3}$ (2.8) x gravitational acceleration (98)

### 2.5.8 Conclusions

Pressure and temperature conditions during regional burial metamorphism and palaeo-geothermal alteration were determined to be:-

a) 88-331 $^{o}C$ under $P_{lith}$ = 274-377 bars and $P_{hyd}$ = 0.7-119 bars in the analcime zone : 231-345 $^{o}C$ under $P_{lith}$ = 388 bars and $P_{hyd}$ - 26-91 bars in the laumontite zone

b) 88-449 $^{o}C$ under $P_{hyd}$ = 0.7 to $\leqslant$120 bars in the palaeo-geothermal plumes.

## Chapter 2.6 Stable isotope analyses in the Midland Valley

### 2.6.1 Aims

1. To determine the isotopic character of metamorphic fluids.
2. To determine carbon and oxygen reservoirs.
3. To determine the significance of co-existing calcite-dolomite pairs.
4. To consider the implications of the previous points to the metamorphic model.

### 2.6.2 Introduction

In the absence of zeolite-water fractionation curves, vein calcite was utilized to determine the isotopic character of the fluids during hydrothermal alteration in the Midland Valley. It is likely that zeolite-water fractionation curves are not available because hydroxyl-bearing minerals have abnormally low $O^{18}/O^{16}$ ratios (Hoefs, 1973), thus suggesting that the hydroxyl group may be lower in $^{18}O$ than the rest of the oxygen in the silicate structure.

Since there is a sparcity of calcite in amygdale and vein assemblages in the Clyde Plateau Lavas, the majority of the data present, is derived from the eastern Midland Valley volcanics. Field studies (chapter 2.2) and petrographic analyses (chapter 2.3) have shown that hydrothermal alteration in the eastern Midland Valley was characterized by:-

i) early greenstone alteration in volcanic plugs and in the basal horizons of the volcanic piles.

ii) later regional burial metamorphic zeolite zones.

The greenstones are believed (chapter 2.2) to have resulted from the interaction of the volcanics either with circulating magmatic, seawater and meteoric water at or near the time of extrusion. This is inferred since the volcanics represent littoral ash-cones and magmatic centres, which were periodically transgressed by the sea (chapter 2.1). Zeolites and associated minerals can be generated both within a geothermal environment (Hattori and Sakai, 1980; Kristmannsdottir and Tomasson, 1978) (such as outlined above), and during burial metamorphism (Coombs *et al*, 1959; Walker 1960b; Houghton, 1982).

### 2.6.3 Notation and basic principles

This chapter is concerned with measuring the variation in isotopic abundance in carbonates. The variation is produced by isotopic fractionation due to physico-chemical effects, and is presumed to be independent of pressure (Hoefs, 1973). Variation is concerned with measuring small changes in the isotope ratios, where the isotope ratios are measured relative to an arbitrary standard.

Oxygen measurements were made relative to SMOW (Standard Mean Ocean Water), as defined by Craig (1961). Carbon measurements were made relative to the Peedee Belemnite (PDB) international standard. SMOW must be analyzed directly by fluorination or by carbon reduction techniques. If, as in this instance, water is analyzed by the $CO_2$-equilibration method (see section 2.6.5), the fractionation factor between $CO_2$ and $H_2O$ must be known at the temperature of equilibration. This is discussed later in this section. The relationship between PDB and SMOW, as defined by Craig (1965), is given by the equations:-

$$SMOW = 1.03086 \quad \delta_{PDB} + 30.86$$

$$PDB = 0.97006 \quad \delta SMOW - 29.94$$

These equations are based on the following fractionation factors at 25 $^{o}C$.

i) 1.0412 for $CO_2$ - $H_2O$

ii) 1.01025 for $H_3PO_4$ - liberated $CO_2$ from calcite

iii) 1.00022 for $H_3PO_4$ - liberated $CO_2$ from PDB-$CO_2$ in equilibrium with SMOW.

In actual practice, two working standards compiled by the National Bureau of Standards (NBS) were used. These are NBS-19 and NBS-20 (Solenhofen Limestone); both have been compared to PDB during this study. Standard values of $\delta^{13}C$, $\delta^{18}O_{PDB}$ and $\delta^{18}O_{SMOW}$, are listed in table 2.6.3., together with similar values for analyzed material.

Partitioning of the isotopes ($^{13}C/^{12}C$ or $^{18}O/^{16}O$) between the mineral and the water with which it is in equilibrium, is defined by the fractionation factor ($\alpha$), where:-

$$\alpha = \frac{RA}{RB}$$

RA = $^{13}C/^{12}C$ or $^{18}O/^{16}O$ in phase A

RB = $^{13}C/^{12}C$ or $^{18}O/^{16}O$ in phase B.

The extent to which this fractionation occurs, is dependent upon the vibrational frequencies of the molecules in the mineral and in the water. Since the fractionation factor is temperature dependant, the values become more similar as temperature increases. The experimentally determined (O'Neil, Clayton and Mayeda, 1969) fractionation factor:-

$$25\ ^{o}C$$

$$\alpha$$

$$H_2O - CaCO_3 = 2.78\ (10^6T^{-2}) - 2.89$$

was used to relate the isotopic composition of the liberated $CO_2$ to that of the parent carbonate during this study.

The fractionation factor ($\alpha$) is related to the delta values by the equation:-

$$1000\ell n\alpha_{A-B} \simeq \Delta A\text{-}B \equiv \delta A - \delta B.$$

Where $\Delta$ = the finite difference between A minus B.

2.6.4 Potential uses of Carbon and Oxygen isotopes

Carbon and oxygen isotopes may be used to define the isotopic compositions of major rock types and fluids during hydrothermal alteration, and to provide geothermometric criteria for mineral formation.

The compositions of the major rock types, as defined by carbon and oxygen isotope ratios, are given in figure 2.6.1. Distinctive

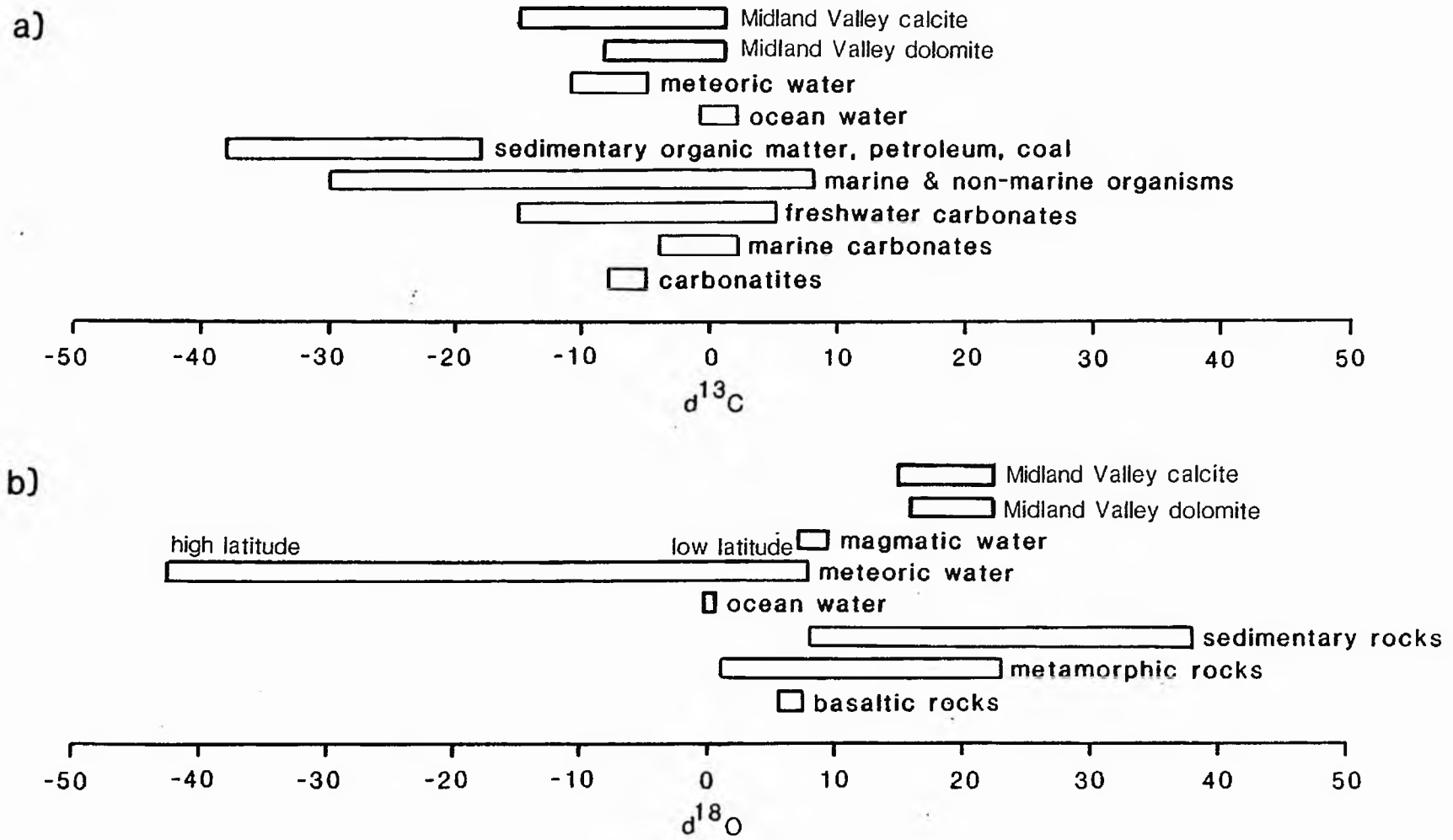


Fig.2.6.1. The range of d 13 C and d 18 O (in ‰ ) values for fluids and major rock types. (after Hoefs, 1973)

$\delta^{13}C$ fields (fig 2.6.1, a) for sedimentary organic matter, marine carbonates and carbonatites are recognized. These have been taken to reflect the organic, carbonate-derived and magmatic carbon fields respectively, as shown on figure 2.6.3. The lack of equivalence (fig. 2.6.1 a) shown by some of the field of sedimentary organic matter (ie $< -30$ $\delta^{13}C$) with that of marine and non-marine organisms, is a function (Hoefs, 1973) of the diagenetic elimination of $^{13}C$-rich carbohydrate proteins from marine sediments. This inadvertently leads to an enrichment of $^{12}C$ in ancient sedimentary organic matter.

The isotopic fields of oceanic, meteoric and magmatic water, are also shown on figure 2.6.1. Oceanic water has a $\delta^{18}O$ value of $0^{o}/oo \pm 1^{o}/oo$. Considering the equatorial latitude (Smith *et al*, 1981) of the Midland Valley for most of the Carboniferous, it is highly likely that the isotopic composition of the seawater would have been affected by evaporation processes. This would have caused an enrichment ($<3^{o}/oo$; Truesdell, 1974) of $\delta^{18}O$ in highly saline waters, as a result of the preferrential enrichment of $\delta^{16}O$ in the vapour phase (Hoefs, 1973). Therefore for any hydrothermal process involving the circulation of saline waters in the Midland Valley a correction factor has to be applied to account for the activity of dissolved salt in the water (see section 2.6.5).

Meteoric water involved in atmospheric circulation shows a wide range of $\delta^{18}O$ ratios. Dansgaard (1964), determined that in tropical regions, water only shows very small $\delta^{18}O$ depletions (0 to $-2^{o}/oo$) relative to SMOW. Whilst at higher latitudes and altitudes fresh water becomes progressively lighter isotopically. For example, Aldaz and Deutsch (1967), determined a $\delta^{18}O$ of $-60^{o}/oo$ for polar snow. These variations are interpreted (Hoefs, 1973) as the products

of fractionation in the atmospheric Rayleigh process, whereby isotopic differences were caused by variations in vapour pressure, ground temperature and evaporation rates.

In equatorial regions, seawater and meteoric water show only minimal variation ($\delta^{18}O$) from SMOW. This makes it difficult to distinguish between the sources of hydrothermal fluids in the Midland Valley, when these two components are involved.

Magmatic water is defined as those fluids that have exchanged chemically and isotopically at magmatic temperatures with a magma system or igneous body. Magmatic water is characterized by $\delta^{18}O$ = 7 to 9°/oo (Hoefs, 1973).

Co-existing dolomite and calcite may be used for thermometry. Northrop and Clayton (1966) and Sheppard and Schwarcz (1970), found that the dolomitic component of certain calcites showed a $\delta^{18}O$ enrichment of 3 to 7°/oo, and was compatible with $O^{18}/O^{16}$ ratios in co-existing quartz. From this it was predicted that dolomite-calcite oxygen-isotope fractionation should be equivalent to quartz-calcite fractionation and hence could be used for geothermometry. The relationship proved to be true for certain ancient sedimentary pairs, where dolomite-water exchange had occurred at >300 °C. There is no evidence (section 2.6.6, below) that dolomites in the Midland Valley were ever at equilibrium with calcite, since small or zero fractionations between dolomite and calcite were encountered. Consequently the application of dolomite-calcite mineral pairs to geothermometery in the Midland Valley (section 2.6.6) has not been attempted.

In the absence of stable co-existing mineral pairs for oxygen-isotope thermometry, the stable-isotope fractionation curves

presented by Friedman and O'Neil (1977), were used to calculate the temperature dependence of calcite-water fractionation factors (see section 2.6.9). The fractionations are correct to ± 0.2 °/oo and the temperatures to ± 5 °C. By establishing the temperature of alteration in this method, it is possible to calculate the nature of the hydrothermal fluid. For example, a fractionation factor yielding a temperature of 20 °C indicates that the fluids were unlikely to have been magmatic or metamorphic; circulation of cool groundwater (either meteoric or seawater) is envisaged.

Additional temperatures of the hydrothermal fluid may be derived from dolomite geothermometry (Sheppard and Schwarcz, 1970). This is discussed in section 2.6.6 and 2.6.7.

### 2.6.5. Effect of salinity on δ-values

In instances where seawater circulation is anticipated a saline correction factor (Truesdell, 1974) has to be applied to the geothermometer. This is because the actual isotope fractionations measured, are between a mineral and a dilute salt solution. The correction factor is dependant upon the concentration and type of salt involved (Truesdell, 1974). The effects of the solutes increase with temperature, up to 275 °C (Truesdell, 1974); ie, over the same temperature range within which the zeolites were formed (see chapter 2.5). Thus the temperature arrived at will be suppressed (because of the salt concentration) relative to the calcite temperature available from the mineral-water curves of Friedman and O'Neil (1977).

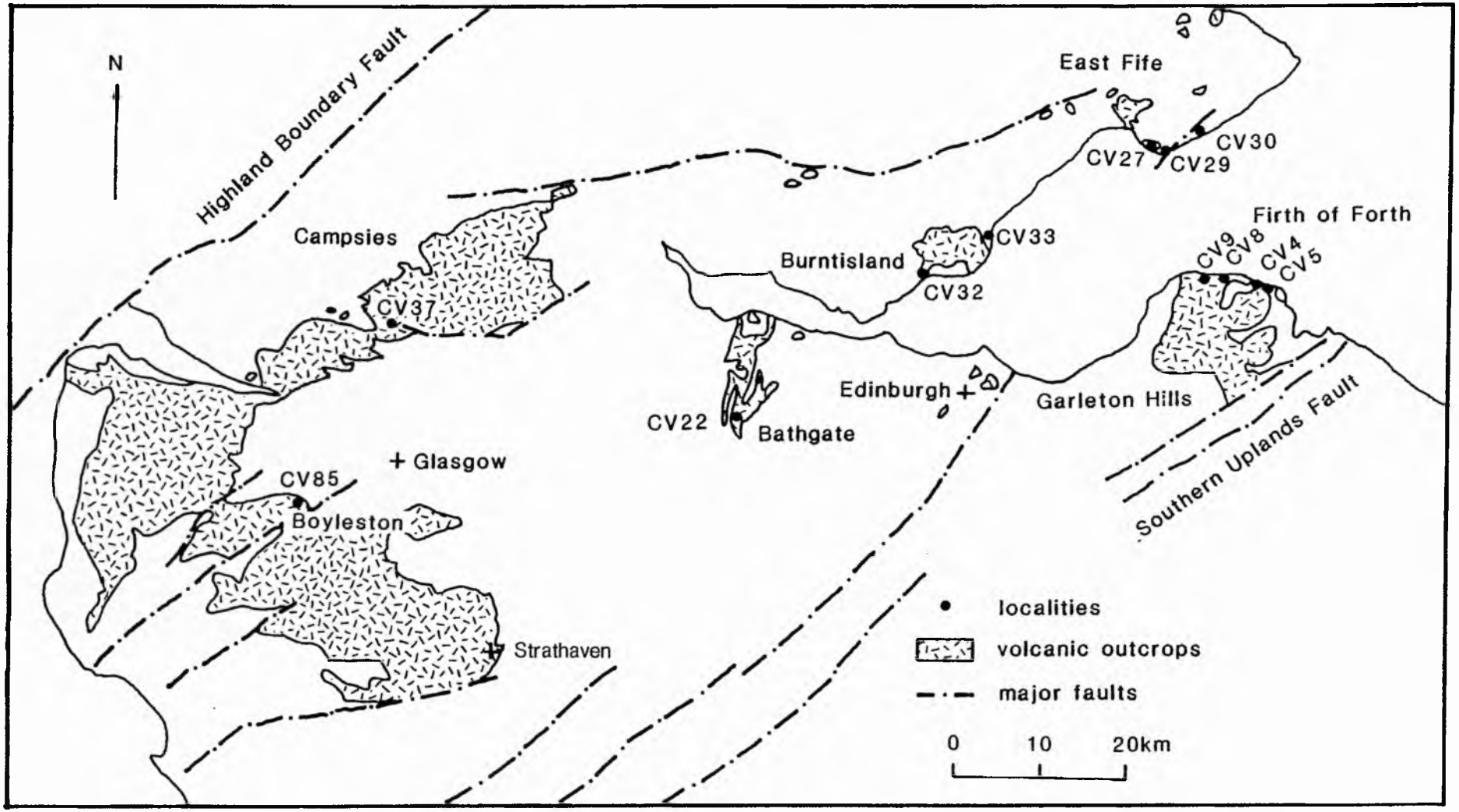


Fig.2.6.2. Locality map for stable isotope data.

Table 2.6.1

| Sample No | Locality | Grid Reference | Host Rock Description | Burial Zone | Underlying strata |
|---|---|---|---|---|---|
| CV4 | Berwick-shire | NT 596 851 | Tuff | Analcime | Calciferous Sandstone |
| CV5 | | NT 603 848 | Tuff | Quartz-calcite | Calciferous Sandstone |
| CV8 | | NT 556 857 | Basalt | Analcime-natrolite | Calciferous Sandstone |
| CV9 | | NT 543 857 | Tuff | Analcime-natrolite | Calciferous Sandstone to Lower Limestone Group |
| CV22 | Bathgate | NS 991 711 | Basalt | Quartz-calcite | Lower Limestone Group |
| CV27 | Fife | NT 461 998 | Tuff + Basalt | Analcime-natrolite | Upper Limestone Group |
| CV29 | | NT 499 993 | Tuff | Analcime-natrolite | Upper and Lower Limestone Group |
| CV30 | | NO 524 014 | Tuff | Quartz-calcite | Upper and Lower Limestone Group |
| CV32 | | NT 212 858 | Tuff | Analcime | Calciferous Sandstone |
| CV33 | | NT 279 883 | Basalt | Analcime | Calciferous Sandstone |
| CV37 | Campsies | NT 616 803 | Basalt | Heulandite | Volcanics |

Table 2.6.1 Localities, rock descriptions and nature of underlying strata of vein calcites.

### 2.6.6 Analytical procedures

**1. Samples and Sample Preparation**

Twelve vein carbonates, sampled from the localities illustrated in figure 2.6.2, were subjected to stable isotope analyses. The relationship of the carbonate to the enclosed rock and to the underlying strata, together with their relative positions in the burial metamorphic scheme, are summmarized in table 2.6.1. For further discussion, refer to chapters 2.1 and 2.2.

Vein carbonate was separated from the whole-rock by hand-picking. Organic matter was removed from crystal faces by floculation in an ultrasonic bath containing either $CaCl_2$ or Na-hexametaphosphate.

$CO_2$ for mass spectrometer analysis was liberated from ground (5-44 $\mu$m) carbonate samples by reaction with 100% phosphoric acid at 25 $^{o}$C (McCrea, 1950). In the case of a discrete dolomitic component being present in the calcite, physical separation of which was impossible, two gas extractions per sample were made. This chemical separation was possible, due to the variable reaction rates of calcite (3 hours) and dolomite (3 days). Scheduling of these collection times was determined by Walters *et al*, (1972), who found that limitation of the particle size to the fractionations quoted above, maximized the fractionation of $CO_2$ collected separately from each phase.

Carbon and oxygen analyses were determined on a McKinney-Nier type Micromass 903 mass spectrometer. Oxygen and carbon measurements were made relative to the standards mentioned in section 2.6.3.

**2. Determination of the dolomite component**

For six of the samples, replacement of $Ca^{2+}$ by $Mg^{2+}$ has

Table 2.6.2

| Sample No | Mol % Mg |
|---|---|
| CV4 | 2.304 |
| CV22 | 3.654 |
| CV29 | 1.634 |
| CV32 | 0.614 |
| CV33 | 0.614 |
| CV37 | 4.334 |

Table 2.6.2 The molecular percentage (mol %) of $Mg^{2+}$ replaced for $Ca^{2+}$ in calcites

occurred. Resolution of the percentage replacement, has been determined by the X-ray technique given in Hutchison (1974). Measurements quoted, are accurate to ± 0.5 mol%. The method is dependant upon the position of the $calcite_{104}$ peak relative to the $silicon_{111}$ peak, in degrees 2θ . These are related through the following equation, such that:-

mol% $MgCO_3$ in calcite = 33.784 (2θ $calcite_{104}$ - 2θ $silicon_{111}$) -32.486

Machine conditions are quoted in Part I of this thesis. The scanning range utilized was 28 to 31 $^{o}CuK\alpha$. The results are collated in table 2.6.2.

The magnesium content of the samples were determined by X-ray diffraction in order to determine the bulk composition of each mechanical mixture subjected to stable isotope analyses. The chemical composition of discrete calcites and dolomites was determined from microprobe analyses, with the aid of the back scatter facility.

**3. Dolomite geothermometry**

The magnesium content of calcite coexisting in the same vein with dolomite forms the basis of the dolomite geothermometer. The mol% $MgCO_3$ (as determined above) is related to the magnesium-calcite solvus geothermometer by the equation:-

$\log MgCO_3 = 1.727 \times 10^{3} T - 0.223$ (after Sheppard and Schwarcz, 1970)

where T = temperature in degrees centigrade.

Table 2.6.3

| Sample No | $CO_2$ Yield $\mu M^2 mg^{-1}$ at 3 hours | $CO_2$ Yield $\mu M^2 mg^{-1}$ at 3 days |
|---|---|---|
| NBS-20 | | |
| NBS-19 | | |
| NBS-20 | 7.75 | |
| | 6.28 | |
| NBS-19 | 7.08 | |
| | 8.33 | |
| CV4 | 4.74 | 0.75 |
| | 4.98 | 0.62 |
| CV5 | 5.63 | |
| CV8 | 7.33 | 0.02 |
| | 7.24 | 0.02 |
| CV9 | 7.75 | 0.02 |
| | 7.69 | |
| CV22 | 4.80 | 0.74 |
| | 3.69 | 0.35 |
| CV27 | 7.3 | |
| CV29 | 7.97 | 0.58 |
| | 7.73 | 0.68 |
| CV30 | 6.76 | |
| CV32 | 7.43 | 0.90 |
| | 7.52 | 0.38 |
| CV33 | 7.11 | 1.01 |
| | 3.09 | gas lost |
| CV37 | 7.07 | 1.40 |
| | 7.03 | 1.42 |

Table 2.6.3 The $d^{13}C$ and $d^{18}O$ values o
eastern Midland Valley.

| Calcite $\delta^{13}C_{PDB}$ | Dolomite $\delta^{13}C_{PDB}$ | Calcite $\delta^{18}O_{PDB}$ | Dolomite $\delta^{18}O_{PDB}$ | Calcite $\delta^{18}O_{SMOW}$ | Dolomite $\delta^{18}O_{SMOW}$ | Dolomite - Calcite $\Delta^{13}C$ | $\Delta^{18}O_{PDB}$ | $\Delta^{18}O_{SMOW}$ |
|---|---|---|---|---|---|---|---|---|
| -1.06 | | -4.14 | | 26.64 | | | | |
| 1.92 | | -2.19 | | 28.65 | | | | |
| -1.50 | | -4.73 | | 26.03 | | | | |
| -1.00 | | -4.50 | | 26.27 | | | | |
| 2.05 | | -2.40 | | 28.43 | | | | |
| 2.04 | | -2.45 | | 28.39 | | | | |
| -6.07 | -7.47 | -12.63 | -13.22 | 17.89 | 17.28 | -1.4 | -0.59 | -0.61 |
| -5.91 | -6.49 | -12.55 | -12.50 | 17.97 | 18.03 | -0.5 | 0.05 | 0.06 |
| -5.91 | | -13.72 | | 16.77 | | | | |
| -1.99 | | -12.06 | | 18.48 | | | | |
| -10.22 | | -12.18 | | 18.35 | | | | |
| -6.16 | not run | -10.57 | | 20.01 | | | | |
| -5.79 | | -10.34 | | 20.25 | | | | |
| -7.59 | -8.16 | -7.91 | -8.48 | 22.75 | 22.16 | -0.77 | -0.57 | -0.59 |
| -7.54 | -8.59 | -7.91 | -8.65 | 22.75 | 21.99 | -1.05 | -0.74 | -0.76 |
| -9.27 | | -10.32 | | 20.27 | | | | |
| -8.48 | not run | -15.18 | not run | 15.26 | not run | | | |
| -8.19 | -8.34 | -15.09 | -14.56 | 15.35 | 15.90 | -0.15 | 0.53 | 0.55 |
| -15.08 | | -9.95 | | 20.66 | | | | |
| -3.34 | -3.31 | -10.93 | -10.59 | 19.64 | 19.99 | 0.03 | 0.34 | 0.35 |
| -3.37 | not run | -11.04 | not run | 19.52 | not run | | | |
| -7.05 | -7.28 | -8.29 | -8.32 | 22.36 | 22.33 | -0.23 | -0.03 | -0.03 |
| -7.21 | | -8.50 | | 22.14 | | | | |
| 0.765 | 0.862 | -13.43 | -13.80 | 17.07 | 16.68 | 0.097 | -0.37 | -0.39 |
| 0.764 | 0.804 | -13.50 | -13.72 | 16.99 | 16.77 | 0.04 | -0.22 | -0.22 |

f calcites and co-existing dolomites from Carboniferous tuffs and basalts of the

$$T\ ^{o}C = \frac{\log MgCO_3 + 0.223}{1.727 \times 10^{3}}$$

The results are collated in table 2.6.2.

This method does not take into account

i) the presence of $FeCO_3$ or $MnCO_3$ in solid solution

or ii) the effect of pressure on solid solution.

Corrections for these have not been determined. Sheppard and Schwarcz (1970) estimate the effects of solid solution to be minimal (± 8°C for 1 mol% $FeCO_3$ or $MnCO_3$). Whereas Goldsmith *et al*, (1955) determined that the solubility of $MgCO_3$ in calcite increases by 1 mol% per 10 kb pressure. The data quoted is correct to 700 °C for pressures up to 2 kb.

### 2.6.7 Isotope results

The results of isotopic analyses are tabulated in table 2.6.3, and are summarized in graphical form on figure 2.6.3, for co-existing calcite and dolomite. The precision achieved for $\delta^{13}C$ was generally better than ± 0.1 °/oo, and for $\delta^{18}O$ SMOW/PDB it was better than ± 0.2 °/oo. $\delta^{13}C$ was not reproducible for three samples. Variation has been attributed to original compositional differences of individual samples within reaction vessels. Thus effecting $\Delta$ $CO_2$ - $CaCO_3$. Analyses of $\delta^{18}O_{SMOW}$ range from 15.26 to 22.75 °/oo; and $\delta^{13}C$

Table 2.6.4 a

| Sample No | Yield $\mu M^2\ mg^{-1}$ | $\delta^{13}C_{PDB}$ | $\delta^{18}O_{PDB}$ | $\delta^{18}O_{SMOW}$ |
|---|---|---|---|---|
| Anal 1c | 6.80 | -9.9 | -15.2 | 14.7 |
| Anal 1d | 7.15 | -9.9 | -14.8 | 15.1 |
| Anal 2c | 7.31 | -9.9 | -15.0 | 14.9 |
| Anal 2d | 7.34 | -10.0 | -15.3 | 14.6 |
| Anal 3b | 6.67 | -10.8 | -13.1 | 16.9 |
| DB 1a | 7.00 | -10.9 | -14.2 | 15.7 |
| DB 1b | 6.54 | -10.7 | -12.1 | 17.9 |
| DB 2b | 6.98 | -9.7 | -11.1 | 18.9 |
| DB 2c | 6.70 | -11.6 | -10.8 | 19.2 |
| DB 5b | 7.46 | -12.7 | -9.4 | 20.7 |
| DB 6b | 8.13 | -12.6 | -8.7 | 21.4 |

Table 2.6.4 $\delta^{13}C$ + $\delta^{18}O$ values for calcite intergrown with analcime from Boyleston Quarry, Barrhead, after D. Banks, pers. comm. 1986. Location equivalent to CV85 of L. Evans.

from 0.862 to -15.08 $^{o}/_{oo}$.

Unpublished $\delta^{18}O$, $\delta^{13}C$ and $\delta D$ values (table 2.6.4) of calcite intergrown with analcime from Boyleston Quarry, Barrhead, are quoted by permission of D Banks. The location is equivalent to CV85 (fig 2.6.1) of L J Evans. Relevant data is plotted in conjunction with analyses from the eastern Midland Valley, on figures 2.6.2 and 2.6.3.

### 2.6.8 Discussion

#### 1. The calcite-dolomite problem

Six of the analysed crystals contained 0.614 to 4.334 mol% $MgCO_3$ (table 2.6.2) in the calcite structure. The magnesium contents are compatible with those of diagenetic calcites (Muir *et al*, 1956) from limestones, which evolved without a volcanic influence. Fractionation ($\Delta$) of $^{13}C$ and $^{18}O$ SMOW between dolomite-calcite varied from 0.09 to -1.05 $^{o}/_{oo}$ and from 0.55 to -0.76 $^{o}/_{oo}$, respectively (table 2.6.3). Clayton and Epstein (1958) and Northrop and Clayton (1966) determined that if dolomite and calcite were precipitated in the same environment, then an isotopic fractionation factor of dol-cc = 6 to 10 $^{o}/_{oo}$ would be observed. Since the $\Delta^{13}C$ and $\Delta^{18}O$ values of all studied dolomite-calcite pairs in the Midland Valley do not exceed $\pm 1$ $^{o}/_{oo}$, dolomite is thought to be an alteration product of crystalline $CaCO_3$.

Microprobe analyses have been obtained for calcite and dolomite in samples CV29, CV33 and CV5. Compositions varied within crystals, as well as from grain to grain, confirming that calcite and dolomite did not equilibrate. Furthermore, solvus temperatures obtained for all dolomites co-existing with calcite, confirm the lack of

equilibration. Sheppard and Schwarcz (1970) and Lattanzi *et al*, (1980) cite negative Δ values as evidence for non-equilibrium fractionation, confirming that the dolomite values were spurious. The $CO_2$ liberated may have been due to the high acid to carbonate ratio in the second extraction, or it may have originated from slow-reacting calcite.

The following factors may have contributed to false values during the extraction proceedure:-

i) Prolonged grinding of calcite-dolomite mixtures. This would have increased the surface area of crystals due to straining, rather than reduced the particle size. Inadvertently, dolomite reaction rates may have been increased at the start of the experiment leading to enhanced $CO_2$ cross-contamination between the largest slow-reacting calcite and the smallest fast-reacting dolomite.

ii) Analyses of too small (<17% of the total gas extracted) a quantity of gas trapped at the end of the experiment (Walters *et al*, 1972). For these reasons, samples yielding <0.1 $\mu M^2$ $mg^{-1}$ $CO_2$ (table 2.6.3) during the second extraction were not analyzed.

**2.1 Carbon and oxygen isotope compositions**

$\delta^{13}C$ and $\delta^{18}O$ values of calcite from the greenstones of the eastern Midland Valley burial-metamorphic sequence, vary between 0 to -15 °/oo (table 2.6.3; 2.6.4) and from 15 to 23 °/oo respectively. $\delta^{13}C$ values contrast significantly with the narrow range (-7 to -4 °/oo) observed in most greenstones (Muelhenbachs and Clayton, 1972; Stakes and O'Neil, 1982); where $\delta^{13}O$ is the result of exchange between the basalts and a homogeneous seawater reservoir. Whilst, $\delta^{18}O$ values correspond to enrichments of 9 to 17 °/oo, when compared

with unaltered submarine basalts (5.5 to 6.5 °/oo, Taylor, 1968; Muehlenbachs and Clayton, 1972). $\delta^{18}O$ values suggest that the calcites were not precipitated directly from magmatic fluids.

The range of $\delta^{13}C$ and $\delta^{18}O$ values encountered in the Midland Valley, is plotted on fig 2.6.1, together with comparative ranges for different rock types and fluids. Measured $\delta^{13}C$ values, fall in the range (fig 2.6.1a) of marine carbonate (including dolomite), organic matter, seawater, meteoric water and magmatic water. $\delta^{18}O$ values, fall in the range (fig 2.6.1b) of metamorphic and sedimentary rocks. Within the Midland Valley, $\delta^{13}C$ values provide the main criteria for distinguishing between fluid sources (see 2.2 below), whilst $\delta^{18}O$ values reflect water/rock ratios (see 2.3 below) and metamorphic conditions (see section 2.6.8).

## 2.2 Sources of hydrothermal fluids

The sources of hydrothermal fluid in the Midland Valley cannot be defined with certainty. Since,

i) $\delta^{18}O$ values reflect the metamorphic event (see section 2.6.8)

ii) $\delta^{18}O$ values for equatorial Carboniferous seawater and meteoric water were similar, and equivalent to 0 °/oo.

iii) no $\delta D$ values are available

iv) the observed $\delta^{13}C$ values characterize pure (?) fluids, but their isotope signature may also have resulted from the mixing of diverse fluids.

Possible sources are discussed below.

In view of the palaeo-environmental conditions (chapter 2.1) experienced by the eastern Midland Valley throughout the Carboniferous, a strong oceanic component to the hydrothermal fluid

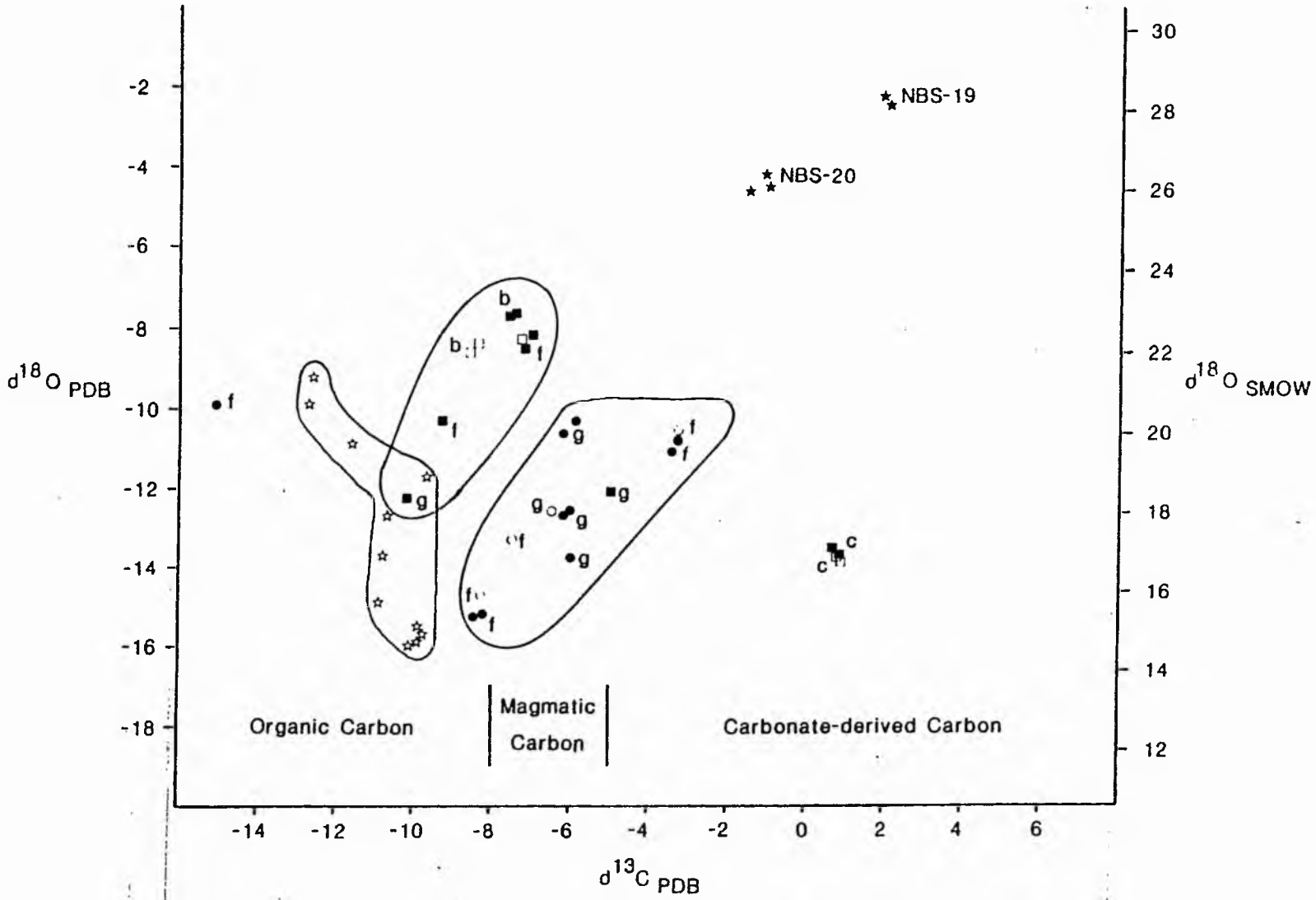


Fig.2.6.3. $\delta^{18}O$ and $\delta^{13}C$ values for co-existing calcite and dolomite from Carboniferous tuffs and basalts of the Midland Valley. (Boyleston data ☆ after D.Banks, pers. comm., 1986). Square symbols - calcite from basalt: circular symbols - calcite from tuffs : closed symbols - calcite:empty symbols - dolomite b Bathgate c Campsies f Fife g Garleton

is to be expected. $\delta^{13}C$ values (fig 2.6.3), for all except CV37, are too depleted to have resulted from the interaction of seawater alone (unless mixing with a depleted, eg organic, substance occurred). The $\delta^{13}C$ values (table 2.6.3) of most samples fall within the expected range (-5 to -11 $^{o}/oo$, Sackett and Moore, 1966) of meteoric fluids and magmatic water, suggesting that meteoric and magmatic water may also have been a major source of hydrothermal fluid. However, if one large homogeneous resevoir was available eg meteoric and magmatic water or seawater, and it exchanged with the basalt throughout the Midland Valley, then the carbon isotope compositions observed from the carbonates should be fairly constant. This condition was noted by Muehlenbachs and Clayton (1972). The scatter (fig 2.6.3) suggests that isolated sources of carbon existed in the Midland Valley, showing variable degrees of exchange with meteoric or oceanic water. The existence of heterogeneous reservoirs is further highlighted by the fact that geographically distinct areas (fig 2.6.3) show a fairly restricted range of $\delta^{13}C$ values. The scatter in the Fife data (fig 2.6.3) is attributed to the fact that individual vents were isolated from one another. This therefore suggests a local control upon the isotopic composition of the fluids in these regions. Possible regional fluid variations are discussed below.

By comparison with figure 2.6.1, $\delta^{13}C$ values for the Campsies (CV37 - table 2.6.3; fig 2.6.3) fall within the range of marine carbonates and oceanic water. The suitability of the Calciferous Sandstone substratum as a source for the fluids is questionable. Particularly since the calcite horizon is separated from the sediments by some 200 m of volcanics (chapter 2.1). Furthermore, it is unlikely that cool groundwater could have penetrated upwards for

this distance, whilst the integrity of the $\delta^{13}C$ ratios in the fluids remained intact. A more plausible explanation is that the fluids were derived from limestones and/or seawater which overlay the volcanics at the close of the Dinantian (chapter 2.1). These fluids would have convectively descended in the vicinity of the cooling Waterhead/Meikle Binn vents (fig 2.1.1).

Calcite from Bathgate (CV22) and from the Garleton Hills (CV4, 5,8,9), plot well within the magmatic carbon field in figure 2.6.3. The two areas are isotopically distinct, Bathgate displaying $\delta^{13}C$ values of -7 to -8 °/oo and the Garleton Hill displaying $\delta^{13}C$ values of -3 to -5 °/oo.

Data from calcite veins at Boyleston (CV85 - fig 2.6.2) lie within the organic carbon field (fig 2.6.3). $\delta^{13}C$ values range from -9 to -12 °/oo (table 2.6.4).

Depleted $^{13}C$ values observed at Boyleston, could have been derived by either:-

i) exchange with $CO_2$ formed from oxidation (burning of organic matter with atmospheric oxygen)
ii) interaction with meteoric waters in adjacent areas
iii) interaction with less depleted oceanic water.

Fife calcites display $\delta^{13}C$ values of -3 to -15 °/oo (table 2.6.3; fig 2.6.3). Mineral assemblages of the altered volcanics (chapter 2.3) are similar in each area sampled. Consequently, the isotopic ($\delta^{13}C$) scatter, is unlikely to be the result of metamorphic variation. The isotope values are therefore attributed to variation in the $\delta^{13}C$ of total dissolved carbon in the fluids of each area.

Depletions in $\delta^{13}C$ of -3 to -8 $^{o}/oo$ may have resulted either from the mixing of magmatic fluids with meteoric or oceanic fluids, or from the exchange of fluids between neighbouring marine sediments and volcanics. Depletions of -8 to -15 ($\delta^{13}C$) are believed to have resulted from the mixing of oxidized organic matter with a mixed magmatic and oceanic/meteoric fluid. CV30 (fig 2.6.3) is particularly depleted in $\delta^{13}C$ (-15 $^{o}/oo$), this may reflect the fact that the surrounding strata is rich in bitumens (Muir *et al*, 1956).

**2.3 Water : Rock ratios**

Figure 2.6.3, shows two $\delta^{18}O$ vs $\delta^{13}C$ fields; one for basalts, and the other for tuffs of the eastern Midland Valley. In part (2.2), it was shown that $\delta^{13}C$ values are similar for basalts and tuffs derived from the same geographical area. The trends shown on figure 2.6.3, are therefore attributed to $\delta^{18}O$ fractionation only. Figure 2.6.3, shows that the carbonate in the tuffs is generally depleted in $\delta^{18}O$ relative to the carbonate in the basalt. The maximum observed $\delta^{18}O$ value (20 $^{o}/oo$) in tuff carbonate, corresponds to a depletion of about -3 $^{o}/oo$ relative to the maximum $\delta^{18}O$ value (22.75 $^{o}/oo$) in basalt carbonate. The negative $\delta^{18}O$ shifts experienced by the tuff carbonate may be interpreted as the product of either :-

i) elevated temperatures in the tuffs during calcite formation
ii) variable water/rock ratios during isotopic exchange
iii) interaction with isotopically lighter fluids

Elevated temperatures are unlikely to have persisted in the

tuffs at the expense of the basalts during calcite formation. Petrographic evidence (chapter 2.3) indicates that similar igneous and metamorphic mineralogies were developed in each rock type, within any particular metamorphic zone. Higher temperature assemblages are only present when overpressurizing occurs (chapter 2.2); this feature does not discriminate between rock regimes. Petrographic evidence (chapter 2.3) however shows that alteration was concentrated in originally porous rocks such as the tuffs, the degree of metamorphic reconstitution decreasing rapidly in phaneritic basalts. Consequently, fluid exchange must have been enhanced in the tuffs relative to the basalt. The oxygen isotope variation seen on figure 2.6.3, must therefore have been a function of variable water/rock ratios. In areas, such as the basalts, where the water/rock ratio was likely to have been low, the reservoir of rock oxygen controls the $\delta^{18}O$ of the fluid (Spooner *et al*, 1974). The oxygen isotope ratio of the rock would have been unaffected because insufficient water would have been available to exchange with the system. In areas, such as the tuffs, where the water/rock ratio was likely to have been high, the $\delta^{18}O$ of the rock would have been modified, and the $\delta^{18}O$ of the fluid would have been invarient.

By inference, tuff carbonates in the Midland Valley characterize high water/rock ratios, whilst basalt carbonates characterize low water/rock ratios. Isotopic variation between the two, indicate that $\delta^{18}O$ $H_2O$ $^{o}/_{oo}$ enrichments are encountered with lower water/rock ratios. Similar observations were made in the prehnite-pumpellyite facies sequence of the Lake District by Thomas (1986). Here samples with low water/rock ratios (0.001) were enriched by 4 $^{o}/_{oo}$ relative to samples with high water/rock ratios

(>1). In this chapter, all volumetric water/rock ratios are quoted as bulk ratios.

The water/rock ratio in any part of the hydrothermal system, would have been related to the rock porosity. Davis and De Weist (1966) determined that for most extrusive basalt sequence, porosity = 1%. The water/rock ratio for material of 1% porosity, equals 0.01 (Spooner *et al*, 1977a, b). However, high water/rock ratios ie >1, were encountered in the Troodos ophiolite complex by Heaton and Sheppard (1977) during zeolite facies alteration. The volume of water available during metamorphism was governed by the pressure and temperature conditions, therefore by inference with Troodos, the water/rock ratio during zeolitization in the eastern Midland Valley is believed to be equivalent ie 1. However ratios less than one may have been encountered, since direct comparison of the effect of fluid flow and circulation mechanisms on water/rock ratios, in an ophiolitic sequence and a burial metamorphic sequence, may not be possible.

The water/rock ratios indicate that flow through the burial metamorphic hydrothermal system of the eastern Midland Valley occurred. Considering that the water/rock ratio for:-

i) a pre-metamorphic basalt, with 1% porosity, = 0.001

ii) a zeolitized basalt = 1

it is apparent that the total amount of water/rock interaction was likely to have been greater than the water/rock ratio in interconnecting pore spaces, therefore flow is assumed.

Interaction with isotopically light fluids may also be invoked to explain the fractionation trends in figure 2.6.3. During zeolitization, pathways for the entry of fluids may have been

intermittent, and the fluid supply itself may have been sporadic. Under such conditions incremental equilibrium exchange conditions may have persisted. In the early stages of flow, isotopic exchange may have produced large $\delta^{18}O$ depletions in the fluid. These isotopically light fluids could interact with the rock below, actually depleting the $\delta^{18}O$ further. The depletion trend would not be reversed until the rocks higher in the sequence had become sufficiently enriched to permit isotopically heavier fluid to penetrate deeper.

### 2.6.9 Variation in stable isotope composition with metamorphism

The oxygen isotope ratios of the carbonate in the Midland Valley would have been controlled by:-

i) the $\delta^{18}O$ values of the fluid involved

ii) the relative volume of the phases present ie the water; rock ratio (see section 2.6.8).

iii) the temperature of fluid interaction

Fluid circulation involved seawater and meteoric water (see section 2.6.8), with a Carboniferous $\delta^{18}O$ isotopic composition near to 0 $^{o}/oo$ (see section 2.6.4). Simple circulation of these fluids through the cooled volcanic rocks cannot account for the observed $\delta^{18}O$ values. This process would have produced depleted $\delta^{18}O$ values in the carbonates relative to the $\delta^{18}O$ (c6 $^{o}/oo$; Hoefs, 1973) of the igneous rocks. The temperature of fluid interaction therefore appears to be the most important variable controlling the observed $\delta^{18}O$ values of carbonates in the Midland Valley.

Fractionations between a mineral and water (where $\delta^{18}O$ = 0 $^{o}/oo$), decrease (Spooner *et al*, 1974) with increasing temperature. For example table 2.6.4 shows that quartz-water (Wenner and Taylor,

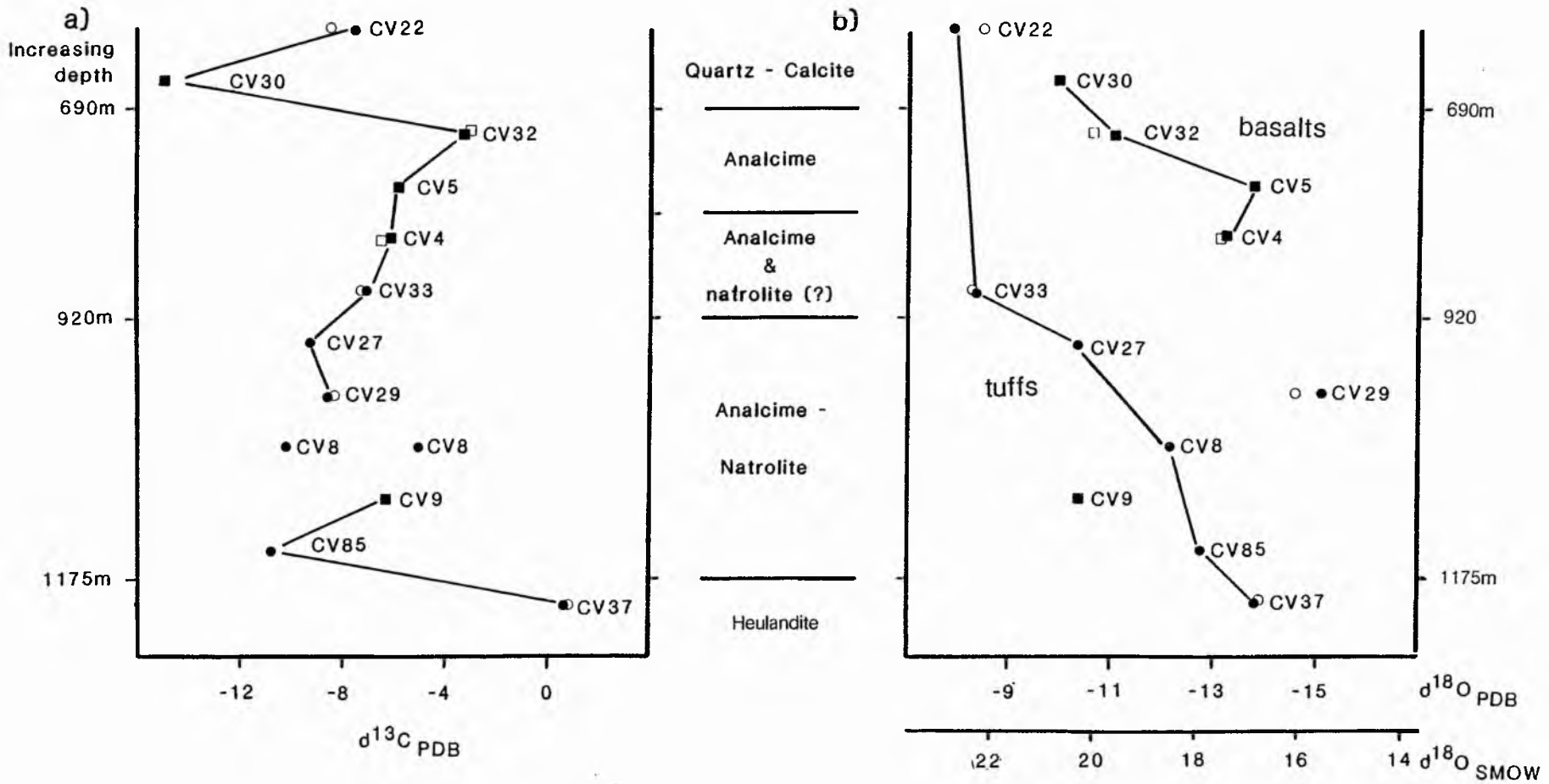


Fig.2.6.4. Burial profile of carbon and oxygen isotope compositions in the Midland Valley.(relative burial depths derived from chapter 2.2.) Square symbols - calcite from basalt: circles - calcite from tuffs. Closed symbols - calcite : open symbols - dolomite.

1971; Clayton *et al*, 1972), chlorite-water (Spooner *et al*, 1974) and calcite-water (Friedman and O'Neil, 1977) fractionations are depleted in $\delta^{18}O$ at increased temperatures.

Table 2.6.4 b

| | 100 °C | 200 °C | 400 °C |
|---|---|---|---|
| Quartz | +23 °/oo | +10 °/oo | +4 °/oo |
| Chlorite | +8 °/oo | +2 °/oo | -2 °/oo |
| Calcite | +17 °/oo | +8 °/oo | +4 °/oo |

Table 2.6.4 Mineral-water fractionations at 100 °C, 200 °C and 400 °C.

$\delta^{18}O$ in the Midland Valley carbonates are seen (fig 2.6.4) to decrease from 22 °/oo to 15 °/oo. The depletion is consistent with an increase in metamorphic grade, as witnessed by the change in the amygdale mineralogy from the quartz-calcite to the analcime-natrolite zone. The association suggests that the observed $\delta^{18}O$ values reflect increased temperatures of fluid interaction with increasing depth. Furthermore, the reduction consumption of $\delta^{18}O$ with burial depth, suggests that metamorphism was related to the entry of oxygenated fluids from above.

$\delta^{18}O$ values in the eastern Midland Valley are compatible with $\delta^{18}O$ values for zeolitized terrains elsewhere in the world (fig 2.6.6). The following $\delta^{18}O$ values are recorded from volcanics and volcanogenic sediments:-

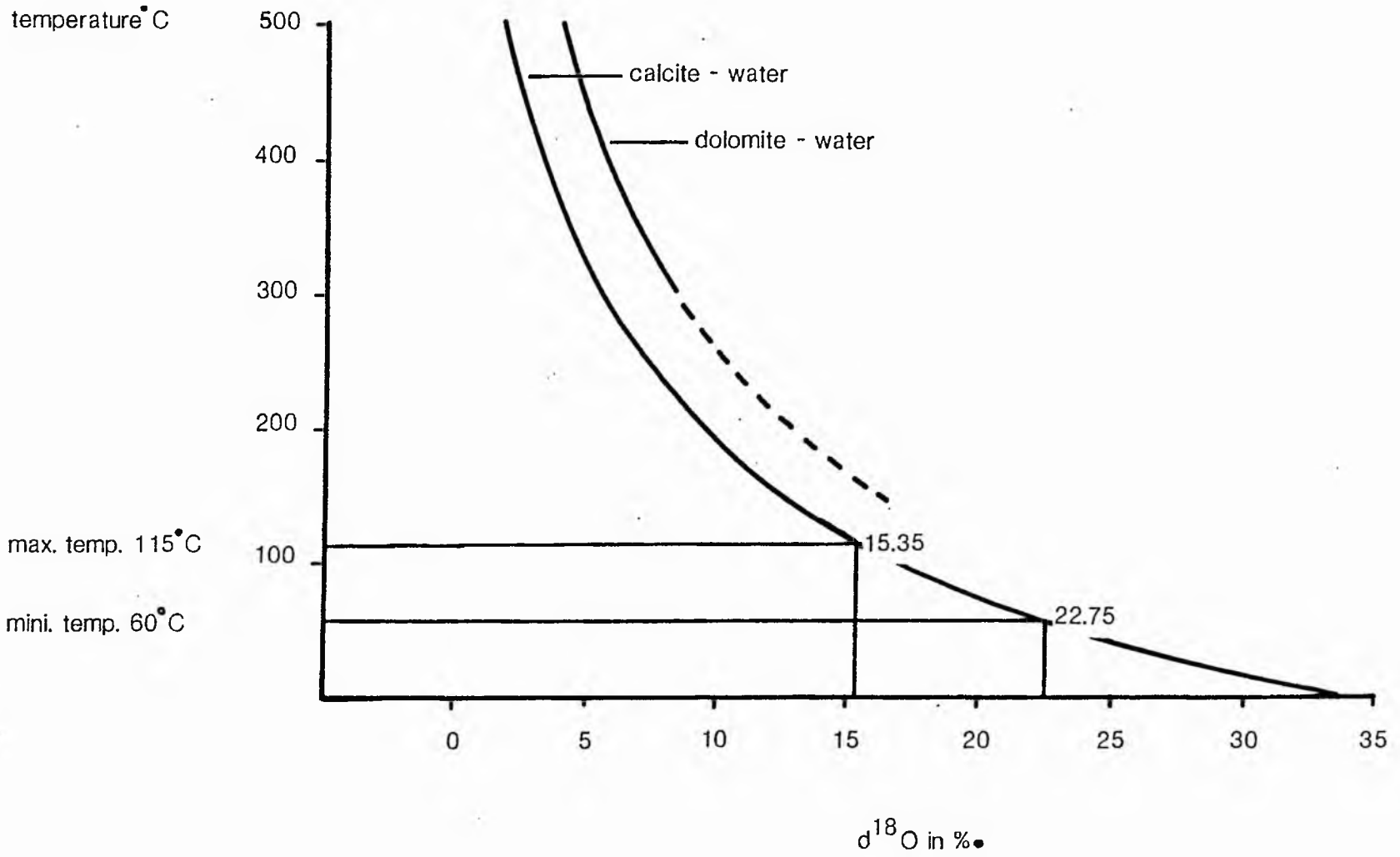


Fig.2.6.5. Temperature dependant calcite - water and dolomite - water fractionation curves (after Friedman and O'Neil, 1977 ).

$\delta^{18}O$ = 15 to 22 °/oo (Suchecki and Land 1983); $\delta^{18}O$ = 11 to 18 °/oo (Matthews and Kolodny, 1978). Not all $\delta^{18}O$ values for zeolitized terrains are comparable, eg:- $\delta^{18}O$ = 6 to 13 °/oo (Spooner *et al*, 1977a, b); $\delta^{18}O$ = -2 to 16 °/oo (Hattori and Sakai, 1980); $\delta^{18}O$ = 0 to -12 °/oo (Sveinbjornsdottir, 1983). This is because oxygen fractionation is dependant upon altitude and latitude of water capture, as well as upon temperature and original fluid isotopic compositions (see section 2.6.5).

In the absence of equilibrium mineral pairs, the calcite-water stable isotope fractionation curves of Friedman and O'Neil (1977) have been used to establish the temperature dependence of the $\delta^{18}O$ values. Fractionation curves (fig 2.6.5) for the partitioning of $CO_2$-$H_2O$ between the parent carbonate and SMOW at 25 °C were determined (*op cit*) from the equation on page 231. The intersection of measured $\delta^{18}O$ values (along the x-axis) with the calcite-water or dolomite-water fractionation curves yield temperatures of crystallization along the y-axis. Minimum and maximum $\delta^{18}O$ values of 15.35 °/oo and 22.75 °/oo are derived from table 2.6.3 and from figure 2.6.3. According to the graphs of Friedman and O'Neil (1977) these yield crystallization temperatures of 120 °C and 60°C respectively. These values are within the range of homogenization temperatures (chapter 2.5) shown by natrolite (120 °C), analcime (120 °C) and calcite (60 °C) within their respective burial zones.

The origin of the metamorphic fluid may be speculated on from oxygen isotope fractionation temperatures, in conjunction with carbon isotope data. Carbon isotope data suggests the involvement of oceanic water in the hydrothermal fluid. The presence of dissolved salts would have depressed the crystallization temperature, hence the

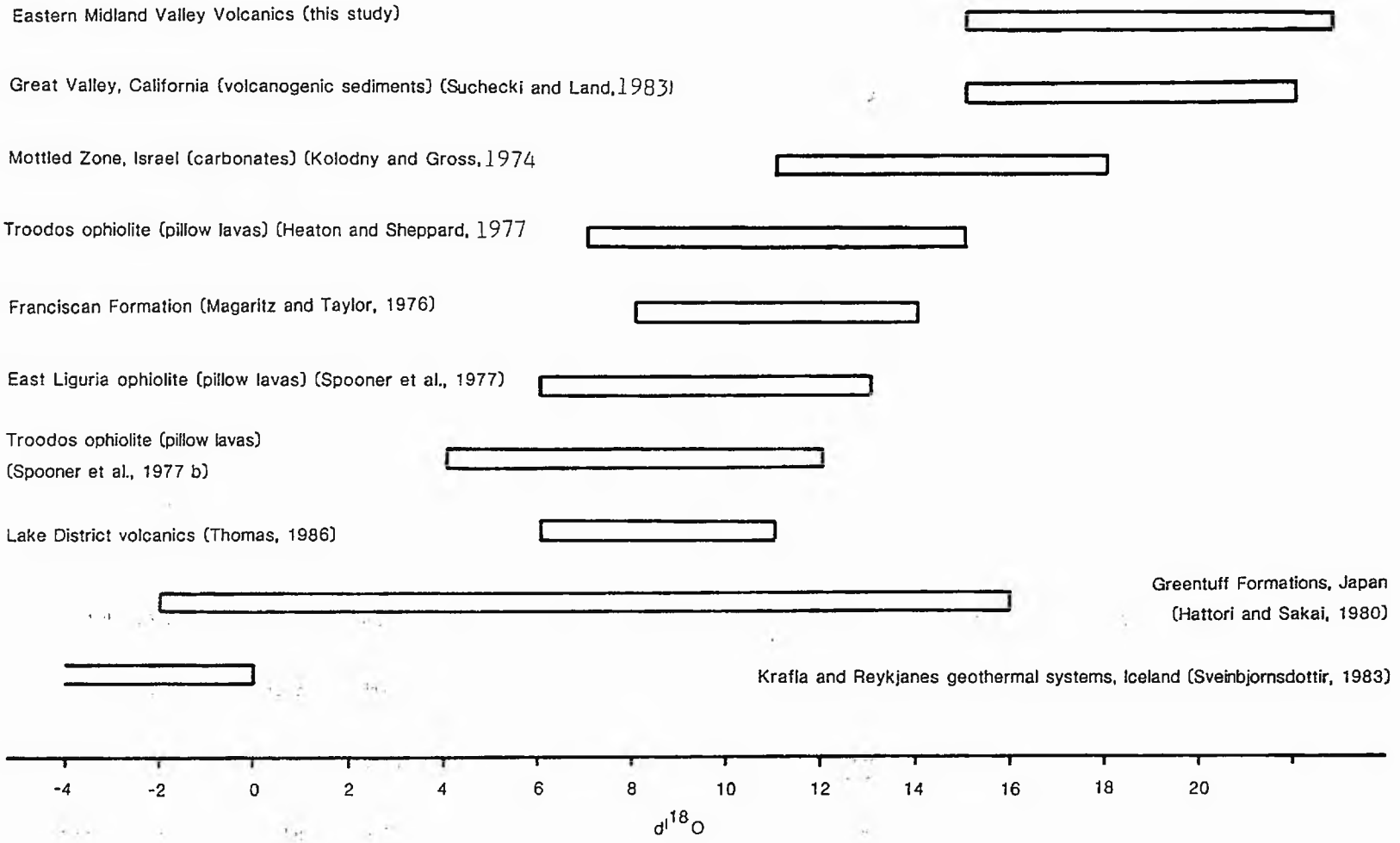


Fig. 2.6.6. Comparison of eastern Midland Valley carbonate $d^{18}O$ values with mineral and whole rock oxygen isotope values from other zeolitized and hydro-thermally altered areas. (Lake District values are from prehnite - pumpellyite facies volcanics.)

correction factors determined by Truesdell (1974) have to be applied to the geothermometric data. The correction factor is dependent upon the composition and concentration of the saline phase. Unfortunately this is not known for the calcites analyzed. Although, fluid inclusion studies (chapter 2.5) have determined the presence of dilute NaCl and $CaCl_2$ at similar burial levels in the Clyde Plateau Lavas. These salt concentrations indicate that the calcite-water $\delta^{18}O$ fractionations determined (table 2.6.3) are too high by -0.1 to 1.6 $^{o}/oo$. This would lead to crystallization in the range 60 - 70 $^{o}C$ and 120 - 140 $^{o}C$ for those $\delta^{18}O$ values recorded at 22 $^{o}/oo$ and 15 $^{o}/oo$ respectively, in table 2.6.3.

The temperatures of the hydrothermal fluids are too great to be representative of either oceanic or meteoric water and are too low to have been derived purely from magmatic fluids. However, Bischoff and Dickinson (1975) showed that seawater and meteoric water adjacent to hot basalt may rapidly (within minutes) acquire temperatures of 100 $^{o}C$, without isotopically exchanging with the rocks. Such fluids may have provided the impetus for the observed $\delta^{18}O$ values, provided that the water : rock ratio was small (Spooner *et al*, 1977a, b) ie $<<1$. In section 2.6.8, the water : rock ratio was thought to be one, consequently the volume of water available would have been too great not to have exchanged with the rock. It is more likely that the heat was obtained from the thermal gradient of the rock during burial. $\delta^{18}O$ values are attributed to the low temperature origin of the metamorphic fluids. $\delta^{13}C$ and $\delta^{18}O$ values indicate that these fluids would have originated from the mixing of magmatic fluids exchanging with marine carbonate and seawater.

### 2.6.9 Conclusions

The isotope values express the intensity of the hydrothermal processes and the magnitude of heat and mass transfer during zeolite facies burial metamorphism.

1. The $\delta^{13}C$ values define pre-metamorphic sources of carbon in the Midland Valley as oceanic and magmatic fluids. $\delta^{13}C$ values, and $\delta^{18}O$, show re-equilbration consistent with zeolite facies metamorphism. Temperatures of metamorphism and the isotopic composition of the metamorphic fluid are expressed by $\delta^{18}O$ values.

2. Geographically distinct (and thus heterogeneous) sources of carbon and oxygen, characterize pre-metamorphic fluids. Metamorphic fluids are re-equilibrated with respect to oxygen isotopes, suggesting one homogeneous reservoir during zeolitization.

3. $MgCO_3$ geothermometry indicates that co-existing calcite-dolomite pairs are not in equilibrium.

4. Isotope values indicate that initial fluid circulation occurred in geographically distinct environments, and was responsible for the production of calcite ± dolomite. $\delta^{18}O$ values provide further evidence that the carbonates re-equilibriated during zeolitization, which was a function of burial metamorphism.

## Chapter 2.7 Discussion

### 2.7.1 Aims

1. To summarize geological knowledge of metamorphism.
2. To produce a metamorphic model.
3. To establish scope for further research.

### 2.7.2 Summary of conclusions

1. Three examples of low grade metamorphism have been recognized in the Carboniferous Volcanics of the Midland Valley of Scotland. These comprise:-

a) greenstone alteration; associated with the circulation of seawater and meteoric water through hot rock shortly after extrusion and with the distillation of heated organic fluids from adjacent sediments.

b) regional low grade burial metamorphism; where amygdales and veins were infilled with zeolites and associated minerals, which formed an orderly vertical zonation with increased burial depth. Locally the lateness of the zeolitization with respect to the main volcanic episode has been established. Regionally the zeolite zones shallow towards the synclinal Central, Ayrshire and Lothian coal basins.

c) palaeo-geothermal plume alteration; narrowly constrained vertical zones of intense Ca-metasomatism which have mineralogical affinities with modern geothermal systems.

2 Metamorphism was thermal and occurred in the analcime and laumontite zones of the zeolite facies. Evidence from mineral stabilities (chapter 2.4), fluid inclusion studies (chapter 2.5) and from stable isotope studies (chapter 2.6) are compatible with metamorphism at a) 140-220 $^{o}C$ at 0.14-0.3 kb in the zeolite zones b) $\leqslant$ 420 $^{o}C$ at 0.18-0.24 kb in the palaeo-geothermal plumes.

3 Metamorphism was characterized by Na- and Ca-metasomatism, related to the breakdown of igneous felspars in the presence of an external fluid (seawater and meteoric water). Mineral stabilities (chapter 2.4) and fluid inclusion data (chapter 2.5) indicate that alteration occurred under conditions of low $XCO_2$. In addition to gradients in aNa and aCa, mineral chemistries also reflect gradients in $aSiO_2$ and aO; the latter two decreasing with increased grade. If these components were derived from seawater then metamorphism may have been related to the entry of oxygenated water from above. This hypothesis is consistent with decreased fractionation of $^{18}O$ (chaper 2.6) with burial depth. The evidence suggests that the dissassociation of $H_2O$ (ie exothermic reactions) from zeolites (which may also have caused an increase in $fO_2$) may have been controlled by the relative rates of fluid access. The generation of $CH_4$ with increased burial depth (chapter 2.5) may have been created during burial metamorphic reactions, associated with the transformation of anorthite, albite and calcite to Ca-zeolites and analcime.

4 Fluid inclusion data indicates that within the fluid system either:-

a) initial hot fluids (saline) mixed with cooler groundwater; or,

b) limited boiling of fluids occurred, associated with a pressure release during the change from lithostatic to hydrostatic pressure during fracturing. The main sources of fluid (chapter 2.6) during metamorphism were seawater and meteoric water plus a small component of sedimentary organic fluid.

5 Water: rock ratios (chapter 2.6) reflect the intensity of the hydrothermal processes in rocks of higher porosity, such that higher temperatures would have been reached at shallower burial depths in tuffs than in basalts, (due to contrasting exchange rates). This may account for why the base of the zeolite zones is encountered higher North of the Clyde where widespread products of phreato-magmatic activity occur, than south of the Clyde.

### 2.7.4 Metamorphic Model

1 Geochronology

The quiet effusion of Dinantian lavas in the western Midland Valley was followed by the deposition of marine Carboniferous sediments and associated explosive volcanicity (chapter 2.1). At Cochno and Bowling, areas of geothermal activity (palaeo-geothermal plumes-chapter 2.2), comparable to those seen at the present day in Iceland and New Zealand, developed in the hot (unmetamorphosed) volcanics. Palaeo-geothermal plumes developed in association with feeder dykes to the volcanics, with minor vents and with faults. In

the eastern Midland Valley the interdigitating nature of the volanics and their extrusion onto wet sediments resulted in the circulation of seawater and meteoric water through the hot rocks. The low temperature greenstones observed (chapter 2.2) are the product of this deuteric alteration. By comparison with present-day extrusives in Iceland and Hawaii (chapter 2.2) it is likely that the bulk of the fresh Carboniferous lavas were characterized by empty vesicles. These fresh basalts would have been uncompacted and very absorbent to precipitation. This would have reduced the heat discharge from the lavas and consequently have inhibited the formation of zeolites immediately following extrusion.

The Carboniferous Volcanics at the present-day are metamorphosed (chapter 2.2). Mineralogical zonations vary from fresh to analcime to laumontite in whole-rock matrix, and from quartz-calcite to analcime to natrolite to stilbite to heulandite to laumontite in amygdales and veins. There are two possible causes for the zeolite zonation:-

i) variation in basalt chemistry with time : early volcanics were basic and became more alkaline with time (chapter 2.1). This is reflected by the change from laumontite to analcime with decreasing burial depth (chapter 2.2; 2.3). However, this mineralogical change also occurs in the Antrim basalts (Walker, 1960a) without a significant change in the basalt chemistry. In the Clyde Plateau Lavas however one would expect to find Ca-zeolites associated with late fractionation of feldspars; analcime and natrolite (chapter 2.2) occur. Furthermore, the same zeolite species are developed locally in a wide range of chemically differentiated lavas. The effect of basalt chemistry upon zeolitization therefore seems to be limited.

ii) regional burial metamorphism: this could only have proceeded once:-

a) The volcanics were saturated with water; the hydrothermal mineralogy developed (chapter 2.2; 2.4) necessitates that an aqueous fluid was involved in the metamorphism.

b) the bulk of the lavas and sediments had accummulated (chapter 2.2).

The main period of volcanicity ended at about 315 Ma (chapter 2.1). At 290 Ma (chapter 2.1) the main faulting episode (associated with dyke intrusion into Carboniferous volcanics and sediments) displaced many zeolite zones, suggesting that zeolitization was almost (?) complete at this time. Zeolitization therefore appears to have occured over a 25-30 Ma episode. In Iceland the maximum period of zeolitization has been determined to be 16 Ma. In Troodos (Cann *et al*, 1985) metamorphism occured over a 0.1 Ma, where fluid temperatures of 200 $^{o}$C have been recorded (however, this is a highly fractured rock, where fluids escaped along faults as opposed to flow through micro-pores and macro-pores - as defined in chapter 2.2).

The thickness of the zeolite zones differs between the eastern Midland Valley and between the north and south Clyde Plateau Lavas. A thick pile in the eastern Midland Valley may have acted as an insulator to heat loss resulting in the development of thicker zones. Where the burial pile was thinner, heat loss may have been rapid; rapid changes in the temperature gradients may have resulted in the development of several contrasting zones. Furthermore higher water: rock ratios in tuffs at the base of the northern Clyde Plateau lavas (chapter 2.6) as opposed to basalts at the base of the southern Clyde Plateau Lavas produced higher temperatures at shallower burial depths

in the former. The height of the water table in the rock pile would also have placed constraints upon the inception of zeolitization. Consequently, low-lying volcanic complexes would have been saturated in water to a higher level than in high lying volcanic complexes. Zeolitization may therefore have been expected to have begun relatively earlier in the life-span of the former system.

The base of the northern Clyde Plateau Lavas is marked by the products of widespread phreatomagmatic activity. By comparison with environments in the eastern Midland Valley, greenstones might be expected to occur in the Clyde Plateau. Greenstones are not developed, suggesting that alteration caused by the circulation of geothermal water completely overshadowed any former deuteric or low temperature greenstone alteration.

Following regional zeolitization, new geothermal systems developed associated with faulting and dyke intrusion at 290 Ma and associated with the intrusion of the Tertiary dykes. (see chapter 2.1)

2 Heat Sources

Mineral chemistry (chapter 2.4) and stable isotope data (chapter 2.6) suggest that the permeable volcanic rocks of the Midland Valley drew in cold seawater and meteoric water. The fluid temperature in the saturated volcanic piles would initialy have been governed by the thermal gradient of the host rock. The volcanic rock as the main heat source is unlikely to have been maintained throughout metamorphism. Its temperature is likely to have been constrained by:-

i) hydration reactions = exothermic.

ii) cooling of the upper (and lower) volcanic surfaces by penetrative hydrothermal circulation.

iii) the flow of hot fluids into fault zones, causing circulation to be centred on these regions and preventing the build-up of large volumes of hot rock through the introduction of major discontinuities in lateral permeability.

The extent of regional zeolitization in the Midland Valley indicates that long term stable geothermal reservoirs existed. The development of a zeolitic mineralogy indicates that the thermal system was water dominated. Consequently some of the heat for metamorphism may also have been provided by exothermic zeolite reactions. Although self-acceleration these reactions (and hence the liberation of heat) may have been controlled by the relative rates of fluid access and heat escape. However fluid circlation in the Midland Valley would have been partly sealed by a Carboniferous cover sequence, ensuring that:-

i) the same water (?) would have been continuously circulated

ii) heat dissipation was restricted and consequently metamorphism was more efficient.

In eastern Iceland, Walker (1960, b) attributed the heat source for zeolitization to the intensity of dyke swarms. This is witnessed by the inflection of the zeolite zones in regions devoid of dykes. In the Midland Valley the main dyke swarm occurs at 290 Ma (chapter 2.1) and outcrops essentially in the Carboniferous sediments. Dyke intensity in the volcanics is not comparable to that observed in eastern Iceland. Therefore although the dykes may have contributed to the overall heat budget, it is unlikely that they were the main

thermal source for metamorphism.

Geophysical evidence (chapter 2.1) suggests that shallow magma chambers existed beneath the Midland Valley during Permo-Carboniferous times. Cann *et al*, (1985) suggest that the heat of crystallization from the magma in such chambers may provide the thermal impetus for low grade metamorphism. Basically, cold water penetrated down through the permeable volcanic rock, to the top of the shallow magma chamber. Here water was heated by conduction through a thin boundary layer. Conduction proceeded from the material to the surface thereby controlling the thermal gradient of the hot rock. This process would have been sluggish due to the low conductivity of the rocks. However, it is likely that heat would have been gradually built up and maintained for a long time, hence reflecting the stability of the geothermal reservoirs.

In addition to conduction, the crystallizing magma would have been responsible (Cann *et al*, 1985) for the venting of hot hydrothermal fluids, which discharged through permeable fault zones. Due to their enhanced permeability, convection would have been vigorous along the faults. In Troodos (Cann *et al*, 1985; Schiffman *et al*, 1987) this has resulted in steep-sided zones containing zoned metabasalt. The products are comparable to those observed in the palaeo-geothermal plumes of the Midland Valley (chapter 2.2). The association of the Troodos zones with sulphide ore deposits (Schiffman *et al*, 1987) suggests that these areas (and by inference the palaeo-geothermal plumes of the Midland Valley) are areas where the fluids vented. At Troodos, boiling of the exhalent fluids on the sea-floor would have led to the precipitation of metals. In the Midland Valley there is an absence of ore-bodies associated with the

palaeo-geothermal plumes. The development of Carboniferous cover sequences necessitates that confining pressures were greater and thus boiling would have occurred deeper in the system. It is predicted that steam would have vented at the surface area. The predicted temperature (340-410 $^{o}$C) of the exhalent fluid, determined by Cann *et al*, (1985) is compatible with temperatures in the palaeo-geothermal plumes of the Midland Valley and with ancient and modern systems in Iceland (Kristmannsdottir and Tommasson, 1978).

3. Fluid access

Fluid may have gained access to the geothermal systems either by:-

i) permeating down through micro- and macro-pore spaces (chapter 2.2; 2.7)

ii) penetration along joint and fault planes

Fault planes both displace the zeolite zones and act as passage-ways for the introduction of fluids. Faulting continued from the Dinantian into the Westphalian (chapter 2.1). As such migration of fluids along these planes must have been episodic; pore spaces developing during movement and becoming increasingly filled with time. In the section (2.2.4) it was shown that faults provide a marked improvement in porosity, therefore pore spaces as fluid channels can hardly have been relevant compared to vein systems.

Hydraulic fracture occurs once $P_{fluid}$ builds up due to the expansion of trapped fluid during metamorphism (Thompson, 1987) and due to the reduction in porosity with time, until it exceeds the tensile strength in the rock. This may have been associated either with the introduction of magma or as a result of seismic failure. In the instance of a seismic event, the region surrounding the

earthquake focus dilates in response to rising tectonic stresses immediately prior to failure. Fractures open, increasing porosity. This causes $P_{fluid}$ in the dilatant zone to decrease resulting in the flow of fluid from the surrounding rock mass into the fracture (Sibson *et al*, 1975). Fluid inclusion data is consistent with this hypothesis, since in chapter 2.5 it was shown that the hottest waters in the palaeo-geothermal plumes (often associated with faults - chapter 2.2) may have been superheated groundwater. With the decreased magnitude of the earthquake, the dilatant cracks relax (Scholz and Kranz, 1974) and fluids are expelled upwards in the easiest direction for fluid migration. Cochno palaeo-geothermal plume (chapter 2.2) is perhaps an example of such seismic pumping of solvent fluids from one crustal environment to another along a fault plane.

At Beith and Boyleston palaeo-geothermal plumes there is geological evidence (chapter 2.2) and fluid inclusion evidence for the lateral migration of palaeo-geothermal plume fluids along lava flow surfaces and along horizontal faults. With time vertical channels for fluid migration become sealed. Sealing necessitates that the migration path of the escaping fluids continues to move upwards until it reaches an impermeable horizon. On reaching such a horizon, fluids must spread laterally. Impermeable horizons may be provided by interbedded sediments, or by previously zeolitized metabasalts where zeolitization has sealed all pore-spaces.

### 2.7.5 Scope for further research

1 To determine variations in major, trace element, stable and radiogenic isotope geochemistry within flow units during

zeolitization with respect to:-

i) increasing burial depth

ii) increasing distance from palaeo-geothermal plume centres

2 To use the fluid extraction gas chromatography line (recently built in the St Andrews University Geology Department) to

i) determine the chemical, stable and radiogenic character of fluid inclusions

ii) model the fluids involved with palaeo-geothermal alteration.

3 To thermodynamically determine reactions characterizing each burial zone.

4 To correlate metamorphic grade in the Carboniferous volcanics with the metamorphic grade in associated sediments. Using the following indexes in the meta-sediments.

i) zeolitization in volcaniclastic sediments

ii) illite crystallinity and clay mineralogy (see Part 1)

iii) vitrinite reflectance

iv) conodont alteration

Aguirre, L., Levi, B. and Offler, R. (1978). Unconformities as mineralogical breaks in the burial metamorphism of the Andes. Contrib. Mineral. Petrol. 66, 361-366.

Aldaz, L. and Deutsch, S. (1967). On a relationship between air temperature and oxygen isotope ratio of snow and firn in the South Pole region. Earth Planet. Sci. Letts. 3, 267.

Alderton, D.H.M. and Rankin, A.H. (1983). The character and evolution of hydrothermal fluids associated with the kaolinized St Austell granite, SW England. J. Geol. Soc. Lond. 140, 297-310.

Allsop, J.M. (1974). Geophysical survey at Spilmersford Borehole, East Lothian, Scotland. Bull. Geol. Survey G.B. 45 p. 63-72.

Alomari, M.I. (1980). Geological investigations of the gravity field of the western Midland Valley of Scotland. Unpub. PhD. thesis Univ. of Glas.

Anderson, F.W. (1951). The Geological Survey bore at Rashiehill, Stirlingshire. Bull. Geol. Surv. G.B. 20.

Anderson, F.W. (1963). The Geological Survey bore at Rashiehill, Stirling (1963). Bull. Geol. Surv. G.B. 20, 43-106.

Anderton, R., Bridges, P.H., Leeder, M.R., and Sellwood, B.W. (1979) Eds. A dynamic statigraphy of the British Isles. A study of crustal evolution. Pub. Allen and Unwin Lond., Boston, Sydney.

Aoki, M. and Minato, H. (1980). Lattice constants of wairakite as a function of chemical composition. Amer. Mineral. 65, 1212-1216.

Bamford, D., Nunn, K., Prodehl, C. and Jacob, B. (1977). LISPB - III. Upper crustal structure of northern Britain. J. Geol. Soc. Lond. 133, 481-8.

Belkin, H. De Vivo, B., Glaielli, G. and Lattarzi, P. (1985). Fluid inclusions in minerals from the geothermal fields of Tuscany, Italy. Geothermics 14, 59-72.

Bergstrom, S.M. (1980). Conodonts as palaeotemperature tools in Ordovician rocks of the Caledonides and adjacent areas in Scandinavia and the British Isles. G.F.F. v. 102 pt. 4 p. 377-92.

Bevins, R.E. (1985). Pumpellyite-dominated metadomain alteration at Builth Wells, Wales - evidence for a fossil submarine hydrothermal system? Min. Mag. 49, 451-465.

Bevins, R.E. and Rowbotham, G. (1983). Low-grade metamorphism within the Welsh sector of the paratectonic Caledonides. Geology J. 18, 141-167.

Biscaye, P.E. (1964). Distinction between kaolinite and chlorite in recent sediments by X-ray diffraction. Amer. Mineral. 49, 1281-1289.

Bischoff, J.L. and Dickson, F.W. (1975). Seawater basalt interaction at 200° and 500 bars. Implications for origin of seafloor heavy metal deposits and regulation of seawater chemistry. Earth. Planet. Sci. Letts. 25, 385-397.

Bluck, B.J. (1983). Role of the Midland Valley of Scotland in the Caledonian orogeny. Trans. Roy. Soc. Edinb. 74, 119-136.

Bluck, B.J. (1984). Pre-Carboniferous history of the Midland Valley of Scotland. Trans. Roy. Soc. Edinb. 75, 275-296.

Boles, J.R. and Coombs, D.S. (1975). Mineral reactions in zeolitic Triassic tuff, Hokonui Hills, New Zealand. Bull. Geol. Soc. Am. 86, 163-173.

Boles, J.R. and Coombs, D.S. (1977). Zeolite facies alteration of sandstones in the Southland Syncline, New Zealand. Am. J. Sci. 277, 982-1012.

Boles, J.R. and Franks, S.G. (1979). Clay diagenesis in Wilcox Sandstones of SW Texas: implications of smectite diagenesis on sandstone cementation. J. Sed. Petrol. 49, 55-70.

Borisenko, A.S. (1977). Study of the salt composition of solutions in gas-liquid inclusions in minerals by the cryometric method. Soviet Geol. and Geophys. 18, 11-19.

Browne, P.R.L. (1978). Hydrothermal alteration in active geothermal fields. Ann. Review Earth Planet. Sci. 6, 229-250.

Burst, J.F. (1959). Postdiagenetic clay-mineral environmental relationship in the Gulf Coast Eocene. Proc. Natl. Conf. Clays Clay Minerals 6th - Natl. Acad. Sci. Natl. Res. Council, Publ., 1957: 327-341.

Burst, J.F. (1969). Diagenesis of Gulf Coast clayey sediments and its possible relation to petroleum migration. Amer. Assoc. Petroleum Geol. Bull. 53, 73-93.

Cameron, I.B. and Stephenson, D. (1985). (Eds.) British Regional Geology: The Midland Valley of Scotland. 3rd edition. BGS NERC. Pub HMSO Lond. 1985.

Cann, J.R., Strens, M.R. and Rice, A.A. (1985). A simple magma-driven thermal balance model for the formation of volcanogenic massive sulphides. Earth Planet. Sci. Letts. 76, 123-134.

Cheng, P. and Minkowycz, W.J. (1977). Free convection about a vertical flat plate embedded in a porous medium, with application to heat transfer from a dyke. J. Geophys. Res. 82, 2040-2044.

Clayton, R.N. and Epstein, S. (1958). The relationship between $O^{18}/O^{16}$ ratios in co-existing quartz, carbonate and iron oxides from various geological deposits. J. Geol. 66, 352-373.

Clayton, R.N., O'Neil, J.R. and Mayeda, T.K. (1972). Oxygen isotope exchange between quartz and water. J. Geophys. Res. 77, 3057.

Clynne, M.A. and Potter, R.W. II (1977). Freezing point depressions of synthetic brines. Geol. Soc. Amer. Abs. with Programe. 9, 930.

Cocks, L.R.M. and Toghill, P. (1973). The biostratigraphy of the Silurian rocks of the Girvan district, Scotland. J. Geol. Soc. Lond. 129, 209-43.

Coombs, D.S. (1952). Cell size, optical properties and chemical composition of laumontite and leonhardite. With a note on regional occurrences in New Zealand. Amer. Mineral. 37, 812-830.

Coombs, D.S. (1954). The nature and alteration of some Triassic sediments from Southland, New Zealand. Trans. Roy. Soc. New Zealand 82, 65-103.

Coombs, D.S. (1971). Present status of the zeolite facies. In: Moleculear Sieve Zeolites eds. Flanigen, E.M.; Sand, L.B. p.p. 317-27. Amer. Chem. Soc. Adv. Chem. Ser. No 101.

Coombs, D.S., Ellis, A.J. Fyfe, W.S. and Taylor, A.M. (1959). The zeolite facies; with comments on the interpretation of hydrothermal syntheses. Geochim. Cosmochim. Acta 17, 53-107.

Coombs, D.S., Kawachi, Y., Houghton, B.F. Hyden, G. Pringle, I.J. and Williams, J.G. (1977). Andradite and andradite-grossular solid

solutions in very low-grade regionally metamorphosed rocks in southern New Zeland. Contrib. Mineral. Petrol. 63, 229-246.

Coombs, D.S., Nakamura, Y. and Vuagnat, M. (1976). Pumpellyite-actinolite facies schists of the Taveyanne Formation near Loeche, Valais, Switzerland. J. Petrol. 17, 440-471.

Coombs, D.S., and Whetten, J.T. (1967). Composition of analcime from sedimentary and burial metamorphic rocks. Geol. Soc. Amer. Bull. 78, 269-282.

Cotton, W.R. (1968). A geophysical survey of the Campsie and Kilpatrick Hills. Uni. of Glasg. PhD. thesis unpub.

Craig, H. (1961). Standard for reporting concentrations of deuterium and oxygen-18 in natural waters. Science 133, 1833.

Craig, H. (1965). The measurement of oxygen isotope palaeo-temperatures. In: Stable isotopes in oceanographic studies and Palaeotemperatures. Spoleto, July 26-27, 1965. Consiglio Nazionale delle Ricerche, Laboratorio di Geologia Nucleare, Pisa, 1-24.

Crawford, M.L. (1981). Phase equilibria in aqueous fluid inclusions: In Hollier, L.S. & Crawford, M.L. (Eds). Short Course. in: Fluid inclusions: Applications to petrology, vol 6. Min. Assoc. Canada 75-100.

Dansgaard, W. (1964). Stable isotope in precipitation. Tellus 16, 436-468.

Davis, S.N. and De Wiest, R.J.M. (1966). Groundwater in igneous and metamorphic rocks. In: Hydrogeology, Chap. 9 pp. 318-345.

Davies, A., McAdam, A.D. and Cameron, I.B. (1986). Geology of The Dunbar district. Mem. Br. Geol. Surv.

Davies, L.H. (1936). The Geology of Inchkeith. Trans. Roy. Soc. Edinb., 58, 753-786.

Davidson, K.A.S., Sola, M., Powell, D.W. and Hall, J. (1984). Geophysical model for the Midland Valley of Scotland. Trans. Roy. Soc. Edinb. 75, 175-182.

Deer, W.A., Howie, R.A. and Zussman, J. (1962). Rock-forming Minerals Vol. 4. Framework Silicates. Longmans.

Deer, W.A., Howie, R.A. and Zussman, J. (1980). An introduction to the rock forming minerals. 12th edition. Pub. Longman Group Ltd.; Lond.

de Souza, H.A.F. (1979). The geochronology of Scottish Carboniferous Volcanism. Edinb. Uni. unpub. PhD. thesis 1979.

Dunoyer de Segonzac, G. (1970). The transformation of clay minerals during diagenesis and low grade metamorphism. Sedimentology 15,

281-346.

Durney, D.W. and Ramsay, J.G. (1973). Incremental Strains Measured by Syntectonic Crystal Growths. In: Gravity and Tectonics (Eds. De Jong, K.A. and Schotten, R.) p. 67-98.

Eichelberger, J.C., Carrigan, C.R., Westrich, H.R. and Price, R.H., (1986). Non-explosive silicic volcanism. Nature 323, 598-602.

Epstein, A.G., Epstein, J.B. and Harris, L.D. (1977). Conodont colour alteration: an index to organic metamorphism. U.S. Geol. Surv. Prof. Pap. 995, 27 p.

Esquevin, J. (1969). Influence de la composition chimique des illites sur la crystallinite. Bull. Centre. Rech. Pau. SNPA 3 147-154.

Evans, A.L., Fitch, F.J., and Miller, J.A. (1973). Potassium-argon age determinations on some British Tertiary Igneous rocks. J. Geol. Soc. Lond. 129, 419-443.

Evarts, R.C. and Schiffman, P. (1983). Submarine hydrothermal metamorphism of the Del Puerto Ophiolite, California. Amer. J. Sci. 283, 289-340.

Everett, D.H. (1961). The thermodynamics of frost damage to porous solids. Trans. Faraday. Soc. 57, 1541-1551.

Eyles, V.A., Simpson, J.B. MacGregor, A.G. (1949). The Geology of central Ayrshire. Mem. Geol. Surv. U.K.

Fettes, D.J., Graham, C.M., Sassi, F.P. and Scolari, A. (1976). The basal spacing of potassic white micas and facies series variations across the Caledonides. Scott. J. Geol. 12, 227-236.

Francis, E.H. (1961). Thin beds of graded tuffs and tuffaceous siltstone in the Carboniferous of Fife. Bull. Geol. Surv. G.B. 17, 191-215.

Francis, E.H. (1978a). The Midland Valley as a rift, seen in connection with Late Palaeozoic rift systems. p. 133-147. In: Ramberg, L.B. and Neumann, E.R. (eds.). Tectonics and Geophysics of Continental Rifts. NATO Advanced Study Institutes Series. Reidel, Dordrecht, 444.

Francis, E.H. (1978b). Igneous activity in a fractured craton: Carboniferous volcanism in northern Britain. In: Bowes, D.R. and Leake, B.E. (Eds.) Crustal evolution in NW Britain and adjacent areas. Spec. Issue Geol. J. No. 10, 279-296

Francis, E.H. (1983). Carboniferous-Permian Igneous Rocks In: The Geology of Scotland. Second Edition Ed. G.Y. Craig. Pub. Scottish Academic Press, Edinburgh. p. 297-320.

Francis, E.H. and Hopgood, A.M. (1970). Volcanism and the Ardross Fault, Fife, Scotland. Scott. J. Geol., 6, 162-185.

Freshney, E.C. (1961). The Cementstone Group of the west Midland Valley of Scotland. PhD thesis, Univ. Glasg. (unpubl.).

Friedman, I. and O'Neil, J.R. (1977). Data of Geochemistry 6th edition (Ed. Fleischer, M) Chapter K.K. Compilation of stable isotope fractionation factors of geochemical interest. Geol. Surv. Prof. Paper 440-KK.

Frost, B.R. (1980). Observations on the boundary between zeolite facies and prehnite-pumpellyite facies. Contrib. Mineral. Petrology 73, 365-373.

Fyfe, W.S., Price, N.J. and Thompson, A.B. (1978). Developments in Geochemistry 1: Fluids in the earth's crust. Pub. Elsevier pp. 383.

Garcia, S.G. and Camazano, M.S. (1968). Differentiation of kaolinite from chlorite by treatment with Dimethyl-sulphoxide. Clay Minerals 7, 447-450.

George, T.N. (1960). The stratigraphical evolution of the Midland Valley. Trans. Geol. Soc. Glasg. 24, 32-107.

George, T.N., Johnson, G.A.L., Mitchell, M., Prentice, J.E., Ramsbottom, W.H.C. Sevastopulo, G.D. and Wilson, R.B. (1976). A correlation of Dinantian rocks in the British Isles. Geol. Soc. Lond. Spec. Rep. No. 7, 87 pp.

Goldsmith, J.R., Graf, J.L. and Joensuu, O.I. (1955). The occurrence of magnesian calcites in nature. Geochim. Cosmochim. Acta 7, 212-230.

Goodchild, J.C. (1903). The natural history of Scottish zeolites and their allies, with special reference to those in the Scottish mineral collection. Trans. Roy. Soc. Glasg. Vol XII - Supplement 88 pp.

Goodlet, G.A. (1957). Lithological variation in the Lower Limestone Group in the Midland Valley of Scotland. Bull. Geol. Surv. G.B. 12, 52-65.

Goswami, G. (1968). A magnetic and chemical study of the titanium bearing ore minerals of Carboniferous igneous rocks of the Midland Valley of Scotland. Unpub. PhD. thesis, Glasg. Uni.

Grabham, G.W. (1925) In: Memoirs of the Geological Survey, Scotland The Geology of the Glasgow District. Pub. HMSO. Revised Edn. by MacGregor, M, Dinham, C.H., Bailey, E.B. and Anderson, E.M.

Grim, R.E. and Bradley, W.C. (1951). High temperature thermal effects of clays and related materials. Amer. Mineral. 36, 182-201.

Grim, R.E. and Kulbichi, G. (1961). Montmorillonite: High temperature reactions and classification. Amer. Mineral. 46, 1329-1369.

Gschwind, M. and Brandenberger, E. (1932). Uber zwei neue

Zeolithvorkommen in Tessin. Schweiz. Min. Petrol. Mitt. 12, 445.

Haas, J.L. (1971) Jr. The effect of salinity on the maximum thermal gradient of a hydrothermal system at hydrostatic pressure. Econ. Geol. 66, 940-946.

Hall, D.H. and Dagley, P. (1970). Regional magnetic anomalies: An analysis of the smoothed Aeromagnetic Map of Great Britain and Northern Ireland. Rep. Inst. Geol. Sci. 70/10.

Hall, J. (1971). A preliminary seismic survey adjacent to the Rashiehill borehole near Slamannan, Stirlingshire. Scott J. Geol. 7, 170-174.

Hall, J. (1973). A seismic reflection survey of the Clyde Plateau Lavas in N. Ayrshire and Renfrewshire. Scott. J. Geol. 9 253-279.

Hall, J. Brewer, J.A., Matthews, D.H. and Warner, M.R. (1984). Crustal structure across the Caledonides from the 'WINCH' seismic reflection profile: influences on the evolution of the Midland Valley. Trans. Roy. Soc. Edinb. 75, 97-112.

Hall, J., Powell, D.W., Warner, M.R., El-Isa, Z.H.M., Adesanya, O. and Bluck, B.J. (1983). Seismological evidence for shallow crystalline basement in the Southern Uplands of Scotland. Nature 305, 418-420.

Hattori, K. and Sakai, H. (1980). Meteoric Hydrothermal Origin of

Calcites in 'Green Tuff' Formations, Miocene Age, Japan. Contrib. Mineral. Petrol. 73, 145-150.

Heaton, T.H.E. and Sheppard, S.M.F. (1977). Hydrogen and oxygen isotopic evidence for sea-water hydrothermal alteration and ore deposition, Troodos complex, Cyprus. In: Volcanic Processes in Ore Genesis (Institute of Mining and Metallurgy and Geological Society, London), p. 42.

Heddle, M.F. (1901). The Mineralogy of Scotland (Edinburgh).

Heddle, M.F. (1924). The Mineralogy of Scotland (Ed. by Goodchild, J.G.) In Hydrous Silicates-Zeolite Division p. 76-112.

Henderson, E.P. and Glass, J.J. (1933). Additional notes on laumontite and thomsonite from Table Mountain, Colorado. Amer. Mineral. 18, 402.

Hey, M.H. (1932). Studies on the zeolites. Part II. Thomsonite (including fareolite) and gonnardite. Min. Mag. 23, 51-125.

Hey, M.H. (1954). A new review of the chlorites. Min. Mag.. 30, 277-292.

Higgins, J.B. and Ribbe, P.H. (1976). The crystal chemistry and space groups of natural and synthetic titanites. Amer. Mineral. 61, 878-888.

Hoefs, J. (1973). Stable Isotope Geochemistry pp. 140. Pub. Springer-Verlag Berlin, Heidelberg, New York 1973.

Hollister, L.S. and Burress, R.C. (1976). Phase equilibria in fluid inclusions for the Khtada Lake metamorphic complex. Geochim. Cosmochim. Acta 40, 163-175.

Houghton, B.F. (1982). Low-grade metamorphism of the Takitimu Group, Western Southland, New Zealand. New Zealand, J. of Geology and Geophys. 25, 1-19.

House, M.R., Richardson, J.B., Chaloner, W.G., Allen, J.R.L., Holland C.H. and Westoll, T.S. (1977). A correlation of Devonian rocks of the British Isles. Spec. Rep. Geol. Soc. Lond. No. 89, 110.

Hower, J. and Mowatt, T.C. (1966). The mineralogy of illite and mixed-layer illite/montmorilonites. Amer. Mineral. 51, 825-854.

Hower, J., Eslinger, E.V., Hower, M.E. and Perry, E.A. (1976). Mechanism of burial metamorphism of argillaceous sediment I. Mineralogic and chemical evidence. Bull. Geol. Soc. Amer. 87, 725-37.

Hsu, L.C. (1980). Hydration and phase relations of grossular-spessartine garnets at $P_{H_2O}$ = 2kb. Contrib. Mineral. Petrol. 71, 407-415.

Hutchinson, C.S. (1974). (Ed.) Laboratory Handbook of Petrographic Techiques. Pub. Wiley and Sons (1974).

Iijima, A. and Harada, K. (1969). Authigenic zeolites in palagonite tuffs on Oahu, Hawaii. Amer. Mineral. 54, 182-197.

Islam, S. and Hesse, R. (1983). The P-T conditions of late-stage diagenesis and low grade metamorphism in The Taconic Best of the Gaspe Peninsula, from fluid inclusions: preliminary results. Current Research, Part B, Geol. Surv. Canada, Paper 83-1B, 145-150.

Johnson, M.R.W., Kelley, T.B., Oliver, G.J.H. and Winter, D.A. (1985). Thermal effects and timing of thrusting in the Mione Thrust zone. J. Geol. Soc. 142, 863-874.

Jolly, W. (1970). Zeolite and prehnite-pumpellyite facies in south central Puerto Rico. Contrib. Mineral. Petrol. 27, 204-224.

Kennedy, W.Q. (1958). The tectonic evolution of the Midland Valley of Scotland. Trans. Geol. Soc. Glasg. 23, 106-133.

King, P. (1977). The secondary minerals of the Tertiary lavas of northern and central Skye - zeolite zonation patterns, their origin and formation. Univ. Aberdeen PhD. thesis (unpub.).

Kisch, H.J. (1980a). Incipient metamorphism of Cambro-Silurian clastic rocks from the Jamtland Supergroup, Central Scandinavian Caledonides, W. Sweden: illite crystallinity and vitrinite

reflectance. J. Geol. Soc. Lond. 137, 271-288.

Kisch, H.J. (1980b). Illite crystallinity and coal rank associated with lowest-grade metamorphism of the Taveyanne grewyacke in the Helvetic Zone of the Swiss Alps. Ecologue. Geol. Helv. 73, 753-77.

Kisch, H.J. (1981). Coal rank and illite crystallinity associated with the zeolite facies of Southland and pumpellyite-bearing facies of Otago, New Zealand. New Zealand J. Geol. and Geophys. 24, 349-360.

Kodama, H. and Oinumai, K. (1963). Identification of kaolin minerals in the presence of chlorite by X-ray diffraction and infra-red adsorption spectra. Clays, Clay Min. 11th Natl. Conf. 236-249.

Kolodny, Y. and Gross, S. (1974). Thermal metamorphism by combustion of organic matter: isotopic and petrological evidence. J. Geol. 82, 489.

Kristmannsdottir, H. (1981). Wollastonite from hydrothermally altered basaltic rocks in Iceland. Min. Mag. 44, 95-99.

Kristmannsdottir, H. and Tomasson, J. (1978). Zeolite Zones in Geothermal Areas in Iceland. In: Natural Zeolites, Occurrence, Properties, Use (Eds. Sand, L.B. and Mumpton F.A.) Pergamon Press Oxford. pg. 277-287.

Kubler, B. (1968). Evaluation quantitative du metamorphisme par la cristallinite de illite: etat des progres realises ces demmieres annees. Bull. Centre Rech. Pau-SNPA. 2, 385-397.

Kubler, B. (1973). La corrensite, indicateur possible de milieu de sedimentation et du degre de transformation d'un sediment (Corrensite a possible guide to the environment of sedimentation and degree of transformation of a sediment) Centre Recherche Pau Bull., 7, 543-556.

Kuniyoshi, S. and Liou, J.G. (1976). Burial metamorphism of the Karmutsen volcanic rocks, north-east Vancouver Island, British Columbia. Am. J. Sci. 276, 1096-1119.

Kuniyoshi, S. and Liou, J.G. (1976b). Contact metamorphism of the Karmutsen volcanics, Vancouver Island, British Columbia. J. Petrol. 17, 73-99.

Lapworth, C. (1882). The Girvan Succession. Q.J.G.S. 38, 357.

Lattanzi, P., Rye, D.M. and Rice, J.M. (1980). Behaviour of $^{13}C$ and $^{18}O$ in carbonates during contact metamorphism at Marysville, Montana: Implications for isotope systematics in impure dolomitic limestones. Amer. J. Sci. 280, 890-906.

Leeder, M.R. (1982). Sedimentology. Processes and Product. Publ. Allen & Unwin, Lond.

Leggett, J.K. (1980). The sedimentological evolution of a Lower Palaeozoic accretionary fore-arc in the Southern Uplands of Scotland. Sedimentology 27, 401-417

Leggett, J.K., McKerrow, W.S. and Casey, D.M. (1982). The anatomy of a Lower Palaeozoic accretionary fore-arc the Southern Uplands of Scotland. In Leggett, J.K. (ed.) Trench-fore-arc geology, 495-520. Spec. Publ. Geol. Soc. Lond. 10.

Leggett, J.K., McKerrow, W.S. and Eales, M.H. (1979). The Southern Uplands of Scotland: A Lower Palaeozoic accretionary prism. J. Geol. Soc. Lond. 136, 755-770.

Liou, J.G. (1974). Stability relations of andradite-quartz in the system Ca-Fe-Si-O-H. Amer. Mineral. 59, 1016-1025.

Liou, J.G., Kim, H.S. and Maruyama, S. (1983). Prehnite-epidote equilibria and their petrologic applications. J. Petrol. 24, 321-342.

Liou, J.G., Maruyama, S. and Cho, M. (1985). Phase equilibria and mineral paragenesis of metabasites in low-grade metamorphism. Min. Mag. 49, 321-333.

Longman, C.D., Bluck, B.J. and Van Breemen, O. (1979). Ordovician conglomerates and the evolution of the Midland Valley. Nature vol. 280, p. 578-581.

Lucas, J. Camez, T. and Millot, G. (1959). Determination pratique aux rayons X des mineraux argileux simples et interstratifies. Bull. Serv. Carte. Geol. Als. Lor. 12 pp. 21-33.

MacDonald, J.G. (1973). Carbon-dioxide metasomatism in the Campsie lavas. Min. Mag. 39, 119-121.

MacDonald, J.G. and White, F. (1981). Petrochemical evidence for the genesis of a Lower Carboniferous transitional basaltic suite in the Midland Valley of Scotland. Trans. Roy. Soc. Edin. 72, 75-88.

Macdonald, R. (1975). Petrochemistry of the Early Carboniferous (Dinantian) lavas of Scotland. (Review Article). Scott. J. Geol. 11, 269-314.

Macdonald, R., Thomas, J.E. and Rizzello, S.A. (1977). Variations in basalt chemistry with time in the Midland Valley province during the Carboniferous and Permian. Scott. J. Geol. 13, 11-22.

MacEwan, D.M.C., (1944). Identification of montmorillonite. Nature, Lond. 154, 577-578.

MacGregor, A.G. (1928). The classification of the Scottish Carboniferous olivene-basalts and mugearites. Trans. Geol. Soc. Glasg. 18, 324-360.

MacGregor. A.G. (1960). Divisions of the Carboniferous on Geological Survey Scottish maps. Bull. Geol. Surv. G.B. 16, 127-30.

MacGregor, M. (1930). Scottish Carboniferous Stratigraphy. Trans. Geol. Soc. Glasg. XVIII, 442-558.

MacGregor, M. and MacGregor, A.G. (1961). The Midland Valley of Scotland (2nd Edit). Br. Reg. Geol. HMSO.

McAdam, A.D. (1974). The petrography of the igneous rocks in Lower Carboniferous (Dinantian) at Spilmersford, East Lothian, Scotland. Bull. Geol. Surv. G.B. 45, 39-46.

McAdam, A.D. and Tulloch, W. (1985). Geology of the Haddington district. Mem. Br. Geol. Surv.

McBirney, A.R. (1984). Igneous Petrology. Pub. Freeman, Cooper and Co., pp. 501.

McCrea, J.M. (1950). On the isotopic chemistry of carbonates and a palaeotemperature scale. J. Chem. Phys. 18, 849-857.

McGiven, A. (1968). Sedimentation and provenance of post-Valention conglomerates up to and including the basal conglomerate of the Lower Old Red Sandstone in the southern part of the Midland Valley of Scotland. PhD Thesis Univ. of Glasgow (unpubl.)

McKerrow, W.S. Leggett, J.K. and Eales, M.H. (1977). Imbricate thrust model of the Southern Uplands of Scotland. Nature 267, 237-239.

Magara, K. (1975). Re-evaluation of montmorillonite dehydration as cause of abnormal pressure and hydrocarbon migration. Amer. Assoc. Petrol. Geol. Bull, 59, 292-302.

Magaritz, M. and Taylor, H.P. Jr. (1976). Oxygen, hydrogen and carbon isotope studies of the Fransiscan Formation, Coastal Ranges, California. Geochim. Cosmochim. Acta 40, 215-234.

Martin-Vivaldi, J.L. and Callego, M.R. (1961). Some problems in the identification of clay minerals in mixtures by X-ray diffraction 11. Chlorite, swelling chlorite, montmorillonite. Clay Min. Bull. 4, 293-298.

Matthews, A. and Kolodny, Y. (1978). Oxygen isotope fractionation in decarbonation metamorphism. The Mottled Zone event. Earth Planet Sci. Letts. 39, 179-192.

Meixner, H., Hey, M.H. and Moss, A.A. (1956). Some new occurrences of gonnardite. Min. Mag. 31, 265.

Merriman, R.J. and Roberts, B. (1985). The survey of white mica crystallinity and polytypes in pelitic rocks of Snowdonia and Llyn, North Wales. Min. Mag. 49, 305-319.

Mitchell, G.H. and Mykura, W. (1962). The geology of the neighbourhood of Edinburgh. Mem. Geol. Surv. U.K.

Miyashiro, A. (1973). Metamorphism and Metamorphic Belts. Pub. Allen and Unwin.

Miyashiro, A. and Seki, Y. (1958). Enlargement of the composition field of epidote and piemontite with rising temperature. Amer. J. Sci. 256, 423-430.

Miyashiro, A. and Shido, F. (1970). Progressive metamorphism in zeolite assemblages. Lithos 3, 251-260.

Monnier, F. (1981). Thermal diagenesis in the Swiss molasse basin: implications for oil generation. Can. J. Earth Sci. 19, 328-342.

Muehlenbachs, K. and Clayton, R.N. (1972). Oxygen isotope geochemistry of submarine greenstones. Can. J. Earth Sci. 9, 471-478.

Muir, A., Hardie, H.G.M., Mitchell, R.L. and Phemister, J. (1956). Memoirs of the geological survey. Special Report on the Mineral Resources of Great Britain Vol XXXVII The Limestones of Scotland. Chemical Analyses and Petrography. Pub HMSO.

Mullis, J. (1979). The system methane-water as a geologic thermometer and barometer from the external part of the Central Alps. Bull. de Mineralogie 102, 526-536.

Munha, J., Fyfe, W.S. and Kerrich, R. (1980). Adularia, the characteristic mineral of felsic spilites. Contrib. Mineral. Petrol.

75, 15-19.

Mykura, W. (1965). White-trap in some Ayrshire Coals. Scott. J. Geol. 1, 176-184.

Mykura, W. (1983). Old Red Sandstone. In: Geology of Scotland. (Ed. Craig, G.Y. 1983. Scottish Academic Press Edinburgh). p. 205-242.

Nadeau, P.H. Wilson, M.J. McHardy, W.J. and Tait, J.M. (1985). The conversion of smectite to illite during diagenesis: evidence from some illitic clays from bentonites and sandstones. Min. Mag. 49, 393-400.

Niskanen, E. (1964). R cation of orientation effects in the quantitative X-ray diffraction analysis of kaolin minerals. Amer. Mineral. 49, 705-714.

Northrop, D.A. and Clayton, R.N. (1966). Oxygen isotope fractionations in systems containing dolomite. J. Geol. 74, 174-196.

Norton, D. and Knapp, R. (1977). Transport phenomena in hydrothermal systems: the nature of porosity. Amer. J. Sci. 277, 913-936.

Novacek, R. (1936). Contribution to the knowledge of Moravian zeolites. Casopis Morav. Zemsk. Mus., Brno, 24, 133.

Oliver, G.J.H. and Leggett, J.K. (1980). Metamorphism in an accretionary prism: prehnite-pumpellyite facies metamorphism of the Southern Uplands of Scotland. Trans. Roy. Soc. Edin.: Earth Sci. 71, 235-246.

Oliver, G.J.H. and Mckerrow, W.S. (1984). Seismological evidence for shallow crystalline basement in Southern Uplands, Scotland. Nature 309 (5963) 89-90.

Oliver, G.J.H., Smellie, J.L., Thomas, L.J., Casey, D.M., Kemp, A.E.S., Evans. L.J., Baldwin, J.R. and Hepworth, B.C. (1984). Early Palaeozoic metamorphic history of the Midland Valley, Southern Uplands-Longford-Down massif and the Lake District, British Isles. Trans. Roy. Soc. Edin. 75, 245-258.

O'Neil, J.R., Clayton, R.N. and Mayeda, T. (1969). Oxygen isotope fractionation in divalent mental carbonates. J. Chem. Phys. 51, 5547-5558.

Padan, A. Kisch, H.J. and Shagam, R. (1982). Use of the lattice parameter $b_o$ of dioctahedral illite/muscovite for the characterization of P.T gradients in incipient metamorphism. Contrib. Mineral. Petrol. 79, 85-95.

Passaglia, E. (1970). The crystal chemistry of chabazites. Amer. Mineral. 55, 1278-1301.

Perry, E.A. and Hower, J. (1970). Burial diagenesis in Gulf Coast pelitic sediments. Clays and Clay Mins. 18, 165-77

Perry, E.A. and Hower, J. (1972). Late-stage dehydration in deeply buried pelitic sediments. Bull. A.A.P.G. 56, 2013-21.

Peters, T. (1965). A water-bearing andradite from the Totalp serpentine (Davos, Switzerland). Amer. Mineral. 50, 1482-1486.

Potter, R.W. II (1977). Pressure corrections for fluid inclusions homogeneization temperatures based on the volumetric properties of the system $NaCl-H_2O$. J. Res. U.S. Geol. Surv. 5, 603-607.

Powers, M.C. (1967). Fluid-release mechanisms in compacting marine mudstones and their importance to oil exploration. Bull. A.A.P.G. 51, 1240-1254.

Pringle, J. (1948). British Regional Geology: The South of Scotland. 2nd edn. H.M.S.O. Edinb.

Ramsbottom, W.H.C., Calver, M.A., Eagar, R.M.C., Hodson, F., Holliday, D.W., Stubblefield, C.J. and Wilson, R.B. (1978). A correlation of Silesian rocks in the British Isles. Spec. Rep. Geol. Soc. Lond. No 10.

Reynolds, R.C. Jr. and Hower, J. (1970). The nature of interlayering in mixed-layer illite-montmorillonite. Clays Clay Mineral. 18, 25-36.

Richardson, J.B. (1967). Some British Lower Devonian spore assemblages and their stratigraphic significance. Rev. Palaeobot. Palynol. 1, 111-129.

Richey, J.E. (1939). The dykes of Scotland. Trans. Edinb. Geol. Soc. 13, 393-435.

Richey, J.E., Anderson, E.M., and MacGregor, A.G. (1930). The geology of North Ayrshire. Mem. Geol. Surv. U.K.

Roberts, B. and Merriman, R.J. (1985). The distinction between Caledonian burial and regional metamorphism in meta pelites from North Wales: an analysis of isocryst patterns. J. Geol. Soc. 142, 615-624.

Roedder, E. (1981). Origin of fluid inclusions and changes that occur after trapping. In: Hollister, L.S. and Crawford, M.L. (eds.) Short course in Fluid Inclusions: Applications to Petrology, vol. 6. Mineralogical Association of Canada, 101-137.

Roedder, E. (1984). Reviews in mineralogy Vol. 12: Fluid Inclusions. Ed. Ribbe, P.H. Publ. Min. Soc. Amer.

Roedder, E. and Bodnar, R.J. (1980). Geologic pressure determinations for fluid inclusion studies. Ann. Rev. Earth Planet. Sci. 8, 263-301.

Rolfe, W.D.I. (1961). The geology of the Hagshaw Hills, Silurian Inlier, Lanarkshire. Trans. Edinb. Geol. Soc. 18, 240-69.

Rolfe, W.D.I. and Fritz, M.A. (1966). Recent evidence for the age of the Hagshaw Hill Silurian inlier, Lanarkshire. Scott. J. Geol. 2, 159-64.

Sackett, W.M. and Moore, W.S. (1966). Isotopic variations of dissolved inorganic carbon. Chem. Geol. 1, 323-328.

Saha, P. (1961). The system $NaAlSiO_4$ (nepheline)-$NaAlSi_3O_8$ (albite) - $H_2O$. Amer. Mineral. 46, 859-884.

Sameshima, T. (1978). Zeolites in tuff beds of the Miocene Waitemata Group, Auckland Province, New Zealand. p. 309-317. In: Natural Zeolites, Occurrence, Properties, Uses (Sand, L.B. and Mumpton, F.A. (eds.) Pergamon Press.

Sameshima, T, (1986). Ferrierite from Tapu, Coromandel Peninsula, New Zealand, and a crystal chemical study of known occurrences. Min. Mag. 50, 63-68.

Sassi, F.P. (1972). The petrological and geological significance of the $b_o$ values of potassic white micas in low-grade metamorphic rocks. An application to the Eastern Alps. Tschermaks Min. Petr. Mitt. 18, 105-113.

Sassi, F.P., Scolari, A. (1974). The $b_o$ value of the potassium white micas as a barometric indicator in low-grade metamorphism of pelitic schists. Contrib. Mineral. Petrol. 45, 143-125.

Schiffman P, Smith, B.M., Varga, R.J. and Moores E.M. 1987. Geometry, conditions and timing of off-axis hydrothermal metamorphism and ore-deposition in the Solea graben. Nature 325, 423-425.

Scholle, P.A. (1979). A Colour Illustrated Guide to Constituents, Textures, Cements and Porosities of Sandstones and Associated Rocks. Bull. A.A.P.G. Memoir 28.

Scholz, C.H. and Kranz, R. (1974). Notes on diltancy revover. J.Geophys. Res. 79, 2132-2135.

Schuiling, R.D. and Vink, B.W. (1967). Stability relations of some titanium minerals (sphene, perovskite, rutile, anatase). Geochim. Cosmochim. Acta 31, 2399-2411.

Seki, Y., Oki, Y., Matsuda, T., Mikami, K. and Okumura, K. (1969). Metamorphism in the Tanzawa Mountains, central Japan. J. Jap. Assoc. Mineral. Petrol. Econ. Geol. 61, 1-29, 50-75.

Selden, P.A. and White, D.E. (1983). A new Silurian arthropod from Lesmahagow Scotland. Spec. pap. in Palaeontology No 30, p. 43-49.

Shepherd, T.J. (1981). Temperature-programmable heating-freezing stage for micro-thermometric analysis of fluid inclusions. Econ.

Geol. 76, 1244-1247.

Shepherd, T.J., Rankin, A.H. and Alderton, D.H.M. (1985). A practical guide to fluid inclusion studies pp. 239. Pub. Blackie - Glasgow.

Sheppard, S.M.F. and Schwarcz, H.P. (1970). Fractionation of carbon and oxygen isotope and magnesium between co-existing metamorphic calcite and dolomite. Contrib. Mineral. Petrol. 26, 161-198.

Sibson, R.H., Moore, J.McM, and Ranking, A.H. (1975). Seismic-pumping - a hydrothermal fluid transport mechanism. J. Geol. Soc. Lond. 131, 653-660.

Smith, A.G., Hurley, A.M. and Briden, J.C. (1981). Phanerozoic palaeocontinental world maps. Cambridged University Press.

Smith, G.F.H., Ashcroft, F.N. and Prior, G.T. (1916). Chabazite and associated minerals from County Antrim. Min. Mag. 17, 274.

Spooner, E.T.C., Beckinsale, R.D., Fyfe, W.S. and Smewing, J.D. (1974). $O^{18}$ enriched ophiolitic metabasic rocks from E Liquria (Italy), Pindos (Greece) and Troodos (Cyprus). Contrib. Mineral. Petrol. 47, 41-62.

Spooner, E.T.C., Beckinsale, R.D., England, P.C. and Senior, A. (1977). Hydration, $^{18}O$ enrichment, + oxidation during ocean floor hydrothermal metamorphism of ophiolitic meta-basic rocks for E.

Liquria, Italy. Geochim. Cosmochim. Acta 41, 857-871.

Spooner, E.T.C., Chapman, H.J. and Smewing J.D. (1977b). Strontium isotopic contaminatio and oxidation during ocean floor hydrothermal metamorphism of the ophiolitic rocks of the Troodos Massif, Cyprus. Geochim. Cosmochim. Acta, 41, 873-890.

Srodon, J. (1980). Precise identification of illite-smectite interstratification by X-ray powder diffraction. Clays Clay Mineral. 28, 401-411.

Stakes, D.S. and O'Neil, J.R. (1982). Mineralogy and stable isotope geochemistry of hydrothermally altered oceanic rocks. Earth Planet. Sci. Letts. Vol 57 No 2, 285-304.

Steiner, A. (1955). Wairakite, the calcium analogue of analcime, a new zeolite mineral. Min. Mag. 30, 691.

Suchecki, R.K. and Land, S.L. (1983). Isotopic geochemistry of burial metamorphosed volcanogenic sediments, Great Valley sequence, Northern California. Geochim. Cosmochim. Acta 47, 1487-1500.

Sukheswala, R.N., Auasia, R.K. and Gangopedhyay, M. (1974). Zeolites and associated secondary minerals in the Deccan Traps of Western India. Min. Mag. 39, 658-671.

Surdam, R.C. (1969). Electron microprobe study of prehnite and pumpellyite from the Karmutsen Group, Vancouver Island, British

Columbia. Amer. Mineral. 54, 256-66.

Sveinbjornsdottir, A.E. (1983). Water-rock interaction in Krafla and Reykjanes geothermal systems, Iceland. J. Geol. Soc. Lond. 140, 549-550.

Taylor, H.P. Jr. (1968). The oxygen isotope geochemistry of igneous rocks. Contrib. Mineral. Petrol. 19, 1-71.

Thirlwall, M.F. (1983). Discussion on implications for Caledonian plate tectonic models of chemical data from volcanic rocks of the British Old Red Sandstone. J. Geol. Soc. Lond. 140, 315-318.

Thomas, L.J. (1986). Low-grade metamorphism and the stable isotope composition of alteration fluids, Lower Palaeozoic Succession, English Lake District. PhD. Thesis: St Andrews Univ.

Thompson, A.B. (1971a). $P_{CO_2}$ in low-grade metamorphism: zeolite carbonate, clay mineral, prehnite relations in the system $CaO-Al_2O_3-SiO_2-CO_2-H_2O$. Contrib. Mineral Petrol. 33, 145-161.

Thompson, A.B. (1971b). Analcite-albite equilibria at low temperatures. Amer. J. Sci. 271, 79-92.

Thompson, A.B. (1987). Some aspects of fluid motion during metamorphism. J. Geo. Soc. Lond. 144, 309-312.

Thorez, J. (1975). Phyllosilicates and clay minerals: a laboratory handbook for their XRD analysis. (Dison, Belg.)

Thorez, J. (1976). Practical identification of clay minerals: a handbook for teachers and students in clay mineralogy (Dison, Belg.).

Tipper, J.C. (1976). The stratigraphy of the North Esk Inlier, Midlothian. Scott. J. Geol. 12, 15-22.

Toulmin III, P. and Clark, Jr. S.P. (1967). Thermal aspects of ore formation. In: Barnes, H.L. Ed. Geochemistry of hydrothermal ore deposits. p. 437-464.

Truesdell, A.H. (1974). Oxygen isotope activities and concentrations in aqueous salt solutions at elevated temperatures - Consequences for isotope geochemistry. Earth Planet. Sci. Letts. 23, 387-396.

Tulloch, A.J. (1979). Secondary Ca-Al Silicates as Low-grade alteration products of granitoid biotite. Contrib. Mineral. Petrol. 69, 105-117.

Upton, B.G.J., Aspen, P. and Hunter, R.H. (1984). Xenoliths and their implications for the deep geology of the Midland Valley of Scotland. Trans. Roy. Soc. Edinb. 75, 65-70.

Utada, M. (1965). Zonal distribution of authigenic zeolites in the Tertiary pyroclastic rocks in Mogami district, Yamagata Prefecture. Sci. Paper Coll. General Education, Univ. Tokyo 15, 173-216.

Velde, B. (1977). Clay Minerals in Natural and Synthetic Systems. Elsevier, Amsterdam, 218 pp.

Velde, B. (1985). Possible chemical controls of illite/smectite compositions during diagenesis. Min. Mag. 49, 387-392.

Vermon, R.H. (1976). Metamorphic Processes Reactions and Microstructure Development. Allen and Unwin.

Walker, G.F. (1949). Distinction of vermiculite, chlorite and montmorillonite in clays. Nature., Lond. 164, 577-578.

Walker, G.P.L. (1951). The amygdale minerals in the Tertiary lavas of Ireland I. The distribution of chabazite habits and zeolites in the Garron Plateau area, County Antrim: Min. Mag. 29, 773-791.

Walker, G.P.L. (1960a). The amygdale minerals in the Tertiary Lavas of Ireland III Regional distribution. Min. Mag 32 503-527.

Walker, G.P.L. (1960b). Zeolite zones and dyke distribution in relation to the structure of the basalts of Eastern Iceland. J. Geol. 68: 515-528.

Walker, G.P.L (1972). Compound and simple lava flows and flood basalts. Bull. Volcan. 35, 579-590.

Walters, L.J., Claypool, G.E. and Choquette, P.W. (1972). Reaction rates and $\delta^{18}O$ variation for the carbonate-phosphoric acid

preparation method. Geochim. Cosmochim. Acta 36, 129-140.

Walton, E.K. (1963). Sedimentation and structure in the Southern Uplands. In: The British Caledonides, Stewart, F.H. and Johnson, M.R.W. (eds.) 71-97 Edinb.: Oliver and Boyd.

Walton, E.K. (1983). Lower Palaeozoic - Stratigraphy p. 105-160. Lower Palaeozoic - Structure and Palaeogeography, p. 139-160. In: Geology of Scotland 2nd Edn. Ed. by Craig, G.Y. 1983. Scottish Academic Press, Edinburgh.

Watson, J. (1983). p. 23-42 In Geology of Scotland 2nd Edn. Ed. by Craig, G.Y. 1983. Scottish Academic Press, Edinburgh.

Weaver, C.E. (1956). The distribution and identification of mixed layer clays in sedimentary rocks. Amer. Mineral. 41, 202-221.

Weaver, C.E. (1960). Possible uses of clay minerals in search for oil. Bull. A.A.P.G. 44, 1505-1518.

Weber, K. (1972). Note on the determination of illite crystallinity. Newes. Jahrb. Mineral. Monatshefte. 6, 267-276.

Weiss, E.J. and Rowland, R.A. (1956). Effect of heat on vermiculite and mixed-layered vermiculite-chlorite. Amer. Mineral. 41., 899-914.

Welton, J.E. (1984). SEM Petrology Atlas for Chevron Oil Field Research Co. Pub. A.A.P.G. Tulsa, Oklahoma.

Wenner, D.B. and Taylor, H.P. (1971). Temperatures of serpentinization of ultramafic rocks based on $^{18}O/^{16}O$ fractionation between coexisting serpentine and magnetite. Contrib. Mineral. Petrol. 32, 165.

Westoll, T.S. (1977). Northern Britain. In House M.R. (ed.). A correlation of the Devonian rocks in the British Isles, 66-93. Spec. Rep. Geol. Soc. Lond. 7.

Whyte, F. and MacDonald, J.G. (1974). Lower Carboniferous volcanicity in the northern part of the Clyde Plateau. Scott. J. Geol. 10, 187-198.

Williams, A. (1959). A structural history of the Girvan district, SW Ayrshire. Trans. Roy. Soc. Edin. 63, 629.

Wilson, M.D. and Pittman, E.D. (1977). Authigenic clays in sandstones: recognition and influence on reservoir properties and palaeoenvironmental analysis. J. Sed. Petrol. 47, 3-31.

Winkler, H.G.F. (1976). Petrogenesis of metamorphic rocks. Fifth Edition. Pub. Springer-Verlag New York. Heidelber, Berlin.

Wise, W.S., Nokleberg, W.J. and Kokinos, M. (1969). Clinoptilolite and ferrierite from Agoura, California. Amer. Mineral. 54, 887-895.

Wise, W.S. and Tschemich, R.W. (1976) Ibid 61, 60-66.

Yajima, S. and Nakamura, T. (1971). Min. J. 6, 343-364.

Yardley, B.W.D. (1975). On some quartz-plagioclase veins in the Connemara schists, Ireland. Geol. Mag. 112, 183-190.

Yermakov, N.P. (1965). Research on the nature of mineral-forming solutions. International Series of Monographs in Earth Sciences 22, p. 473, Pergamon.

Yoder, H.S. (1960). Stability relations of grossularite. J. Geol. 58, 221-253.

Appendix 1.3.1

| SAMPLE NO | G R | DIFFRACTOGRAMS/TREATMENTS | | | | | | | |
|---|---|---|---|---|---|---|---|---|---|
| | | Hb-rel | $b_o$ | Untreated | EG | Heat | HCl | DMSO | MgCl/EG |
| 2 | NX167 952 | * | * | * | * | * | * | * | * |
| 3 | NX168 954 | * | * | * | * | * | * | * | * |
| 4 | NX176 958 | * | * | * | * | * | * | * | * |
| 5 | NX177 960 | * | * | * | * | * | * | * | * |
| 6 | NX180 963 | * | * | * | * | * | * | * | * |
| 7 | NX210 978 | * | * | * | * | * | * | * | * |
| 8 | NX207 970 | * | * | * | * | * | * | * | * |
| 9 | NX214 973 | * | * | * | * | * | * | * | * |
| 10 | NX219 975 | * | * | * | * | * | * | * | * |
| 11 | NX225 976 | * | * | * | * | * | * | * | * |
| 12 | NX234 983 | * | * | * | * | * | * | * | * |
| 13 | NX237 980 | * | * | * | * | * | * | * | * |
| 14 | NX247 991 | * | * | * | * | * | * | * | * |
| 15 | NX265 999 | * | * | * | * | * | * | * | * |
| 16 | NX334 023 | * | * | * | * | * | | * | * |
| 17 | NX327 019 | * | * | * | * | * | * | * | * |
| 18 | NX315 017 | * | * | * | * | * | | | * |
| 19 | NX373 046 | * | * | * | * | * | * | * | * |
| 20 | NX357 036 | * | | * | * | * | * | * | * |
| 21 | NX347 036 | * | * | * | * | * | * | * | * |
| 22 | NX293 007 | * | * | * | * | * | * | * | * |
| 23 | NX241 034 | * | * | * | * | * | * | * | * |
| 24 | NX258 041 | * | * | * | * | * | * | * | * |
| 25 | NX268 042 | * | * | * | * | * | * | * | * |
| 26 | NX274 039 | * | * | * | * | * | * | * | * |
| 27 | NT156 577 | * | * | * | * | * | * | * | * |
| 28 | NT157 586 | * | * | * | * | * | * | * | * |
| 29 | NT159 594 | * | * | * | * | | * | * | * |
| 30 | NT147 586 | * | * | * | * | * | * | * | * |
| 31 | NT146 596 | * | * | * | * | * | * | * | * |
| 32 | NT145 581 | * | * | * | * | * | | | * |
| 33 | NT147 572 | * | * | * | * | * | * | * | * |
| 34 | NT167 624 | * | * | * | * | * | * | | * |
| 35 | NT177 624 | * | * | * | * | * | * | * | * |
| 36 | NT188 619 | * | * | * | * | * | * | * | * |
| 37 | NT199 635 | * | * | * | * | * | * | * | * |
| 38 | NS749 373 | * | * | * | * | * | * | * | * |
| 39 | NS738 353 | * | * | * | * | * | | * | * |
| 40 | NX250 986 | * | * | * | * | * | * | * | * |
| 41 | NS745 253 | * | * | * | * | * | * | * | * |
| 42 | NS746 260 | * | * | * | * | * | * | * | * |
| 43 | NS750 269 | * | * | * | * | * | * | * | * |
| 44 | NS754 278 | * | * | * | * | * | * | * | * |
| 45 | NS762 279 | * | * | * | * | * | * | * | * |
| 46 | NS778 291 | * | * | * | * | * | * | | * |
| 47 | NS773 298 | * | * | * | * | * | * | * | * |
| 48 | NS782 283 | * | * | * | * | * | * | | * |
| 49 | NS942 384 | * | * | * | | * | * | * | * |
| 50 | NS730 384 | * | * | * | * | * | * | * | * |
| 51 | NS739 387 | * | * | * | * | * | * | * | * |
| 52 | NS734 338 | * | * | * | * | * | * | * | * |
| 53 | NS729 329 | * | * | * | * | * | * | * | * |
| 54 | NS749 359 | * | * | * | * | * | * | * | * |
| 55 | NS733 317 | * | * | * | * | * | * | * | * |
| 56 | NS718 309 | * | * | * | | * | * | * | * |
| 57 | NS696 303 | * | * | * | * | * | * | | * |
| 58 | NS680 321 | * | * | * | * | * | * | * | * |
| 59 | NS679 337 | * | * | * | * | * | * | * | * |
| 60 | NS658 367 | * | * | * | * | * | * | * | * |
| 61 | NS688 314 | * | * | * | * | * | | | * |
| 62 | NS614 325 | * | * | * | * | * | * | | * |
| 62A | NS614 325 | * | * | * | * | * | | | * |
| 63 | NS629 309 | * | * | * | * | * | | | * |
| 64 | NT172 597 | * | * | * | * | * | * | * | * |
| 65 | NT172 592 | * | * | * | * | * | * | * | * |
| 66A | NT132 565 | * | * | * | * | * | | * | * |
| 66B | NT131 565 | * | * | * | | * | | * | * |
| 67 | NT129 563 | * | * | * | * | * | * | * | * |
| 68 | NT129 568 | * | * | * | * | * | * | * | * |
| 69 | NT128 573 | * | * | * | * | * | * | * | * |
| 70 | NT143 577 | * | * | * | * | * | * | * | * |
| 71 | NT137 567 | * | * | * | * | * | * | * | * |
| 72 | NT141 579 | * | * | * | | * | * | * | * |
| 73 | NT145 591 | * | * | * | * | * | * | * | * |
| 74 | NT153 584 | * | * | * | * | * | * | * | * |
| 75 | NT159 590 | * | * | * | * | * | | * | * |
| 76 | NT156 580 | * | * | * | * | * | * | * | * |
| 77 | NX338 029 | * | * | * | * | | * | * | * |
| 78 | NX229 978 | * | * | * | * | * | * | * | * |
| 79 | NX228 979 | * | * | * | * | * | * | * | * |
| 80 | NX229 983 | * | * | * | * | * | * | * | * |
| 81 | NX229 991 | * | * | * | * | * | * | * | * |
| 82 | NX236 983 | * | * | * | * | * | * | * | * |
| 83 | NX251 992 | * | * | * | * | * | * | * | * |
| 84 | NX251 995 | * | | * | * | * | * | * | * |

Hb-rel - illite crystallinity parameter

$b_o$ - lattice spacing parameter

EG - ethylene glycolated samples

Heat - head treated (to 600 °C) samples

HCl - hydrochloric acid treated samples

DMSO - dimethol-sulphoxide treated samples

MgCl/EG - magnesium chloride saturated, ethylene glycolated samples

Appendix 1.3.2

| Locality and Sample Number | $10b_{rel}$ | $b_o$ | I/M ratio | MINERALOGY | | | | | | | | | | Calcite | Assemblage |
|---|---|---|---|---|---|---|---|---|---|---|---|---|---|---|---|
| | | | | Chlorite | Kaolinite | Vermiculite | Illite | MIXED LAYERS I/M (R) | I/M (IRR) | C-I | C-V | I-V | | | |
| 2 | 160.6 | 9.010 | M-0%; 20% | * | | | * | * | | | | | | | a 2 |
| 3 | | 9.037 | | * | | | | | | | | | | | 1 |
| 4 | | 9.043 | M-0% | | | * | * | | | | * | | | * | 1 |
| 5 | | 9.037 | M-0%; 40% | | | | * | * | | * | | | | * | 4 |
| 6 | | 9.041 | M-0% | * | | | * M | | | | | | | | 1 |
| 7 | 125.8 | 8.965 | M-0% | | | | * | | | * | | | | | 1 |
| 8 | 108.1 | | M-0% | * | | | * V | | | | | * | (IRR) | | 1 |
| 9 | 120.0 | 9.060 | M-0% | * | * | | * | | | | | | | | 1 |
| 10 | 113.2 | 9.019 | M-0%; 30% | * | minor | | * | * | | | | | | | a 3 |
| 11 | 140.0 | 9.047 | M-0% | * | * minor | | * | | | | | | | | 1 |
| 12 | 112.3 | 9.041 | M-0% | * | * | | * | | | | | | | | 1 |
| 13 | 111.4 | 9.026 | M-0% | * | | | * V | | | | | * | (IRR) | * | 1 |
| 14 | 131.4 | 9.011 | M-0% | * | * | | * | | | | | | | * | 1 |
| 15 | 149.2 | 9.062 | M-0%; 20% | * | | | * M | * | | | | | | | a 2 |
| 16 | 89.7 | 9.061 | M-0%; 20% | * | | | * | * | | | | | | | a 2 |
| 17 | 116.6 | 9.030 | M-0%; 20% | | * | * | | * | | | * | | | | b 2 |
| 18 | 124.2 | 9.029 | M-0%; 30% | * | | | * | | * | | | | | | |
| 19 | 127.8 | 9.047 | M-0%; 30% | * | | | * | * | | * | | | | | b 3 |
| 20 | 141.9 | | M-0%; 30% | * | | | * | * | | | | | | | a 3 |
| 21 | 143.2 | 9.050 | M-0% | * | | | * M | | | | | | | * | 1 |
| 22 | 158.4 | 9.044 | M-0% | * | * | | * V | | | | | | | * | 1 |
| 23 | 110.9 | 9.037 | M-0% | * | * | * | * M | | | | | | | * | 1 |
| 24 | 182.5 | | M-0% | | * | | * M | | | | | | | * | 1 |
| 25 | | 9.031 | | | * | | | | | | | | | | 1 |
| 26 | 122.7 | 9.027 | M-20% | * | | | | * | | | | | | * | a 2 |
| 27 | 95.2 | 9.029 | M-0% | * | | * | * | | | | | | | | 1 |
| 28 | 111.1 | | M-0%; 20% | * | * | * | * M | * | | | | | | * | a 2 |
| 29 | 111.2 | 9.035 | M-0%; 20% | * | | | * | * | | | | | | | a 2 |
| 30 | 106.5 | 9.005 | M-0%; 40% | * | | | * | * | | | | | | | 2 |
| 31 | 119.6 | 9.008 | M-0%; 40% | | | | * | * | | * | | | | | 2 |
| 32 | | 8.981 | M-0%; 20% | | | | * | * | | | | | | | a 2 |
| 33 | 119.4 | 9.030 | M-0% | * | | * | * | | | | | | | * | 1 |
| 34 | 129.3 | 9.047 | M-0% | * | | * | * M | | * | | | | | | 1 |
| 35 | 95.6 | 9.037 | M-0% | * | | * | * M | | * | | | | | * | 1 |
| 36 | 159.7 | 9.004 | M-0%; 20% | * | | | * | * | | | | | | | a 2 |
| 37 | 97.8 | 9.006 | M-100% | | * | | | * | | | | | | | 3 |
| 38 | 153.6 | 9.023 | M-0%; 30% | * | * | | * | * | | | | | | | a 3 |
| 39 | 108.7 | 9.051 | M-0% | * | | | * M | | | | | | | | 1 |
| 40 | 113.3 | 9.039 | M-0% | | | | | | | | | | | * | 1 |
| 41 | 167.8 | 9.008 | M-0% | * | minor | | * V | | | | | | | | 1 |
| 42 | 98.4 | 9.050 | M-0% | * | * | | * V | | | | | | | * | 1 |
| 43 | 170.4 | 9.014 | M-0% | * | | * | * M | | | | | | | | 1 |
| 44 | 116.7 | 9.023 | M-0% | | * | | * M | | | | | | | | 1 |
| 45 | | 9.026 | M-0%; 40% | * | | | * | * | | | | | | * | 4 |
| 46 | 146.5 | 9.016 | M-0% | * | | | * V | | | | | | | | 1 |
| 47 | 109.1 | 9.008 | | * | | | | | | | | * | | | |
| 48 | 143.0 | 9.029 | M-0% | * | | * | * M | | * | | | | | | 1 |
| 49 | 110.9 | 9.032 | M-0% | * | | | * V | | | | | | | * | 1 |
| 50 | 133.6 | 9.031 | | * | | | | | | | | * | | * | |
| 51 | 139.6 | 9.020 | M-0%; 25% | | | | * | * | | * | | | | * | b 3 |
| 52 | 137.3 | 9.041 | M-0% | | | | * M | | | * | | | | * | 1 |
| 53 | 141.4 | 9.023 | M-0%; 30% | | | | * | * | | * | | | | * | b 3 |
| 54 | 126.3 | 9.027 | M-5% | | | | | * | | * | | | | * | |
| 55 | 134.9 | 9.020 | M-0% | | * | | * V | | | | | | | | 1 |
| 56 | 164.3 | 9.027 | M-5% | * | minor | | | * | | | | | | * | 1 |
| 57 | 190.0 | 9.019 | M-0%; 20% | | * | | * | * | | * | | | | | b 2 |
| 58 | 149.1 | 9.023 | | * | | | | | | | * | * | | | 2 |
| 59 | 148.8 | 9.041 | M-0%; 25% | minor | * | | * | * | | | | (IRR) | | | a 2 |
| 60 | 114.8 | | M-0% | ** | | | * | | | | * | | | | 1 |
| 61 | 187.5 | 9.019 | M-0%; 10% | * | | | * | * | | | | (IRR) | | | a 3 |
| 62 | 114.2 | 9.008 | M-30% | | * | | * | | | | | | | | a 3 |
| 62A | 137.5 | 9.052 | M-0%; 30% | | | | * | | * | | | | | * | b 3 |

Appendix 1.3.2 continued

| Locality and Sample Number | $Hb_{rel}$ | $b_o$ | I/M ratio | MINERALOGY | | | | | | | | | | | Assemblage |
|---|---|---|---|---|---|---|---|---|---|---|---|---|---|---|---|
| | | | | Chlorite | Kaolinite | Montmorillonite | Illite | MIXED LAYERS I/M(R) | I/M(IRR) | C-M | C-V | I-V | Calcite | | |
| 63 | 145.6 | 9.014 | M=0%; 30% | * | | | * | * | | | | | | | a 3 |
| 64 | 100.3 | 9.030 | M=0% | | | | * | | | * | | | | | 1 |
| 65 | 137.3 | 9.026 | M=0%; 30% | | | | * | * | | * | | | | | b 3 |
| 66A | 142.9 | 9.016 | | | | | | | | | * | * | * | | |
| 66B | 129.3 | 9.014 | M=0%; 30% | | | | * | * | | * | | | | | |
| 67 | 137.1 | 9.013 | M=0%; 20% | * | | | * | * | | | | | | | |
| 68 | 166.7 | 9.034 | M=0%; 20% | | | | * | * | | | * | | | | |
| 69 | 153.2 | 9.008 | M=0%; 20% | * | | | * | * | | | * (IRR) | | | | |
| 70 | 103.3 | 9.041 | M=0%; 20% | | | | * | * | | * | | | | | b 2 |
| 71 | 143.3 | 9.016 | M=0% | * | | | * | | | | | | * | | 1 |
| 72 | 137.6 | 8.997 | M=0%; 20% | | | | * | * | | * | | | | | b 2 |

| Locality and Sample No | $Hb_{rel}$ | $b_o$ | I/M Ratio | MINERALOGY | | | | | | | | | | | Assemblage |
|---|---|---|---|---|---|---|---|---|---|---|---|---|---|---|---|
| | | | | Chlorite | Kaolinite | Montmorillonite | Illite | MIXED LAYERS I/M(R) | I/M(IRR) | C-M | C-V | I-V | Calcite | | |
| 73 | 109.9 | | M = 0% | * | | | * | | | | | | * | | 1 |
| 74 | 140.8 | 9.038 | M=0%; 20% | | | | * | * | | * | | | | | b 2 |
| 75 | 147.8 | 9.022 | M = 0% | * | | | | | | | * | | | | 1 |
| 76 | 120.8 | 9.049 | | | minor * | | | | | * | * | | | | |
| 77 | 180.0 | 9.032 | M=0%; 40% | * | | * | $*_M$ | * | * | | | | | | 4 |
| 78 | 140.4 | 9.009 | M = 0% | * | | | * | | | | | | | | 1 |
| 79 | 132.8 | 9.042 | M = 5% | * | | | | * | | | | | | | 1 |
| 80 | 145.2 | 9.075 | | * | | | $*_V$ | | | | | | | | 1 |
| 81 | 134.0 | 9.038 | | | | | $*_V$ | | | | | * | | | 1 |
| 82 | 125.4 | 8.978 | M = 0% | * | | | $*_M$ | | | | | | | | 1 |
| 83 | 160.1 | 9.039 | M = 0% | * | minor * | | $*_V$ | | | | | | | | 1 |
| 84 | 136.4 | 9.004 | M = 0% | | minor * | * | $*_M$ | | | | | | | | 1 |

$Hb_{rel}$, $b_o$, I-M ratio and clay mineralogy per locality

KEY: I/M = illite-montmorillonite; I-V = illite-vermiculite; C-M = chlorite-montmorillonite; C-V = chlorite-vermiculite; (R) = regularly interstratified; (IRR) = randomly interstratified; M = amount of montmorillonite interstratified in illite structure.
$*_M$ = illite with montmorillonite behaviour; $*_V$ = illite with vermiculite behaviour

Appendix 1.4.1

| Sample No | Litho | Crystallinity mm | Crystallinity °2θ |
|---|---|---|---|
| 2 | P | 12.3 | 0.62 |
| 7 | P | 6.3 | 0.33 |
| 8 | P | 6.2 | 0.31 |
| 9 | P | 6.1 | 0.30 |
| 10 | P | 6.3 | 0.33 |
| 11 | P | 7.0 | 0.34 |
| 12 | P | 6.4 | 0.33 |
| 13 | P | 6.1 | 0.30 |
| 14 | P | 8.8 | 0.45 |
| 15 | P | 10.0 | 0.50 |
| 16 | P | 6.8 | 0.34 |
| 17 | P | 6.2 | 0.30 |
| 18 | P | 7.7 | 0.40 |
| 19 | P | 7.0 | 0.34 |
| 20 | P | 7.3 | 0.35 |
| 21 | P | 7.2 | 0.35 |
| 22 | P | 6.9 | 0.34 |
| 23 | P | 5.8 | 0.28 |
| 24 | S | 9.2 | 0.46 |
| 26 | P | 6.4 | 0.33 |
| 27 | P | 5.9 | 0.30 |
| 29 | P | 6.6 | 0.33 |
| 30 | P | 6.7 | 0.33 |
| 31 | C | 6.8 | 0.34 |
| 33 | P | 6.2 | 0.30 |
| 34 | P | 7.2 | 0.36 |
| 35 | P | 5.2 | 0.25 |
| 36 | P | 9.4 | 0.47 |
| 37 | C | 15.2 | 0.77 |
| 38 | P | 7.7 | 0.37 |
| 39 | P | 6.3 | 0.33 |
| 40 | P | 6.8 | 0.34 |
| 41 | S | 18.8 | 0.95 |
| 42 | S(P) | 9.6(7.2) | 0.48(0.36) |
| 43 | S | 8.5 | 0.43 |
| 44 | S | 6.0 | 0.29 |
| 45 | P | 7.6 | 0.37 |
| 46 | P | 5.9 | 0.30 |
| 47 | P | 7.6 | 0.38 |
| 48 | P | 7.6 | 0.38 |
| 49 | P | 6.1 | 0.29 |
| 50 | P | 7.6 | 0.39 |
| 51 | P | 7.4 | 0.38 |
| 52 | P | 8.2 | 0.43 |
| 53 | P | 8.1 | 0.42 |
| 54 | P | 6.8 | 0.34 |
| 55 | P | 8.0 | 0.39 |
| 56 | P | 8.6 | 0.44 |
| 57 | P | 9.5 | 0.46 |
| 58 | P | 8.1 | 0.42 |
| 59 | P | 8.1 | 0.42 |
| 60 | P | 5.7 | 0.27 |
| 61 | P | 9.6 | 0.47 |
| 62 | S(P) | 7.6(6.7) | 0.38(0.32) |
| 63 | P | 7.3 | 0.35 |
| 64 | P | 5.8 | 0.28 |
| 65 | P | 8.3 | 0.40 |
| 66A | P | 7.8 | 0.38 |
| 66B | P | 7.1 | 0.35 |
| 67 | C | 8.5 | 0.43 |
| 68 | P | 8.6 | 0.44 |
| 69 | P | 8.4 | 0.42 |
| 70 | P | 6.3 | 0.33 |
| 71 | P | 8.5 | 0.43 |
| 72 | P | 7.2 | 0.36 |
| 73 | P | 6.7 | 0.32 |
| 74 | P | 7.0 | 0.35 |
| 75 | P | 8.0 | 0.39 |
| 76 | P | 6.8 | 0.33 |
| 77 | S | 9 | 0.45 |
| 78 | P | 7.0 | 0.35 |
| 79 | P | 6.6 | 0.33 |
| 80 | P | 7.2 | 0.36 |
| 81 | P | 6.7 | 0.34 |
| 82 | P | 10.7 | 0.53 |
| 83 | P | 7.5 | 0.37 |
| 84 | P | 6.8 | 0.34 |

Appendix 1.4.1 Crystallinity values (Kubler Index).
KEY- Litho lithology; P pelite; S sandstone; C conglomerate.

APPENDIX 2.2.1

| Sample No | Grid Reference | Secondary Minerals in veins‡ and amygdales* | Recognised in field | Identification confirmed by | | | Additional Secondary minerals identified in laboratory |
|---|---|---|---|---|---|---|---|
| | | | | XRD | T/S | Probe | |
| CV1 | NT 276 726 | Quartz‡, Analcime‡ | * | | | | |
| CV2 | NT 268 734 | Analcime‡ | | | * | * | Calcite*, analcime‡ |
| CV3 | NT 268 734 | | | | * | | Analcime‡‡, natrolite‡ |
| CV4 | NT 596 851 | Calcite‡, barytes‡ | * | | * | * | Ikoite‡, analcime‡, calcite‡‡, natrolite‡ |
| CV5 | NT 603 848 | | | | * | | |
| CV6 | NT 621 835 | Quartz‡, calcite‡, barytes‡ | * | | | | |
| CV7 | NT 568 856 | Calcite‡ | * | * | * | | Celestine‡ |
| CV8 | NT 556 857 | Calcite‡, quartz‡ | * | | * | * | |
| CV9 | NT 543 857 | Calcite‡ | * | | * | * | Analcime‡ |
| CV10 | | Calcite‡ | * | | | | |
| CV11 | NT 501 860 | Calcite‡, dolomite‡ | * | * | * | | Analcime* |
| CV12 | NT 517 840 | Calcite‡, barytes‡ | * | | | | |
| CV13 | NT 555 840 | | | | * | | |
| CV14 | NT 545 824 | Quartz‡ | * | | * | | Analcime‡ |
| CV15 | NT 573 764 | | | | * | | |
| CV16 | NT 589 768 | Calcite‡ | * | | * | | |
| CV17 | NT 576 730 | | | | | | |
| CV18 | NT 511 760 | Haematite‡ | * | | * | | |
| CV19 | NT 103 789 | | | | * | | |
| CV20 | NT 059 740 | | | | * | | quartz‡ |
| CV21 | NT 228 720 | | | | * | | Calcite‡ |
| CV22 | NS 991 711 | Calcite‡ | * | | * | | |
| CV23 | NS 998 728 | | | | | | |
| CV24 | NS 988 727 | Pyrite‡ | * | | * | | Quartz* |
| CV25 | NO 422 025 | Calcite‡ | * | | | | |
| CV26 | NO 431 023 | Calcite‡ | * | | * | | Analcime‡ |
| CV27 | NT 461 998 | Calcite‡* | * | | * | | Analcime‡‡ |
| CV28 | NO 453 006 | Calcite‡, Quartz‡, Analcime‡, Natrolite‡* | * | * | * | * | |
| CV29 | NT 499 993 | Calcite‡, gonnardite* | * | | * | * | Quartz*, analcime*‡, natrolite‡* |
| CV30 | NO 524 014 | Calcite‡, ferrierite‡ | * | | * | * | Samidine‡, analcime‡ |
| CV31 | NO 433 049 | | | | * | | Quartz*, analcime*‡ |
| CV32 | NT 212 858 | Calcite‡* | * | | * | * | dolomite‡, quartz‡, ferrierite‡ |
| CV33 | NT 279 883 | Calcite‡, quartz‡, barytes‡ | * | * | * | | |
| CV34 | NT 277 875 | Calcite*, labradorite* barytes*‡ | * | * | * | | |
| CV35 | NT 274 869 | Calcite‡, analcime‡ | * | * | * | * | Analcime* |
| CV36 | NT 267 861 | Calcite‡*, analcime*‡, barytes* | * | * | * | | |
| CV37 | NS 616 803 | Calcite*, quartz* | * | | * | | |
| CV38 | NS 634 853 | Calcite‡, quartz*, heulandite* | * | | * | | Analcime‡* |
| CV39 | NS 835 839 | Calcite‡, pyrite‡ | * | | * | * | Quartz‡*, penninite‡*, analcime‡ |
| CV40 | NS 632 827 | Quartz* | * | | * | | Calcite‡ |
| CV41 | NS 628 807 | Ferrierite*, stilbite* | * | * | * | | Calcite* |
| CV42 | NS 627 892 | Stilbite*, heulandite* | * | * | * | * | Analcime*, sphene*‡ |
| CV43 | NS 631 881 | Heulandite | | | * | | Analcime‡ |

APPENDIX 2.2.1 continued

| Sample No | Grid Reference | Secondary Minerals in veins‡ and amygdales* | Recognised in Field | Identification confirmed by | | | Additional Secondary minerals identified in laboratory |
|---|---|---|---|---|---|---|---|
| | | | | XRD | T/S | Probe | |
| CV44 | NS 443 739 | Analcime*‡, thomsonite*‡, prehnite*‡ | * | * | * | | |
| CV45 | NS 389 607 | Quartz | * | * | | | |
| CV46 | NS 331 617 | Calcite*, Quartz*, Labradorite*, Analcime*‡, Laumontite*‡ | * | * | * | * | Analcime‡ |
| CV47 | NS 353 618 | Analcime*, Natrolite* | * | * | * | | Cristobolite*, analcime‡ |
| CV48 | NS 356 652 | Haematite | * | | | | |
| CV49 | NS 352 662 | Quartz*‡ | * | * | * | | Sphene‡, analcime‡ |
| CV50 | NS 347 671 | | | | * | | Natrolite‡, analcime‡ |
| CV51 | NS 345 723 | Calcite‡, labradorite‡ | * | * | * | | Cristobolite* |
| CV52 | NS 511 813 | Calcite‡, barytes‡, analcime*, natrolite* | * | * | * | | Analcime‡‡ |
| CV53 | NS 494 798 | Calcite*, analcime*, haematite* | * | * | * | | Analcime‡ Sphene‡, natrolite* |
| CV54 | NS 495 787 | Natrolite | * | | | | |
| CV55 | NS 496 784 | Barytes‡, calcite* | * | * | * | * | Chlorite‡ |
| CV56 | NS 491 773 | Barytes‡ | * | * | * | | Haematite‡, sphene‡, analcime‡ |
| CV57 | NS 215 582 | Labradorite‡ | * | * | * | | Analcime‡‡ |
| CV58 | NS 274 747 | | | | | | |
| CV59 | NS 268 736 | Natrolite‡*, wairakite*‡ | * | * | * | * | Sphene‡, haematite‡ |
| CV60 | NS 268 727 | | | | * | | Sphene‡ |
| CV61 | NS 263 717 | | | | * | | Analcime‡ |
| CV62 | NS 253 705 | Natrolite‡*, analcime* | * | * | * | * | |
| CV63 | NS 252 696 | Stilbite, chabazite rankinite | * | * | * | | |
| CV64 | NS 250 685 | Stilbite‡, chabazite‡, rankinite‡ | * | * | | | |
| CV65 | NS 247 672 | Stilbite*, chabazite*, rankinite* | * | * | | | |
| CV66 | NS 234 656 | | | | * | * | |
| CV67 | NS 228 648 | | | | * | | Quartz*, calcite* |
| CV68 | NS 222 638 | | | | * | | |
| CV69 | NS 358 555 | Thomsonite*, natrolite, Analcime, wairakite, Hydrogrossular*, Prehnite‡*‡, haematite‡ | * | * | * | * | Epidote*, analcime‡, mesolite* |
| CV70 | NS 382 571 | | | | | | |
| CV71 | NS 478 578 | Calcite | * | | | | |
| CV72 | NS 358 537 | Quartz, natrolite‡ | * | * | | | |
| CV73 | NS 507 543 | Quartz | * | | * | | Calcite‡ |
| CV74 | NS 493 528 | | | | * | | |
| CV75 | NS 474 558 | Calcite‡ | * | | * | | |
| CV76 | NS 457 529 | Analcime‡ | * | * | * | | Prehnite‡, sphene‡, analcime‡ |
| CV77 | NS 572 524 | Calcite* | * | | * | | |
| CV78 | NS 568 549 | Quartz*, prehnite* | * | * | * | * | Sphene‡, analcime‡ |
| CV79 | NS 646 490 | Calcite*, dolomite* | * | * | * | | |
| CV80 | NS 727 915 | Analcime‡*, heulandite‡* | * | * | * | * | Analcime‡, sphene‡ |

APPENDIX 2.2.1 continued

| Sample No | Grid Reference | Secondary Minerals in veins‡ and amygdales* | Recognition in field | Identification confirmed by | | | Additional Secondary minerals identified in laboratory |
|---|---|---|---|---|---|---|---|
| | | | | XRD | T/S | Probe | |
| CV81 | NS 727 925 | Calcite*, stilbite*, heulandite*, mordenite* | * | * | * | | Analcime |
| CV82 | NS 728 908 | Quartz*, labradorite* stilbite‡*, analcime‡* | * | * | * | | |
| CV83 | NS 727 888 | Laumontite‡ | * | * | * | | |
| CV84 | NS 724 879 | | | | * | * | Albite‡*‡ |
| CV85 | NS 492 598 | Prehnite‡* | * | | * | * | Analcime‡*, wairakite‡*, thomsonite‡*, sphene*, calcite*, haematite‡ |
| CV86 | NS 369 735 | Analcime, stilbite* prehnite*‡ | * | * | * | * | Sphene‡, quartz*, calcite*, analcime‡ albite*‡ |
| CV87 | NS 326 698 | Calcite‡, clinoptilolite‡, heulandite‡ | * | * | * | * | Quartz‡, analcime‡ |
| CV88 | NS 399 746 | | | | * | | Sphene‡, quartz*, calcite*‡, analcime |
| CV89 | NS 486 743 | Thomsonite‡*, prehnite‡* | * | * | * | * | Analcime*, |
| CV90 | NS 479 749 | Thomsonite*‡ | * | * | * | * | Prehnite‡, sphene‡ |
| CV91 | NS 480 756 | Thomsonite*‡ | * | * | * | * | Analcime‡, sphene‡, albite‡ |
| CV92 | NS 555 768 | | | | * | | Quartz*, calcite*, stilbite*, analcime‡ |
| CV93 | NS 526 769 | Thomsonite, laumontite | * | * | * | * | Cristobalite*, analcime*, chabazite*, natrolite*, wairakite, gonnnarite* |
| CV94 | NS 438 774 | Clinoptilolite‡, stilbite* | * | * | * | | Analcime‡, calcite* |
| CV95 | NS 434 765 | | * | | * | * | Stilbite‡‡, laumontite‡, sphene‡, albite‡ |
| CV96 | NS 636 796 | | | | | | Calcite‡*, sphene‡, quartz*, |
| CV97 | NS 675 920 | Quartz*, laumontite haematite* | * | * | * | * | Analcime*‡‡, albite‡ |
| CV98 | NS 683 922 | Laumontite | | * | | | |
| CV100 | NS 767 678 | | | | * | | Quartz*, calcite*‡, haematite* |
| | | | | | * | | |
| CV102 | NS 483 745 | | | | * | | Analcime*, natrolite*, |
| CV103 | NS 478 753 | | | | * | | Thomsonite*, analcime‡ |
| CV104 | NS 476 753 | | | | * | | Cristobolite*, |
| CV105 | NS 474 753 | Thomsonite‡ | | | * | | |
| CV106 | NS 552 771 | | | | | | |
| CV107 | NS 546 772 | | | | * | | |
| CV108 | NS 540 773 | | | | | | |
| CV109 | NS 539 770 | | | | * | | Calcite‡, |
| CV110 | NS 535 778 | | | | * | | Calcite‡, |
| CV111 | NS 435 772 | | | | * | | Analcime‡ |
| CV112 | NS 435 770 | Heulandite*, stilbite*‡ | * | * | * | * | Sphene*, quartz*, |
| CV113 | NS 434 769 | | | | | | |
| CV114 | NS 619 805 | | | | * | | Haematite‡, calcite‡, |
| CV115 | NS 616 802 | | | | | | |
| CV116 | NS 616 800 | | | | * | | Calcite* |
| CV117 | NS 618 800 | | | | * | | Calcite*‡, quartz*, |
| CV118 | NS 625 799 | | | | * | | |
| CV119 | NS 633 797 | | | | | | |
| CV 120 | NS 676 920 | | | | | | |
| CV121 | NS 682 922 | | | | * | | Quartz‡*, analcime‡ |
| CV122 | NS 689 924 | | | | | | |
| CV123 | NS 686 926 | | | | | | |
| CV124 | NT 214 871 | Quartz*, calcite‡, ferrierite‡‡ | * | * | | | |

APPENDIX 2.2.1

| Sample No | Grid Reference | Secondary Minerals in Veins‡ and amygdales* | Recognised in field | Identification confirmed by | | | Additional secondary minerals identified in laboratory |
|---|---|---|---|---|---|---|---|
| | | | | XRD | T/S | Probe | |
| CV125 | NT 223 873 | Calcite‡ | * | | | | |
| CV126 | NT 232 872 | Calcite | | | | | |
| CV127 | NT 255 883 | Quartz*, calcite*‡ | * | | | | |
| CV128 | NT 260 881 | Quartz*, calcite*, | * | | | | |
| CV 129 | NT 263 877 | Calcite*‡, Quartz*‡, | * | | | | |
| CV130 | NT 254 864 | Calcite‡ | * | | | | |
| CV131 | NT 254 866 | Natrolite*‡ | * | | | | |
| CV132 | NT 254 867 | Quartz*‡, calcite*‡ chalcedony | * | | | | |
| CV133 | NT 259 866 | Quartz*, calcite* | * | | | | |
| CV134 | NT 259 866 | Analcime*, natrolite*‡ | * | | | | |
| CV135 | NT 253 874 | Quartz*, calcite*, | * | | | | |
| CV136 | NT 267 864 | Quartz*, calcite*, | * | | | | |
| CV137 | NS 346 606 | Laumontite‡, analcime* | * | | | | |
| CV138 | NS 701 893 | Heulandite* | * | | | | |
| CV139 | NS 459 758 | Heulandite*, stilbite* | * | | | | |
| CV140 | NS 499 739 | Heulandite* | * | | | | |
| CV141 | NS 691 921 | Stilbite*, quartz* | * | | | | |

APPENDIX 2.2.1 Amygdale and Vein Assemblages in the Carboniferous Volcanics of the Midland Valley, Scotland: Localities.

* - amygdale mineral
‡ - vein mineral
‡‡ - replacement mineral

Appendix 2.2.1 continued

| Sample No | Grid Reference | Secondary Minerals in Veins‡ and Amygdales* | Recognised in field | Identification confirmed by | | | Additional minerals identified in laboratory |
|---|---|---|---|---|---|---|---|
| | | | | XRD | T/S | Probe | |
| L1 | NS4774 7534 | Empty vesicles | * | | | | |
| L2 | NS4782 7521 | Calcite‡, quartz‡, clays‡ | * | | | | |
| L4 | NS4778 7516 | Quartz‡, Analcime‡ | * | | | | |
| L8 | NS4765 7510 | Analcime‡ | * | | | | |
| L9 | NS4782 7499 | Analcime* | * | | | | |
| L10 | N4780 7493 | Natrolite‡, analcime*, chlorite‡ | * | | | | |
| L11 | NS4785 7487 | Thomsonite‡*, analcime* | * | | | | |
| L12 | NS4789 7484 | Analcime*, thomsonite‡ | * | | * | | |
| L13 | NS4794 7480 | Prehnite‡, thomsonite‡, analcime* | * | | | | |
| L14 | NS4798 7474 | Prehnite‡, thomsonite‡, analcime*‡, nimite (ni-chl) | * | | | | |
| L15 | NS4799 7464 | Analcime*, thomsonite* | * | | | | |
| L16 | NS4840 7432 | Analcime* | * | | | | |
| L17 | NS4876 7414 | Natrolite* | * | | | | |

Appendix 2.2.1 continued

| Sample No | Grid Reference | Secondary Minerals in Veins‡ and Amygdales* | Recognised in field | Identified confirmed by | | | Additional minerals identified in laboratory |
|---|---|---|---|---|---|---|---|
| | | | | XRD | T/S | Probe | |
| *1 | NS 35 55 | Haematite‡, chlorite‡ | | | | | |
| *2 | " " | Chlorite‡, epidote* | | | | | |
| *3 | " " | Epidote*‡, calcite*, chlorite*, prehnite*, analcime* | | | | | |
| *4 | " " | Epidote* | | | * | | |
| *5 | " " | Epidote*, calcite* | | | | | |
| *6 | " " | | | | | | |
| *7 | " " | Clays‡, calcite‡ | | | | | |
| *8 | " " | Thomsonite* | | | | | |
| CV69A | " " | | | | | | |
| CV69B(1) | " " | | | | | | |
| CV69B(11) | " " | | | | | | |
| CV69D | " " | Thomsonite* | | | | | |
| CV69I | " " | | | | | | |
| CV69J | " " | Epidote‡, garnet‡ (hydrogrossular) | | | | * | |

Appendix 2.2.2

| Mineal | Area | Found in |
|---|---|---|
| Analcime | Kellie Law, Fife | Basalt |
| | North of Abden shipyard, Kinghorn | Associated with calcite in veins in agglomerate |
| | Rock & Spindle, St Andrews. | Basalt |
| | Craighall, Ceres | |
| | Oprosite Sheep Craigs, North Berwick | with natrolite in tuff |
| | Canty Bay | with natrolite |
| | Rugged Knowe | with natrolite in basalt intrusives and veins in tuff |
| | Salisbury Crags, Edinburgh | with natrolite |
| | Castle Rock, Edinburgh | in cavities in basalt |
| | Muirdock Tunnel, Milngavie | with laumonite |
| | Bishopton railway tunnel, Renfrewshire | with prehnite |
| | Kilmalcolm, Renfrewshire | |
| Thomsonite | at Kilmalcolm | |
| | Hills S of Port Glasgow | |
| | Bishopston | on prehnite |

Appendix 2.2.2

Zeolite localities described by Heddle (1924) and incorporated in text.

| Mineral | Analcime 1 | 2 | 3 | 4 | 5 | 6 | 7 | 8 | 9 | 10 | 11 | 12 | 13 | 14 | 15 | 16 | 17 | 18 | 19 | 20 | 21 | 22 | 23 | 24 | 25 | 26 |
|---|---|---|---|---|---|---|---|---|---|---|---|---|---|---|---|---|---|---|---|---|---|---|---|---|---|---|
| PP/B No | CV4PA (15) | CV62 (13) | CV86 (1) | CV86 (7) | CV3 (1) | CV35 (2) | CV35 (13) | CV288 (13) | CV288 (14) | CV69K (29) | CV69K (30) | CV28 (2) | CV28 (7) | CV59B (2) | CV59B (6) | CV59B (14) | CV59B (15) | CV69K (8) | CV69K (9) | CV69K (10) | CV69K (11) | CV69K (20) | CV69K (21) | CV69K (23) | CV69K (24) | CV69K (25) |
| $SiO_2$ | 54.64 | 52.07 | 55.88 | 57.13 | 54.55 | 53.54 | 53.07 | 52.53 | 50.46 | 55.73 | 56.77 | 52.70 | 53.47 | 54.83 | 53.99 | 55.54 | 53.76 | 55.49 | 54.91 | 55.76 | 55.12 | 55.90 | 55.08 | 55.24 | 55.37 | 55.15 |
| $TiO_2$ | 0.01 | 0.01 | - | - | 0.02 | - | - | 0.03 | - | 0.01 | - | - | - | - | - | 0.06 | - | 0.01 | - | - | - | 0.01 | - | - | - | - |
| $Al_2O_3$ | 23.04 | 26.84 | 23.31 | 23.02 | 22.56 | 23.76 | 23.59 | 30.03 | 29.03 | 22.74 | 23.25 | 29.68 | 31.12 | 22.32 | 22.39 | 22.39 | 24.71 | 22.22 | 22.30 | 22.31 | 21.92 | 22.29 | 22.04 | 22.30 | 21.92 | 22.17 |
| FeO | - | 0.05 | - | 0.03 | - | - | - | 0.05 | - | - | - | 0.10 | - | - | 0.03 | - | 0.16 | - | 0.06 | 0.01 | 0.04 | - | 0.06 | 0.02 | - | 0.04 |
| MnO | 0.01 | 0.06 | - | 0.04 | - | - | - | - | 0.01 | 0.01 | 0.04 | - | - | 0.01 | - | - | 0.07 | 0.01 | 0.03 | 0.01 | - | - | - | - | 0.01 | - |
| MgO | 0.03 | - | - | 0.01 | - | - | 0.01 | - | - | - | - | 0.10 | - | - | 0.06 | 0.05 | 0.02 | 0.01 | - | - | - | 0.02 | - | 0.01 | 0.02 | - |
| CaO | 0.09 | 0.14 | 0.06 | - | 0.30 | 0.29 | 0.36 | 0.06 | 0.06 | 0.03 | 0.05 | 0.03 | 0.05 | 0.11 | 0.09 | 0.06 | 0.67 | 0.03 | - | - | 0.02 | 0.04 | 0.03 | 0.05 | 0.06 | 0.08 |
| $Na_2O$ | 13.61 | 11.61 | 13.03 | 12.51 | 12.98 | 13.76 | 13.90 | 12.29 | 13.43 | 13.07 | 12.89 | 12.95 | 12.51 | 13.14 | 13.40 | 13.14 | 13.05 | 13.03 | 13.06 | 13.05 | 13.16 | 12.43 | 12.53 | 12.57 | 12.60 | 12.70 |
| $K_2O$ | 0.01 | 0.02 | 0.03 | 0.03 | 0.03 | 0.03 | 0.03 | 0.01 | 0.02 | 0.04 | 0.07 | 0.05 | 0.03 | 0.03 | 0.01 | 0.06 | 0.17 | 0.07 | 0.02 | 0.06 | 0.03 | 0.05 | 0.03 | 0.04 | 0.02 | 0.02 |
| $P_2O_5$ | - | 0.10 | - | - | - | - | - | - | - | 0.03 | - | - | - | - | 0.06 | 0.19 | 0.09 | - | - | - | - | 0.03 | - | - | 0.04 | 0.02 |
| NiO | - | 0.12 | - | - | - | - | - | 0.10 | 0.02 | - | - | - | - | 0.07 | 0.10 | - | - | - | - | - | - | - | - | - | 0.05 | 0.10 |
| $Cr_2O_3$ | - | 0.01 | - | - | - | - | - | 0.05 | - | - | - | - | - | - | 0.01 | 0.04 | 0.01 | - | - | - | - | 0.04 | 0.01 | 0.01 | 0.02 | - |
| BaO | - | 0.09 | - | - | - | - | - | 0.21 | 0.09 | 0.10 | 0.19 | - | - | 0.05 | 0.12 | 0.15 | 0.30 | - | - | - | - | 0.09 | 0.18 | 0.13 | 0.04 | 0.05 |
| SrO | 0.01 | 0.05 | - | - | - | 0.05 | 0.01 | 0.04 | 0.02 | 0.01 | - | 0.05 | 0.09 | - | 0.01 | - | - | - | 0.04 | - | 0.01 | - | - | 0.04 | 0.05 | - |
| TOTAL | 91.49 | 91.14 | 92.29 | 92.77 | 90.44 | 91.43 | 90.59 | 95.37 | 93.14 | 91.81 | 93.26 | 95.66 | 97.27 | 90.62 | 90.40 | 91.58 | 92.82 | 90.87 | 90.22 | 91.12 | 90.30 | 90.92 | 89.93 | 90.21 | 90.20 | 90.48 |
| Recalculated on the basis of 6 oxygens | | | | | | | | | | | | | | | | | | | | | | | | | | |
| Si | 2.01 | 1.91 | 2.02 | 2.05 | 2.02 | 1.97 | 1.97 | 1.85 | 1.83 | 2.03 | 2.03 | 1.84 | 2.10 | 2.03 | 2.01 | 2.03 | 1.96 | 2.01 | 2.04 | 2.05 | 2.04 | 2.05 | 2.05 | 2.05 | 2.05 | 2.04 |
| Ti | - | - | - | - | - | - | - | - | - | - | - | - | - | - | - | - | - | 0.01 | - | - | - | - | - | - | - | - |
| Al | 1.00 | 1.16 | 1.00 | 0.97 | 0.99 | 1.03 | 1.03 | 1.24 | 1.24 | 0.97 | 0.98 | 1.34 | 0.91 | 0.97 | 0.98 | 0.97 | 1.06 | 0.96 | 0.97 | 0.96 | 0.96 | 0.97 | 0.97 | 0.97 | 0.95 | 0.97 |
| Fe | - | - | - | - | - | - | - | - | - | - | - | - | - | - | - | - | 0.01 | - | - | - | - | - | - | - | - | - |
| Mn | - | - | - | - | - | - | - | - | - | - | - | - | - | - | 0.01 | - | - | - | - | - | - | - | - | - | - | - |
| Mg | - | - | - | - | - | - | - | - | - | - | - | - | - | - | 0.01 | - | - | - | - | - | - | - | - | - | - | - |
| Ca | - | 0.02 | - | - | 0.01 | 0.01 | 0.01 | - | - | - | - | - | - | 0.02 | 0.01 | - | 0.02 | - | - | - | - | - | - | - | - | - |
| Na | 0.97 | 0.83 | 0.92 | 0.87 | 0.93 | 0.98 | 0.97 | 0.86 | 0.91 | 0.92 | 0.89 | 0.89 | 0.89 | 0.94 | 0.97 | 0.93 | 0.92 | 0.93 | 0.94 | 0.93 | 0.95 | 0.88 | 0.90 | 0.90 | 0.91 | 0.91 |
| K | - | - | - | - | - | - | - | - | - | - | 0.01 | - | - | - | - | - | 0.01 | - | - | - | - | - | - | - | - | - |
| Ni | - | 0.01 | - | - | - | - | - | - | - | - | - | - | - | - | 0.01 | - | - | - | - | - | - | - | - | - | - | - |
| Ca | - | 0.01 | - | - | - | - | - | - | - | - | - | - | - | - | - | - | - | - | - | - | - | - | - | - | - | - |
| Cr | - | - | - | - | - | - | - | - | - | - | - | - | - | - | - | - | - | - | - | - | - | - | - | - | - | - |
| Ba | - | - | - | - | - | - | - | 0.01 | - | - | 0.01 | - | - | - | - | 0.01 | 0.01 | - | - | - | - | - | 0.01 | - | - | - |
| Sr | - | - | - | - | - | - | - | - | - | - | - | - | - | - | - | - | - | - | - | - | - | - | - | - | - | - |
| IX | 0.97 | 0.86 | 0.92 | 0.87 | 0.94 | 0.99 | 0.98 | 0.85 | 0.94 | 0.92 | 0.91 | 0.89 | 0.89 | 0.95 | 1.00 | 0.94 | 0.97 | 0.94 | 0.94 | 0.93 | 0.95 | 0.88 | 0.91 | 0.90 | 0.91 | 0.91 |
| IY | 1.00 | 1.16 | 1.00 | 0.97 | 0.99 | 1.03 | 1.03 | 1.24 | 1.24 | 0.97 | 0.98 | 1.34 | 0.91 | 0.97 | 0.98 | 0.97 | 1.06 | 0.96 | 0.97 | 0.96 | 0.96 | 0.97 | 0.97 | 0.97 | 0.95 | 0.97 |
| IZ | 2.01 | 1.98 | 2.02 | 2.05 | 2.02 | 1.97 | 1.97 | 1.85 | 1.83 | 2.03 | 2.03 | 1.84 | 2.10 | 2.03 | 2.01 | 2.03 | 1.96 | 2.04 | 2.04 | 2.05 | 2.04 | 2.05 | 2.05 | 2.05 | 2.05 | 2.04 |

Appendix 2.4.1 Electron microprobe analyses of analcime

| Mineral | Natrolite 1 | 2 | 3 | 4 | 5 | 6 | 7 | 8 | 9 | 10 | 11 | 12 |
|---|---|---|---|---|---|---|---|---|---|---|---|---|
| PT/S No | CV93 (33) | CV93 (9) | CV28 (3) | CV28 (4) | CV28 (5) | CV28 (6) | CV59B (4) | CV59B (5) | CV59B (7) | CV59B (13) | CV59B (16) | CV59B (17) |
| $SiO_2$ | 48.04 | 46.60 | 47.88 | 47.41 | 47.42 | 47.44 | 47.25 | 47.76 | 47.68 | 46.35 | 64.48 | 46.16 |
| $TiO_2$ | - | - | 0.02 | - | - | 0.06 | 0.02 | - | - | 0.02 | - | 0.01 |
| $Al_2O_3$ | 29.11 | 26.75 | 26.94 | 26.13 | 26.48 | 26.92 | 24.96 | 25.78 | 24.50 | 26.44 | 26.44 | 26.40 |
| FeO | - | 0.05 | 0.01 | 0.02 | - | 0.02 | 0.30 | 0.11 | 0.24 | 0.17 | 0.08 | 0.13 |
| MnO | 0.06 | - | 0.03 | 0.02 | 0.05 | 0.05 | - | 0.03 | 0.04 | - | - | - |
| MgO | 0.02 | - | - | 0.02 | 0.07 | 0.03 | 0.01 | 0.03 | - | 0.03 | - | 0.06 |
| CaO | 0.06 | 0.05 | 0.02 | 0.01 | 0.08 | 0.02 | 0.42 | 0.40 | 0.58 | 0.82 | 0.30 | 0.64 |
| $Na_2O$ | 15.85 | 15.94 | 15.35 | 15.61 | 15.46 | 15.96 | 14.32 | 15.38 | 14.68 | 14.81 | 14.16 | 14.20 |
| $K_2O$ | 0.04 | 0.02 | 0.04 | 0.04 | 0.01 | - | 0.07 | - | 0.03 | - | 0.04 | - |
| $P_2O_5$ | - | 0.04 | - | - | - | - | 0.04 | 0.23 | - | 0.03 | 0.17 | - |
| NiO | 0.01 | - | - | - | - | - | - | - | - | 0.09 | 0.04 | 0.04 |
| $Cr_2O_3$ | - | - | - | - | - | - | 0.03 | 0.08 | - | - | - | - |
| SrO | 0.14 | 0.11 | - | - | - | - | 0.27 | - | 0.06 | 0.21 | 0.17 | 0.10 |
| BaO | 0.04 | - | - | - | - | 0.07 | - | - | 0.07 | - | - | - |
| TOTAL | 93.37 | 89.56 | 90.29 | 89.26 | 89.57 | 90.55 | 87.69 | 89.80 | 87.88 | 88.97 | 87.88 | 87.74 |
| Recalculated on the basis of 80 oxygens | | | | | | | | | | | | |
| Si | 23.52 | 23.84 | 24.19 | 24.28 | 24.18 | 23.99 | 24.64 | 24.32 | 24.80 | 23.92 | 24.08 | 24.00 |
| Ti | - | - | 0.01 | - | - | 0.02 | - | - | - | - | - | - |
| $Al^{+3}$ | 16.80 | 16.16 | 16.04 | 15.77 | 15.91 | 16.05 | 15.36 | 15.44 | 15.04 | 16.08 | 16.16 | 16.16 |
| Fe | - | - | 0.03 | 0.01 | - | 0.01 | 0.16 | 0.08 | 0.08 | 0.08 | - | 0.08 |
| Mn | - | - | 0.13 | 0.01 | 0.02 | 0.02 | - | - | - | - | - | - |
| Mg | - | - | - | 0.01 | 0.05 | 0.03 | - | - | - | - | - | 0.08 |
| Ca | - | - | 0.13 | 0.01 | 0.05 | 0.01 | 0.24 | 0.24 | 0.32 | 0.48 | 0.16 | 0.32 |
| Na | 15.04 | 15.84 | 15.03 | 15.50 | 15.28 | 15.65 | 14.48 | 15.20 | 14.80 | 14.80 | 14.24 | 14.32 |
| K | - | - | - | - | 0.01 | - | 0.16 | - | - | - | - | - |
| P | - | - | - | - | - | - | - | 0.08 | - | - | 0.08 | - |
| Ni | - | - | - | - | - | - | - | - | - | - | - | - |
| Cr | - | - | - | - | - | - | - | - | - | - | - | - |
| Sr | - | - | - | - | - | - | 0.16 | - | - | 0.08 | 0.08 | - |
| Ba | - | - | - | - | - | - | - | - | - | - | - | - |
| ΣX | 15.04 | 15.84 | 15.33 | 15.54 | 15.41 | 15.74 | 15.20 | 15.60 | 15.20 | 15.44 | 14.56 | 14.80 |
| ΣY | 40 32 | 40.00 | 40.23 | 40.05 | 40.09 | 40.04 | 40.00 | 39.76 | 39.84 | 40.24 | 40.24 | 40.24 |
| ΣZ | | | | | | | | | | | | |

Appendix 2.4.2 Electron microprobe analyses of natrolite

| Mineral | Thomsonite 1 | 2 | 3 | 4 | 5 | 6 | 7 | 8 | 9 | 10 | 11 | 12 | 13 | 14 | 15 | 16 | 17 |
|---|---|---|---|---|---|---|---|---|---|---|---|---|---|---|---|---|---|
| PT/S No | CV3CVA (7) | CV3CVA (8) | CV93 (1) | CV93 (3) | CV93 (4) | CV93 (32) | CV93 (37) | CV93 (38) | CV93 (41) | CV93 (13) | CV93 (14) | CV69X (19) | CV69X (25) | CV93 (7) | CV93 (6) | CV93 (11) | CV93 (12) |
| $SiO_2$ | 39.48 | 39.19 | 39.29 | 37.21 | 38.78 | 40.33 | 38.59 | 38.72 | 39.40 | 38.52 | 39.26 | 38.16 | 38.71 | 38.72 | 39.97 | 38.81 | 39.68 |
| $TiO_2$ | 0.03 | 0.01 | 0.03 | 0.02 | - | 0.01 | - | 0.03 | 0.01 | - | - | - | - | 0.01 | - | - | - |
| $Al_2O_3$ | 29.87 | 29.57 | 28.56 | 27.86 | 28.68 | 29.59 | 28.89 | 29.21 | 29.26 | 28.53 | 28.22 | 30.58 | 29.63 | 29.09 | 28.23 | 28.27 | 28.01 |
| FeO | 0.56 | 0.18 | - | 0.04 | 0.19 | 0.04 | 0.09 | 0.03 | 0.02 | 0.04 | 0.01 | 0.02 | - | 0.01 | 0.04 | - | 0.09 |
| MnO | 0.01 | 0.05 | - | 0.02 | - | - | 0.01 | - | - | 0.01 | - | - | 0.01 | 0.05 | - | - | 0.03 |
| MgO | 0.25 | 0.05 | 0.02 | - | 0.02 | - | 0.01 | 0.03 | - | 0.01 | 0.01 | 0.01 | - | - | - | 0.02 | - |
| CaO | 11.23 | 11.71 | 11.61 | 11.36 | 11.80 | 11.88 | 12.41 | 12.67 | 12.13 | 11.81 | 11.86 | 11.92 | 11.31 | 12.30 | 11.11 | 11.20 | 11.46 |
| $Na_2O$ | 3.92 | 4.51 | 5.10 | 4.67 | 4.73 | 4.72 | 4.82 | 3.96 | 4.80 | 4.74 | 4.98 | 3.59 | 4.18 | 4.62 | 5.22 | 4.97 | 5.14 |
| $K_2O$ | 1.31 | 0.02 | 0.03 | 0.04 | 0.09 | 0.04 | 0.07 | 0.01 | 0.12 | 0.02 | - | 0.02 | 0.02 | 0.05 | 0.03 | 0.01 | 0.05 |
| $P_2O_5$ | - | - | - | 0.06 | 0.03 | 0.11 | - | - | 0.06 | 0.03 | 0.04 | - | 0.08 | 0.06 | 0.07 | 0.08 | 0.07 |
| NiO | - | - | - | - | 0.01 | - | 0.02 | - | - | 0.03 | - | - | - | 0.16 | - | - | 0.03 |
| $Cr_2O_3$ | - | - | 0.03 | - | - | - | 0.02 | - | - | 0.09 | - | 0.07 | 0.03 | - | - | 0.02 | 0.04 |
| SrO | - | - | 0.44 | 0.43 | 0.55 | 0.26 | 0.50 | 0.58 | 0.49 | 0.27 | 0.17 | 0.59 | 0.52 | 0.28 | 0.23 | 0.16 | 0.19 |
| BaO | 0.12 | - | - | - | 0.04 | - | - | - | 0.04 | 0.04 | - | - | 0.02 | 0.01 | 0.01 | 0.03 | 0.05 |
| TOTAL | 86.78 | 85.29 | 85.11 | 81.71 | 84.92 | 86.98 | 85.45 | 85.24 | 86.33 | 84.14 | 84.55 | 84.96 | 84.51 | 85.36 | 84.91 | 83.57 | 84.77 |
| Recalculated on the basis of 80 oxygens | | | | | | | | | | | | | | | | | |
| Si | 21.15 | 21.20 | 21.44 | 21.12 | 21.20 | 21.44 | 21.04 | 21.04 | 21.20 | 21.20 | 21.52 | 20.72 | 21.12 | 21.12 | 21.76 | 21.44 | 21.68 |
| Ti | 0.01 | 0.01 | - | - | - | - | - | - | - | - | - | - | - | - | - | - | - |
| $Al^{+3}$ | 18.86 | 18.85 | 18.32 | 18.64 | 18.48 | 18.48 | 18.56 | 18.72 | 18.56 | 18.56 | 18.24 | 19.60 | 19.04 | 18.64 | 18.08 | 18.40 | 18.00 |
| Fe | 0.25 | 0.08 | - | - | 0.08 | - | - | - | - | - | - | - | - | - | - | - | - |
| Mn | 0.01 | 0.03 | - | - | - | - | - | - | - | - | - | - | - | - | - | - | - |
| Mg | 0.20 | 0.04 | - | - | - | - | - | - | - | - | - | - | - | - | - | - | - |
| Ca | 6.44 | 6.79 | 6.80 | 6.88 | 6.96 | 6.72 | 7.28 | 7.36 | 6.96 | 6.96 | 6.96 | 6.96 | 6.64 | 7.20 | 6.48 | 6.64 | 6.72 |
| Na | 4.07 | 4.73 | 5.36 | 5.12 | 5.04 | 4.88 | 5.12 | 4.16 | 5.04 | 5.04 | 5.28 | 3.76 | 4.40 | 4.88 | 5.52 | 5.36 | 5.44 |
| K | 0.90 | 0.02 | - | - | 0.08 | - | 0.08 | - | 0.08 | - | - | - | - | - | - | - | - |
| P | - | - | - | - | - | 0.08 | - | - | - | - | - | - | - | - | - | - | - |
| Ni | - | - | - | - | - | - | - | - | - | - | - | - | - | - | - | - | - |
| Cr | - | - | - | - | - | - | - | - | - | - | - | - | - | - | - | - | - |
| Sr | - | - | 0.16 | 0.16 | 0.16 | 0.08 | 0.16 | 0.16 | 0.16 | 0.16 | 0.08 | 0.16 | 0.16 | 0.08 | 0.08 | 0.08 | 0.08 |
| Ba | 0.03 | - | - | - | - | - | - | - | - | - | - | - | - | - | - | - | - |
| ΣX | 11.91 | 11.70 | 12.32 | 12.16 | 12.32 | 11.76 | 12.64 | 11.68 | 12.24 | 12.16 | 12.32 | 10.88 | 11.20 | 12.16 | 12.08 | 12.08 | 12.14 |
| ΣY | 40.01 | 40.05 | 39.76 | 39.76 | 39.68 | 39.92 | 39.60 | 39.76 | 39.76 | 39.76 | 39.76 | 40.32 | 40.16 | 39.76 | 39.84 | 39.84 | 39.68 |
| ΣZ | | | | | | | | | | | | | | | | | |

Appendix 2.4.3 Electron microprobe analyses of thomsonite

| Mineral | Gonnardite 1 | 2 | 3 | 4 |
|---|---|---|---|---|
| PT/S No | CV29C (5) | CV29C (6) | CV29C (7) | CV93 (2) |
| $SiO_2$ | 42.04 | 40.88 | 37.99 | 41.42 |
| $TiO_2$ | - | 0.04 | - | 0.02 |
| $Al_2O_3$ | 29.03 | 28.24 | 27.62 | 25.71 |
| FeO | 0.27 | 1.45 | 3.86 | - |
| MnO | - | 0.02 | - | 0.03 |
| MgO | 0.27 | 1.51 | 2.27 | - |
| CaO | 7.03 | 7.80 | 8.97 | 6.15 |
| $Na_2O$ | 8.96 | 7.11 | 5.03 | 9.28 |
| $K_2O$ | 0.04 | 0.04 | 0.03 | 0.03 |
| $P_2O_5$ | - | - | - | 0.08 |
| NiO | - | - | - | 0.05 |
| $Cr_2O_3$ | - | - | - | - |
| SrO | - | - | - | 0.24 |
| BaO | - | 0.02 | 0.10 | 0.03 |
| TOTAL | 87.64 | 87.11 | 85.87 | 83.04 |
| Recalculated on the basis of 80 oxygens | | | | |
| Si | 22.09 | 21.73 | 20.82 | 22.96 |
| Ti | - | 0.02 | - | - |
| $Al^{+3}$ | 17.98 | 17.69 | 17.85 | 16.80 |
| $Fe^{+3}$ | 0.12 | 0.65 | 1.77 | - |
| Mn | - | 0.01 | - | - |
| Mg | 0.22 | 1.20 | 1.85 | - |
| Ca | 3.96 | 4.45 | 5.27 | 3.68 |
| Na | 9.13 | 7.33 | 5.35 | 10.00 |
| K | - | 0.03 | 0.02 | - |
| P | - | - | - | - |
| Ni | - | - | - | - |
| Cr | - | - | - | - |
| Sr | - | - | - | 0.03 |
| Ba | - | - | 0.02 | - |
| ΣX | 13.43 | 13.69 | 14.28 | 13.71 |
| ΣY | 40.07 | 39.42 | 38.67 | 39.76 |
| ΣZ | | | | |

Appendix 2.4.4 Electron microprobe analyses of gonnardite

| Mineral | Mesolite 1 | 2 | Gmelinite |
|---|---|---|---|
| PI/S No | CV69 (8) | CV69(10) | (9) |
| $SiO_2$ | 41.26 | 40.66 | 50.32 |
| $TiO_2$ | 0.05 | - | - |
| $Al_2O_3$ | 28.94 | 29.90 | 20.56 |
| FeO | 0.10 | 0.09 | 0.05 |
| MnO | - | - | 0.05 |
| MgO | - | - | - |
| CaO | 10.50 | 11.75 | 7.38 |
| $Na_2O$ | 5.68 | 5.02 | 6.23 |
| $K_2O$ | 0.03 | 0.02 | - |
| $P_2O_5$ | 0.07 | 0.02 | - |
| NiO | 0.06 | - | - |
| $Cr_2O_3$ | 0.10 | - | 0.03 |
| SrO | 0.52 | 0.36 | 0.11 |
| BaO | 0.17 | - | 0.94 |
| TOTAL | 87.48 | 84.82 | 84.82 |
| Recalculated on the basis of 30 oxygens (mesolite) + 48 oxygens (gmelinite) | | | |
| Si | 8.19 | 8.04 | 8.04 |
| Ti | - | - | - |
| $Al_{+3}$ | 6.75 | 6.96 | 6.96 |
| Fe | 0.03 | 0.03 | 0.03 |
| Mn | - | - | - |
| Mg | - | - | - |
| Ca | 2.22 | 2.49 | 2.49 |
| Na | 2.19 | 1.92 | 1.92 |
| K | - | - | - |
| P | - | - | - |
| Ni | - | - | - |
| Cr | 0.03 | - | - |
| Sr | 0.06 | 0.03 | 0.03 |
| Ba | - | - | - |
| ΣX | 4.53 | 4.47 | 4.47 |
| ΣY | 14.94 | 15.00 | 15.45 |
| ΣZ | | | |

Appendix 2.4.5 Electron microprobe analyses of mesolite and gmelinite

| Mineral | Laumontite 1 | 2 | 3 | 4 | 5 | 6 |
|---|---|---|---|---|---|---|
| PT/S No | CV93 (46) | CV93 (47) | CV93 (53) | CV93 (51) | CV93 (54) | CV93 (19) |
| $SiO_2$ | 51.26 | 51.36 | 52.30 | 52.22 | 51.09 | 51.81 |
| $TiO_2$ | - | - | - | 0.01 | 0.09 | - |
| $Al_2O_3$ | 21.34 | 21.73 | 21.57 | 21.64 | 21.35 | 21.23 |
| FeO | 0.03 | 0.02 | 0.02 | 0.04 | 1.26 | 0.04 |
| MnO | 0.07 | 0.01 | 0.02 | 0.01 | 0.01 | 0.01 |
| MgO | - | - | - | - | - | 0.01 |
| CaO | 12.13 | 11.29 | 11.31 | 11.93 | 11.80 | 11.32 |
| $Na_2O$ | 0.04 | 0.02 | 0.08 | 0.10 | 0.08 | 0.15 |
| $K_2O$ | 0.65 | 1.18 | 0.81 | 0.72 | 0.62 | 0.96 |
| $P_2O_5$ | 0.07 | 0.08 | 0.07 | 0.03 | 0.08 | 0.05 |
| NiO | - | 0.01 | - | 0.05 | - | 0.04 |
| $Cr_2O_3$ | - | - | 0.01 | - | 0.05 | 0.02 |
| SrO | 0.16 | 0.26 | 0.20 | 0.19 | 0.11 | 0.19 |
| BaO | - | - | - | 0.02 | 0.05 | - |
| TOTAL | 85.70 | 85.96 | 86.39 | 86.96 | 86.59 | 85.83 |
| Recalculated on the basis of 48 oxygens | | | | | | |
| Si | 15.98 | 15.98 | 16.13 | 16.03 | 15.89 | 16.13 |
| Ti | - | - | - | - | - | - |
| $Al_{+3}$ | 7.82 | 7.97 | 7.82 | 7.82 | 7.82 | 7.78 |
| Fe | - | - | - | - | 0.34 | - |
| Mn | - | - | - | - | - | - |
| Mg | - | - | - | - | - | - |
| Ca | 4.03 | 3.74 | 3.74 | 3.94 | 3.94 | 3.79 |
| Na | - | - | 0.05 | 0.05 | 0.05 | 0.10 |
| K | 0.24 | 0.48 | 0.34 | 0.29 | 0.24 | 0.38 |
| P | - | - | - | - | - | - |
| Ni | - | - | - | - | - | - |
| Cr | - | - | - | - | - | - |
| Sr | 0.05 | 0.05 | 0.05 | 0.05 | - | 0.05 |
| Ba | - | - | - | - | - | - |
| X | 4.32 | 4.27 | 4.18 | 4.33 | 4.57 | 4.32 |
| ΣY | 23.80 | 23.95 | 23.95 | 23.85 | 23.71 | 23.91 |
| ΣZ | | | | | | |

Appendix 2.4.6 Electron micrprobe analyses of laumontite

| Mineral | Chabazite 1 | 2 | 3 | 4 |
|---|---|---|---|---|
| PT/S No | CV93 (50) | CV93 (52) | CV93 (57) | CV93 (59) |
| $SiO_2$ | 47.29 | 48.22 | 48.89 | 49.70 |
| $TiO_2$ | 0.01 | - | - | 0.02 |
| $Al_2O_3$ | 20.61 | 21.36 | 20.62 | 20.75 |
| FeO | 0.98 | 1.40 | 0.03 | - |
| MnO | - | 0.06 | 0.03 | 0.02 |
| MgO | 0.48 | 0.70 | 0.05 | 0.01 |
| CaO | 8.92 | 8.34 | 11.47 | 11.82 |
| $Na_2O$ | 0.06 | 0.04 | 0.03 | 0.04 |
| $K_2O$ | 1.76 | 2.13 | 0.64 | 0.66 |
| $P_2O_5$ | 0.04 | 0.08 | 0.08 | 0.05 |
| NiO | 0.01 | - | - | - |
| $Cr_2O_3$ | - | - | - | 0.03 |
| SrO | 0.20 | 0.14 | 0.17 | 0.18 |
| BaO | - | 0.01 | 0.02 | 0.02 |
| TOTAL | 80.36 | 82.48 | 82.03 | 83.30 |
| Recalculated on the basis of 72 oxygens | | | | |
| Si | 23.76 | 23.62 | 23.90 | 23.90 |
| Ti | - | - | - | - |
| Al | 12.17 | 12.31 | 11.80 | 11.81 |
| Fe | 0.43 | 0.58 | - | - |
| Mn | - | - | - | - |
| Mg | 0.36 | 0.50 | - | - |
| Ca | 4.82 | 4.39 | 5.98 | 6.12 |
| Na | 0.07 | 0.07 | - | 0.07 |
| K | 1.15 | 1.30 | 0.43 | 0.43 |
| P | - | - | - | - |
| Ni | - | - | - | - |
| Cr | - | - | - | - |
| Sr | 0.07 | 0.07 | 0.07 | 0.07 |
| Ba | - | - | - | - |
| ΣX | 6.90 | 6.91 | 6.48 | 6.69 |
| ΣY | 35.93 | 35.93 | 35.78 | 35.71 |
| ΣZ | | | | |

Appendix 2.4.7 Electron microprobe analyses of chabazite

| Mineral | Wairakite 1 | 2 | 3 |
|---|---|---|---|
| FT/S No | CV69X (19) | CV69X (22) | CV93 (18) |
| $SiO_2$ | 51.10 | 53.16 | 50.33 |
| $TiO_2$ | - | 0.02 | - |
| $Al_2O_3$ | 20.93 | 21.74 | 20.06 |
| FeO | - | 0.02 | 0.06 |
| MnO | - | - | - |
| MgO | - | - | 0.02 |
| CaO | 10.12 | 10.69 | 10.48 |
| $Na_2O$ | 0.34 | 0.23 | 0.21 |
| $K_2O$ | 0.60 | 0.69 | 1.08 |
| $P_2O_5$ | 0.14 | - | 0.02 |
| NiO | - | 0.03 | 0.01 |
| $Cr_2O_3$ | 0.01 | - | 0.03 |
| SrO | 0.14 | 0.18 | 0.13 |
| BaO | - | 0.01 | 0.03 |
| Recalculated on the basis of 6 oxygens | | | |
| Si | 2.03 | 2.03 | 2.03 |
| Ti | - | - | - |
| $Al^{+3}$ | 0.98 | 0.98 | 0.95 |
| Fe | - | - | - |
| Mn | - | - | - |
| Mg | - | - | - |
| Ca | 0.43 | 0.44 | 0.46 |
| Na | 0.02 | 0.02 | 0.02 |
| K | 0.03 | 0.04 | 0.05 |
| P | 0.01 | - | - |
| Ni | - | - | - |
| Cr | - | - | - |
| Sr | 0.01 | 0.01 | - |
| Ba | - | - | - |
| ΣX | 0.50 | 0.51 | 0.48 |
| ΣY | 0.98 | 0.98 | 0.95 |
| ΣZ | 2.03 | 2.03 | 2.03 |

Appendix 2.4.7 Electron microprobe analyses of wairakite

| Mineral | Ferrierite | |
|---|---|---|
| PT/S No | CV32 (16) | CV32 (18) |
| $SiO_2$ | 69.92 | 71.11 |
| $TiO_2$ | 0.07 | 0.07 |
| $Al_2O_3$ | 10.84 | 10.82 |
| FeO | 0.69 | 0.34 |
| MnO | - | - |
| MgO | 2.06 | 1.99 |
| CaO | 0.18 | 0.22 |
| $Na_2O$ | 1.13 | 1.16 |
| $K_2O$ | 3.94 | 3.40 |
| $P_2O_5$ | - | - |
| NiO | - | - |
| $Cr_2O_3$ | - | - |
| SrO | - | - |
| BaO | 0.09 | 0.10 |
| TOTAL | 88.92 | 89.21 |
| Recalculated on the basis of 72 oxygens | | |
| Si | 30.22 | 30.43 |
| Ti | 0.02 | 0.02 |
| $Al_{+3}$ | 5.52 | 5.46 |
| $Fe^{+3}$ | 0.25 | 0.12 |
| Mr | - | - |
| Mg | 1.33 | 1.27 |
| Ca | 0.08 | 0.10 |
| Na | 0.95 | 0.96 |
| K | 2.17 | 1.86 |
| P | - | - |
| Ni | - | - |
| Cr | - | - |
| Sr | - | - |
| Ba | 0.02 | 0.02 |
| $\Sigma X$ | 4.82 | 4.35 |
| $\Sigma Y$ | 35.74 | 35.89 |
| $\Sigma Z$ | | |

Appendix 2.4.8 Electron microprobe analyses of ferrierite.

| Mineral | Albite 1 | 2 | 3 | 4 | 5 | 6 | 7 | 8 | 9 | 10 | 11 | 12 |
|---|---|---|---|---|---|---|---|---|---|---|---|---|
| PT/S No | CV86 (1) | CV86 (2) | CV86 (3) | CV86 (5) | CV86 (6) | CV89 S71 (8) | CV69 (12) | CV69 (14) | CV93 (5) | CV93 (10) | CV97 (12) | CV89 (40) |
| $SiO_2$ | 70.76 | 70.53 | 70.26 | 70.57 | 71.00 | 72.04 | 67.36 | 65.61 | 66.72 | 66.67 | 68.97 | 67.28 |
| $TiO_2$ | 0.02 | - | - | 0.02 | - | - | 0.01 | 0.02 | 0.04 | 0.01 | - | 0.04 |
| $Al_2O_3$ | 20.12 | 20.51 | 20.20 | 20.56 | 20.09 | 20.33 | 19.75 | 20.22 | 19.13 | 19.10 | 20.48 | 20.20 |
| FeO | 0.06 | 0.36 | 0.02 | 0.33 | - | - | 0.03 | - | 0.21 | - | 0.43 | - |
| MnO | - | 0.10 | 0.04 | 0.02 | - | 0.06 | 0.01 | 0.01 | 0.01 | - | - | 0.20 |
| MgO | - | - | 0.02 | 0.07 | 0.01 | 0.03 | - | - | 0.16 | - | 0.31 | - |
| CaO | 0.01 | 0.19 | 0.05 | 0.40 | 0.05 | 0.09 | 0.22 | 3.23 | 0.57 | 0.30 | 0.28 | 0.16 |
| $Na_2O$ | 12.11 | 11.34 | 11.30 | 11.00 | 11.17 | 11.53 | 11.42 | 10.91 | 11.95 | 12.00 | 11.76 | 9.90 |
| $K_2O$ | - | - | 0.02 | 0.06 | 0.04 | 0.07 | 0.05 | 0.03 | 0.04 | 0.09 | 0.02 | 0.02 |
| $P_2O_5$ | - | - | - | - | - | - | - | - | - | 0.01 | - | 0.10 |
| NiO | - | - | - | - | - | - | 0.04 | - | - | - | - | - |
| $Cr_2O_3$ | - | - | - | - | - | - | - | - | 0.01 | 0.05 | - | 0.07 |
| SrO | - | - | - | - | - | - | 0.27 | 0.26 | 0.28 | 0.27 | - | 0.14 |
| BaO | 0.04 | - | 0.02 | - | 0.04 | - | 0.02 | - | - | - | - | 0.06 |
| TOTAL | 103.12 | 102.93 | 101.93 | 103.03 | 102.40 | 104.141 | 99.18 | 100.29 | 99.12 | 98.50 | 102.25 | 98.17 |
| Recalculated on the basis of 32 oxygens | | | | | | | | | | | | |
| Si | 11.98 | 11.95 | 12.00 | 11.95 | 12.06 | 12.04 | 11.90 | 11.58 | 11.84 | 11.90 | 11.82 | 11.90 |
| Ti | - | - | - | - | - | - | - | - | - | - | - | - |
| $Al^{+3}$ | 4.02 | 4.10 | 4.07 | 4.10 | 4.02 | 4.01 | 4.10 | 4.22 | 4.00 | 4.00 | 4.14 | 4.22 |
| Fe | 0.01 | 0.05 | - | 0.05 | - | - | - | - | 0.03 | - | 0.06 | - |
| Mn | - | - | 0.01 | - | - | 0.01 | - | - | - | - | - | 0.03 |
| Mg | - | - | 0.01 | 0.02 | - | 0.01 | - | - | 0.03 | - | 0.08 | - |
| Ca | - | 0.03 | 0.01 | 0.07 | 0.01 | 0.02 | 0.03 | 0.61 | 0.10 | 0.06 | 0.05 | 0.03 |
| Na | 3.98 | 3.73 | 3.74 | 3.61 | 3.68 | 3.74 | 3.90 | 3.74 | 4.13 | 4.16 | 3.91 | 3.39 |
| K | - | - | 0.01 | 0.01 | 0.01 | 0.02 | - | - | - | 0.03 | - | - |
| P | - | - | - | - | - | - | - | - | - | - | - | - |
| Ni | - | - | - | - | - | - | - | - | - | - | - | - |
| Cr | - | - | - | - | - | - | - | - | - | - | - | - |
| Sr | - | - | - | - | - | - | 0.03 | 0.03 | 0.03 | 0.03 | - | - |
| Ba | - | - | - | - | - | - | - | - | - | - | - | - |
| IX | 3.99 | 3.81 | 3.78 | 3.76 | 3.70 | 3.80 | 3.96 | 4.38 | 4.32 | 4.28 | 4.10 | 3.45 |
| IY | 4.02 | 4.10 | 4.07 | 4.10 | 4.02 | 4.01 | 4.10 | 4.22 | 4.00 | 4.00 | 4.14 | 4.22 |
| IZ | 11.98 | 11.95 | 12.00 | 11.95 | 12.06 | 12.04 | 11.90 | 11.58 | 11.84 | 11.90 | 11.82 | 11.90 |
| An | 0.08 | 0.90 | 0.24 | 1.95 | 0.24 | 0.45 | 0.81 | 13.97 | 2.27 | 1.50 | 1.31 | 0.94 |
| Ab | 99.92 | 99.07 | 99.63 | 97.78 | 99.51 | 99.12 | 99.19 | 86.03 | 97.73 | 97.75 | 98.60 | 99.06 |
| Or | - | 0.03 | 0.13 | 0.33 | 0.24 | 0.43 | - | - | - | 0.75 | 0.08 | - |

Appendix 2.4.9 Electron microprobe analyses of albite

| Mineral | 13 | 14 | 15 | 16 | 17 | 18 | 19 | 20 | 21 | 22 | 23 |
|---|---|---|---|---|---|---|---|---|---|---|---|
| PT/S No | CV89 (41) | CV98 (16) | CV93 (20) | CV93 (21) | CV80 (3) | CV80 (7) | CV3 (1) | CV259B (1) | CV59B (3) | CV46 (6) | CV85 (10) |
| $SiO_2$ | 69.02 | 65.59 | 67.03 | 67.24 | 67.45 | 66.05 | 67.91 | 65.57 | 66.89 | 69.16 | 68.40 |
| $TiO_2$ | - | 0.16 | - | - | 0.03 | 0.33 | 0.05 | - | - | - | 0.02 |
| $Al_2O_3$ | 20.25 | 19.05 | 19.31 | 19.24 | 19.47 | 19.99 | 19.60 | 20.39 | 20.84 | 19.52 | 19.26 |
| FeO | 0.12 | 0.30 | 0.09 | - | 0.05 | 0.80 | 0.05 | 0.11 | 0.01 | 0.23 | 0.03 |
| MnO | 0.02 | - | 0.03 | 0.02 | 0.11 | 0.01 | 0.02 | 0.08 | 0.09 | 0.02 | 0.04 |
| MgO | - | 0.25 | 0.04 | - | 0.03 | 0.05 | 0.05 | 0.17 | - | 0.03 | 0.02 |
| CaO | 0.30 | 0.65 | 0.41 | 0.46 | 0.08 | 0.17 | 0.46 | 1.29 | 0.10 | 0.14 | 0.10 |
| $Na_2O$ | 10.01 | 11.80 | 11.96 | 12.00 | 11.89 | 10.99 | 11.20 | 10.84 | 11.11 | 11.57 | 11.99 |
| $K_2O$ | 0.08 | 0.05 | 0.05 | 0.02 | 0.01 | 0.28 | 0.06 | 0.09 | - | 0.17 | 0.02 |
| $P_2O_5$ | - | 0.01 | - | - | 0.13 | 0.42 | - | - | - | - | - |
| NiO | - | 0.06 | - | - | - | 0.07 | - | - | 0.02 | - | - |
| $Cr_2O_3$ | - | 0.01 | - | 0.01 | 0.09 | - | - | 0.07 | - | - | - |
| Sr | 0.29 | 0.21 | 0.32 | 0.19 | 0.17 | 0.24 | - | 0.63 | 0.43 | - | - |
| BaO | 0.01 | - | - | 0.09 | - | - | 0.07 | 0.06 | 0.13 | - | 0.04 |
| TOTAL | 100.10 | 98.14 | 99.24 | 99.27 | 99.51 | 99.40 | 99.49 | 99.90 | 100.51 | 100.84 | 98.72 |
| Si | 12.00 | 11.78 | 11.87 | 11.90 | 11.87 | 11.68 | 11.93 | 11.58 | 11.71 | 11.99 | 12.12 |
| Ti | - | 0.03 | - | - | - | 0.03 | 0.01 | - | - | - | - |
| $Al^{+3}$ | 4.16 | 4.03 | 4.03 | 4.00 | 4.03 | 4.16 | 4.06 | 4.38 | 4.29 | 3.99 | 3.77 |
| Fe | 0.03 | 0.03 | - | - | - | 0.13 | 0.01 | 0.03 | - | 0.03 | - |
| Mn | - | - | - | - | 0.03 | - | - | - | - | - | 0.01 |
| Mg | - | 0.06 | - | - | - | - | 0.01 | 0.03 | - | 0.01 | 0.01 |
| Ca | 0.06 | 0.13 | 0.06 | 0.10 | - | 0.03 | 0.09 | 0.26 | 0.19 | 0.03 | 0.02 |
| Na | 3.36 | 4.10 | 4.10 | 4.13 | 4.06 | 3.78 | 3.82 | 3.71 | 3.78 | 3.89 | 0.12 |
| K | 0.03 | - | - | - | - | 0.06 | 0.01 | 0.03 | - | 0.04 | 0.01 |
| P | - | - | - | - | 0.03 | 0.06 | - | - | - | - | - |
| Ni | - | - | - | - | - | - | - | - | - | - | - |
| Cr | - | - | - | - | - | - | - | - | - | - | - |
| Sr | 0.03 | 0.03 | 0.03 | 0.03 | 0.03 | 0.03 | - | 0.06 | 0.03 | - | - |
| Ba | - | - | - | - | - | - | - | - | - | - | - |
| IX | 3.51 | 4.38 | 4.19 | 4.26 | 4.15 | 4.12 | 3.94 | 4.12 | 4.00 | 4.00 | 4.17 |
| IY | 4.16 | 4.03 | 4.03 | 4.00 | 4.03 | 4.16 | 4.06 | 4.38 | 4.29 | 3.99 | 3.77 |
| IZ | 12.00 | 11.78 | 11.87 | 11.90 | 11.87 | 11.68 | 11.93 | 11.58 | 11.71 | 11.99 | 12.12 |
| An | 1.85 | 3.03 | 1.54 | 2.27 | - | 0.83 | 2.27 | 6.44 | 4.84 | 0.66 | 0.43 |
| Ab | 97.28 | 96.97 | 98.46 | 97.73 | 100.00 | 97.52 | 97.40 | 92.8 | 95.16 | 98.41 | 99.44 |
| Or | 0.93 | - | - | - | - | 1.65 | 0.33 | 0.8 | - | 0.94 | 0.12 |

| Mineral | Plagioclase 1 | Labradorite 1 | 2 | 3 | Andesine 1 |
|---|---|---|---|---|---|
| PT/S No | CV30A (9) | CV35 (15) | CV32 (20) | CV66 (3) | CV66 (12) |
| $SiO_2$ | 48.55 | 50.86 | 51.45 | 53.69 | 56.90 |
| $TiO_2$ | 0.08 | 0.09 | 0.14 | 0.43 | 0.07 |
| $Al_2O_3$ | 32.61 | 30.34 | 30.90 | 28.02 | 26.17 |
| FeO | 0.53 | 1.02 | 0.67 | 0.88 | 0.75 |
| MnO | - | - | - | - | - |
| MgO | 0.09 | 0.43 | 0.13 | 0.10 | 0.08 |
| CaO | 15.94 | 13.15 | 13.56 | 11.37 | 8.96 |
| $Na_2O$ | 2.53 | 3.60 | 3.44 | 4.78 | 5.70 |
| $K_2O$ | 0.13 | 0.29 | 0.23 | 0.37 | 0.57 |
| $P_2O_5$ | - | - | - | 0.13 | - |
| NiO | - | - | - | 0.05 | 0.06 |
| $Cr_2O_3$ | - | - | - | - | 0.23 |
| BaO | - | - | - | 0.02 | 0.11 |
| TOTAL | 100.46 | 99.78 | 100.52 | 99.59 | 99.62 |
| Recalculated on the basis of 32 oxygens | | | | | |
| Si | 8.88 | 9.31 | 9.33 | 9.79 | 10.30 |
| Ti | 0.01 | 0.01 | 0.02 | - | - |
| $Al^{+3}$ | 7.03 | 6.55 | 6.60 | 6.02 | 5.60 |
| $Fe^{+3}$ | 0.08 | 0.16 | 0.10 | 0.13 | 0.13 |
| Mn | - | - | - | - | - |
| Mg | 0.03 | 0.12 | 0.04 | 0.03 | 0.03 |
| Ca | 3.12 | 2.58 | 2.63 | 2.24 | 1.73 |
| Na | 0.90 | 1.28 | 1.21 | 1.70 | 2.02 |
| K | 0.03 | 0.07 | 0.05 | 0.10 | 0.13 |
| P | - | - | - | 0.03 | |
| Ni | - | - | - | - | - |
| Cr | - | - | - | - | - |
| Sr | - | - | - | - | 0.03 |
| Ba | - | - | - | - | - |
| ΣX | 4.17 | 4.22 | 4.05 | 4.23 | 4.07 |
| ΣY | 7.03 | 6.55 | 6.60 | 6.02 | 5.60 |
| ΣZ | 8.88 | 9.31 | 9.33 | 9.79 | 10.30 |
| An | 77.12 | 65.71 | 67.62 | 55.53 | 44.63 |
| Ab | 22.14 | 32.56 | 31.00 | 42.04 | 52.07 |
| Or | 0.74 | 1.73 | 1.38 | 2.38 | 3.30 |

Appendix 2.4.10 Electron microprobe analyses of plagioclase

| Mineral | Adularia 1 | 2 | Oligoclase 1 | 2 | 3 |
|---|---|---|---|---|---|
| PT/S No | CV69 (1) | CV28 (1) | CV9 (5) | CV66 (4) | CV66 (9) |
| $SiO_2$ | 63.61 | 64.40 | 65.59 | 70.44 | 69.50 |
| $TiO_2$ | - | 0.03 | - | 0.38 | 0.73 |
| $Al_2O_3$ | 18.56 | 18.84 | 18.15 | 13.53 | 15.66 |
| FeO | 0.02 | - | 0.38 | 2.03 | 1.14 |
| MnO | 0.04 | 0.04 | - | 0.06 | 0.12 |
| MgO | - | - | 0.33 | 0.27 | 0.04 |
| CaO | 0.03 | 0.01 | 0.13 | 0.38 | 0.34 |
| $Na_2O$ | 1.12 | 1.05 | 0.03 | 1.36 | 3.21 |
| $K_2O$ | 14.44 | 14.89 | 16.33 | 9.49 | 8.69 |
| $P_2O_5$ | - | - | - | 0.10 | 0.02 |
| NiO | 0.04 | - | - | - | - |
| $Cr_2O_3$ | - | - | - | 0.03 | - |
| SrO | 0.24 | - | - | 0.16 | 0.20 |
| BaO | 0.51 | 0.68 | 0.01 | 0.21 | 0.09 |
| TOTAL | 98.61 | 99.94 | 100.95 | 98.44 | 99.74 |
| Recalculated on the basis of 32 oxygens | | | | | |
| Si | 11.90 | 11.91 | 12.05 | 12.83 | 12.48 |
| Ti | - | - | - | 0.06 | 0.10 |
| $Al^{+3}$ | 4.10 | 4.11 | 3.93 | 2.91 | 3.33 |
| $Fe^{+3}$ | - | - | 0.06 | 0.32 | 0.16 |
| Mn | - | 0.01 | - | - | 0.03 |
| Mg | - | - | 0.01 | 0.06 | - |
| Ca | - | - | 0.03 | 0.06 | 0.06 |
| Na | 0.42 | 0.38 | 0.01 | 0.48 | 1.12 |
| K | 3.46 | 3.51 | 3.83 | 2.21 | 1.98 |
| P | - | - | - | - | - |
| Ni | - | - | - | - | - |
| Cr | - | - | - | - | - |
| Sr | 0.03 | - | - | 0.03 | 0.03 |
| Ba | 0.03 | 0.05 | - | - | - |
| ΣX | 3.94 | 3.95 | 3.94 | 3.22 | 3.48 |
| ΣY | 4.10 | 4.11 | 3.93 | 2.91 | 3.33 |
| ΣZ | 11.90 | 11.91 | 12.05 | 12.83 | 12.48 |
| Ab | - | 0.05 | 0.67 | 2.33 | 2.02 |
| An | 10.74 | 9.66 | 0.23 | 7.44 | 35.35 |
| Or | 89.26 | 90.285 | 99.09 | 80.23 | 62.63 |

Appendix 2.4.11 Electron microprobe analyses of K-spar

| Mineral | Prehnite 1 | 2 | 3 | 4 | 5 | 6 | 7 | 8 | 9 | 10 | 11 | 12 | 13 | 14 | 15 | 16 | 17 | 18 |
|---|---|---|---|---|---|---|---|---|---|---|---|---|---|---|---|---|---|---|
| PT/S | CV69X (1) | CV69 (15) | CV69 (16) | CV69X (2) | CV69 (20) | CV69X (17) | CV69X (18) | CV69X (24) | CV69X (26) | CV69X (28) | CV69 (1) | CV69 (2) | CV69 (3) | CV69 (4) | CV69 (5) | CV69 (9) | CV69 (10) | CV69 (13) |
| $SiO_2$ | 41.49 | 43.13 | 42.71 | 40.05 | 37.79 | 43.94 | 43.74 | 43.20 | 43.26 | 43.43 | 43.28 | 43.37 | 43.50 | 43.45 | 43.30 | 42.96 | 43.50 | 43.07 |
| $TiO_2$ | 0.05 | 0.08 | 0.01 | 0.01 | 0.13 | 0.04 | - | - | 0.03 | 0.02 | 0.03 | 0.08 | 0.04 | 0.09 | 0.07 | 0.01 | 0.10 | 0.07 |
| $Al_2O_3$ | 22.50 | 22.78 | 21.08 | 20.84 | 20.00 | 22.05 | 23.98 | 22.85 | 24.12 | 24.54 | 23.71 | 22.65 | 22.89 | 22.94 | 22.69 | 24.20 | 23.41 | 22.99 |
| FeO | 0.22 | 1.78 | 3.16 | 2.27 | 3.89 | 2.50 | 0.38 | 1.75 | 0.21 | 0.06 | 0.72 | 1.90 | 0.74 | 1.62 | 1.90 | 0.52 | 1.52 | 1.55 |
| MnO | 0.05 | 0.03 | 0.02 | 0.07 | 0.05 | 0.05 | 0.06 | 0.04 | 0.04 | 0.08 | 0.03 | 0.03 | - | 0.11 | 0.09 | 0.12 | 0.05 | 0.04 |
| MgO | 0.02 | 0.02 | - | 0.41 | 0.10 | 0.03 | 0.06 | 0.28 | - | - | - | - | - | 0.02 | 0.01 | - | 0.02 | - |
| CaO | 25.79 | 26.95 | 26.46 | 24.35 | 21.98 | 24.82 | 25.28 | 24.29 | 23.67 | 26.14 | 26.77 | 26.57 | 27.00 | 26.52 | 26.59 | 27.02 | 27.10 | 26.56 |
| $Na_2O$ | 0.01 | 0.03 | 0.19 | 0.06 | 0.71 | 0.24 | 0.04 | 0.05 | 0.48 | 0.04 | 0.11 | 0.19 | 0.21 | 0.12 | 0.19 | 0.13 | 0.15 | 0.16 |
| $K_2O$ | - | 0.04 | 0.03 | 0.02 | 0.84 | - | 0.05 | 0.02 | 0.02 | 0.01 | 0.04 | 0.05 | 0.03 | 0.02 | 0.04 | 0.09 | 0.01 | 0.04 |
| $P_2O_5$ | - | 0.19 | 0.16 | 0.02 | 0.17 | - | 0.06 | - | 0.09 | - | 0.25 | 0.21 | 0.22 | 0.18 | 0.18 | 0.27 | 0.25 | 0.17 |
| NiO | - | - | 0.02 | - | - | - | 0.11 | 0.01 | - | 0.03 | 0.04 | - | 0.02 | - | 0.01 | - | - | - |
| $Cr_2O_3$ | 0.02 | 0.01 | - | - | - | 0.06 | - | - | 0.01 | - | 0.02 | - | - | - | - | - | - | - |
| SrO | 0.17 | - | 0.10 | 0.07 | 0.27 | 0.08 | 0.85 | 0.15 | 0.14 | 0.15 | 0.02 | 0.12 | 0.62 | 0.10 | 0.12 | 0.15 | 0.03 | 0.11 |
| BaO | 0.03 | 0.04 | 0.05 | 0.08 | - | 0.02 | - | - | - | - | - | 0.02 | - | 0.06 | 0.04 | - | - | - |
| TOTAL | 90.35 | 95.08 | 93.99 | 88.23 | 85.93 | 93.83 | 94.61 | 92.64 | 92.08 | 94.50 | 95.02 | 95.19 | 95.27 | 95.24 | 95.23 | 95.47 | 96.14 | 94.76 |
| Recalculated on the basis of 22 oxygens | | | | | | | | | | | | | Recalculated on the basis of 22 oxygens | | | | | |
| Si | 6.05 | 6.01 | 6.09 | 6.05 | 5.94 | 6.20 | 6.09 | 6.14 | 6.12 | 6.03 | 6.01 | 6.05 | 6.03 | 6.05 | 6.05 | 5.94 | 6.01 | 6.03 |
| Ti | - | - | - | - | 0.02 | - | - | - | - | - | - | - | - | - | - | - | - | - |
| $Al^{+3}$ | 3.87 | 3.74 | 3.54 | 3.72 | 3.72 | 3.67 | 3.94 | 3.83 | 4.03 | 4.00 | 3.87 | 3.72 | 3.74 | 3.76 | 3.74 | 3.94 | 3.81 | 3.78 |
| Fe | 0.02 | 0.20 | 0.37 | 0.29 | 0.51 | 0.29 | 0.04 | 0.20 | 0.02 | - | 0.09 | 0.22 | 0.20 | 0.20 | 0.22 | 0.07 | 0.18 | 0.18 |
| Mn | - | - | - | - | - | - | - | - | - | - | - | - | - | 0.02 | - | 0.02 | - | - |
| Mg | - | - | - | 0.09 | 0.02 | - | 0.02 | 0.07 | - | - | - | - | - | - | - | - | - | - |
| Ca | 4.03 | 4.03 | 4.05 | 3.94 | 3.70 | 3.74 | 3.78 | 3.70 | 3.59 | 3.89 | 3.98 | 3.96 | 4.00 | 3.96 | 3.98 | 4.00 | 4.00 | 3.98 |
| Na | - | 0.07 | 0.04 | 0.02 | 0.22 | 0.07 | - | 0.02 | 0.13 | - | 0.02 | 0.04 | 0.07 | 0.02 | 0.04 | 0.04 | 0.04 | 0.04 |
| K | - | - | - | - | 0.18 | - | - | - | - | - | - | - | - | - | - | 0.02 | - | - |
| F | - | 0.02 | 0.02 | - | 0.02 | - | - | - | - | - | 0.02 | 0.02 | 0.02 | 0.02 | 0.02 | 0.02 | 0.02 | 0.02 |
| Ni | - | - | - | - | - | - | - | - | - | - | - | - | - | - | - | - | - | - |
| Cr | - | - | - | - | - | - | - | - | - | - | - | - | - | - | - | - | - | - |
| Sr | 0.02 | - | - | - | 0.02 | - | - | 0.02 | 0.02 | 0.02 | - | - | - | - | - | 0.02 | - | - |
| Ba | - | - | - | - | - | - | - | - | - | - | - | - | - | - | - | - | - | - |
| ΣX | 4.05 | 4.12 | 4.11 | 4.05 | 4.18 | 3.81 | 3.80 | 3.83 | 3.74 | 3.91 | 4.02 | 4.02 | 4.09 | 4.02 | 4.04 | 4.12 | 4.06 | 4.04 |
| ΣY | 3.89 | 3.94 | 3.91 | 4.01 | 4.23 | 3.96 | 3.98 | 4.03 | 4.05 | 4.00 | 3.96 | 3.94 | 3.94 | 3.96 | 3.96 | 4.01 | 3.99 | 3.96 |
| ΣZ | 6.05 | 6.01 | 6.09 | 6.05 | 5.94 | 6.20 | 6.09 | 6.14 | 6.12 | 6.03 | 6.01 | 6.05 | 6.03 | 6.05 | 6.05 | 5.94 | 6.01 | 6.03 |

Appendix 2.4.12 Electron microprobe analyses of prehnite

| Mineral | Epidote 1 | 2 | 3 | 4 | 5 | 6 |
|---|---|---|---|---|---|---|
| PT/S No | CV69 (17) | CV69 (18) | CV69 (19) | CV69 (21) | CV69 (22) | CV69 (26) |
| $SiO_2$ | 37.95 | 37.04 | 36.83 | 37.67 | 35.24 | 37.24 |
| $TiO_2$ | 0.06 | 0.16 | 0.04 | 0.30 | 0.13 | 0.32 |
| $Al_2O_3$ | 23.55 | 17.86 | 24.07 | 22.33 | 19.35 | 21.86 |
| FeO | 11.65 | 15.99 | 11.13 | 12.62 | 12.55 | 12.40 |
| MnO | 0.15 | 0.03 | 0.06 | 0.14 | 0.06 | 0.24 |
| MgO | 0.10 | 0.02 | 0.02 | 0.06 | 0.11 | - |
| CaO | 23.94 | 22.94 | 24.01 | 23.16 | 20.97 | 22.84 |
| $Na_2O$ | - | 0.02 | 0.01 | - | 0.02 | 0.08 |
| $K_2O$ | 0.01 | 0.03 | 0.03 | - | 0.03 | 0.08 |
| $P_2O_5$ | 0.18 | 0.23 | 0.23 | 0.17 | 0.22 | 0.09 |
| $Cr_2O_3$ | - | 0.01 | 0.01 | 0.05 | 0.05 | - |
| SrO | 0.11 | 0.12 | 0.30 | 0.16 | 0.20 | 0.25 |
| BaO | 0.04 | - | 0.06 | - | 0.03 | - |
| TOTAL | 97.78 | 94.49 | 96.80 | 96.70 | 88.96 | 95.40 |
| Recalculated on the basis of 12 oxygens | | | | | | |
| Si | 2.96 | 3.07 | 2.90 | 2.99 | 3.05 | 3.00 |
| Ti | - | 0.01 | - | 0.02 | 0.01 | 0.02 |
| $Al_{+3}$ | 2.16 | 1.75 | 2.23 | 2.09 | 1.97 | 2.08 |
| Fe | 0.76 | 1.12 | 0.73 | 0.84 | 0.91 | 0.84 |
| Mn | 0.01 | - | - | 0.01 | - | 0.01 |
| Mg | 0.01 | - | - | 0.01 | 0.01 | - |
| Ca | 2.00 | 2.04 | 2.03 | 1.97 | 1.94 | 1.97 |
| K | - | - | - | - | - | 0.01 |
| P | 0.01 | 0.01 | 0.01 | 0.01 | 0.01 | - |
| Na | - | - | - | - | - | 0.01 |
| Cr | - | - | - | - | - | - |
| Sr | - | - | 0.01 | 0.01 | 0.01 | 0.01 |
| Ba | - | - | - | - | - | - |
| ΣX | 2.03 | 2.05 | 2.05 | 2.01 | 1.98 | 2.01 |
| ΣY | 2.92 | 2.88 | 2.96 | 2.95 | 2.88 | 2.94 |
| ΣZ | 2.96 | 3.07 | 2.90 | 2.99 | 3.05 | 3.00 |

Appendix 2.4.13 Electron microprobe analyses of epidote

| Mineral | Hydro-grossular 1 | 2 | 3 | 4 | 5 |
|---|---|---|---|---|---|
| PT/S No | CV69 (24) | CV69 (27) | CV69 (29) | CV69 (30) | CV69 (31) |
| $SiO_2$ | 30.66 | 28.75 | 37.24 | 37.50 | 34.96 |
| $TiO_2$ | 0.02 | - | 0.04 | - | 0.05 |
| $Al_2O_3$ | 6.87 | 0.15 | 14.21 | 12.76 | 8.34 |
| FeO | 16.75 | 24.87 | 10.76 | 12.24 | 16.85 |
| MnO | 0.26 | 0.10 | 0.23 | 0.25 | 0.17 |
| MgO | 0.04 | 0.03 | 0.64 | 0.04 | 0.04 |
| CaO | 29.87 | 28.69 | 36.67 | 35.76 | 35.29 |
| $Na_2O$ | 0.06 | 0.05 | 0.01 | - | 0.10 |
| $K_2O$ | 0.04 | 0.15 | - | 0.05 | 0.02 |
| $P_2O_5$ | 0.18 | 0.16 | 0.26 | 0.21 | 0.25 |
| NiO | 0.03 | - | 0.01 | 0.06 | - |
| $Cr_2O_3$ | - | 0.01 | - | 0.04 | 0.02 |
| SrO | - | 0.06 | 0.12 | 0.04 | 0.18 |
| BaO | 0.02 | - | - | - | 0.04 |
| TOTAL | 84.80 | 83.02 | 99.61 | 98.95 | 96.22 |
| Recalculated on the basis of 23 oxygens | | | | | |
| Si | 5.87 | 6.00 | 5.75 | 5.87 | 5.84 |
| Ti | - | - | - | - | - |
| $Al^{+3}$ | 1.51 | 0.05 | 2.60 | 2.35 | 1.63 |
| Fe | 2.67 | 4.35 | 1.38 | 1.61 | 2.35 |
| Mn | 0.05 | 0.02 | 0.02 | 0.02 | 0.02 |
| Mg | - | - | 0.02 | - | - |
| Ca | 6.12 | 6.44 | 6.07 | 6.00 | 6.33 |
| Na | 0.02 | 0.02 | - | - | - |
| K | - | 0.05 | - | - | - |
| P | 0.02 | 0.02 | 0.02 | 0.02 | 0.05 |
| Ni | - | - | - | - | - |
| Cr | - | - | - | - | - |
| Sr | - | - | - | - | 0.02 |
| Ba | - | - | - | - | - |
| ΣX | 6.21 | 6.55 | 6.13 | 6.04 | 6.42 |
| ΣY | 4.21 | 4.40 | 3.98 | 3.96 | 3.98 |
| ΣZ | 5.87 | 6.00 | 5.75 | 5.87 | 5.84 |

Appendix 2.4.14 Electron microprobe analyses of hydrogarnets

| Mineral | Chlorite 1 | 2 | 3 | 4 | 5 | 6 | 7 | 8 | 9 | 10 | 11 | 12 | 13 | 14 | 15 | 16 | 17 | 18 | 19 | 20 | 21 | 22 | 23 | 24 | 25 | 26 | 27 |
|---|---|---|---|---|---|---|---|---|---|---|---|---|---|---|---|---|---|---|---|---|---|---|---|---|---|---|---|
| PP/B No | CV46 (1) (1) | CV41 (5) | CV38 (7) | CV8 (10) | CV112 (6) | CV112 (7) | CV86 (4) | CV86871 (9) | CV598 (13) | CV8r (16) | CV9 (1) | CV9 (1) | CV30A (10) | CV35 (11) | CV45K (23) | CV45K (27) | CV54K (28) | CV30 (28) | CV30 (29) | CV90 (30) | CV90 (31) | CV90 (32) | CV90 (33) | CV90 (35) | CV90 (38) | CV84 (39) | CV84 (42) | CV84 (41) |
| $SiO_2$ | 31.55 | 31.69 | 34.27 | 32.88 | 37.52 | 36.85 | 31.87 | 34.99 | 33.34 | 34.77 | 28.85 | 26.94 | 33.95 | 36.05 | 30.43 | 31.34 | 23.84 | 26.46 | 26.76 | 25.89 | 26.85 | 27.22 | 28.56 | 29.66 | 30.24 | 29.05 | 32.25 |
| $TiO_2$ | - | 0.05 | 0.78 | 0.09 | 0.03 | 0.04 | 0.08 | 0.11 | - | 0.33 | - | 0.06 | - | 0.01 | 0.04 | 0.10 | 0.15 | - | 0.01 | - | - | 0.13 | - | - | 0.05 | - | - |
| $Al_2O_3$ | 12.50 | 12.09 | 14.05 | 13.24 | 11.70 | 11.78 | 15.80 | 16.27 | 14.90 | 17.04 | 18.64 | 18.42 | 14.01 | 13.87 | 15.19 | 15.59 | 14.01 | 12.73 | 14.10 | 17.27 | 12.95 | 15.82 | 13.22 | 13.54 | 15.98 | 15.80 | 20.43 |
| FeO | 27.97 | 28.52 | 15.68 | 23.81 | 16.60 | 18.80 | 22.27 | 11.15 | 9.60 | 11.90 | 31.66 | 33.33 | 20.32 | 13.62 | 26.16 | 26.11 | 25.62 | 25.78 | 24.21 | 26.53 | 26.38 | 21.87 | 28.65 | 28.11 | 22.68 | 26.68 | 11.34 |
| MnO | - | 0.21 | 0.34 | 0.25 | 0.24 | 0.38 | 0.30 | 0.21 | - | 0.23 | 0.03 | 0.11 | 0.36 | 0.16 | 0.36 | 0.37 | 0.35 | 0.26 | 0.39 | 0.45 | 0.35 | 0.53 | 0.34 | 0.45 | 0.34 | 0.62 | 0.66 |
| MgO | 14.38 | 14.35 | 22.02 | 16.17 | 21.57 | 20.42 | 14.48 | 22.75 | 26.54 | 21.75 | 9.30 | 8.75 | 18.14 | 23.00 | 13.15 | 14.48 | 12.33 | 10.63 | 10.97 | 11.64 | 10.66 | 9.62 | 10.99 | 13.06 | 13.58 | 10.68 | 17.24 |
| CaO | 0.50 | 0.87 | 0.76 | 1.30 | 0.32 | 0.40 | 0.51 | 0.26 | 0.15 | 0.21 | 0.22 | 0.21 | 0.44 | 0.75 | 0.41 | 0.61 | 0.39 | 0.37 | 0.39 | 0.14 | 0.34 | 2.23 | 0.57 | 0.25 | 0.35 | 0.17 | 0.33 |
| $Na_2O$ | 0.07 | 0.01 | 0.28 | 0.07 | 0.09 | 0.11 | 0.04 | 0.16 | 0.12 | 0.29 | 0.05 | - | 0.09 | 0.30 | 0.01 | 0.04 | 0.04 | 0.05 | 0.05 | 0.02 | 0.08 | 0.23 | 0.11 | 0.04 | 0.09 | - | 0.03 |
| $K_2O$ | 0.05 | 0.11 | 0.12 | - | - | 0.11 | 0.11 | 0.05 | 0.05 | 0.34 | 0.13 | - | 0.35 | 0.24 | 0.05 | 0.04 | 0.02 | 0.39 | 0.58 | 0.30 | 0.61 | 0.55 | 0.17 | 0.11 | 0.25 | - | 0.08 |
| $P_2O_5$ | - | - | - | - | - | - | - | - | - | 0.19 | - | - | - | - | - | 0.03 | 0.12 | 0.01 | 0.11 | 0.02 | 0.03 | 1.77 | - | 0.02 | 0.06 | 0.06 | 0.30 |
| BaO | - | - | - | - | - | - | - | - | - | 0.03 | - | - | - | - | - | - | - | - | - | 0.04 | 0.05 | 0.03 | 0.02 | 0.02 | - | - | 0.02 |
| $Cr_2O_3$ | - | - | - | - | - | - | - | - | - | - | - | - | - | - | - | - | 0.05 | 0.02 | - | 0.02 | - | 0.01 | 0.08 | - | 0.01 | - | 0.02 |
| SrO | - | - | - | - | - | - | - | - | - | - | - | - | - | - | - | - | 0.09 | 0.08 | 0.05 | 0.12 | - | 0.01 | - | 0.01 | - | - | 0.05 |
| NiO | - | - | - | 0.04 | - | 0.01 | - | 0.12 | - | 0.07 | - | - | - | - | - | - | 0.04 | 0.03 | - | 0.07 | - | 0.07 | 0.01 | - | 0.01 | - | 0.02 |
| TOTAL | 87.03 | 87.72 | 89.30 | 87.65 | 88.07 | 88.70 | 85.68 | 86.07 | 84.50 | 87.40 | 88.64 | 87.82 | 87.66 | 88.00 | 86.04 | 88.71 | 77.00 | 76.72 | 77.62 | 83.31 | 78.28 | 80.09 | 82.70 | 85.08 | 83.59 | 87.06 | 86.44 |
| Recalculated on the basis of 28 oxygens | | | | | | | | | | | | | | | | | | | | | | | | | | | |
| Si | 6.75 | 6.77 | 6.69 | 6.83 | 7.88 | 7.29 | 6.72 | 6.66 | 6.63 | 6.72 | 6.16 | 5.91 | 6.90 | 7.00 | 6.52 | 6.50 | 5.80 | 6.90 | 6.64 | 5.91 | 6.90 | 6.22 | 6.55 | 6.52 | 6.55 | 6.22 | 6.91 |
| Ti | - | - | 0.11 | 0.01 | - | 0.01 | 0.01 | 0.01 | - | 0.06 | - | 0.01 | - | 0.01 | - | 0.01 | 0.03 | - | - | - | - | 0.03 | - | - | - | - | - |
| Al iv | 1.25 | 1.23 | 1.31 | 1.17 | 0.12 | 0.71 | 1.28 | 1.34 | 1.37 | 1.28 | 1.84 | 2.09 | 1.10 | 0.99 | 1.48 | 1.50 | 2.12 | 1.50 | 1.36 | 2.09 | 1.50 | 1.78 | 1.45 | 1.48 | 1.45 | 1.78 | 1.50 |
| Al vi | 1.50 | 1.92 | 2.11 | 2.07 | 2.50 | 2.04 | 2.65 | 2.31 | 2.13 | 2.78 | 2.86 | 2.67 | 3.26 | 3.28 | 3.42 | 2.90 | 1.98 | 2.19 | 2.46 | 2.56 | 2.19 | 2.67 | 2.14 | 2.05 | 2.61 | 1.98 | 3.34 |
| Fe | 5.01 | 5.10 | 2.56 | 4.16 | 2.73 | 3.11 | 3.92 | 1.76 | 1.56 | 1.85 | 5.65 | 6.11 | 3.46 | 3.22 | 4.70 | 4.54 | 5.29 | 5.35 | 4.87 | 5.03 | 5.35 | 4.17 | 5.49 | 5.21 | 4.12 | 5.76 | 2.24 |
| Mn | 0.04 | 0.04 | 0.04 | 0.05 | 0.04 | 0.03 | 0.05 | 0.03 | - | 0.04 | 0.01 | 0.01 | 0.04 | 0.01 | 0.04 | 0.04 | 0.08 | 0.08 | 0.08 | 0.08 | 0.08 | 0.11 | 0.06 | 0.08 | 0.06 | 0.11 | 0.11 |
| Mg | 4.59 | 4.57 | 6.41 | 5.01 | 6.32 | 6.02 | 4.55 | 7.30 | 7.87 | 6.27 | 2.93 | 2.86 | 5.49 | 6.38 | 4.20 | 4.48 | 4.54 | 3.84 | 3.98 | 3.38 | 3.84 | 3.38 | 3.75 | 4.31 | 4.40 | 4.48 | 5.18 |
| Ca | 0.12 | 0.15 | 0.16 | 0.29 | 0.07 | 0.09 | 0.13 | 0.05 | 0.03 | 0.06 | 0.05 | 0.05 | 0.10 | 0.16 | 0.08 | 0.14 | 0.11 | 0.08 | 0.08 | 0.03 | 0.08 | 0.56 | 0.14 | 0.06 | 0.08 | 0.03 | 0.08 |
| Na | 0.03 | 0.01 | 0.11 | 0.03 | 0.03 | 0.08 | 0.03 | 0.06 | 0.05 | 0.11 | 0.02 | - | 0.09 | 0.11 | - | - | 0.03 | 0.03 | 0.03 | - | 0.03 | 0.11 | 0.06 | 0.03 | 0.03 | 0.03 | 0.03 |
| K | 0.01 | 0.03 | 0.03 | - | - | - | 0.03 | 0.08 | 0.01 | 0.06 | 0.04 | - | - | 0.04 | - | - | - | 0.20 | 0.17 | 0.03 | 0.20 | 0.17 | 0.06 | 0.03 | 0.08 | - | 0.03 |
| P | - | - | - | - | - | - | - | - | - | 0.08 | - | - | - | - | - | - | 0.03 | - | 0.03 | - | - | 0.34 | - | - | - | - | 0.03 |
| Mn | - | - | - | - | - | - | - | - | - | 0.03 | - | - | - | - | - | - | - | - | - | - | - | - | - | - | - | - | - |
| Cr | - | - | - | - | - | - | - | - | - | - | - | - | - | - | - | - | - | - | - | - | - | - | 0.03 | - | - | - | - |
| Sr | - | - | - | - | - | - | - | - | - | - | - | - | - | - | - | - | - | - | - | 0.03 | - | - | - | - | - | - | - |
| Ba | 0.01 | - | - | 0.01 | - | - | - | 0.08 | - | - | - | - | - | - | - | - | - | - | - | - | - | - | - | - | - | - | - |
| IX | 11.71 | 11.72 | 11.55 | 11.57 | 11.29 | 11.34 | 11.35 | 15.40 | 11.65 | 11.33 | 11.53 | 11.72 | 11.46 | 12.55 | 11.48 | 11.56 | 12.05 | 11.77 | 11.65 | 11.78 | 11.77 | 11.28 | 11.93 | 11.77 | 11.38 | 11.56 | 11.01 |
| IT | 8.00 | 8.00 | 8.00 | 8.00 | 8.00 | 8.00 | 8.00 | 8.00 | 8.00 | 8.00 | 8.00 | 8.00 | 8.00 | 8.00 | 8.00 | 8.00 | 8.00 | 8.00 | 8.00 | 8.00 | 8.00 | 8.00 | 8.00 | 8.00 | 8.00 | 8.00 | 8.00 |
| TH | | | | | | | | | | | | | | | | | | | | | | | | | | | |

Appendix 2.4.15 Electron microprobe analyses of chlorite

| Mineral | Sphene 1 | 2 | 3 | 4 | 5 | 6 | 7 | 8 | 9 |
|---|---|---|---|---|---|---|---|---|---|
| PI/S No | CV93 (6) | CV69K (20) | CV93 (15) | CV69K (15) | CV69K (20) | CV90 (23) | CV90 (25) | CV90 (26) | CV93 (39) |
| $SiO_2$ | 30.99 | 33.40 | 30.69 | 29.51 | 35.17 | 32.35 | 27.87 | 29.87 | 29.80 |
| $TiO_2$ | 27.74 | 28.04 | 29.69 | 31.27 | 27.00 | 29.27 | 28.73 | 29.28 | 29.30 |
| $Al_2O_3$ | 5.87 | 5.33 | 5.01 | 3.61 | 6.27 | 4.70 | 4.94 | 4.25 | 5.33 |
| FeO | 2.54 | 3.23 | 2.24 | 1.66 | 2.33 | 1.78 | 2.40 | 3.16 | 2.54 |
| MnO | 0.04 | 0.03 | 0.01 | 0.04 | 0.05 | – | – | 0.13 | – |
| MgO | 0.44 | 0.07 | 0.05 | – | – | – | – | 0.33 | 0.40 |
| CaO | 27.37 | 25.02 | 28.80 | 26.85 | 24.21 | 25.08 | 26.32 | 26.16 | 28.54 |
| $Na_2O$ | 0.10 | 0.65 | 0.01 | 0.07 | 1.91 | 0.89 | – | 0.17 | 0.05 |
| $K_2O$ | 0.06 | 0.03 | 0.01 | 0.05 | 0.03 | 0.05 | – | 0.09 | 0.06 |
| $P_2O_5$ | 0.22 | 0.01 | 0.27 | – | – | 0.11 | 0.01 | 1.16 | 0.11 |
| NiO | – | 0.01 | – | – | 0.02 | 0.02 | 0.03 | – | 0.02 |
| $Cr_2O_3$ | – | – | 0.02 | 0.05 | 0.05 | 0.02 | 0.06 | – | 0.02 |
| SrO | 0.08 | 0.13 | 0.14 | 0.11 | – | 0.11 | 0.04 | 0.04 | 0.13 |
| BaO | 0.14 | 0.94 | – | 1.02 | 0.68 | 0.93 | 0.86 | 0.98 | 0.18 |
| TOTAL | 95.59 | 96.79 | 96.94 | 94.24 | 97.72 | 95.31 | 91.26 | 95.62 | 96.48 |
| Si | 4.00 | 4.00 | 4.00 | 4.00 | 4.00 | 4.00 | 4.00 | 4.00 | 4.00 |
| Ti | 2.70 | 2.70 | 2.85 | 3.12 | 2.53 | 2.85 | 2.96 | 2.87 | 2.85 |
| Al | 0.89 | 0.78 | 0.76 | 0.57 | 0.93 | 0.72 | 0.80 | 0.65 | 0.82 |
| $Fe^{+3}$ | 0.27 | 0.34 | 0.25 | 0.19 | 0.25 | 0.19 | 0.29 | 0.34 | 0.27 |
| Mn | – | – | – | – | – | – | – | 0.02 | – |
| Mg | 0.08 | 0.02 | – | – | – | – | – | 0.06 | 0.08 |
| Ca | 3.80 | 3.42 | 3.95 | 3.82 | 3.23 | 3.48 | 3.88 | 3.69 | 3.95 |
| Na | 0.02 | 0.15 | – | 0.02 | 0.46 | 0.23 | – | 0.04 | 0.02 |
| K | 0.02 | – | – | – | – | – | – | 0.02 | – |
| P | 0.02 | – | 0.04 | – | – | 0.29 | – | 0.13 | 0.02 |
| Ni | – | – | – | – | – | – | – | – | – |
| Cr | – | – | – | – | – | – | – | – | – |
| Sr | – | 0.02 | 0.02 | – | – | – | – | – | 0.02 |
| Ba | – | 0.04 | – | 0.06 | 0.04 | 0.04 | 0.04 | 0.06 | – |
| IX | 3.94 | 3.65 | 4.01 | 3.90 | 3.73 | 3.77 | 3.92 | 3.98 | 4.09 |
| IY | 3.86 | 3.82 | 3.86 | 3.88 | 3.71 | 3.76 | 4.05 | 3.86 | 3.94 |
| IZ | 4.00 | 4.00 | 4.00 | 4.00 | 4.00 | 4.00 | 4.00 | 4.00 | 4.00 |

| 10 | 11 | 12 | 13 | 14 | 15 | 16 | 17 |
|---|---|---|---|---|---|---|---|
| CV93 (44) | CV93 (49) | CV93 (55) | CV97 (10) | CV62 (4) | (12) | (9) | (1) |
| 32.00 | 26.98 | 37.22 | 31.56 | 30.98 | 31.52 | 32.80 | 36.49 |
| 29.98 | 23.98 | 24.41 | 29.55 | 29.41 | 30.86 | 32.26 | 19.89 |
| 5.27 | 5.69 | 7.29 | 5.11 | 5.14 | 4.95 | 2.64 | 8.49 |
| 2.22 | 7.78 | 0.01 | 1.95 | 1.51 | 2.74 | 2.67 | 2.74 |
| – | 0.12 | – | – | – | – | – | 0.06 |
| – | 1.63 | 0.07 | 0.58 | – | 0.31 | 0.38 | 2.88 |
| 28.82 | 24.48 | 24.43 | 29.01 | 23.82 | 27.49 | 27.47 | 20.57 |
| 0.96 | 0.04 | 2.59 | – | 0.06 | 0.06 | 0.03 | 2.42 |
| 0.03 | 0.07 | 0.03 | – | 0.03 | 0.03 | – | 0.55 |
| 0.19 | 1.36 | 0.16 | 0.03 | 0.13 | 0.05 | – | – |
| 0.02 | 0.01 | 0.02 | – | – | 0.04 | – | – |
| – | – | 0.03 | – | – | 0.12 | – | – |
| 0.06 | 0.04 | 0.04 | – | 0.14 | – | – | – |
| 0.07 | 0.13 | 0.13 | – | 1.65 | 1.76 | 1.07 | 0.76 |
| 99.62 | 92.31 | 96.37 | 97.79 | 92.87 | 99.93 | 99.32 | 94.85 |
| 4.00 | 4.00 | 4.00 | 4.00 | 4.00 | 4.00 | 4.00 | 4.00 |
| 2.81 | 2.47 | 2.28 | 2.82 | 2.95 | 2.91 | 3.04 | 1.90 |
| 0.08 | 0.91 | 1.06 | 0.77 | 0.80 | 0.74 | 0.39 | 1.27 |
| 0.23 | 0.89 | – | 0.21 | 0.17 | 0.29 | 0.29 | 0.30 |
| – | 0.02 | – | – | – | – | – | – |
| – | 0.34 | – | – | – | 0.06 | 0.08 | 0.54 |
| 3.84 | 3.61 | 3.25 | 3.95 | 3.38 | 3.71 | 3.70 | 2.80 |
| 0.23 | 0.02 | 0.63 | – | 0.02 | 0.02 | – | 0.60 |
| – | 0.02 | – | – | – | – | – | 0.09 |
| 0.02 | 0.15 | 0.02 | – | 0.02 | – | – | – |
| – | – | – | – | – | – | – | – |
| – | – | – | – | – | 0.02 | – | – |
| – | – | – | – | 0.02 | – | – | – |
| – | – | – | – | 0.10 | 0.10 | 0.06 | 0.04 |
| 4.00 | 4.00 | 4.00 | 4.00 | 4.00 | 4.00 | 4.00 | 4.00 |
| 3.12 | 4.27 | 3.34 | 3.80 | 3.92 | 3.94 | 3.72 | 3.47 |
| 3.99 | 3.71 | 4.61 | 4.01 | 4.10 | 3.95 | 4.11 | 4.61 |

Appendix 2.4.16 Electron microprobe analyses of sphene

Appendix 2.4.17

| Element | Standards |
|---|---|
| Si | Wollastonite |
| Ti | Rutile |
| Al | Corundum |
| | Orthoclase |
| Fe | Garnet |
| | Ferrite |
| | METAL |
| Mn | METAL |
| | Ferrite |
| Mg | Periclase |
| Ca | Wollastonite |
| Na | Jadeite |
| K | Orthoclase |
| P | Beeson Apatite |
| Ni | METAL |
| Sr | Celestine |
| Ba | Barytes |

Appendix 2.4.17 Microprobe standards per element

Appendix 2.5.1 Fluid inclusion analyses

| Crystal | Sample No | Inclusion No | Inclusion Type | Tf °C | Tlm °C | wt% NaCl equiv | Th °C | Ts °C | Ts °C |
|---|---|---|---|---|---|---|---|---|---|
| Analcime | CV47 | 1 | L+V | -29.7 | | | 281 | | |
| | | 2 | L+V | -40.1 | +0.4 | 0 | 214 | | |
| | | 3 | L+V | | | | 210 | | |
| | | 4 | L+V | | | | 301 | | |
| | | 5 | S+L+V | | | 38 | 181.2 | 307 | |
| | | 6 | L+V | | | | 308 | | |
| | | 7 | L+V | | | | 168.3 | | |
| | | 8 | L+V | | | | 157.9 | | |
| | | 10 | L+V | | | | 176.4 | | |
| | | 11 | L+V | | | | 158.2 | | |
| | | 12 | L+V | | | | 123 | | |
| Calcite (co-existing with analcime) | CV85 (after D. Banks pers. comm 1986) | Anal 1 | L+V | -39/-48 | -0.8 | 1.39 | 147 | | |
| | | Anal 2 | L+V | -42/-47 | -0.9 | 1.59 | 151 | | |
| | | Anal 3 | L+V | -36/-44 | -0.6 | 1.05 | 101 | | |
| | | Anal 4 | L+V | -38/-50 | -0.7 | 1.27 | 133 | | |
| | | Anal 5 | L+V | -34/-48 | -1.1 | 1.90 | 148 | | |
| Natrolite | CV59C | 1 | L+V | | | | 326 | | |
| | | 2 | L+V | | | | 261 | | |
| | | 3 | L+V | | | | 175.5 | | |
| | | 4 | L+V | | | | 318 | | |
| | CV59B | 1 | V+L | -33.5 | -7.5 | 11.3 | 347 | | |
| | | 2 | V+L | | +2.1 | 0 | 322 | | |
| | | 3 | L+V | | | | 311 | | |
| Heulandite | CV94 | 1 | L+V | | -4.2 | 6.9 | 133 | | |
| | | 2 | L+V | -38.4 | -13.6 | 17.8 | 169.3 | | |
| | | 3 | L+V | -57.9 | -10.7 | 14.9 | 169 | | |
| | | 4 | L+V | -69.5 | -19.5 | 22.4 | 102.8 | | |
| | | 5 | L+V | -77.3 | -23.1 | 25.3 | 119 | | |
| | | 8 | L+V | | -16.4 | 20.2 | 164.9 | | |
| | | 9 | L+V | -50.2 | -4.0 | 6.6 | 152.4 | | |
| | | 10 | L+V | -42.3 | +0.1 | 0 | 88.8 | | |
| | | 11 | L+V | -39.8 | -3.8 | 6.3 | 172.1 | | |
| | | 12 | L+V | -89.3 | -25.5 | 26.8 | 128.5 | | |
| | | 13 | L+V | -72.1 | -18.1 | 21.5 | 113 | | |
| | | 14 | L+V | -60.1 | -9.1 | 13.2 | 154.7 | | |
| | | 15 | L+V | | | | 136.2 | | |
| | | 16 | L+V | -38.0 | -0.2 | 0.2 | 157.5 | | |
| | | 17 | L+V | -86.1 | -26.0 | 27.3 | 166.2 | | |
| | | 18 | L+V | | | | 178.8 | | |
| | | 19 | L+V | | | | 162.1 | | |
| | | 20 | L+V | | | | 178.8 | | |
| | | 21 | L+V | | | | 153 | | |
| | | 22 | L+V | | | | 151.8 | | |
| | | 23 | L+V | | -8.1 | 12 | 163.4 | | |
| | | 24 | L+V | -37.7 | +1.5 | 0 | 122 | | |
| | | 25 | L+V | -57.3 | -8.3 | 12.3 | 135.7 | | |
| | | 26 | L+V | | | | 302 | | |
| | | 29 | V+L | -41.6 | 0 | 0 | 361 | | |
| | | 31 | L+V | | | | 136.9 | | |
| | | 32 | L+V | -54.6 | -6.1 | 9.5 | 123.4 | | |
| | | 33 | L+V | -46.7 | -7.9 | 11.8 | 220 | | |
| | | 34 | L+V | -47.1 | -7.6 | 11.4 | 225 | | |
| Laumontite | CV97AL25 | 1 | L+V | | | | 231 | | |
| | CV97AL26 | 1 | L+V | | | | 356 | | |
| | | 2 | V+L | | | | 153.7 | | |
| | | 3 | V+L | | | | 151.6 | | |
| | | 4 | L+V | | | | 310 | | |
| | | 5 | V+L | | | | 305 | | |
| | | 6 | S+L+V | -36.4 | | 42 | 251 | 368 | |

| | | | | | | | | |
|---|---|---|---|---|---|---|---|---|
| Laumontite | CV97AL26 (cont) | 7<br>8 | S+L+V<br>V+L | -39.8 | | 42 | 227<br>405 | 372 |
| Thomsonite | CV69(1) | 1 | L+V | -72.9 | -19.4 | 22.4 | 250 | |
| | | 3 | L+V | -50.4 | -12.3 | 16.6 | 243 | |
| | | 4 | L+V | -76.6 | -21.6 | 24.0 | 270 | |
| | | 5 | L+V | -50.2 | -12.8 | 17.0 | 261 | |
| | | 6 | L+V | -54.5 | -12.3 | 16.6 | 244 | |
| | | 7 | L+V | -55.1 | -12.3 | 16.6 | 243 | |
| | | 8 | L+V | -69.8 | -13.4 | 17.6 | 264 | |
| | | 9 | L+V | -57.1 | -11.8 | 16.1 | 250 | |
| | | 10 | L+V | -66.5 | -18.3 | 21.6 | 246 | |
| | | 11 | L+V | -57.4 | -12.1 | 16.4 | 251 | |
| | | 12 | L+V | -71.4 | -19.6 | 22.5 | 350 | |
| | | 13 | L+V | | 0.0 | 0 | 249 | |
| | | 14 | L+V | -50.8 | -13.5 | 17.7 | 271 | |
| | | 15 | L+V | -68.4 | -12.2 | 16.5 | 253 | |
| | | 16 | S+L+V | | | 43 | | 374 |
| | | 17 | L+V | -74.8 | -17.8 | 21.3 | 250 | |
| | | 18 | L+V | -76.4 | -20.4 | 23 | 550 | |
| | | 19 | L+V | -53.2 | -11.4 | 15.7 | 247 | |
| | | 20 | L+V | -82.1 | -22.8 | 25.3 | 323 | |
| | | 23 | L+V | -69.6 | -14.5 | 18.6 | 272 | |
| | | 24 | L+V | -122 | -25.0 | 26.5 | 280 | |
| | | 25 | L+V | -65.7 | -9.3 | 13.4 | 268 | |
| | | 26 | L+V | -76.6 | -23.2 | 25.2 | 550 | |
| | | 28 | L+V | -53.8 | -13.9 | 18 | 275 | |
| | | 29 | L+V | -56.4 | -14.3 | 18.4 | 273 | |
| | | 30 | V+L | -53.0 | -16.6 | 20.3 | 477 | |
| | | 32 | L+V | -51.9 | -15.8 | 19.7 | 348 | |
| | | 33 | L+V | -70.9 | -14.8 | 18.1 | 293 | |
| | | 34 | L+V | -58.4 | -15.1 | 19.1 | 284 | |
| | | 36 | L+V | -101.0 | -15.0 | 19 | 291 | |
| | | 37 | L+V | -82.4 | -33.1 | 31.7 | 224 | |
| | | 38 | L+V | -85.0 | -27.9 | 28.0 | 187 | |
| | | 39 | L+V | -54.67 | -15.6 | 19.5 | 440 | |
| | | 40 | L+V | | | | 207 | |
| | | 41 | L+V | -66.6 | -18.2 | 21.5 | 119.6 | |
| | | 42 | L+V | -83.3 | -26.3 | 27.3 | 370 | |
| Thomsonite | CV69(1) (cont) | 43 | L+V | -66.7 | -25.7 | 27.0 | 414 | |
| | | 44 | L+V | -69.7 | -26.3 | 27.3 | 274 | |
| | | 45 | L+V | -82.5 | -26.4 | 27.4 | 195.6 | |
| | | 47 | L+V | -79.3 | -22.3 | 24.6 | 184.9 | |
| | | 48 | L+V | -77.7 | -21.9 | 24.5 | 295 | |
| | | 49 | L+V | -76.9 | -22.4 | 24.7 | 271 | |
| | | 50 | S+L+V | -77.5 | -23.0 | 47.0 | | 410 |
| | | 51 | L+V | -81.1 | -21.8 | 24.3 | 181 | |
| | | 52 | S+L+V | -85.2 | -22.3 | 37.5 | | 299 |
| | | 53 | S+L+V | -79.8 | -22.4 | 40.0 | | 352 |
| | | 54 | L+V | -81.6 | -21.9 | 24.5 | 187.8 | |
| | | 55 | S+L+V | -80.9 | -27.4 | 28.2 | 352 | 352 |
| | | 56 | L+V | -73.9 | | | 350 | |
| | | 58 | S+L+V | -74.6 | -29.4 | 56.0 | 180 | 493 |
| Prehnite | L12 | 1 | L+V | -63.6 | -12.7 | 17 | 532 | |
| | | 3 | L+V | -67.1 | -14.0 | 18.1 | 379 | |
| | | 5 | L+V | -60.3 | -11.0 | 15.2 | 400 | |
| | | 6 | L+V | -41.2 | -0.5 | 0.9 | 146.9 | |
| | | 10 | L+V | -46.4 | -10.5 | 14.7 | 124.0 | |
| | | 12 | L+V | -66.7 | -15.4 | 19.4 | 88.9 | |
| | | 13 | L+V | -46.7 | -10.4 | 14.6 | 400 | |
| | | 14 | L+V | -59.6 | -10.5 | 14.7 | 246 | |
| | | 15 | L+V | -63.0 | -10.9 | 15.1 | 449 | |
| | | 16 | L+V | -66.7 | -15.8 | 19.7 | 88.9 | |
| | | 17 | L+V | -60.7 | -11.8 | 16.1 | 400 | |
| | | 18 | L+V | -66.8 | -15.1 | 19.1 | 142.1 | |
| | | 19 | L+V | -60.0 | -15.9 | 19.8 | 164.9 | |
| | | 20 | S+L+V | -66.7 | | | 389 | |
| | CV69 | 1 | L+V | | -13.8 | 18 | 179.9 | |
| | | 2 | L+V | | -12.5 | 16.8 | 180.3 | |
| | | 3 | S+L+V | | 0.6 | 57.0 | 358 | 459 |
| | | 4 | L+V | -64.0 | -13.6 | 17.8 | 224 | |
| | | 5 | L+V | -72.7 | -13.6 | 17.8 | 406 | |

APPENDIX Whole rock chemical data.

| Sample No. | CV3 | CV5 | CV8 | CV9 | CV19 | CV20 | CV22 | CV26 | CV27 | CV28 | CV29 | CV30A | CV30B |
|---|---|---|---|---|---|---|---|---|---|---|---|---|---|
| Weight % | 100.689 | 100.012 | 99.853 | 100.017 | 100.000 | 100.137 | 99.168 | 100.752 | 100.045 | 99.889 | 99.971 | 100.703 | 100.330 |
| $SiO_2$ | 45.343 | 29.177 | 44.804 | 47.975 | 48.916 | 42.918 | 42.829 | 59.239 | 43.767 | 49.881 | 36.763 | 44.241 | 46.032 |
| $TiO_2$ | 3.603 | 1.472 | 2.168 | 1.231 | 1.443 | 2.660 | 2.724 | 0.971 | 2.202 | 1.958 | 2.598 | 1.887 | 2.362 |
| $Al_2O_3$ | 14.117 | 7.915 | 18.245 | 9.348 | 9.980 | 13.668 | 14.326 | 17.373 | 12.244 | 12.002 | 13.377 | 10.079 | 19.434 |
| $Fe_2O_3$ | 4.052 | 1.466 | 7.653 | 0.501 | -0.336 | 6.563 | 3.186 | 6.423 | 1.459 | 4.816 | 4.110 | 2.104 | 6.018 |
| FeO | 7.600 | 5.450 | 4.500 | 5.300 | 7.690 | 5.700 | 8.260 | 1.250 | 7.920 | 4.460 | 6.890 | 7.600 | 3.700 |
| MnO | 0.190 | 0.135 | 0.098 | 0.152 | 0.115 | 0.168 | 0.219 | 0.042 | 0.100 | 0.120 | 0.154 | 0.199 | 0.141 |
| MgO | 5.263 | 5.341 | 0.524 | 2.170 | 7.712 | 8.126 | 7.712 | 1.467 | 10.680 | 9.107 | 8.092 | 8.236 | 3.62 |
| CaO | 8.204 | 23.747 | 13.097 | 14.518 | 6.645 | 6.261 | 8.728 | 1.373 | 3.563 | 2.821 | 9.644 | 8.516 | 10.317 |
| $Na_2O$ | 2.862 | 1.250 | 4.418 | 1.240 | 0.608 | 3.823 | 2.458 | 5.981 | 2.863 | 0.430 | 1.387 | 0.506 | 3.481 |
| $K_2O$ | 2.039 | 1.030 | 0.025 | 2.300 | 3.449 | 0.272 | 0.873 | 3.180 | 2.257 | 5.080 | 3.030 | 2.238 | 1.258 |
| $P_2O_5$ | 1.172 | 0.324 | 0.313 | 0.494 | 0.316 | 0.745 | 0.736 | 0.514 | 0.611 | 0.419 | 0.559 | 0.453 | 0.356 |
| L.O.I. | 5.400 | | | | | | | 2.800 | 11.500 | 8.300 | 12.600 | 13.800 | 3.200 |
| TOTAL | 100.689 | 100.012 | 99.853 | 100.017 | 100.000 | 100.137 | 99.168 | 100.613 | 100.045 | 99.889 | 99.971 | 100.703 | 100.330 |
| Th ppm | 7 | - | 14 | 4 | 3 | 4 | 5 | 6 | 9 | 4 | 6 | 6 | - |
| Mn | 0.18 | 0.144 | 0.183 | 0.161 | 0.121 | 0.182 | 0.211 | 0.042 | 0.109 | 0.135 | 0.160 | 0.206 | 0.138 |
| V | 292 | 208 | 335 | 127 | 190 | 269 | 264 | 89 | 218 | 228 | 307 | 209 | 250 |
| Cr | 0 | 248 | 131 | 97 | 262 | 221 | 123 | - | 252 | 197 | 286 | 230 | - |
| Hf | 3 | 4 | 1 | 5 | 4 | 4 | 5 | 6 | 5 | 4 | 4 | 3 | 4 |
| Ni | 0 | 74 | 80 | 67 | 187 | 170 | 131 | 8 | 212 | 166 | 181 | 275 | 12 |
| Cu | 12 | 18 | 7 | 19 | 25 | 39 | 38 | 17 | 47 | 53 | 57 | 27 | 23 |
| Zn | 47 | 160 | 124 | 26 | 117 | 98 | 127 | 78 | 62 | 33 | 66 | 60 | 65 |
| Rb | 40 | 22 | 24 | 44 | 54 | 3 | 5 | 67 | 42 | 58 | 40 | 29 | 21 |
| Sr | 796 | 491 | 724 | 254 | 383 | 351 | 1205 | 386 | 331 | 109 | 403 | 140 | 1192 |
| Y | 29 | 14 | 20 | 27 | 28 | 24 | 25 | 35 | 32 | 25 | 28 | 22 | 24 |
| Zr | 227 | 128 | 168 | 244 | 234 | 294 | 410 | 294 | 316 | 197 | 253 | 187 | 327 |
| Nb | 36 | 35 | 28 | 37 | 33 | 55 | 58 | 10 | 64 | 50 | 48 | 37 | 25 |
| Ce | 96 | 112 | 73 | 111 | 67 | 98 | 148 | 79 | 132 | 37 | 94 | 108 | 66 |
| La | 42 | 59 | 22 | 48 | 50 | 52 | 51 | 18 | 58 | 28 | 36 | 33 | 11 |
| $TiO_2$ | 3.397 | 1.569 | 2.733 | 1.309 | 1.573 | 2.625 | 2.625 | 0.921 | 2.277 | 2.074 | 2.778 | 1.971 | 2.217 |
| Ba | 820 | 756 | 578 | 378 | 722 | 497 | 839 | 499 | 736 | 357 | 906 | 356 | 410 |
| Pb | 6 | 2 | 20 | 7 | 3 | 12 | 1 | 5 | 3 | 1 | 4 | 2 | - |

# Whole rock chemistry data continued

| CV32 | CV33 | CV34 | CV35 | CV37 | X1 | X2 | X3 | X4 | X6 | X7 | X8 | CV69A | CV69B1 | CV69B2 | CV94LAL-V | CV94LAL-V | CV95HML | CV95UAL-V | CV111UAL-V | CV111UAL-V | CV112HML |
|---|---|---|---|---|---|---|---|---|---|---|---|---|---|---|---|---|---|---|---|---|---|
| 99.882 | 100.106 | 99.437 | 100.369 | 99.800 | 100.004 | 100.028 | 99.773 | 99.409 | 100.572 | 100.254 | 100.003 | 99.508 | 100.598 | 99.884 | 100.248 | 100.231 | 100.958 | 100.001 | 100.002 | 100.228 | 99.997 |
| 38.157 | 37.914 | 36.426 | 41.995 | 45.488 | 40.876 | 39.567 | 43.397 | 44.277 | 53.871 | 38.496 | 47.187 | 45.220 | 46.083 | 49.165 | 55.281 | 49.424 | 55.330 | 50.899 | 45.099 | 46.463 | 44.685 |
| 1.721 | 1.394 | 2.882 | 2.034 | 2.050 | 2.031 | 3.445 | 2.816 | 2.143 | 1.066 | 0.456 | 2.636 | 2.721 | 3.279 | 2.472 | 2.214 | 3.070 | 1.845 | 2.465 | 3.583 | 3.547 | 2.360 |
| 9.524 | 16.282 | 14.479 | 12.709 | 14.296 | 21.560 | 18.773 | 17.898 | 14.553 | 14.431 | 19.522 | 17.637 | 16.338 | 17.088 | 17.974 | 12.933 | 15.492 | 16.830 | 16.734 | 17.444 | 17.949 | 14.867 |
| 0.713 | 1.505 | 1.962 | 4.046 | 9.872 | 11.370 | 4.721 | 5.449 | 7.117 | 1.543 | 2.411 | 5.367 | 2.114 | 4.751 | 8.112 | 14.697 | 9.555 | 9.364 | 13.649 | 7.279 | 7.834 | 4.276 |
| 7.300 | 8.100 | 7.830 | 7.820 | 8.610 | 4.000 | 9.727 | 7.700 | 5.400 | 8.000 | 4.493 | 5.856 | 9.417 | 8.190 | 3.784 | - | 3.636 | 1.743 | - | 3.939 | 3.820 | 7.368 |
| 0.263 | 0.163 | 0.135 | 0.227 | 0.135 | 0.144 | 0.471 | 0.283 | 0.247 | 0.183 | 0.079 | 0.178 | 0.196 | 0.136 | 0.121 | 0.100 | 0.145 | 0.120 | 0.072 | 0.452 | 0.473 | 0.260 |
| 6.360 | 4.397 | 10.367 | 13.343 | 3.265 | 4.397 | 7.913 | 5.574 | 7.198 | 5.769 | 0.395 | 4.871 | 5.726 | 4.316 | 2.611 | 2.657 | 4.623 | 2.160 | 0.811 | 6.102 | 6.022 | 8.021 |
| 18.013 | 10.102 | 7.849 | 6.587 | 3.928 | 0.914 | 1.636 | 2.889 | 6.013 | 9.487 | 30.089 | 3.870 | 8.503 | 6.010 | 3.146 | 4.356 | 6.063 | 2.857 | 3.613 | 4.037 | 4.688 | 10.052 |
| 1.719 | 2.512 | 1.436 | 3.041 | 2.702 | 0.532 | 2.354 | 4.591 | 4.858 | 2.609 | 0.273 | 6.075 | 3.957 | 5.438 | 5.297 | 3.336 | 2.985 | 6.897 | 6.438 | 3.306 | 4.500 | 1.998 |
| 0.765 | 2.383 | 2.338 | 1.100 | 0.514 | 5.686 | 2.554 | 1.890 | 0.565 | 1.097 | 0.042 | 0.436 | 0.645 | 0.022 | 2.421 | 0.927 | 1.159 | 0.652 | 0.567 | 1.924 | 0.935 | 0.791 |
| 0.363 | 0.254 | 0.564 | 0.399 | 1.184 | 0.110 | 0.187 | 0.331 | 0.239 | 0.186 | 0.130 | 0.290 | 0.225 | 0.376 | 0.531 | 0.379 | 0.475 | 0.957 | 0.803 | 0.680 | 0.566 | 0.401 |
| 15.600 | 14.100 | 12.000 | 6.200 | 6.800 | 7.880 | 7.600 | 5.000 | 5.200 | 1.200 | 3.600 | 4.950 | 3.400 | 4.000 | 3.000 | 3.400 | 3.200 | 2.000 | 3.950 | 5.720 | 3.200 | 4.100 |
| 99.882 | 100.080 | 99.437 | 100.369 | 99.800 | 99.560 | 100.028 | 99.773 | 99.409 | 100.572 | 100.254 | 100.003 | 99.508 | 100.598 | 99.884 | 100.248 | 99.827 | 100.765 | 100.001 | 99.565 | 99.997 | 99.997 |
| - | - | 9 | 1 | - | 16 | - | - | 1 | 4 | - | - | - | - | - | 1 | - | 7 | 4 | 6 | 2 | 1 |
| 0.271 | 0.155 | 0.143 | 0.204 | 0.135 | 0.152 | 0.477 | 0.299 | 0.288 | 0.190 | 0.095 | 0.200 | 0.219 | 0.167 | 0.125 | 0.067 | 0.131 | 0.114 | 0.090 | 0.449 | 0.434 | 0.271 |
| 224 | 239 | 385 | 225 | 65 | 167 | 404 | 273 | 355 | 261 | 164 | 286 | 312 | 223 | 243 | 359 | 289 | 70 | 95 | 269 | 253 | 338 |
| 329 | 348 | 473 | 490 | - | 46 | 54 | 97 | 165 | 133 | - | 28 | 28 | 2 | 63 | 15 | - | - | - | - | 18 | 178 |
| 2 | 1 | 5 | 4 | 4 | 7 | 3 | 3 | 2 | 4 | 1 | 3 | 3 | 2 | 3 | 6 | 3 | 6 | 5 | 5 | 6 | 4 |
| 201 | 130 | 244 | 326 | 2 | 43 | 57 | 59 | 121 | 67 | 11 | 41 | 54 | 19 | 55 | 21 | 16 | 5 | 8 | 2 | 6 | 121 |
| 48 | 35 | 39 | 51 | 5 | 12 | 80 | 33 | 39 | 98 | 134 | 43 | 44 | 46 | 30 | 19 | 3 | 12 | 32 | 14 | 20 | 28 |
| 39 | 44 | 38 | 138 | 105 | 88 | 216 | 134 | 242 | 87 | 31 | 99 | 98 | 115 | 106 | 31 | 53 | 63 | 37 | 267 | 252 | 102 |
| 7 | 14 | 33 | 18 | 5 | 178 | 74 | 57 | 17 | 33 | 5 | 8 | 11 | 2 | 70 | 10 | 28 | 16 | 12 | 42 | 43 | 19 |
| 533 | 85 | 452 | 296 | 69 | 139 | 360 | 361 | 580 | 189 | 76 | 1120 | 759 | 534 | 364 | 701 | 608 | 542 | 508 | 552 | 556 | 463 |
| 22 | 17 | 33 | 26 | 40 | 55 | 25 | 28 | 25 | 34 | 11 | 21 | 20 | 24 | 21 | 43 | 29 | 41 | 31 | 37 | 36 | 29 |
| 195 | 85 | 237 | 174 | 408 | 452 | 242 | 193 | 145 | 169 | 19 | 124 | 136.5 | 150 | 164 | 305 | 207 | 363 | 334 | 295 | 288 | 184 |
| 22 | 9 | 47 | 29 | 47 | 50 | 33 | 23 | 15 | 3 | - | 10 | 12 | 15 | 21 | 57 | 33 | 73 | 38 | 55 | 52 | 27 |
| 64 | 15 | 144 | 47 | 195 | 190 | 32 | 94 | 17 | 40 | - | 21 | 58 | 38 | 100 | 127 | 142 | 175 | 152 | 123 | 124 | 97 |
| 13 | - | 28 | 4 | 63 | 48 | - | 7 | 7 | 15 | - | - | 8 | 2 | 30 | 32 | 16 | 62 | 39 | 34 | 36 | 15 |
| 1.661 | 1.605 | 2.972 | 1.754 | 1.873 | 2.102 | 3.186 | 2.666 | 2.118 | 1.173 | 0.496 | 2.338 | 2.193 | 3.053 | 2.349 | 2.993 | 2.699 | 1.626 | 2.370 | 3.325 | 3.256 | 2.448 |
| 430 | 58 | 635 | 364 | 190 | 647 | 563 | 196 | 229 | 354 | - | 116 | 332 | 65 | 348 | 289 | 436 | 337 | 193 | 587 | 552 | 356 |
| 7 | 2 | 2 | - | - | 34 | 17 | 14 | 26 | 8 | 4 | 5 | 12 | 3 | 18 | 5 | 8 | 9 | 3 | 8 | 7 | - |

Whole rock chemistry data continued.

| CV69I | CV69J | L1MML | L1LAL-V | CV91MML | L2MML | L4MML | CV105MML | L9MML | L8MML | L10MML | L11MML | L12MML | L12LAL-V | L13MML | L13UAL-V | L14MML | L15MML | CV88MML | CV89UAL-V | L16MML |
|---|---|---|---|---|---|---|---|---|---|---|---|---|---|---|---|---|---|---|---|---|
| 99.616 | 99.765 | 101.218 | 100.452 | 99.817 | 100.959 | 100.721 | 100.489 | 100.401 | 100.232 | 100.821 | 100.817 | 100.951 | 99.997 | 100.696 | 101.053 | 100.000 | 99.934 | 99.982 | 99.973 | 100.507 |
| 46.542 | 48.870 | 48.951 | 54.188 | 50.004 | 46.357 | 45.472 | 50.113 | 48.168 | 49.130 | 46.476 | 48.458 | 48.519 | 38.564 | 47.997 | 44.621 | 49.801 | 47.714 | 48.079 | 48.569 | 47.198 |
| 2.959 | 2.148 | 2.780 | 2.609 | 3.218 | 2.372 | 2.357 | 3.050 | 2.884 | 3.021 | 3.672 | 2.719 | 2.737 | 2.240 | 2.578 | 2.969 | 2.585 | 2.736 | 2.858 | 2.556 | 2.364 |
| 16.279 | 16.924 | 17.948 | 16.118 | 13.419 | 13.510 | 13.542 | 16.712 | 17.590 | 16.364 | 14.476 | 18.121 | 18.173 | 19.203 | 17.685 | 17.060 | 17.577 | 18.025 | 18.041 | 18.324 | 20.486 |
| 5.446 | 7.343 | 7.289 | 10.473 | 4.406 | 7.504 | 5.680 | 8.540 | 5.263 | 6.946 | 5.960 | 3.524 | 8.628 | 10.882 | 6.812 | 9.428 | 2.876 | 4.759 | 9.669 | 6.444 | 3.548 |
| 7.781 | 2.451 | 4.444 | 1.754 | 8.951 | 5.500 | 7.113 | 3.365 | 6.337 | 5.612 | 8.200 | 7.500 | 3.636 | 1.009 | 4.286 | 4.265 | 8.011 | 6.346 | 2.574 | 3.697 | 5.891 |
| 0.139 | 0.109 | 0.174 | 0.087 | 0.201 | 0.306 | 0.301 | 0.387 | 0.480 | 0.208 | 0.236 | 0.263 | 0.154 | 0.114 | 0.193 | 0.127 | 0.290 | 0.289 | 0.168 | 0.210 | 0.284 |
| 3.921 | 1.426 | 3.574 | 1.653 | 4.613 | 8.680 | 8.765 | 3.440 | 4.736 | 4.172 | 4.467 | 4.656 | 3.129 | 0.340 | 3.086 | 2.250 | 3.952 | 3.672 | 3.345 | 3.426 | 3.949 |
| 5.938 | 12.326 | 6.732 | 2.519 | 5.607 | 10.750 | 10.795 | 5.917 | 3.984 | 5.993 | 7.051 | 5.625 | 3.352 | 21.750 | 5.741 | 6.734 | 2.996 | 6.212 | 6.261 | 4.138 | 5.169 |
| 4.321 | 5.374 | 4.466 | 8.261 | 3.041 | 1.794 | 1.733 | 4.500 | 4.983 | 4.643 | 4.172 | 4.288 | 4.516 | 1.089 | 4.751 | 3.209 | 5.709 | 4.248 | 4.574 | 5.782 | 4.094 |
| 1.567 | 0.073 | 1.367 | 0.061 | 2.174 | 0.697 | 0.705 | 0.935 | 1.051 | 0.988 | 1.007 | 1.033 | 2.353 | 0.019 | 2.339 | 0.091 | 1.009 | 1.141 | 0.719 | 0.089 | 1.944 |
| 0.318 | 0.249 | 0.399 | 0.334 | 0.689 | 0.279 | 0.268 | 0.566 | 0.422 | 0.533 | 0.597 | 0.398 | 0.350 | 0.344 | 0.352 | 0.426 | 0.353 | 0.388 | 0.408 | 0.428 | 0.326 |
| 3.800 | 2.200 | 2.600 | 2.200 | 2.200 | 3.600 | 3.200 | 2.600 | 3.800 | 2.000 | 3.600 | 3.400 | 5.000 | 4.330 | 4.400 | 9.400 | 3.950 | 3.700 | 3.000 | 5.900 | 4.600 |
| 99.616 | 100.087 | 100.624 | 100.452 | 99.817 | 100.959 | 100.721 | 100.489 | 100.401 | 100.232 | 100.821 | 100.817 | 100.951 | 99.997 | 100.220 | 100.860 | 100.000 | 99.934 | 99.982 | 99.973 | 100.507 |
| - | - | - | - | 2 | 1 | 2 | 1 | 2 | 7 | 1 | 2 | 1 | - | - | - | 2 | 3 | 3 | 2 | - |
| 0.148 | 0.122 | 0.174 | 0.094 | 0.199 | 0.281 | 0.293 | 0.360 | 0.527 | 0.202 | 0.248 | 0.296 | 0.173 | 0.134 | 0.219 | 0.153 | 0.332 | 0.304 | 0.169 | 0.248 | 0.305 |
| 306 | 252 | 263 | 170 | 378 | 266 | 398 | 271 | 288 | 317 | 420 | 286 | 248 | 249 | 263 | 261 | 299 | 305 | 288 | 287 | 290 |
| 49 | 15 | - | - | - | - | 388 | - | - | - | - | - | - | - | - | 5 | - | - | - | 4 | - |
| 4 | 2 | 3 | 3 | 4 | 4 | 2 | 4 | 4 | 4 | 3 | 3 | 3 | 3 | 4 | 1 | 4 | 4 | 4 | 3 | 4 |
| 49 | 31 | 6 | 6 | 11 | 7 | 266 | 8 | 6 | 6 | - | 4 | 4 | 7 | 6 | 7 | 9 | 5 | 5 | 8 | 6 |
| 64 | 13 | 22 | 19 | 12 | 22 | 24 | 15 | 18 | 13 | 24 | 23 | 19 | 10 | 19 | 20 | 35 | 23 | 17 | 33 | 18 |
| 108 | 50 | 99 | 91 | 115 | 101 | 79 | 129 | 173 | 87 | 134 | 109 | 124 | 36 | 117 | 115 | 102 | 144 | 88 | 83 | 115 |
| 37 | 4 | 24 | 5 | 46 | 27 | 16 | 19 | 13 | 14 | 11 | 16 | 48 | 4 | 44 | 7 | 14 | 16 | 11 | 3 | 28 |
| 1168 | 377 | 474 | 200 | 377 | 828 | 355 | 499 | 881 | 488 | 307 | 531 | 660 | 302 | 1143 | 242 | 962 | 1319 | 478 | 957 | 1313 |
| 23 | 23 | 29 | 23 | 46 | 31 | 20 | 36 | 31 | 36 | 40 | 27 | 31 | 28 | 27 | 29 | 29 | 29 | 35 | 29 | 24 |
| 173 | 116 | 200 | 188 | 285 | 212 | 128 | 276 | 214 | 269 | 271 | 196 | 195 | 150 | 187 | 203 | 186 | 203 | 205 | 187 | 171 |
| 14 | 7 | 22 | 24 | 8 | 22 | 12 | 41 | 24 | 40 | 37 | 22 | 23 | 14 | 20 | 22 | 20 | 21 | 24 | 23 | 18 |
| 37 | 28 | 75 | 36 | 150 | 63 | 43 | 111 | 78 | 95 | 65 | 69 | 60 | 45 | 40 | 52 | 43 | 61 | 55 | 51 | 34 |
| 7 | - | 9 | - | 47 | 11 | 4 | 35 | 19 | 33 | 19 | 16 | 11 | 4 | 7 | 11 | 9 | 5 | 10 | 17 | 4 |
| 2.739 | 2.315 | 2.631 | 2.396 | 3.173 | 2.552 | 2.115 | 2.819 | 2.457 | 2.612 | 3.334 | 2.688 | 2.369 | 1.993 | 2.137 | 2.385 | 2.333 | 2.373 | 2.682 | 2.568 | 2.215 |
| 1622 | 13 | 882 | 19 | 700 | 496 | 201 | 440 | 542 | 4.290 | 385 | 337 | 484 | 26 | 722 | 165 | 564 | 652 | 444 | 92 | 639 |
| 18 | 5 | 32 | 75 | 8 | 17 | 6 | 15 | 39 | 6 | 10 | 55 | 17 | 108 | 10 | 9 | 61 | 10 | 27 | 155 | 29 |